NUTRIENT LIMITATION ALTERS METABOLISM, CR(VI) RESPONSE, AND BIOFILM MATRIX COMPOSITION IN *DESULFOVIBRIO VULGARIS* HILDENBOROUGH

by

Lauren Christine Franco

A dissertation submitted in partial fulfillment
of the requirements for the degree

of

Doctor of Philosophy

in

Microbiology and Immunology

MONTANA STATE UNIVERSITY
Bozeman, Montana

November 2017

©COPYRIGHT

by

Lauren Christine Franco

2017

All Rights Reserved

ACKNOWLEDGEMENTS

Looking back on the last seven years of graduate school, I can't help but think that I have been very fortunate to spend the better part of a decade living and studying in Montana surrounded by some of the best people I know. There were challenges, of course, but the support system that is the Center for Biofilm Engineering at MSU and all of the people that work there made it so that help was never hard to find. First, I must thank my advisor, Professor Matthew Fields, for being supportive, patient, and an all-around great mentor throughout this process. He has been a great example of leadership and professionalism, while still being approachable and kind. I would also like to thank my committee members, Christine Foreman, Brent Peyton, and Mike Franklin for their invaluable insight and input throughout my time here. After every meeting, I have felt grateful for their contributions and humbled by their intellect.

I want to acknowledge that my experience as a graduate student would not have been nearly as successful and fulfilling without CBE friends and labmates past and present that have become like my family here -- Heidi, Kristen, James, Sara, Kara, Hannah, Luisa, Chiachi, Luke, Laura, Isaac, Katie, Anna, and Greg. Graduate school would not have been the same without all of your intellectual input and lessons in winter, outdoor activities, and life in general. Also, to the Molecular Biosciences Program and the Department of Energy for funding throughout the years. Lastly, I have to thank my family for being beacons of support from afar and letting me find my own path.

TABLE OF CONTENTS

1. INTRODUCTION 1

Nutrient Limitation 1
Sulfate-Reducing Microorganisms 2
Applications of Sulfate Reducing Bacteria 3
Desulfovibrio vulgaris Hildenborough 6
Heavy Metal and Radionuclide Reduction in *Desulfovibrio* 8
Cr(V) Reduction in *D. vulgaris* 9
Biofilm Physiology 10
The Biofilm Matrix 11
Biofilm Resistance to Heavy Metal and Radionuclide Toxicity 15
Physiology of *D. vulgaris* Biofilms 17
Research Objectives 18
References 21

2. Cr(VI) REDUCTION AND PHYSIOLOGICAL TOXICITY IS IMPACTED BY RESOURCE RATIO IN *DESULFOVIBRIO VULGARIS* HILDENBOROUGH 31

Contributions of Authors 31
Manuscript Information 32
Abstract 33
Introduction 34
Materials and Methods 36
Strains and Growth Conditions 36
Experimental Design 38
Cr(VI) Reduction Analysis 38
Analytical Techniques 39
Mutant Generation 39
Results 41
Temperature Affects *D. vulgaris* Growth and Cr(VI) Reduction/Toxicity Under a Balanced Resource Ratio 41
Resource Ratio Imbalance Affects *D. vulgaris* Cr(VI) Reduction and Tolerance 46
Electron Donor-Limitation (EDL) 46
Electron Acceptor-Limitation (EAL) 47

TABLE OF CONTENTS CONTINUED

Viability 48
Growth with Increased Sulfate....49
Growth with Normalized Sulfate Levels 50
Sulfate Permease Mutants....51
Ascorbate 53
Discussion....54
References....61
Supplemental Figures 66

3. NUTRIENT LIMITATION CAUSES DECLINE IN METABOLITES IMPORTANT FOR CELL CYCLE PROGRESSION IN BACTERIAL BIOFILM....70

Contributions of Authors 70
Manuscript Information Page 71
Abstract....72
Introduction....73
Materials and Methods....75
Sample Collection....76
Biomass Analyses 76
Metabolomic Analysis of Biofilm 76
Results....77
Biofilm Growth under Nutrient-Limited and Balanced Conditions 77
Metabolomic Analysis of *D. vulgaris* Biofilm 79
Discussion....86
References....92

4. EXTRACELLULAR MEMBRANE STRUCTURES IN *DESULFOVIBRIO VULGARIS* HILDENBOROUGH BIOFILMS 95

Contributions of Authors 95
Manuscript Information 97
Abstract....98
Introduction....99
Materials and Methods....101

TABLE OF CONTENTS CONTINUED

Bacterial Strains and Growth Conditions 101
Sample Collection 102
Biomass Analyses 102
Imaging Methods 103
Fluorescence Microscopy 103
High Pressure Freezing and Freeze Substitution 103
Transmission Electron Microscopy 104
Volume Electron Microscopy 104
Energy Dispersive Spectroscopy 105
Biofilm Exposure to Cr(VI) 105
Cytochrome Staining and Heme Quantification 106
Results 107
2D TEM Imaging of *Desulfovibrio vulgaris* Biofilms 107
Large Volume 3D SBF/SEM Imaging 111
Elemental Analysis of Extracellular Metal Deposits 113
Underlying Metal Deposition Sites are Biological Membranes 115
The Effect of Nutrient Limitation on Cr(VI) Toxicity in *D. vulgaris* Biofilms 119
Discussion 122
References 129

5. OUTER MEMBRANE VESICLES AND ASSOCIATED PROTEINS PRODUCED BY *DESULFOVIBRIO VULGARIS* BIOFILMS 133

Contributions of Authors 133
Manuscript Information Page 134
Abstract 135
Introduction 136
Materials and Methods 138
Bacterial Strains and Growth Conditions 138
Isolation of Outer Membrane Vesicles 139
Transmission Electron Microscopy 140
Nucleic Acid Detection 140
Proteomic Analysis 140
Results and Discussion 141
Outer Membrane Vesicles and Tubes 141
Proteomic Analysis of OMVs 146

TABLE OF CONTENTS CONTINUED

References 151

6. EPILOGUE 156

References 167

REFERENCES CITED 170

APPENDICES 197

APPENDIX A: Supplemental Figures 198
Introduction 199
Materials and Methods 199
Results 200

APPENDIX B: *Desulfovibrio carbinoliphilus* Oakridgensis, Spp. Nov., an Organic Acid-Oxidizing, Sulfate-Reducing Bacterium Isolated from Uranium(VI)-Contaminated Groundwater 202
Contributions of Authors 202
Manuscript Information Page 203
Abstract 204
Introduction 205
Materials and Methods 206
Results and Discussion 211
References 218
Supplemental Figures 221

APPENDIX C: Autonomous Metabolomics for Rapid Metabolite Identification in Global Profiling 227
Contributions of Authors 227
Manuscript Information Page 228

APPENDIX D: Comprehensive Bioimaging with Fluorinated Nanoparticles Using Breathable Liquids 237
Contributions of Authors 237
Manuscript Information Page 238

LIST OF TABLES

Table Page

1. Strains used in this study 67

2. Primers used in this study 67

3. Lactate and Sulfate concentrations for the different nutrient ratios and biomass yields based on lactate and sulfate consumption 79

4. List of metabolites down-regulated under the EAL condition.....81

5. List of metabolites up-regulated under the EAL condition 83

6. Proteins identified in purified OMV samples 144

7. Summary of substrate and electron acceptor utilization of FW-101 isolate and closely related strains 216

LIST OF FIGURES

Figure Page

1. Growth of *D. vulgaris* at 20 and 30°C with 0 and 50μM Cr(VI) under EAL, BAL, and EDL 44

2. Cr(VI) reduction at 20 and 30°C with 100 and 50μM Cr(VI) under EAL, BAL, and EDL 45

3. Growth with 50μM Cr(VI) and increasing sulfate concentrations....50

4. Growth with 50μM Cr(VI) and normalized sulfate concentrations....51

5. Growth of sulfate permease mutants with 0 and 50 μM Cr(VI) 53

6. Growth with 50μM Cr(VI) and ascorbate....54

7. Schematic of EAL, BAL, and EDL scenarios 59

8. Lactate, acetate, sulfate concentrations over growth with 0 and 50μM Cr(VI)....66

9. Protein, carbohydrate, and sulfide concentrations in biofilms grown under EAL, BAL, and EDL 78

10. Cloud plot of dysregulated metabolites 80

11. Pathways down-regulated under EAL 84

12. Large-scale microscopic analysis of biofilm Grown under EAL, BAL, and EDL 108

13. TEM images of extracellular structures....110

14. 3D reconstruction of extracellular membrane structures 112

LIST OF FIGURES CONTINUED

Figure Page

15. 3D images of 40 x 40 x 100μm biofilm with and without cells 113

16. EDS elemental mapping of metal deposits 114

17. Differential staining of extracellular membrane structures 116

18. FAME content of biofilm.....118

19. Viability in EAL, BAL, EDL biofilm.....118

20. Planktonic growth of scraped biofilm with Cr(VI).....121

21. Protein gel with cytochrome stain.....122

22. TEM images of isolated OMVs 143

23. SEM images of biofilm grown at different temperatures 201

24. Phylogenetic tree of 16s small subunit RNA.....212

25. Phylogenetic tree of *dsr*AB gene 213

26. Growth of *D. carbinoliphilus* Oakridgensis
at different temperatures 221

27. Growth of *D. carbinoliphilus* Oakridgensis
at different pH values.....222

28. Growth of *D. carbinoliphilus* Oakridgensis
with different substrates.....223

29. Growth of *D. carbinoliphilus* Oakridgensis
with different nitrogen sources 224

30. Growth of *D. carbinoliphilus* Oakridgensis
with different electron acceptors.....225

LIST OF FIGURES CONTINUED

Figure Page

31. Growth of *D. carbinoliphilus* Oakridgensis with Cr(VI) and U(VI) 226

ABSTRACT

Sulfate-reducing bacteria (SRB) are a diverse group of anaerobic microorganisms that live in anoxic environments and play critical roles in biogechemical cycling, namely linkages between the carbon and sulfur cycles. *Desulfovibrio vulgaris* Hildenborough (DvH) is a model organism for SRB that has been studied for its ability to reduce toxic heavy metals to insoluble forms and its involvement in microbially induced corrosion in oil pipelines and other industrial settings. The described work investigated how the availability of electron donor/carbon sources and electron acceptors affected Cr(VI) reduction, metabolism, and biofilm growth and composition in DvH. DvH was grown planktonically at 20°C and 30°C in batch mode or as a biofilm under continuous flow at 20°C. In the second chapter of this dissertation, it is established that electron acceptor-limitation (EAL) predisposes cells to Cr(VI) toxicity compared to a balanced electron donor to electron acceptor (BAL) condition and electron donor-limited (EDL) condition. The effect of nutrient limitation on DvH biofilms is investigated, and microscopy revealed unique extracellular membranous structures that have not previously been observed. The extracellular structures were heterogeneously distributed, connected to cells, co-localized with metal precipitates, and more prevalent under EAL compared to BAL condition. Differential staining indicated that the structures were composed of lipid, consistent with the observation that these structures are membrane derived. Metabolomic analysis revealed an up-regulation of fatty acids under the EAL condition, which was confirmed and quantified via GC-MS. Down-regulated metabolites for biofilm grown under the EAL condition included those involved in DNA turnover, N-cycling, and peptidoglycan turnover, indicating that EAL may induce a switch from growth to fatty acid production that may coordinate with alternative electron transfer mechanisms. Outer membrane vesicles (OMVs) were purified from DvH biofilm and proteins detected in OMVs included porins, lipoproteins, hydrogenases, and oxidative stress response proteins. The results presented here show that nutrient limitation and resource ratio affect DvH physiology in both biofilm and planktonic growth modes. The analysis of the DvH biofilm matrix highlights the importance of investigating extracellular capabilities that are unique to the biofilm growth mode and has implications for activities and physiological states in the environment.

CHAPTER ONE

INTRODUCTION

Nutrient Limitation

Across trophic levels, availability of nutrients determines growth rate, population size, and competition between organisms. In the microbial world, the effect of nutrient limitation on community structure and metabolism is an area of interest due to the desire to utilize and/or control microbial growth and metabolism. On a global scale, limitation of N, P, or Fe in oceans determines primary productivity, which subsequently affects global carbon flux and nutrient availability below the photic zone and to higher trophic levels (Moore et al. 2013). On a smaller scale, nutrient limitation can affect microbial community structure, with organisms that are capable of growth on low concentrations of substrates outcompeting other microbes, also known as the resource ratio theory (Mello et al. 2016). In a monoculture or coculture, nutrient limitation has been shown to affect microbial metabolism, physiology and interactions with other organisms. For example, some sulfate-reducing bacteria experiencing sulfate limitation can produce hydrogen as an electron sink. The production of hydrogen can attract hydrogenotrophic bacteria or archaea such as methanogens and initiate a syntrophic relationship (Brileya et al. 2013).

The work presented here investigates the effect of nutrient limitation, in the form of electron donor/carbon limitation and electron acceptor/sulfate limitation on the sulfate-

reducing bacterium, *Desulfovibrio vulgaris* Hildenborough. Moreover, nutrient limitation is also examined in terms of a "resource ratio," or how the ratio of concentration of carbon source/electron donor to sulfate/electron acceptor affects physiology. Previous work has shown that electron acceptor-limitation (oxygen limitation) in *Shewanella oneidensis* induces the production of extracellular nanowires and increases gene expression for certain cytochromes, while electron acceptor-limitation in *Geobacter sulfurreducens* also caused an increase in expression genes involved in the utilization of alternative terminal electron acceptors (Gorby et al. 2006; Bansal et al. 2013; Barchinger et al. 2016). Similarly, electron donor/carbon source limitation can result in an increase in abundance of transporter proteins, proteins involved in utilizing alternative carbon sources, and adjusted ribosome content to reflect slower growth rates (Gaal et al. 1997; Liu and Ferenci 1998; Marozava et al. 2014).

Sulfate-Reducing Microorganisms

Sulfate reducing microorganisms (SRM) are ubiquitous in nature and play an important role in the global sulfur cycle by reducing sulfate to sulfide. SRM are a phylogenetically diverse group of prokaryotes, consisting of gram-negative (belonging to δ-*Proteobacteria*) and gram-positive (belonging to *Firmicutes* and *Nitrospira*) bacteria, and archaea (*Crenarchaeota*, *Euryarchaeota*) (Castro 2000). SRM inhabit a variety of different environments including terrestrial subsurface environments, marine and freshwater sediments, and animal guts (Widdel 1988; Rey et al. 2013). SRM have been

isolated from cold environments, such as arctic sediments, hot environments such as hydrothermal vents and hot spring sediments, acidic, and hypersaline environments (Knoblauch et al. 1999; Fishbain et al. 2003; Foti et al. 2007; Alazard et al. 2010; Frank et al. 2013). Given the wide distribution of the sulfate reducing metabolism, it is apparent that these organisms play an essential role in ecosystem function and global nutrient cycling.

SRM are responsible for an estimated 12-29% of organic carbon oxidation in anoxic seafloor sediments and up to 50% in wetland environments (Blodau et al. 2007; Keller and Bridgham 2007; Bowles et al. 2014), making them major drivers of carbon cycling in these environments. SRB are important microbial community members, consuming H_2, organic acids, short chain and long chain fatty acids, and other carbon compounds, while also producing reduced sulfur compounds and influencing the redox state of the local environment (Muyzer and Stams 2008). SRB are also linked to microbial methane production through syntrophic relationships with methanogenic archaea in which methanogens consume hydrogen produced by SRB (Stams and Plugge 2009; McInerney et al. 2009).

Applications of Sulfate-Reducing Bacteria

Currently, SRB are recognized for both the beneficial role they play in the reduction of heavy metal pollutants to insoluble forms and the problems they cause in industrial settings such as corrosion of steel and oil souring in pipelines and reservoirs.

The role of SRBs in corrosion has been heavily researched because of the cost associated with repairing infrastructure that has been compromised (Koch and United States. Federal Highway Administration 2002). The current model for corrosion caused by SRB is bimodal in that the H_2S produced by SRB is corrosive in itself and also some SRB are capable of using metallic iron as their sole electron donor (Enning et al. 2012; Enning and Garrelfs 2014). Oil souring is also caused by the production of H_2S and therefore it is of keen interest to better understand how to inhibit the growth of SRB (Hubert and Voordouw 2007).

SRB have also been extensively studied due to their ability to reduce heavy metals such as U(VI), Cr(VI), Se(VI), and Tc(VII) both chemically, by reacting with sulfide to produce insoluble metal-sulfides, and enzymatically (Lovley et al. 1993; Lovley and Phillips 1994; Lloyd et al. 1998; Hockin and Gadd 2003). Interest in using naturally occurring SRB for bioremediation of such heavy metal pollutants in contaminated sites has been explored as a more economical and environmentally friendly treatment than traditional chemical pump and treat methods (Tyagi et al. 2011). Pilot studies have analyzed the effectiveness of biostimulation strategies at contaminated field sites by injecting a carbon source and electron donor into the subsurface and tracking contaminant concentrations and microbial community composition over time. At one such site, the DOE Rifle site in Colorado, acetate was injected as the stimulant, which resulted in a substantial reduction in U(VI) levels (from 1-1.5µM to 0.05-0.1µM) (Williams et al. 2011). *In situ* incubations of sediment columns during acetate

amendment lead to the conclusion that U(VI) reduction occurs through multiple redox pathways, including enzymatic reduction followed by binding of U(IV) with biomass and abiotic reduction via FeS embedded in extracellular matrix materials in SRB biofilms. (Williams et al. 2011; Bargar et al. 2013)

At another site, the DOE Oak Ridge site in Tennessee (FRC), contaminated groundwater is characterized by low pH, high levels of nitrate and U(VI) (Spain and Krumholz 2011). Previous studies have demonstrated reduction of nitrate and uranium levels in the subsurface upon bio-stimulation with ethanol at the FRC, and during bio-stimulation an increase was observed in DNA sequences corresponding to SRB (Hwang et al. 2009). Injections of emulsified vegetable oil (EVO) resulted in decreased U(VI) concentrations from between 9.1 and 3.8 μM to less than 1μM across all wells and resulted in an initial increase in SRB from the *Desulforegula* genus along with *Veillonellaceae* (belonging to *Firmicutes*). Post injection, after the EVO had been degraded to acetate, NO_3^-, Fe(III), SO_4^{2-}, and U(VI) reduction decreased and was attributed to members of the *Comamonadaceae*, *Geobacteriaceae*, and *Desulfobacterales* (Gihring et al. 2011). However, further work is needed to fully develop and parameterize the proper constraints to model heavy metal bioremediation in both groundwater and sediments and better understand the physiology of important populations.

Cr(VI) and U(VI) are also groundwater contaminants at the Hanford site in Washington that have been targeted for bioremediation. A 2004 injection of hydrogen release compound (HRC), a glycerol and polylactate mixture that also releases hydrogen

upon hydrolysis, into a Cr(VI) contaminated area resulted in a significant decrease in Cr(VI) and an increase in *Pseudomonas, Desulfovibrio,* and *Geobacter* in the groundwater (Faybishenko et al. 2008). The increase in relative abundance of dissimilatory metal-reducing bacteria such as SRB and Fe(III) reducers during these field-scale pilot studies is telling of the important role that they play in heavy metal and radionuclide reduction at contaminated sites.

Desulfovibrio vulgaris Hildenborough

Desulfovibrio vulgaris Hildenborough is a model organism for studying the sulfate-reducing metabolism and SRB-metal interactions. *D. vulgaris* is a gram-negative bacterium belonging to the δ-*Proteobacteria* that was isolated from clay soil in Hildenborough, England in 1946. The DvH genome was sequenced and published in 2004 and has aided in the elucidation of many metabolic pathways and gene functions (Heidelberg et al. 2004). *D. vulgaris* generates ATP through coupling the oxidation of carbon sources/electron donors with the reduction of sulfate to sulfide. Carbon, typically in the form of organic acids and alcohols, is incompletely oxidized to acetate, resulting in a nearly 1:1 stoichiometric output of acetate to carbon input (*e.g.*, lactate). When lactate is provided as the carbon source, it is first oxidized to pyruvate, then to acetyl-CoA via lactate dehydrogenase and then pyruvate:ferredoxin dehydrogenase. Acetyl-CoA is then used for substrate-level phosphorylation to generate one ATP per lactate (Keller and Wall 2011a).

Sulfate reduction in *D. vulgaris* requires an initial input of energy (1 ATP) to activate sulfate and form adenosine phosphosulfate (APS). APS is then reduced by the APS reductase to bisulfite (HSO_3^-), which requires the hydrolysis of the pyrophosphate and two electrons. Bisulfite is reduced to sulfide (HS^-) using six electrons via the dissimilatory sulfite reductase and another ATP molecule is required to convert the AMP produced during APS reduction to ADP. Two lactate molecules are required to reduce one sulfate molecule, resulting in a 2:1 ratio of lactate to sulfate needed for a "balanced" nutrient ratio. Because two ATP molecules are produced during lactate oxidation and two are consumed during sulfate reduction, resulting in a net gain of zero ATP, cells must have another way to conserve energy. Oxidative phosphorylation via ATP synthase is thought to be the mechanism for additional ATP production and to yield one net ATP, 6-12 protons must be pumped for every molecule of sulfate reduced (Bargar et al. 2013). Membrane potential (Δp) can be generated via multiple proposed pathways, including hydrogen cycling, in which protons and electrons produced during the oxidation of lactate or pyruvate are used to produce H_2 via a cytoplasmic hydrogenase and then the H_2 can diffuse across the membrane where it can be re-oxidized by periplasmic hydrogenases. Electrons can then flow through the cytochrome c network in the periplasm and inner membrane to be used in the sulfate reduction pathway and the protons are pumped back across the membrane via ATP synthase (Odom 1981; Keller and Wall 2011). Additionally, the ferredoxin:NADH oxidoreductase Rnf is required when substrate-level phosphorylation is not possible and can pump ions across the

membrane, contributing to (Δp), and transfer electrons to NAD^+ where they are donated to the sulfate reduction pathway via Hrd/flx protein complex that couples ferredoxin reduction with DsrC reduction (Ramos et al. 2015).

Heavy Metal and Radionuclide Reduction in *Desulfovibrio*

Another aspect of the *D. vulgaris* metabolism that has been subject to study is its ability to reduce heavy metals and radionuclides. Mechanisms for heavy metal/radionuclide reduction have been identified, but more study is necessary to fully understand responses to heavy metal toxicity and reduction. Cr(VI) was selected for study in this work due to its prevalence at the Department of Energy superfund site in Hanford, WA and Cr(VI) is also a prevalent contaminant at many DOE sites. Cr is the seventh most abundant element on earth and exists primarily as Cr(VI) or Cr(III). Cr(VI), which is typically associated with oxygen as chromate (CrO_4^{2-}) or dichromate ($Cr_2O_7^{2-}$) ions, is considered the more toxic form of Cr due to its solubility in water. Cr(III) is usually associated with organic matter in the environment, exists as an oxide, hydroxide, or sulfur compound, and is generally less soluble and therefore less mobile than Cr(VI) (McGrath 1995).

Cr(VI) Reduction in *D. vulgaris*

Because sulfate and chromate are chemical analogues, it is hypothesized that chromate can enter the cell through sulfate permeases in *D. vulgaris*. Chromate uptake through sulfate transport systems has been shown in other organisms such as

Pseudomonas fluorescens, *Escherichia coli*, and *Salmonella typhimurium* (Pardee et al. 1966; Ota et al. 1971; Karbonowska et al. 1977; Ohtake et al. 1987; Sirko et al. 1990). Once inside the cell, multiple mechanisms for enzymatic Cr(VI) reduction by *D. vulgaris* are possible and this is probably because there is no specific chromate reductase enzyme, but rather enzymes that can use multiple substrates. Cytochrome c_3 has been shown to function as both a Cr(VI) and U(VI) reductase and purified cytochrome c_3 and hydrogenase in the presence of H_2 as the electron donor can reduce Cr(VI) to Cr(III) (Lovley and Phillips 1994). A cytochrome c_3 mutant in a different *Desulfovibrio* sp. (*D. desulfuricans*), had a slower U(VI) reduction rate than wild type and U(VI) reduction in the mutant was slower when H_2 was the electron donor compared to lactate or pyruvate, further indicating that there is more than one Cr(VI) and/or U(VI) reduction pathway (Payne et al. 2002). Additionally, nitroreductase enzymes in *Escherichia coli* and *Vibrio harveyi* have been shown to also function as chromate reductases (Kwak et al. 2003a; Robins et al. 2013a), and unpublished microarray data shows that the nitroreductase in *D. vulgaris* is upregulated when Cr(VI) is present (Kwak et al. 2003b; Robins et al. 2013b)).

Although *D. vulgaris* is capable of Cr(VI) reduction, energy production during Cr(VI) reduction is not linked to growth and Cr(VI) reduction intermediates such as Cr(V) and hydroxyl radicals have toxic and mutagenic effects on the cell (Chardin et al. 2002; Klonowska et al. 2008). One example of this is reduction of Cr(VI) to Cr(V) by NAD(P)H, $FADH_2$, or glutathione can create hydroxyl radicals when H_2O_2 is present, causing intracellular damage to DNA (Kawanishi et al. 1986; Shi and Dalal 1990a; Shi

and Dalal 1990b; Kadiiska et al. 1994; Itoh et al. 1995). Intracellular Cr(III) can also have mutagenic effects by forming adducts with phosphate groups of DNA strands and preventing or causing errors in replication (Nishio and Uyeki 1985; Bridgewater et al. 1994). Because intracellular Cr(III) can cause DNA replication errors, it is advantageous to the organism to export Cr(III) out of the cell quickly. *D. vulgaris* has a few different potential mechanisms for defense against chromate toxicity, including *chr*A, a chromate transporter that is critical to chromate efflux in *P. aeruginosa*, *mer*P, a mercury transporter, and *acr*A, a subunit of a multidrug efflux pump (Alvarez et al. 1999; Pimentel et al. 2002). These three genes were up-expressed in *D. vulgaris* when exposed to Cr(VI) (Fields *et al.*, unpublished results). It has been shown that Cr(III) that has been reduced from Cr(VI) is located on the cell surface, in the cytoplasmic and outer membranes, and the periplasmic space (Goulhen et al. 2005). This is consistent with the evidence that periplasmic and membrane bound hydrogenases and cytochromes are involved in Cr(VI) reduction and then Cr(III) is excreted from the cytoplasm.

Biofilm Physiology

Microorganisms attached to a surface, known as a biofilm, have distinct characteristics and growth physiology compared to planktonic counterparts in the bulk aqueous phase. The biofilm growth mode is thought to be the primary growth mode for microorganisms in a wide range of environments and because of this it is important to understand the components of microbial biofilms that make them unique (Hall-Stoodley

et al. 2004). Moreover, microorganisms associated with sediments (*i.e.*, biofilms) play an important role in nutrient and contaminant cycling and this unique physiology must be considered when trying to understand metal fate in the environment. One of the defining characteristics of the biofilm growth mode is the production of an extracellular matrix, also known as EPS (extracellular polymeric substances). The extracellular matrix can be composed of many different materials depending on the organism and the environment and can account for 50-90% of the total organic matter of a biofilm (Christensen and Characklis 1990; Nielsen et al. 1997). The biofilm matrix aids in microbial attachment to surfaces and other cells and determines the unique structure of biofilms, which affects nutrient and waste transport and the formation of microenvironments within the biofilm. A description of the major matrix components and examples of their proposed functions follows.

The Biofilm Matrix

Polysaccharides. Polysaccharides were originally assumed to be the majority of biofilm matrices, but now protein, nucleic acids, lipids, and other macromolecules are also recognized as important matrix components. Polysaccharide is a general term used for linked, repeating sugar molecules. Polysaccharides in biofilm matrices can exist as homopolysaccharides and/or heteropolysaccharides and contribute to attachment and morphology/structure in many organisms. Organisms often produce more than one type of polysaccharide, as is the case for *P. aeruginosa* that produces alginate, Pel, and Psl. *P.*

aeruginosa with a mutation in the σ-factor that regulates alginate production, results in an overproduction of alginate and a "mucoid" phenotype with increased resistance to antimicrobials (Hentzer et al. 2001). *P. aeruginosa* biofilms deficient in alginate production can still form biofilms due to the Pel and Psl polysaccharides. The Pel polysaccharide is a glucose-rich polysaccharide important for pellicle formation at the air-liquid interface and Psl is a mannose- and galactose-rich polysaccharide that is important for cell-cell and cell-surface attachment (Friedman and Kolter 2004; Ma et al. 2006). The exopolysaccharides produced by *P. aeruginosa* are examples of the diversity of polysaccharides that can be produced by one species/strain and the specific role that each can play in biofilm attachment, structure, and function; however, it appears that there is little conservation in exopolysaccharide production and function across microbial biofilms.

Proteins. Proteins are also integral components of microbial biofilm matrices and the roles of specific proteins in biofilm formation, structure, and function have been elucidated in many microorganisms. Both enzymatic and structural proteins have been detected in biofilm matrices. Extracellular enzymes are involved in degradation of matrix materials during times of starvation or to enable dispersal (Vats and Lee 2000; Zhang and Bishop 2003). Structural proteins, such as pili and flagella, are also important parts of many biofilm matrices with flagellar and pili mutations in some organisms causing changes in biofilm morphology compared to wild-type (*E. coli, P. aeruginosa,*

Streptococcus pyogenes) (Pratt and Kolter 1998; Klausen et al. 2003; Kimura et al. 2012). A variety of other biofilm matrix proteins have distinct functions specific to a particular microorganism (Flemming and Wingender 2010), for example LapA in *Pseudomonas* species (Ivanov et al. 2012).

DNA. Another biofilm matrix component that is important for the structure of some biofilms is extracellular DNA. Strategies for release/secretion of eDNA from cells differs from organism to organism with some using cell lysis as a release mechanism, while others package eDNA into membrane vesicles for release or have a yet unidentified secretion mechanism (Molin and Tolker-Nielsen 2003; Liao et al. 2014). Treatment of organisms with DNase has been shown to either prevent biofilm formation and/or disband established biofilms without having an effect of the organisms themselves, indicating the importance of eDNA for maintaining biofilm structure (Whitchurch 2002; Liao et al. 2014; Sena-Vélez et al. 2016). Further, visualization of eDNA in biofilms has shown DNA in the extracellular matrix can form extensive networks and connect cells across channels within the biofilm (Böckelmann et al. 2006; Jurcisek and Bakaletz 2007). In *P. aeruginosa* biofilms, eDNA has also been shown to protect against aminoglycosides, indicating that eDNA may play more than a structural role for some organisms (Chiang et al. 2013). The genomic content of the eDNA in biofilm matrices has also been investigated and, again, varies according to the organism studied. In a bacterial isolate from the Saskatchewan River, isolated eDNA from the biofilm matrix

was similar to genomic DNA, but treatment with restriction endonucleases and DNA fingerprinting resulted in slightly different banding patterns (Böckelmann et al. 2006). Alternatively, eDNA isolated from *P. aeruginosa* and subjected to the same fingerprinting analysis as above, revealed no differences between genomic and extracellular DNA (Steinberger and Holden 2005).

Lipids. Lipids have also been reported as a component of biofilm matrices in some organisms, but have not been as well studied as polysaccharides, proteins, or eDNA. *Serratia marcescens* produces serrawettins, hydrophobic molecules composed of hydroxy fatty acids that aid in colony biofilm spreading by reducing surface tension at the interface of different phases (Matsuyama and Nakagawa 1996). More recently, it has been found that matrix in mixed species biofilms that form on membrane bioreactors for wastewater treatment is composed largely of lipid rather than protein or polysaccharide, however these free lipids may be the product of dead cell debris (Inaba et al. 2017). While literature often cites lipids as being a potential component of biofilm matrices, there are few detailed reports on their abundance, composition, and function and is therefore an area in which more study is needed.

Outer Membrane Vesicles. The last component of biofilm matrices that will be highlighted here is outer membrane vesicles (OMVs). OMVs are small (20-250 nm) bilayer structures that bleb from the outer membrane of cells and carry cellular components in and on them. OMVs are thought to be produced by all Gram-negative

bacteria and also some Gram-positive bacteria and archaea (Ellen et al. 2009; Lee et al. 2009; Kulp and Kuehn 2010). The OMVs thus far studied can be a combination of proteins, DNA, and small molecules and have been implicated in many different processes from pathogenesis to horizontal gene transfer (Yaron et al. 2000; Kuehn 2005). Interestingly, OMVs produced by biofilm cells have distinct protein profiles compared to those produced by the same organism growing planktonically, suggesting that OMVs could play a unique role in biofilms (Schooling and Beveridge 2006; Park et al. 2015; Grande et al. 2015).

Biofilm Resistance to Heavy Metal and Radionuclide Toxicity

The biofilm growth mode is prevalent in many different environments and biofilm characteristics, such as increased resistance to antimicrobials or other external stressors, may be attributed to the presence of a heterogeneous matrix containing protective elements. Studies have shown that biofilms can have increased resistance to external stressors such as changes in water availability, UV radiation, or the presence of antibiotics or heavy metals compared to planktonic cells (Elasri and Miller 1999; Harrison et al. 2005; Chang et al. 2007), but it can be difficult to delineate the combined attributes of inherent physiology unique to the biofilm and intrinsic physical characteristics of being in biofilm itself.

The effect of heavy metals on biofilms compared to planktonic cells is of interest due to the potential for indigenous microorganisms to interact with high concentrations of

heavy metals and/or radionuclides at contaminated sites and to better understand how corroding biofilms interact with metals. Microorganisms in these contaminated subsurface environments exist predominantly as biofilms, and therefore it is important to investigate how microbes interact with metals in the biofilm growth mode (Dar et al. 2013). In *P. aeruginosa*, cells growing as a biofilm were twice as resistant to lead compared to planktonic cells and 600 times as resistant to copper. The authors of this study propose that increased Cu and Pb resistance in *P. aeruginosa* biofilms could be due to metal complexation with EPS components, which has been demonstrated in other organisms (Kaplan et al. 1987; McLean et al. 1990; Kim et al. 1996; Teitzel and Parsek 2003). *Pseudomonas putida* biofilm exposed to Cr(VI) increases production of extracellular carbohydrate, protein, and DNA compared to biofilm not exposed to Cr(VI), further supporting the hypothesis that the extracellular matrix of a biofilm is involved in metal resistance (Priester et al. 2006).

Interactions of sulfate reducing biofilms with metals has also been investigated and studies have observed that naturally occurring, multispecies SRB biofilms contain metals such as selenium and zinc immobilized in the matrix (Hockin and Gadd 2003; Labrenz and Banfield 2004). In monoculture biofilms of *Desulfovibrio desulfuricans* exposed to lead or U(VI), the amount of Pb(II) or U(VI) immobilized in the biofilm was dependent on sulfide production, as chemical reduction of Pb(II) or U(VI) by sulfide was the dominant mode of metal reduction in these biofilms. Biogenic U(VI) reduction also contributed to the overall immobilization of U(VI) in the biofilm, but the ratio of abiotic

to biotic reduction is unclear (Beyenal et al. 2004; Beyenal and Lewandowski 2004). The production of sulfide by SRB is advantageous for increasing metal reduction and immobilization through abiotic means; however, the presence of sulfide also makes it very challenging to investigate the biotic response of the organisms.

Physiology of *D. vulgaris* Biofilms

Limited research has been done to characterize the properties and characteristics of *D. vulgaris* biofilms or other SRB compared to other model organisms such as *P. aeruginosa*, *E. coli*, or *S. aureus*, but the work that has been done has laid a good foundation for understanding gene expression and protein regulation in the biofilm vs. planktonic growth mode. Clark *et al.* (2012) observed that biofilm cells have altered electron flow pathways, decreased amino acid and nucleotide biosynthesis, and decreased cell wall and membrane biosynthesis, which all point to an altered metabolic state compared to exponentially growing planktonic cells. Further, carbohydrate metabolism was altered, with a reported decrease in gluconeogenesis related genes and an increase in glycerol uptake and utilization related genes. Expression of transporter genes was also altered, with genes for ABC transporters, two other transporter proteins, and a type I secretion system protein being up-expressed under biofilm conditions along with a type III secretion system protein also that had increased abundance. In addition, recent results showed the important role of a type I secretion system for biofilm formation in *D. vulgaris* Hildenborough (De León et al. 2017). The increase in expression/abundance of

particular transporter/secretion systems for biofilm cells is perhaps indicative of an increase of small molecules, proteins, or other substrates entering and exiting the cell and/or biofilm matrix compared to planktonic cells (Clark et al. 2012).

Previous results with *D. vulgaris* indicated that biofilms on glass did not contain an extensive exopolysaccharide matrix, used protein filaments to form biofilm between cells and the silica oxide surfaces, and the filaments appeared to be flagella (Clark et al., 2007). The data suggested that *D. vulgaris* used flagella for more than a means of locomotion to a surface, but also used flagella, or modified flagella, to establish and/or maintain biofilm structure (Clark et al. 2007). Proteomic analysis of the extracellular fraction of *D. vulgaris* biofilm revealed 188 proteins. Noteworthy is a highly abundant protein that contains a vonWillebrand factor domain, which can be involved in cell adhesion, pattern formation, and signal transduction. In addition, abundant in the extracellular fraction are two outer membrane porin proteins whose function in the biofilm matrix is unknown (Clark et al. 2012; Zeng et al. 2017).

Research Objectives

The overarching theme of this work is the effect of nutrient limitation, in the form of electron donor/carbon or electron acceptor limitation, on the growth and response of *D. vulgaris* Hildenborough to Cr(VI) stress in both planktonic and biofilm growth modes. Limitation of electron donors/carbon sources or electron acceptors is a scenario the SRB likely encounter in natural environments as well as engineered systems. For example, in

the context of bioremediation, electron donor/carbon sources are injected into the subsurface during biostimulation regimes that can create an electron acceptor-limited (EAL) environment. In offshore oil wells, ocean water is typically injected into the well to recover the remaining oil, but in doing so they are injecting ~30mM sulfate, creating an electron donor/carbon limited (EDL) system. Better understanding of how nutrient limitation affects *D. vulgaris* planktonic growth, biofilm production, and response to Cr(VI) could contribute to better microbial control in engineered systems and better understanding of how SRB interact with their environment and other organisms in natural settings. Further, most studies investigating the physiological response of dissimilatory metal reducing bacteria have cultured them at 30°C, an optimal growth temperature in terms of growth rates, but not always an environmentally relevant temperature. The research presented in Chapter 2 compared planktonic growth and Cr(VI) reduction at 20 and 30°C to determine how temperature affected rate of Cr(VI) reduction in addition to how nutrient limitation affected *D. vulgaris* tolerance to Cr(VI).

Based on the findings from Chapter 2, we decided that further investigation into how nutrient limitation affected biofilm growth in *D. vulgaris* was warranted. For some of the more in-depth analysis and experiments, the EAL and BAL conditions were chosen for comparison with the BAL condition being a “control” in which lactate and sulfate concentrations are “balanced” and the EAL being the “stressed” or “limited” condition. To limit sample number, the EDL condition was omitted in a few instances. To understand how nutrient limitation affected the metabolism of *D. vulgaris* biofilm under

sulfate-limiting conditions (EAL), the metabolite profiles from biofilm grown under EAL and BAL conditions were compared. These results are presented in Chapter 3 and the data from this experiment was also used for metabolomic method and data analysis development, which is presented in Appendices C and D.

Because of the inherent heterogeneity, gradient and micro-niche formation in biofilms, *D. vulgaris* biofilms grown under EAL and BAL conditions were also compared using high resolution microscopy and differential staining techniques to detect such differences within a biofilm. The observations made during these experiments regarding the extracellular matrix of the biofilm are presented in Chapter 4 and lead to the development of methods to isolate fractions of the extracellular matrix. Outer membrane vesicles were isolated from *D. vulgaris* biofilms grown under EAL and BAL conditions and analyzed via proteomic methods. The results of these experiments are detailed in Chapter 5.

While studying model organisms such as *D. vulgaris* Hildenborough is useful and practical due to the body of literature available for reference, it is becoming increasingly apparent that model organisms are not always representative of the systems in which we are interested. The work presented here strives to apply some field-relevant parameters to the growth of a model organism, but moving forward, relevant field isolates should be selected for study. The first steps toward this goal are presented in Appendix B: the growth characterization of a sulfate reducing bacterial isolate from the Oak Ridge FRC, *Desulfovibrio carbinoliphilus* Oakridgensis.

REFERENCES CITED

Alazard D, Joseph M, Battaglia-Brunet F, Cayol J-L, Ollivier B (2010) Desulfosporosinus acidiphilus sp. nov.: a moderately acidophilic sulfate-reducing bacterium isolated from acid mining drainage sediments. Extremophiles 14:305–312.

Alvarez AH, Moreno-Sánchez R, Cervantes C (1999) Chromate efflux by means of the ChrA chromate resistance protein from Pseudomonas aeruginosa. J Bacteriol 181:7398–7400.

Bansal R, Helmus RA, Stanley BA, Zhu J, Liermann LJ, Brantley SL, Tien M (2013) Survival during long-term starvation: global proteomics analysis of Geobacter sulfurreducens under prolonged electron-acceptor limitation. J Proteome Res 12:4316–4326.

Barchinger SE, Pirbadian S, Sambles C, Baker CS, Leung KM, Burroughs NJ, El-Naggar MY, Golbeck JH (2016) Regulation of Gene Expression in Shewanella oneidensis MR-1 during Electron Acceptor Limitation and Bacterial Nanowire Formation. Appl Environ Microbiol 82:5428–5443.

Bargar JR, Williams KH, Campbell KM, Long PE, Stubbs JE, Suvorova EI, Lezama-Pacheco JS, Alessi DS, Stylo M, Webb SM, Davis JA, Giammar DE, Blue LY, Bernier-Latmani R (2013) Uranium redox transition pathways in acetate-amended sediments. Proceedings of the National Academy of Sciences 110:4506–4511.

Beyenal H, Lewandowski Z (2004) Dynamics of lead immobilization in sulfate reducing biofilms. Water Res 38:2726–2736.

Beyenal H, Sani RK, Peyton BM, Dohnalkova AC, Amonette JE, Lewandowski Z (2004) Uranium immobilization by sulfate-reducing biofilms. Environ Sci Technol 38:2067–2074.

Blodau C, Mayer B, Peiffer S, Moore TR (2007) Support for an anaerobic sulfur cycle in two Canadian peatland soils. J Geophys Res. doi: 10.1029/2006jg000364

Böckelmann U, Janke A, Kuhn R, Neu TR, Wecke J, Lawrence JR, Szewzyk U (2006) Bacterial extracellular DNA forming a defined network-like structure. FEMS Microbiol Lett 262:31–38.

Bowles MW, Mogollón JM, Kasten S, Zabel M, Hinrichs K-U (2014) Global rates of marine sulfate reduction and implications for sub-sea-floor metabolic activities. Science 344:889–891.

Bridgewater LC, Manning FC, Woo ES, Patierno SR (1994) DNA polymerase arrest by adducted trivalent chromium. Mol Carcinog 9:122–133.

Brileya KA, Connolly JM, Downey C, Gerlach R, Fields MW (2013) Taxis toward hydrogen gas by Methanococcus maripaludis. Sci Rep 3:3140.

Castro H (2000) Phylogeny of sulfate-reducing bacteria. FEMS Microbiol Ecol 31:1–9.

Chang W-S, van de Mortel M, Nielsen L, Nino de Guzman G, Li X, Halverson LJ (2007) Alginate production by Pseudomonas putida creates a hydrated microenvironment and contributes to biofilm architecture and stress tolerance under water-limiting conditions. J Bacteriol 189:8290–8299.

Chardin B, Dolla A, Chaspoul F, Fardeau ML, Gallice P, Bruschi M (2002) Bioremediation of chromate: thermodynamic analysis of the effects of Cr(VI) on sulfate-reducing bacteria. Appl Microbiol Biotechnol 60:352–360.

Chiang W-C, Nilsson M, Jensen PØ, Høiby N, Nielsen TE, Givskov M, Tolker-Nielsen T (2013) Extracellular DNA shields against aminoglycosides in Pseudomonas aeruginosa biofilms. Antimicrob Agents Chemother 57:2352–2361.

Christensen BE, Characklis WG (1990) Physical and chemical properties of biofilms. In: Characklis WG, Marshall KC (eds) Biofilms. Wiley, New York, pp 93–103

Clark ME, Edelmann RE, Duley ML, Wall JD, Fields MW (2007) Biofilm formation in Desulfovibrio vulgaris Hildenborough is dependent upon protein filaments. Environ Microbiol 9:2844–2854.

Clark ME, He Z, Redding AM, Joachimiak MP, Keasling JD, Zhou JZ, Arkin AP, Mukhopadhyay A, Fields MW (2012) Transcriptomic and proteomic analyses of Desulfovibrio vulgaris biofilms: carbon and energy flow contribute to the distinct biofilm growth state. BMC Genomics 13:138.

Dar SA, Tan H, Peacock AD, Jaffe P, N'Guessan L, Williams KH, Strycharz-Glaven S (2013) Spatial Distribution ofGeobacteraceaeand Sulfate-Reducing Bacteria DuringIn SituBioremediation of Uranium-Contaminated Groundwater. Remediation Journal 23:31–49.

De León KB, Zane GM, Trotter VV, Krantz GP, Arkin AP, Butland GP, Walian PJ, Fields MW, Wall JD (2017) Unintended Laboratory-Driven Evolution Reveals Genetic Requirements for Biofilm Formation by Desulfovibrio vulgaris Hildenborough. MBio. doi: 10.1128/mBio.01696-17

Elasri MO, Miller RV (1999) Study of the response of a biofilm bacterial community to UV radiation. Appl Environ Microbiol 65:2025–2031.

Ellen AF, Albers S-V, Huibers W, Pitcher A, Hobel CFV, Schwarz H, Folea M, Schouten S, Boekema EJ, Poolman B, Driessen AJM (2009) Proteomic analysis of secreted membrane vesicles of archaeal Sulfolobus species reveals the presence of endosome sorting complex components. Extremophiles 13:67–79.

Enning D, Garrelfs J (2014) Corrosion of iron by sulfate-reducing bacteria: new views of an old problem. Appl Environ Microbiol 80:1226–1236.

Enning D, Venzlaff H, Garrelfs J, Dinh HT, Meyer V, Mayrhofer K, Hassel AW, Stratmann M, Widdel F (2012) Marine sulfate-reducing bacteria cause serious corrosion of iron under electroconductive biogenic mineral crust. Environ Microbiol 14:1772–1787.

Faybishenko B, Hazen TC, Long PE, Brodie EL, Conrad ME, Hubbard SS, Christensen JN, Joyner D, Borglin SE, Chakraborty R, Williams KH, Peterson JE, Chen J, Brown ST, Tokunaga TK, Wan J, Firestone M, Newcomer DR, Resch CT, Cantrell KJ, Willett A, Koenigsberg S (2008) In situ long-term reductive bioimmobilization of Cr(VI) in groundwater using hydrogen release compound. Environ Sci Technol 42:8478–8485.

Fishbain S, Dillon JG, Gough HL, Stahl DA (2003) Linkage of high rates of sulfate reduction in Yellowstone hot springs to unique sequence types in the dissimilatory sulfate respiration pathway. Appl Environ Microbiol 69:3663–3667.

Flemming H-C, Wingender J (2010) The biofilm matrix. Nat Rev Microbiol. doi: 10.1038/nrmicro2415

Foti M, Sorokin DY, Lomans B, Mussman M, Zacharova EE, Pimenov NV, Kuenen JG, Muyzer G (2007) Diversity, activity, and abundance of sulfate-reducing bacteria in saline and hypersaline soda lakes. Appl Environ Microbiol 73:2093–2100.

Frank KL, Rogers DR, Olins HC, Vidoudez C, Girguis PR (2013) Characterizing the distribution and rates of microbial sulfate reduction at Middle Valley hydrothermal vents. ISME J 7:1391–1401.

Friedman L, Kolter R (2004) Genes involved in matrix formation in Pseudomonas aeruginosa PA14 biofilms. Mol Microbiol 51:675–690.

Gaal T, Bartlett MS, Ross W, Turnbough CL Jr, Gourse RL (1997) Transcription regulation by initiating NTP concentration: rRNA synthesis in bacteria. Science 278:2092–2097.

Gihring TM, Zhang G, Brandt CC, Brooks SC, Campbell JH, Carroll S, Criddle CS, Green SJ, Jardine P, Kostka JE, Lowe K, Mehlhorn TL, Overholt W, Watson DB, Yang Z, Wu W-M, Schadt CW (2011) A Limited Microbial Consortium Is Responsible for Extended Bioreduction of Uranium in a Contaminated Aquifer. Appl Environ Microbiol 77:5955–5965.

Gorby YA, Yanina S, McLean JS, Rosso KM, Moyles D, Dohnalkova A, Beveridge TJ, Chang IS, Kim BH, Kim KS, Culley DE, Reed SB, Romine MF, Saffarini DA, Hill EA, Shi L, Elias DA, Kennedy DW, Pinchuk G, Watanabe K, Ishii S 'ichi, Logan B, Nealson KH, Fredrickson JK (2006) Electrically conductive bacterial nanowires produced by Shewanella oneidensis strain MR-1 and other microorganisms. Proc Natl Acad Sci U S A 103:11358–11363.

Goulhen F, Gloter A, Guyot F, Bruschi M (2005) Cr(VI) detoxification by Desulfovibrio vulgaris strain Hildenborough: microbe–metal interactions studies. Appl Microbiol Biotechnol 71:892–897.

Grande R, Di Marcantonio MC, Robuffo I, Pompilio A, Celia C, Di Marzio L, Paolino D, Codagnone M, Muraro R, Stoodley P, Hall-Stoodley L, Mincione G (2015) Helicobacter pylori ATCC 43629/NCTC 11639 Outer Membrane Vesicles (OMVs) from Biofilm and Planktonic Phase Associated with Extracellular DNA (eDNA). Front Microbiol 6:1369.

Hall-Stoodley L, Costerton JW, Stoodley P (2004) Bacterial biofilms: from the natural environment to infectious diseases. Nat Rev Microbiol 2:95–108.

Harrison JJ, Turner RJ, Ceri H (2005) Persister cells, the biofilm matrix and tolerance to metal cations in biofilm and planktonic Pseudomonas aeruginosa. Environ Microbiol 7:981–994.

Heidelberg JF, Seshadri R, Haveman SA, Hemme CL, Paulsen IT, Kolonay JF, Eisen JA, Ward N, Methe B, Brinkac LM, Daugherty SC, Deboy RT, Dodson RJ, Durkin AS, Madupu R, Nelson WC, Sullivan SA, Fouts D, Haft DH, Selengut J, Peterson JD, Davidsen TM, Zafar N, Zhou L, Radune D, Dimitrov G, Hance M, Tran K, Khouri H, Gill J, Utterback TR, Feldblyum TV, Wall JD, Voordouw G, Fraser CM (2004) The genome sequence of the anaerobic, sulfate-reducing bacterium Desulfovibrio vulgaris Hildenborough. Nat Biotechnol 22:554–559.

Hentzer M, Teitzel GM, Balzer GJ, Heydorn A, Molin S, Givskov M, Parsek MR (2001) Alginate overproduction affects Pseudomonas aeruginosa biofilm structure and function. J Bacteriol 183:5395–5401.

Hockin SL, Gadd GM (2003) Linked redox precipitation of sulfur and selenium under

anaerobic conditions by sulfate-reducing bacterial biofilms. Appl Environ Microbiol 69:7063–7072.

Hubert C, Voordouw G (2007) Oil field souring control by nitrate-reducing Sulfurospirillum spp. that outcompete sulfate-reducing bacteria for organic electron donors. Appl Environ Microbiol 73:2644–2652.

Hwang C, Wu W, Gentry TJ, Carley J, Corbin GA, Carroll SL, Watson DB, Jardine PM, Zhou J, Criddle CS, Fields MW (2009) Bacterial community succession during in situ uranium bioremediation: spatial similarities along controlled flow paths. ISME J 3:47–64.

Inaba T, Hori T, Aizawa H, Ogata A, Habe H (2017) Architecture, component, and microbiome of biofilm involved in the fouling of membrane bioreactors. NPJ Biofilms Microbiomes 3:5.

Itoh M, Nakamura M, Suzuki T, Kawai K, Horitsu H, Takamizawa K (1995) Mechanism of chromium(VI) toxicity in Escherichia coli: is hydrogen peroxide essential in Cr(VI) toxicity? J Biochem 117:780–786.

Ivanov IE, Boyd CD, Newell PD, Schwartz ME, Turnbull L, Johnson MS, Whitchurch CB, O'Toole GA, Camesano TA (2012) Atomic force and super-resolution microscopy support a role for LapA as a cell-surface biofilm adhesin of Pseudomonas fluorescens. Res Microbiol 163:685–691.

Jurcisek JA, Bakaletz LO (2007) Biofilms formed by nontypeable Haemophilus influenzae in vivo contain both double-stranded DNA and type IV pilin protein. J Bacteriol 189:3868–3875.

Kadiiska MB, Xiang Q-H, Mason RP (1994) In vivo Free Radical Generation by Chromium (VI): An Electron Spin Resonance Spin-Trapping Investigation. Chem Res Toxicol 7:800–805.

Kaplan D, Christiaen D, Arad SM (1987) Chelating Properties of Extracellular Polysaccharides from Chlorella spp. Appl Environ Microbiol 53:2953–2956.

Karbonowska H, Wiater A, Hulanicka D (1977) Sulphate permease of Escherichia coli K12. Acta Biochim Pol 24:329–334.

Kawanishi S, Inoue S, Sano S (1986) Mechanism of DNA cleavage induced by sodium chromate(VI) in the presence of hydrogen peroxide. J Biol Chem 261:5952–5958.

Keller JK, Bridgham SD (2007) Pathways of anaerobic carbon cycling across an ombrotrophic-minerotrophic peatland gradient. Limnol Oceanogr 52:96–107.

Keller KL, Wall JD (2011) Genetics and Molecular Biology of the Electron Flow for Sulfate Respiration in Desulfovibrio. Front Microbiol. doi: 10.3389/fmicb.2011.00135

Kim S-Y, Kim J-H, Kim C-J, Oh D-K (1996) Metal adsorption of the polysaccharide produced from Methylobacterium organophilum. Biotechnol Lett 18:1161–1164.

Kimura KR, Nakata M, Sumitomo T, Kreikemeyer B, Podbielski A, Terao Y, Kawabata S (2012) Involvement of T6 pili in biofilm formation by serotype M6 Streptococcus pyogenes. J Bacteriol 194:804–812.

Klausen M, Heydorn A, Ragas P, Lambertsen L, Aaes-Jørgensen A, Molin S, Tolker-Nielsen T (2003) Biofilm formation by Pseudomonas aeruginosa wild type, flagella and type IV pili mutants. Mol Microbiol 48:1511–1524.

Klonowska A, Clark ME, Thieman SB, Giles BJ, Wall JD, Fields MW (2008) Hexavalent chromium reduction in Desulfovibrio vulgaris Hildenborough causes transitory inhibition of sulfate reduction and cell growth. Appl Microbiol Biotechnol 78:1007–1016.

Knoblauch C, Jørgensen BB, Harder J (1999) Community size and metabolic rates of psychrophilic sulfate-reducing bacteria in Arctic marine sediments. Appl Environ Microbiol 65:4230–4233.

Koch GH, United States. Federal Highway Administration (2002) Corrosion Cost and Preventive Strategies in the United States.

Kuehn MJ (2005) Bacterial outer membrane vesicles and the host-pathogen interaction. Genes Dev 19:2645–2655.

Kulp A, Kuehn MJ (2010) Biological functions and biogenesis of secreted bacterial outer membrane vesicles. Annu Rev Microbiol 64:163–184.

Kwak YH, Lee DS, Kim HB (2003) Vibrio harveyi nitroreductase is also a chromate reductase. Appl Environ Microbiol 69:4390–4395.

Labrenz M, Banfield JF (2004) Sulfate-Reducing Bacteria-Dominated Biofilms That Precipitate ZnS in a Subsurface Circumneutral-pH Mine Drainage System. Microb Ecol. doi: 10.1007/s00248-003-1025-8

Lee E-Y, Choi D-Y, Kim D-K, Kim J-W, Park JO, Kim S, Kim S-H, Desiderio DM, Kim Y-K, Kim K-P, Gho YS (2009) Gram-positive bacteria produce membrane vesicles: proteomics-based characterization of Staphylococcus aureus-derived membrane vesicles. Proteomics 9:5425–5436.

Liao S, Klein MI, Heim KP, Fan Y, Bitoun JP, Ahn S-J, Burne RA, Koo H, Brady LJ, Wen ZT (2014) Streptococcus mutans extracellular DNA is upregulated during growth in biofilms, actively released via membrane vesicles, and influenced by components of the protein secretion machinery. J Bacteriol 196:2355–2366.

Liu X, Ferenci T (1998) Regulation of porin-mediated outer membrane permeability by nutrient limitation in Escherichia coli. J Bacteriol 180:3917–3922.

Lloyd JR, Nolting H -F, Solé VA, Bosecker K, Macaskie LE (1998) Technetium reduction and precipitation by sulfate-reducing bacteria. Geomicrobiol J 15:45–58.

Lovley DR, Phillips EJ (1994) Reduction of Chromate by Desulfovibrio vulgaris and Its c(3) Cytochrome. Appl Environ Microbiol 60:726–728.

Lovley DR, Widman PK, Woodward JC, Phillips EJ (1993) Reduction of uranium by cytochrome c3 of Desulfovibrio vulgaris. Appl Environ Microbiol 59:3572–3576.

Ma L, Jackson KD, Landry RM, Parsek MR, Wozniak DJ (2006) Analysis of Pseudomonas aeruginosa conditional psl variants reveals roles for the psl polysaccharide in adhesion and maintaining biofilm structure postattachment. J Bacteriol 188:8213–8221.

Marozava S, Röling WFM, Seifert J, Küffner R, von Bergen M, Meckenstock RU (2014) Physiology of Geobacter metallireducens under excess and limitation of electron donors. Part II. Mimicking environmental conditions during cultivation in retentostats. Syst Appl Microbiol 37:287–295.

Matsuyama T, Nakagawa Y (1996) Surface-active exolipids: analysis of absolute chemical structures and biological functions. J Microbiol Methods 25:165–175.

McGrath SP (1995) Chromium and Nickel. In: Heavy Metals in Soils. pp 152–178

McInerney MJ, Sieber JR, Gunsalus RP (2009) Syntrophy in anaerobic global carbon cycles. Curr Opin Biotechnol 20:623–632.

McLean RJ, Beauchemin D, Clapham L, Beveridge TJ (1990) Metal-Binding Characteristics of the Gamma-Glutamyl Capsular Polymer of Bacillus licheniformis ATCC 9945. Appl Environ Microbiol 56:3671–3677.

Mello BL, Alessi AM, McQueen-Mason S, Bruce NC, Polikarpov I (2016) Nutrient availability shapes the microbial community structure in sugarcane bagasse compost-derived consortia. Sci Rep. doi: 10.1038/srep38781

Molin S, Tolker-Nielsen T (2003) Gene transfer occurs with enhanced efficiency in biofilms and induces enhanced stabilisation of the biofilm structure. Curr Opin Biotechnol 14:255–261.

Moore CM, Mills MM, Arrigo KR, Berman-Frank I, Bopp L, Boyd PW, Galbraith ED, Geider RJ, Guieu C, Jaccard SL, Jickells TD, La Roche J, Lenton TM, Mahowald NM, Marañón E, Marinov I, Moore JK, Nakatsuka T, Oschlies A, Saito MA, Thingstad TF, Tsuda A, Ulloa O (2013) Processes and patterns of oceanic nutrient limitation. Nat Geosci 6:701–710.

Muyzer G, Stams AJM (2008) The ecology and biotechnology of sulphate-reducing bacteria. Nat Rev Microbiol 6:441–454.

Nielsen PH, Jahn A, Palmgren R (1997) Conceptual model for production and composition of exopolymers in biofilms. Water Sci Technol. doi: 10.1016/s0273-1223(97)00318-1

Nishio A, Uyeki EM (1985) Inhibition of DNA synthesis by chromium compounds. J Toxicol Environ Health 15:237–244.

Odom J (1981) Hydrogen cycling as a general mechanism for energy coupling in the sulfate-reducing bacteria, Desulfovibrio sp. FEMS Microbiol Lett 12:47–50.

Ohtake H, Cervantes C, Silver S (1987) Decreased chromate uptake in Pseudomonas fluorescens carrying a chromate resistance plasmid. J Bacteriol 169:3853–3856.

Ota N, Galsworthy PR, Pardee AB (1971) Genetics of sulfate transport by Salmonella typhimurium. J Bacteriol 105:1053–1062.

Pardee AB, Prestidge LS, Whipple MB, Dreyfuss J (1966) A binding site for sulfate and its relation to sulfate transport into Salmonella typhimurium. J Biol Chem 241:3962–3969.

Park AJ, Murphy K, Surette MD, Bandoro C, Krieger JR, Taylor P, Khursigara CM (2015) Tracking the Dynamic Relationship between Cellular Systems and Extracellular Subproteomes in Pseudomonas aeruginosa Biofilms. J Proteome Res 14:4524–4537.

Payne RB, Gentry DM, Rapp-Giles BJ, Casalot L, Wall JD (2002) Uranium Reduction by Desulfovibrio desulfuricans Strain G20 and a Cytochrome c3 Mutant. Appl Environ Microbiol 68:3129–3132.

Pimentel BE, Moreno-SÃ¡nchez R, Cervantes C (2002) Efflux of chromate byPseudomonas aeruginosacells expressing the ChrA protein. FEMS Microbiol Lett

212:249–254.

Pratt LA, Kolter R (1998) Genetic analysis of Escherichia coli biofilm formation: roles of flagella, motility, chemotaxis and type I pili. Mol Microbiol 30:285–293.

Priester JH, Olson SG, Webb SM, Neu MP, Hersman LE, Holden PA (2006) Enhanced exopolymer production and chromium stabilization in Pseudomonas putida unsaturated biofilms. Appl Environ Microbiol 72:1988–1996.

Ramos AR, Grein F, Oliveira GP, Venceslau SS, Keller KL, Wall JD, Pereira IAC (2015) The FlxABCD-HdrABC proteins correspond to a novel NADH dehydrogenase/heterodisulfide reductase widespread in anaerobic bacteria and involved in ethanol metabolism inDesulfovibrio vulgaris Hildenborough. Environ Microbiol 17:2288–2305.

Rey FE, Gonzalez MD, Cheng J, Wu M, Ahern PP, Gordon JI (2013) Metabolic niche of a prominent sulfate-reducing human gut bacterium. Proc Natl Acad Sci U S A 110:13582–13587.

Robins KJ, Hooks DO, Rehm BHA, Ackerley DF (2013) Escherichia coli NemA Is an Efficient Chromate Reductase That Can Be Biologically Immobilized to Provide a Cell Free System for Remediation of Hexavalent Chromium. PLoS One 8:e59200.

Schooling SR, Beveridge TJ (2006) Membrane Vesicles: an Overlooked Component of the Matrices of Biofilms. J Bacteriol 188:5945–5957.

Sena-Vélez M, Redondo C, Graham JH, Cubero J (2016) Presence of Extracellular DNA during Biofilm Formation by Xanthomonas citri subsp. citri Strains with Different Host Range. PLoS One 11:e0156695.

Shi XL, Dalal NS (1990) NADPH-dependent flavoenzymes catalyze one electron reduction of metal ions and molecular oxygen and generate hydroxyl radicals. FEBS Lett 276:189–191.

Sirko A, Hryniewicz M, Hulanicka D, Böck A (1990) Sulfate and thiosulfate transport in Escherichia coli K-12: nucleotide sequence and expression of the cysTWAM gene cluster. J Bacteriol 172:3351–3357.

Spain AM, Krumholz LR (2011) Nitrate-Reducing Bacteria at the Nitrate and Radionuclide Contaminated Oak Ridge Integrated Field Research Challenge Site: A Review. Geomicrobiol J 28:418–429.

Stams AJM, Plugge CM (2009) Electron transfer in syntrophic communities of anaerobic

bacteria and archaea. Nat Rev Microbiol 7:568–577.

Steinberger RE, Holden PA (2005) Extracellular DNA in single- and multiple-species unsaturated biofilms. Appl Environ Microbiol 71:5404–5410.

Teitzel GM, Parsek MR (2003) Heavy metal resistance of biofilm and planktonic Pseudomonas aeruginosa. Appl Environ Microbiol 69:2313–2320.

Tyagi M, da Fonseca MMR, de Carvalho CCCR (2011) Bioaugmentation and biostimulation strategies to improve the effectiveness of bioremediation processes. Biodegradation 22:231–241.

Vats N, Lee SF (2000) Active detachment of Streptococcus mutans cells adhered to epon-hydroxylapatite surfaces coated with salivary proteins in vitro. Arch Oral Biol 45:305–314.

Whitchurch CB (2002) Extracellular DNA Required for Bacterial Biofilm Formation. Science 295:1487–1487.

Widdel F (1988) Microbiology and ecology of sulfate- and sulfur-reducing bacteria. In: Zehnder AJB (ed) Biology of anaerobic microorganisms. Wiley & Sons, New York, pp 469–575

Williams KH, Long PE, Davis JA, Wilkins MJ, Lucie N'Guessan A, Steefel CI, Yang L, Newcomer D, Spane FA, Kerkhof LJ, McGuinness L, Dayvault R, Lovley DR (2011) Acetate Availability and its Influence on Sustainable Bioremediation of Uranium-Contaminated Groundwater. Geomicrobiol J 28:519–539.

Yaron S, Kolling GL, Simon L, Matthews KR (2000) Vesicle-mediated transfer of virulence genes from Escherichia coli O157:H7 to other enteric bacteria. Appl Environ Microbiol 66:4414–4420.

Zeng L, Wooton E, Stahl DA, Walian PJ (2017) Identification and Characterization of the Major Porin of Desulfovibrio vulgaris Hildenborough. J Bacteriol. doi: 10.1128/JB.00286-17

Zhang X, Bishop PL (2003) Biodegradability of biofilm extracellular polymeric substances. Chemosphere 50:63–69.

CHAPTER TWO

Cr(VI) REDUCTION AND PHYSIOLOGICAL TOXICITY IS IMPACTED BY RESOURCE RATIO IN *DESULFOVIBRIO VULGARIS* HILDENBOROUGH

Contribution of Authors and Co-Authors

Manuscript in Chapter 2

Author: Lauren C. Franco

Contributions: Developed experimental design, performed experiments, analyzed data, wrote and revised the manuscript.

Co-Author: Grant Zane

Contributions: Created mutant strains, wrote and revised the manuscript.

Co-Author: Sadie Steinbeisser

Contributions: Performed experiments.

Co-Author: Judy Wall

Contributions: Created mutant strains, wrote and revised the manuscript.

Co-Author: Matthew W. Fields

Contributions: Developed experimental design, analyzed data, wrote and revised the manuscript.

Manuscript Information Page

Lauren C. Franco, Grant Zane, Sadie Steinbeisser, Judy Wall, Mathew W. Fields

Applied Microbiology and Microbiology

Status of Manuscript:
____ Prepared for submission to a peer-reviewed journal
__x_ Officially submitted to a peer-review journal
____ Accepted by a peer-reviewed journal
____ Published in a peer-reviewed journal

Springer Berlin Heidelberg
August 14, 2017

Abstract

Desulfovibrio spp. are capable of heavy metal reduction and are well-studied systems for understanding metal fate and transport in anaerobic environments. *Desulfovibrio vulgaris* Hildenborough was grown under environmentally-relevant conditions (*i.e.*, temperature and nutrient limitation) to elucidate the impacts of Cr(VI) reduction on cellular physiology. Growth at 20°C was slower than 30°C and the presence of 50 μM Cr(VI) caused extended lag times for all conditions, but once resumed the growth rate was similar to that without Cr(VI). Cr(VI) reduction rates were greatly diminished at 20°C for both 50 μM and 100 μM Cr(VI), particularly for the electron acceptor limited (EAL) condition in which Cr(VI) reduction was much slower, the growth lag much longer (200 h), and viability decreased compared to balanced (BAL) and electron donor limited (EDL) conditions. Similar results were observed between the different resource ratio conditions when the sulfate levels were normalized (10 mM), and these results indicated that resource ratio (donor:acceptor) impacted *D. vulgaris* response to Cr(VI) and not merely sulfate limitation. When sulfate levels were increased in the presence of Cr(VI), cellular responses improved via a shorter lag time to growth. The results suggest that temperature and resource ratios greatly impacted the extent of Cr(VI) toxicity, Cr(VI) reduction, and the subsequent cellular health via Cr(VI) influx and overall metabolic rate. The results also emphasized the need to perform experiments at lower temperatures with nutrient limitation to make accurate predictions of heavy metal reduction rates as well as physiological states in the environment.

Introduction

Chromium is a naturally occurring trace element that is widely used for industrial purposes (*i.e.*, metallurgy, leather tanning) and has become a major pollutant of soil and groundwater (Barnhart 1997; Zayed and Terry 2003; Dhal et al. 2013). Hexavalent chromium is soluble and can easily be transported across cell membranes whereas trivalent chromium is mostly insoluble and therefore not as toxic to cells. Cr(VI) is a known mutagen and carcinogen, although it appears that chromium toxicity is largely caused by reactive intermediates such as Cr(V) or hydroxyl radicals produced during Cr(VI) reduction and Cr(III) forming adducts with DNA or natural organic matter (Nriagu and Nieboer 1988; Aiyar et al. 1991; Zhitkovich et al. 1995; 2013; Gustafsson et al. 2014).

Desulfovibrio species are model sulfate-reducing bacteria (SRB) and have been shown to reduce metals, metalloids, and radionuclides (Heidelberg et al. 2004; Klonowska et al. 2008). Previous work with purified enzymes and whole cells has shown that *D. vulgaris* is capable of reducing Cr(VI) via hydrogenases and cytochrome c3, but cells are unable to use Cr(VI) as a terminal electron acceptor linked to growth (Lovley and Phillips 1994; Chardin et al. 2002; Elias et al. 2004). One promising approach for treatment of contaminated environments is *in situ* biostimulation, the process of promoting indigenous microbial activity via the addition of carbon, nitrogen, phosphorus, and/or energy sources (Tyagi et al. 2011). Typically, microbial activity is promoted

through the addition of carbon/energy sources as soluble substrates and/or more recalcitrant, complex substrates that degrade more slowly (Faybishenko et al. 2008). For example, biostimulation has been used successfully to reduce contaminants at the Cr(VI) contaminated 100-H area of the Hanford Site in south-central Washington state. Injections of electron donors such as polylactate hydrogen-release compound (HRC) into the subsurface have been shown to stimulate Cr(VI)-reducing microorganisms such as *Desulfovibrio* spp. and other metal-reducing bacteria *in situ* (Zhang et al. 2015).

Electron donors and electron acceptors are rarely balanced according to metabolic stoichiometry for a particular organism or guild. In fact, it is common practice to stimulate growth of existing microorganisms by injecting an excess electron donor into the subsurface, creating an electron acceptor limited environment. Previous studies have reported that substrate limitation can increase Cr(VI) susceptibility (Chardin et al. 2002), and injections of electron donor without a corresponding increase in electron acceptor creates unbalanced electron donor to acceptor ratios. However, little is known about the physiological responses of metal-reducing populations in the context of unbalanced ratios that occur as a consequence of stimulated conditions. In addition, metal-reducing bacteria are often studied at optimal growth temperatures (between 30 and 40°C) although much lower temperatures are experienced *in situ*. A previous study examined uranium reduction in a sulfate-reducing consortium at 10, 20, and 30°C, and observed that growth and reduction kinetics were affected by temperature (Boonchayaanant et al. 2008). Therefore, it is important to understand the growth characteristics of

microorganisms that are capable of heavy metal immobilization, such as SRB, under typical field conditions to accurately assess and predict ability and rate of contaminant immobilization. To our knowledge, previous studies have not evaluated Cr(VI) effects on SRB growth and reduction rates at a temperature lower than 30°C under unbalanced stoichiometries of electron donors and acceptors.

Materials and Methods

Strains and Growth Conditions

The *Desulfovibrio vulgaris* Hildenborough culture was acquired from Dr. Romy Chakraborty (Lawrence Berkeley National Laboratory). LS4D medium (Borglin et al. 2009) (modified to 2.5 μM resazurin and 130 μM riboflavin in Thauer's vitamins (Brandis et al. 1981)) was prepared anoxically by boiling water under oxygen-free N_2 gas, adding medium components, and dispensing into N_2 gassed tubes or serum bottles sealed with butyl stoppers and aluminum crimp seals as previously described (Klonowska et al. 2008). LS4D medium was modified to alter electron donor (lactate) to electron acceptor (sulfate) ratios: 60 mM to 30 mM (balanced, or 20:10), 50 mM to 10 mM (electron acceptor-limited), and 18 mM to 50 mM (electron donor-limited or 5:10). The medium was not prepared with a reducing agent to avoid abiotic Cr(VI) reduction. Inocula for all experiments unless otherwise noted were grown in the same electron donor to acceptor ratio (*i.e.*, inoculum grown in balanced medium was

inoculated into balanced medium). Cultures were grown at ambient room temperature (approximately 20°C) unless otherwise stated.

Inocula for all experiments were prepared by washing mid-exponential phase (approximately 0.4 OD_{600}) cultures to remove sulfide as previously described (Klonowska et al. 2008). To do this, cultures (9 ml aliquots) were harvested by centrifugation at 5,750×*g* for 10 min at room temperature. The supernatant was removed anoxically and aseptically by needle attached to a vacuum flask under constant flow of N_2 gas to maintain neutral pressure. Pellets were then re-suspended in 9 ml fresh LS4D medium that contained lactate and sulfate concentrations of the respective growth condition and washed once more, after which the pellets were re-suspended and concentrated in 1 ml fresh LS4D. Concentrated cell cultures were inoculated into 25 ml balch tubes with LS4D medium (15 ml) that contained Cr(VI) (potassium chromate) at 0, 50, and 100 μM to an OD_{600} between 0.06 and 0.07. Growth was monitored by optical density (600 nm) and samples of 0.2 to 0.5 ml were withdrawn throughout the growth cycle to monitor Cr(VI), lactate, acetate, and sulfate concentrations. All experiments were performed in triplicate. Ascorbate, which has been shown to reduce Cr(VI) to Cr(III) and form short-lived Cr(V) and Cr(IV) intermediates and Cr(III)-ascorbate complexes (Cieăślak-Golonka et al. 1992; Stearns and Wetterhahn 1994), was added to cultures with and without Cr(VI) to determine the effect that complexed Cr(III) had on growth. Cells were prepared as described above and inoculated into electron acceptor-limited LS4D medium that contained either 50 μM sodium ascorbate, 50 μM potassium

chromate, 50 μM sodium ascorbate and 50 μM potassium chromate, or 50 μM potassium chromate added prior to inoculation and 50 μM sodium ascorbate added 3 hours post-inoculation.

Experimental Design

In order to determine the physiological responses and Cr(VI) reduction rates under field relevant conditions, *D. vulgaris* was grown under three conditions of resource ratios with and without Cr(VI) (50 and 100 μM) at 20°C. A ratio of 60:30 (or 20:10) mM (lactate:sulfate) was used for balanced (BAL), 50:10 mM for electron-acceptor limited (EAL), and 18:50 (5:10) mM for electron-donor limited (EDL). Cell cultures were washed of sulfides to observe cellular responses to field relevant levels of Cr(VI). Cr(VI) reduction rates, growth rates, biomass yields ($Y^{sulfate}$), and viability were measured to assess physiological responses. Similar levels of lactate (electron-donor) were tested with increasing levels of sulfate (electron-acceptor) and showed the role of Cr(VI) influx, metabolism, and toxicity on cell viability and Cr(VI) reduction.

Cr(VI) Reduction Analysis

Cr(VI) reduction was measured by quantifying Cr(VI) concentrations over time using the diphenylcarbazide method with Hach ChromaVer 3 reagent (Hach Company, Loveland, CO) as previously described (Viamajala et al. 2002; Klonowska et al. 2008) except that absorbance was read in disposable cuvettes (Plastibrand, Germany) at 540 nm. Cells were removed by filtration (0.22 μm) so that only Cr(VI) in the filtrate was

measured. Primary and secondary Cr(VI) reduction rates were calculated from bi-phasic decline Cr(VI) levels and the culture density did not change significantly from inoculation during the time in which the rates were calculated. Cr(VI) in uninoculated medium and cultures containing heat-killed cells were also measured.

Analytical Techniques

Lactate and acetate concentrations were measured by HPLC (Dionex) with an Aminex HPX-87H ion exclusion column. Sulfate concentrations were measured by ion chromatography (Dionex) with an IonPac AS11 column (Dionex). All samples were measured in triplicate. Cell viability was measured via the most probable number (MPN) method at 3 and 48 hours. Washed cells were inoculated into fresh LS4D medium (~0.07 OD_{600}) that was electron donor to acceptor balanced or electron acceptor-limited and contained 0 or 50 μM K_2CrO_4. Subsamples were removed and serially diluted with LS4D medium that contained sodium sulfide as a reducing agent. MPN cultures were incubated at 30°C for three weeks at which point the MPN for each condition was calculated (Jarvis et al. 2010).

Mutant Generation

Construction of the mutants lacking the annotated sulfate permease genes, *sulP,* was accomplished similarly to the generation of marker-less deletion strains in the uracil phosphoribosyltransferase (*upp*, pyrimidine salvage pathway enzyme) deletion mutant (JW710; resistant to 5-fluoro uracil, 5FU) of *Desulfovibrio vulgaris* Hildenborough

(Keller et al. 2009). In short, two plasmids were necessary for each gene deletion. The first (marker-exchange) plasmid, contained the antibiotic-resistance cassette encoding the aminoglycoside-3'-phosphotransferase (*npt*, Km^r) driven by the native promoter (P_{npt}) followed by the *upp* gene (P_{npt}-*npt*-*upp*) and was exchanged with the gene of interest (selected with the kanamycin analog G418). The second (marker-less deletion) plasmid was used for removing the cassette that conferred sensitivity to 5FU (selected with 5FU) resulting in the in-frame, marker-less deletion. Following each transformation, putative transformants were screened for phenotypes with spectinomycin, 5FU and G418 to determine the probability that a double homologous recombination event took place rather than a single recombination event resulting in plasmid insertion. Three of the isolates with correct phenotypes were further confirmed by Southern blot analysis and one selected as the confirmed deletion strain. Multiple deletions were obtained through an iterative process of transforming the appropriate parental strain with the marker-exchange/marker-less deletion plasmids and selecting for the appropriate resistances. A total of nine plasmids were constructed for generating the deletion strains of the three putative sulfate-permease genes (Table S1). Each marker-exchange plasmid was initially constructed with only the *npt* gene and no *upp* gene, as done in other studies (Parks et al. 2013; Lovley and Phillips 1994; Li and Elledge 2007). These plasmids were later modified to include the *upp* gene as the second gene in an artificial operon driven by P_{npt}. This was accomplished by PCR amplifying the plasmid with a pair of primers that allowed for the addition of the counter-selectable feature by the SLIC (sequence- and

ligation- independent cloning) technique (Li and Elledge 2007). The construct for a marker-less, in-frame deletion plasmid was produced by PCR amplification of the original marker-exchange plasmid with primers that excluded the kanamycin-resistance marker and ligated closed using the SLIC procedure. The regions of each plasmid necessary for homologous recombination were sequenced (DNA core, University of Missouri, Columbia) to determine fidelity to the published sequence. These plasmids were transformed into JW710 for the single deletion strains or into one of the marker-less deletion strains to generate strains deleted of multiple genes. All primers are listed in Table S2.

Results

Temperature Affects *D. vulgaris* Growth and Cr(VI) Reduction/Toxicity Under A Balanced Resource Ratio

D. vulgaris was grown at both 20°C and 30°C, with 0 and 50 μM Cr(VI), to assess differences in growth rate, biomass yield, and Cr(VI) tolerance at different resource ratios. Under balanced ratio conditions, *D. vulgaris* had a 3.6-fold slower growth rate (0.03 h^{-1}) at 20°C compared to growth at 30°C (0.12 h^{-1}) (Figure 1C and D). When exposed to Cr(VI) under balanced conditions, *D. vulgaris* could tolerate and reduce Cr(VI) faster at 30°C compared to at 20°C. At 30°C, only a small growth rate difference (10% lower) was observed when cells were exposed to 50 μM Cr(VI) (Figure 1C and D). At 20°C and BAL conditions, cells exposed to 50 μM Cr(VI) had an extended

lag time (~100 h), but the subsequent growth rate was similar to cultures without Cr(VI) (Figure 1D). In addition, the $Y^{Sulfate}$ values were similar between 0 and 50 μM Cr(VI) once growth was complete. Even under balanced conditions at 20°C, exposure to 100 μM Cr(VI) caused variable growth and greatly extended lags even though Cr(VI) levels declined (Figure 2D). For EDL and EAL conditions at 20°C, 100 μM Cr(VI) caused culture death and incomplete Cr(VI) reduction (Figure 2). Therefore, growth at 50 μM Cr(VI) was selected as a sub-toxic level to elucidate physiological responses across the tested resource ratios. At 20°C and 30°C, cultures with and without Cr(VI) under balanced conditions utilized lactate and produced equimolar levels of acetate until sulfate was depleted (Figure S1C). In the presence of 50 μM Cr(VI) under balanced conditions, lactate and sulfate were not utilized during the growth lag, and growth coincided with the utilization of lactate and sulfate (Figure S1D).

Temperature also affected *D. vulgaris* ability to reduce Cr(VI) (50 or 100 μM) under balanced conditions. At 30°C, 50 μM Cr(VI) was reduced at a rate of 23.63±0.12 μM Cr(VI)/h whereas at 20°C, 50 μM Cr(VI) was reduced at an initial rate of 10.81±2.14 μM Cr(VI)/h and a secondary rate of 1.51±0.18 μM Cr(VI)/h (average O.D. 0.08)). At 30°C, 100 μM Cr(VI) was reduced at an initial rate of 22.53±0.78 μM Cr(VI)/h and a secondary rate of 0.45±0.22 μM Cr(VI)/h (average O.D. of 0.08)). At 20°C, 100 μM Cr(VI) was reduced at an initial rate of 14.21±0.58 μM Cr(VI)/h and a secondary rate of 0.42±0.15 μM Cr(VI)/h (average O.D. 0.07)) (Figure 2C, D). Ultimately, a decrease in

temperature caused significant decreases in *D. vulgaris* Cr(VI) reduction rates under the balanced condition.

Previous work has highlighted many different enzymes that are capable of Cr(VI) reduction in *D. vulgaris* (Lovley and Phillips 1994; Chardin et al. 2003a; Li and Krumholz 2009a), but these studies have been conducted at temperatures selected for maximal growth. Temperature effects on *D. vulgaris* growth and Cr(VI) reduction were pronounced and emphasized the need to study microorganisms at temperatures that are field relevant in order to provide improved estimates for ecosystem function (*e.g.*, Cr(VI) reduction). The difference in Cr(VI) reduction and growth at 20°C compared to 30°C is likely due to the combination of a slower growth rate (*i.e.*, slower overall metabolism) at 20°C and the temperature dependence of enzyme reaction rates. When U(VI) reduction was measured at 20°C and 30°C in a sulfate-reducing consortium, pseudo second-order rate constants for uranium reduction tripled with the 10°C increase in temperature (Boonchayaanant et al. 2008), further emphasizing the role that temperature plays in microbial processes such as heavy metal reduction. Our results showed that the rate of Cr(VI) reduction during *D. vulgaris* growth was approximately 2-fold slower at 20°C compared to 30°C and the slower Cr(VI) reduction likely contributed to the increased Cr(VI) toxicity.

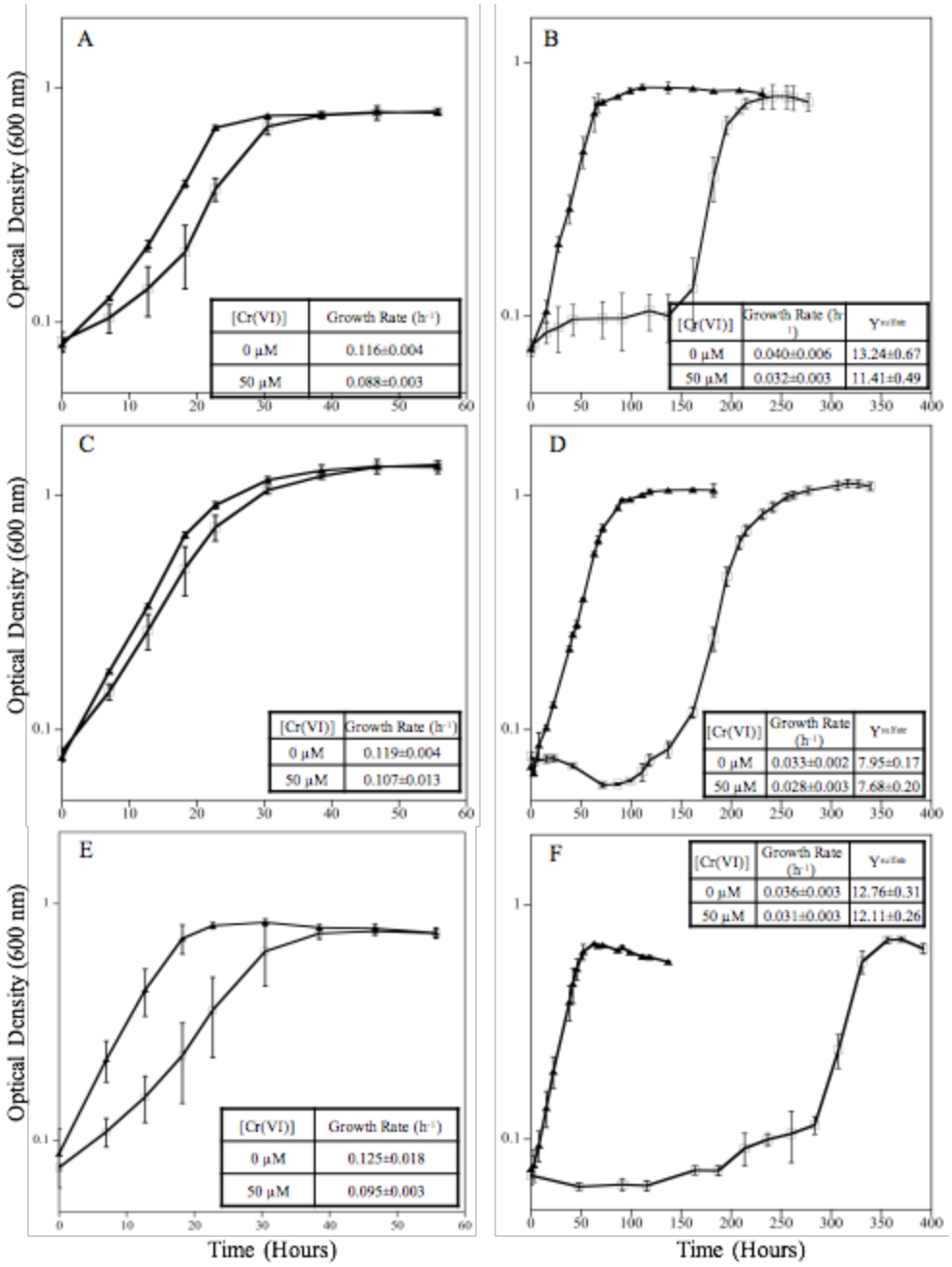


Figure 1. Growth of *D. vulgaris* at 30°C (a, c, and e) and 20°C (b, d and f) under EDL (a,b), BAL (c,d), and EAL (e,f) conditions with 0 (●) and 50 (□) µM Cr(VI). Growth rates (h^{-1}) and growth yields (grams of protein/moles sulfate consumed) are overlaid for each condition.

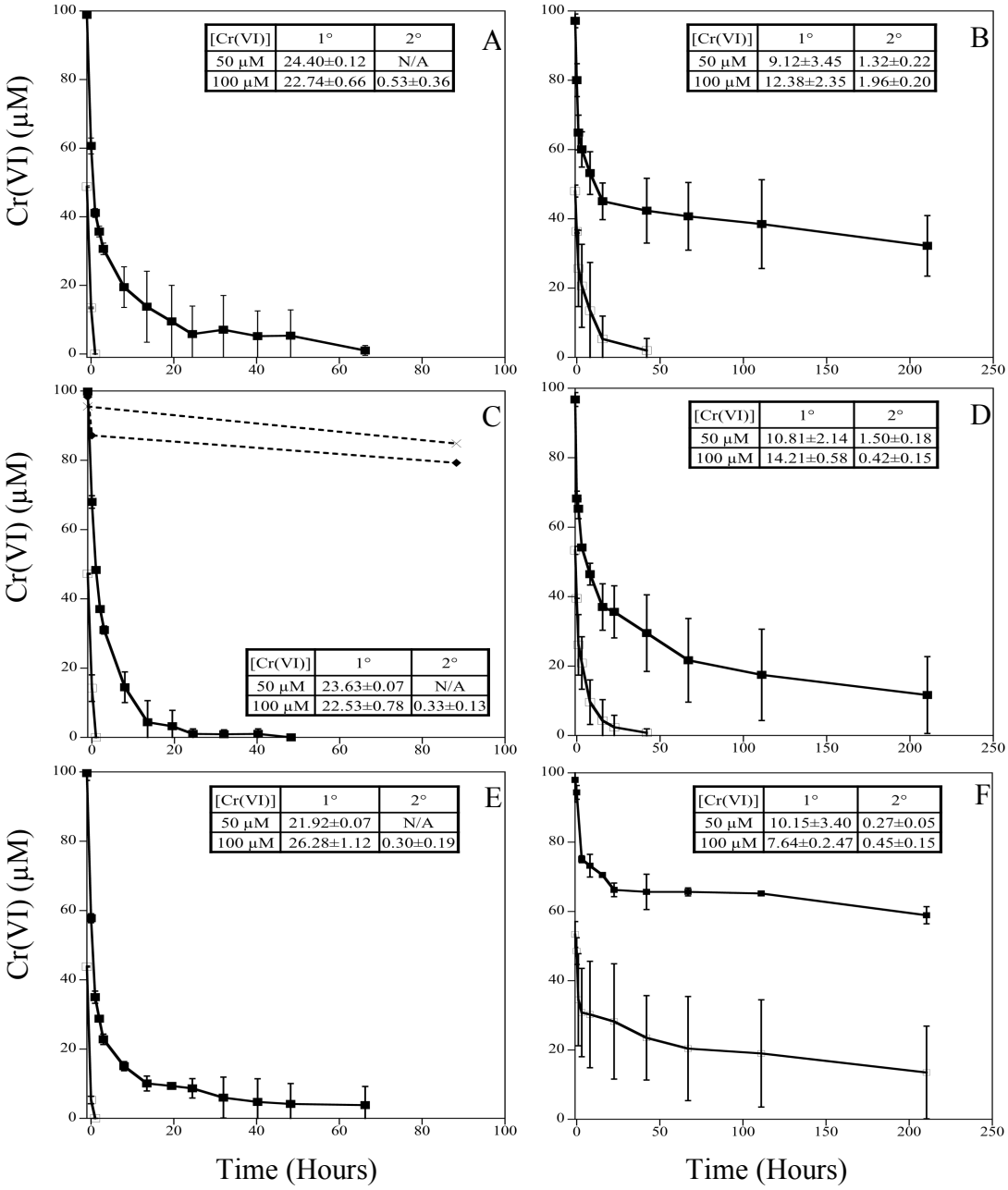


Figure 2. Cr(VI) reduction at 30°C (a, c, and e) and 20°C (b, d and f) under EDL (a,b), BAL (c,d), and EAL (e,f) conditions with 50 (○) and 100 (■) µM Cr(VI). Dashed lines indicate heat-killed (◆) and uninoculated controls (x) (C). Cr(VI) reduction rates (µM Cr(VI)/hr) (primary and secondary) are overlaid for each condition.

Resource Ratio Imbalance Affects *D. vulgaris* Cr(VI) Reduction and Tolerance

Electron-Donor Limitation (EDL). *D. vulgaris* was grown at both 20°C and 30°C, with 0 and 50 μM Cr(VI) to assess differences in growth rate, biomass yield, and Cr(VI) tolerance under electron-donor limitation. Under EDL conditions, *D. vulgaris* had a 2.9-fold slower growth rate (0.04 h^{-1}) at 20°C compared to growth at 30°C (0.12 h^{-1}) (Figure 1A, B). When exposed to Cr(VI) under EDL conditions, *D. vulgaris* could tolerate and reduce Cr(VI) faster at 30°C compared to 20°C, but to a lesser extent than under balanced conditions. At 30°C and exposure to Cr(VI), the growth rate declined 25% (Figure 1A). At 20°C, cells exposed to 50 μM Cr(VI) had an extended lag time that was longer than the balanced condition (~125 h), but the subsequent growth rate was similar to the no Cr(VI) treatment (Figure 1B). At 20°C, cultures without Cr(VI) under EDL conditions utilized lactate and produced equimolar levels of acetate until lactate was depleted (Figure S1A). In the presence of 50 μM Cr(VI) under EDL conditions, lactate and sulfate were not utilized during the growth lag, and growth coincided with the utilization of lactate and sulfate (Figure S1B).

Temperature also affected *D. vulgaris* ability to reduce Cr(VI) under EDL conditions. At 30°C, 50 μM Cr(VI) was reduced at an initial rate of 24.40±0.12 μM Cr(VI)/h (average O.D. of 0.08)) similar to the balanced condition, but at 20°C, 50 μM Cr(VI) was reduced at an initial rate of 9.12±3.45 μM Cr(VI)/h and a secondary rate of 1.32±0.22 μM Cr(VI)/h (average O.D. of 0.07)). At 30°C, 100 μM Cr(VI) was reduced at an initial rate of 22.74±0.66 μM Cr(VI)/h and a secondary rate of 0.53±0.36 μM Cr(VI)/h

(average OD 0.08). At 20°C, 100 μM Cr(VI) was reduced at a rate of 12.38±2.35 μM Cr(VI)/h that slowed to 1.96±0.20 μM Cr(VI)/h (average O.D. 0.08) (Figure 2A, B). Ultimately, the decrease in temperature caused a decrease in Cr(VI) reduction rates and the electron donor limitation with 50 μM Cr(VI) caused a 25 h increase in lag time compared to the balanced condition with 50 μM Cr(VI).

Electron-Acceptor Limitation (EAL). *D. vulgaris* was grown at both 20°C and 30°C, with 0 and 50 μM Cr(VI) to assess differences in growth rate, biomass yield, and Cr(VI) tolerance under electron-acceptor limitation. Under EAL conditions, *D. vulgaris* had a 3.5-fold slower growth rate (0.04 h^{-1}) at 20°C compared to growth at 30°C (0.13 h^{-1}) (Figure 1E and F). When exposed to Cr(VI) under EAL conditions, *D. vulgaris* could tolerate and reduce Cr(VI) faster at 30°C compared to at 20°C but to a much lesser extent than balanced conditions. At 30°C and exposure to Cr(VI), the growth rate declined 24% (Figure 1E). At 20°C, cells exposed to 50 μM Cr(VI) had an extended lag time that was longer than the balanced or EDL condition (~200 h), and the subsequent growth rate was 15% slower than no Cr(VI) treatment (Figure 1F). At 20°C, cultures without Cr(VI) under EAL conditions utilized lactate and produced equimolar levels of acetate until sulfate was depleted (Figure S1E). In the presence of 50 μM Cr(VI) under EAL conditions, lactate and sulfate were not utilized during the growth lag, and growth coincided with the utilization of lactate and sulfate after 200 h (Figure S1F).

Temperature also affected the ability of *D. vulgaris* to reduce Cr(VI) under EAL conditions. At 30°C, 50 μM Cr(VI) was reduced at an approximate rate of 21.92±0.07 μM Cr(VI)/hr (average O.D. of 0.08) and at 20°C 50 μM Cr(VI) was reduced at an initial rate of 10.15±3.40 μM Cr(VI)/h, which then slowed to 0.27±0.05 μM Cr(VI)/h (average O.D. of 0.08). At 30°C, 100 μM Cr(VI) was reduced at an initial rate of 26.28±1.12 μM Cr(VI)/h that slowed to 0.30±0.19 μM Cr(VI)/h (average OD 0.08) and at 20°C, 100 μM Cr(VI) was initially reduced at a rate of 7.64±2.47 μM Cr(VI)/h, that slowed to 0.45±0.15 μM Cr(VI)/h (average O.D. 0.07). Ultimately, under the EAL condition and 20°C, 50 μM Cr(VI) caused an extended growth lag (approximately 200 h) with prolonged exposure to higher Cr(VI) levels compared to the balanced and EDL conditions.

Viability

To assess if Cr(VI) caused more cell death in EAL grown *D. vulgaris* compared to cells under BAL conditions, the most probable number method was used to compare viability during the lag phases at 20°C. Viability after three hours of exposure to Cr(VI) was two orders of magnitude lower under EAL conditions compared to BAL conditions (4.7×10^3 cells/ml vs. 4.7×10^5 cells/ml). At 48 hours post-Cr(VI) exposure, the cells under both conditions were starting to recover, but the EAL cells still had decreased viability (2.1×10^4 cells/ml vs. 1.2×10^6 cells/ml). Viability for both EAL and BAL cells was similar under the respective condition without Cr(VI) (approximately 10^8 cells/ml).

Growth with Increasing Sulfate Concentrations

To explain the observation that sulfate limitation (EAL condition) resulted in increased Cr(VI) susceptibility, it was hypothesized that chromate competed with sulfate through sulfate permeases/transporters in *D. vulgaris* under the tested growth conditions. Previous work in different organisms has shown that the cellular uptake of chromate oxyanions can occur through sulfate permeases (Pepi and Baldi 1992; Appenroth et al. 2008; Aguilar-Barajas et al. 2011) and chromate was previously shown to block sulfate accumulation and reduction completely in *Desulfovibrio desulfuricans* (Cypionka 1989). To determine if increased sulfate levels could alleviate intracellular stress and damage under the EAL condition, cells were inoculated into medium that contained 50 mM lactate, increasing sulfate concentrations (10, 20, 30, and 50 mM sulfate) and 50 μM Cr(VI). In addition, the inoculum cells were either grown in a BAL or EAL condition. Results showed that increasing sulfate concentration did not provide protection from Cr(VI) toxicity, but inoculum grown under EAL conditions (Figure 3A) showed an increased lag time when inoculated into EAL medium compared to inoculum grown under BAL conditions was inoculated into EAL medium (Figure 3B). These results indicated that the electron donor to acceptor ratio that *D. vulgaris* is grown in prior to Cr(VI) exposure can impact the cellular response in a way that predisposes the cells to increased Cr(VI) susceptibility.

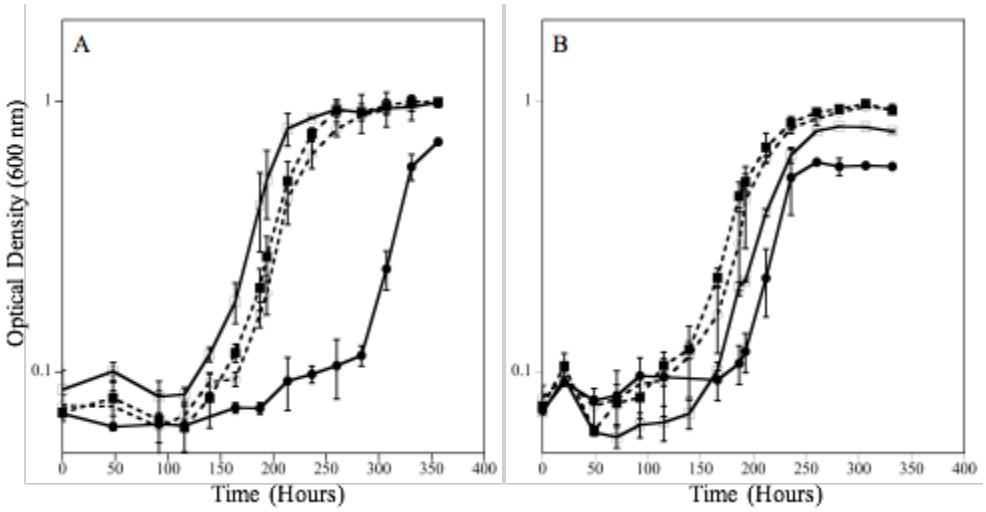


Figure 3. Growth at 20°C with 50 µM Cr(VI) and increasing sulfate levels of 10 mM (●), 20 mM (□), 30 mM (■), and 50 mM (○) inoculated with cells grown under EAL conditions (a) or BAL conditions (b).

Growth with Normalized Sulfate Levels

Because *D. vulgaris* was the most affected by Cr(VI) under the EAL condition (50:10 mM), Cr(VI) exposure was normalized to nutrient ratios with 10 mM sulfate in order to see if increased Cr(VI) susceptibility is caused by sulfate concentration or the ratio of lactate to sulfate (BAL -20:10 mM; EDL - 5:10 mM, and EAL -50:10 mM). The 20:10 balanced condition lagged for approximately 100 hours similar to the 60:30 mM ratio (Figure 4). These results indicate that it is not only the sulfate concentration that affects Cr (VI) toxicity, but also the ratio of electron acceptor to electron donor.

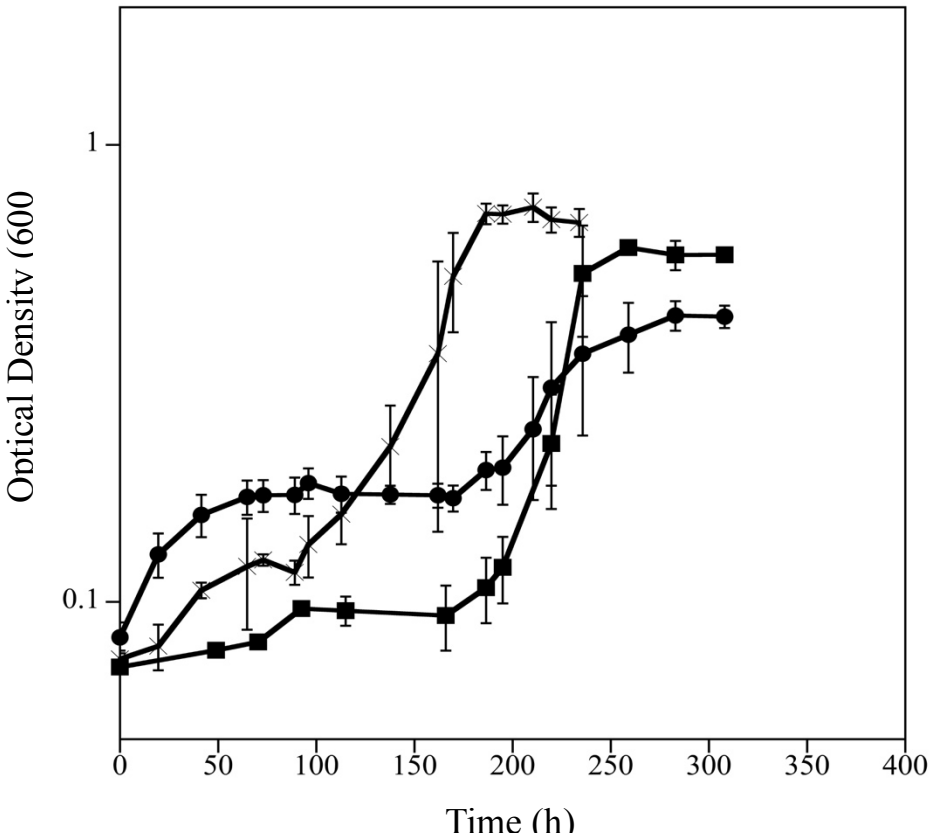


Figure 4. Growth at 20°C with 50 µM Cr(VI) and lactate to sulfate ratios normalized to 10 mM sulfate. Normalized ratios were EDL (5 mM: 10 mM - ●), BAL (20 mM:10 mM - X), and EAL (50 mM:10 mM - ■).

Sulfate Permease Mutants

To further understand the role of sulfate permeases in exposure to Cr(VI) in *D. vulgaris*, a search of the annotated genome revealed three genes designated as *sulP* that are presumptive sulfate permeases in *D. vulgaris* Hildenborough (microbesonline.org). Three individual sulfate permease mutants (ΔDVU0053, ΔDVU0279, ΔDVU1999) and a triple mutant in which all three sulfate permease genes were knocked out were

constructed. The wild-type, three individual mutants, and the triple mutant had similar growth rates and yields when grown via lactate-dependent sulfate respiration without Cr(VI) at 20°C under BAL conditions (Figure 5, data not shown for individual mutants). These results indicated that *D. vulgaris* Hildenborough has other mechanisms of sulfate influx (specific and/or non-specific) in addition to the presumptively annotated transporters. When grown in the presence of 50 μM Cr(VI), the triple mutant had a longer lag time by approximately 40 hours compared to wild-type cells grown under BAL conditions (Figure 5). These results indicated that the absence of the annotated sulfate permeases did not prevent Cr(VI) from entering and harming the cells and that triple mutant cells had decreased ability to regulate Cr(VI) influx and/or sulfate influx even under balanced conditions. The results suggested that the unidentified mechanism(s) by which Cr(VI) can enter the cell are not as tightly linked to Cr(VI) reduction and/or the alternative mechanisms for sulfate transport have a strong affinity for Cr(VI) that results in increased Cr(VI) sensitivity.

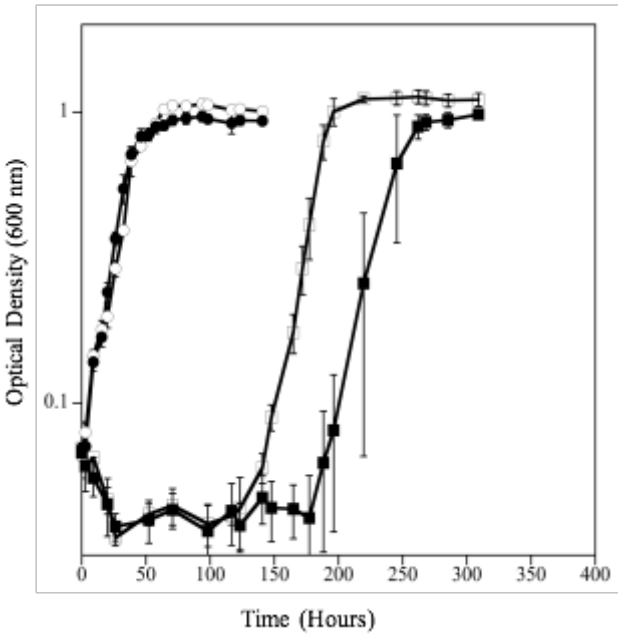


Figure 5. Growth of wild type *D. vulgaris* (○) and sulfate permease triple mutant (●) without Cr(VI) and with 50 µM Cr(VI) (□,■) at 20°C under BAL conditions.

Ascorbate

D. vulgaris was also grown with Cr(VI) in the presence of ascorbate to determine if a reducing/complexing agent could prevent or alleviate Cr(VI) cellular toxicity. Cell growth was compared between cells grown with and without 50 µM Cr(VI), with 50 µM Cr(VI) and 50 µM ascorbate added concurrently, with 50 µM Cr(VI) and 50 µM ascorbate added 3 hours post inoculation, and with 50 µM ascorbate only. When Cr(VI) and ascorbate were added concurrently, *D. vulgaris* cells grew similar to the control without Cr(VI), indicating that the reduced/complexed Cr compounds were not toxic and cells were most likely able to maintain viability (Figure 6). If ascorbate was added 3 hours post-inoculation, the cells were still impacted, but not as drastically as without

ascorbate. Approximately 30 µM Cr(VI) remained in solution when the ascorbate was added at the 3 h time point, which might explain why the lag time for this condition was shorter than the condition in which 50 µM Cr(VI) was added without ascorbate.

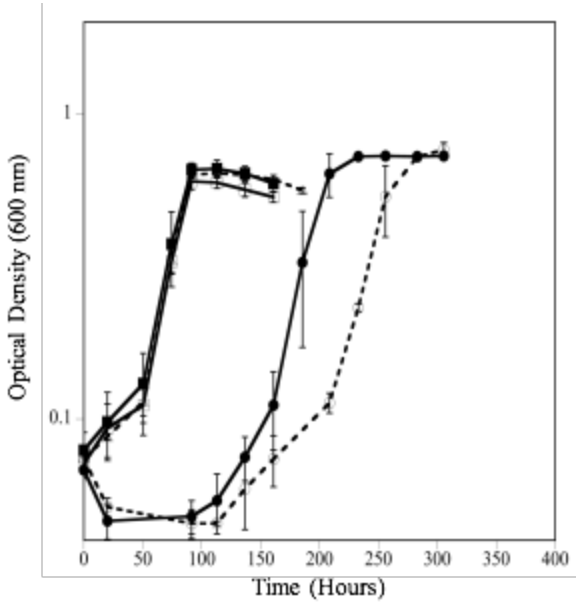


Figure 6. Growth of *D. vulgaris* during Cr(VI) and ascorbate exposure at 20°C under EAL conditions. Cells were exposed to 50 µM Cr(VI) and 50 µM ascorbate (■), 50 µM Cr(VI) added prior to inoculation and 50 µM ascorbate added at 3 h post-inoculation (●), 50 µM ascorbate (△), 50 µM Cr(VI) (○), or medium only (□).

Discussion

The mechanism for Cr(VI) reduction in *Desulfovibrio* spp. is not well-understood, but it is hypothesized that Cr(VI) enters the cell and is reduced to Cr(III) by cytochrome c_3, periplasmic hydrogenases, and possibly thioredoxin reductase (Chardin et al. 2003; Lovley and Phillips 1994; Li and Krumholz 2009). After the Cr(VI) is reduced to Cr(III),

the Cr(III) is either excreted from the cell or remains in the inner or outer membrane of the cell (Goulhen et al. 2005). It has also been shown that the presence of Cr(VI) alters the metabolism of *Desulfovibrio* spp. by transiently uncoupling lactate oxidation and sulfate reduction and causing lactate to be used for energy production or to lower the redox potential of the medium without concurrent growth at 30°C (Chardin et al. 2002; Klonowska et al. 2008). The redox couple for Cr(VI) reduction to Cr(III) is 1.41V (Nriagu and Nieboer 1988); however, *D. vulgaris* Hildenbourough is not known to conserve energy from Cr(VI) reduction and most data indicate that direct and indirect Cr(VI) reduction is linked to detoxification (Chardin et al. 2002; Klonowska et al. 2008). However, microbial fuel cells have recently been shown to reduce Cr(VI) with anode electrons (Habibul et al. 2016); and therefore, improved understanding of electron movement from the bulk phase to heavy metals under different conditions is needed.

Waters contaminated with heavy metals can be deficient in electron donors, electron acceptors, and/or carbon sources related to desired microbial activities, and the exact relationship between growth, activity, and substrate utilization is more challenging to understand when the activity of interest is not directly linked to growth. Previous studies have compared different electron donors ranging from organic acids, alcohols, carbohydrates, and polysaccharides to stimulate Cr(VI) reduction with pure cultures, mixed consortia, and *in situ* (Liamleam and Annachhatre 2007; Zhang et al. 2015). Geets et al. (2006) tested the removal of Zn, Cd, Co, and Ni from contaminated groundwater in

column experiments and concluded that additional experiments were needed to better understand the interplay between sulfate-, metal-, and carbon source concentrations.

The electron donor to electron acceptor ratio had a very strong effect on Cr(VI) reduction by *D. vulgaris* at both 20° and 30°C, with the EAL condition at 20°C being the most detrimentally affected. To explain this, we hypothesized that because chromate (CrO_4^{2-}) and sulfate (SO_4^{2-}) are structural analogues, the amount of sulfate in the environment affects the rate at which sulfate versus chromate enters the cell. It has been shown that Cr(VI) can enter cells through sulfate transport systems in numerous bacteria including, *Pseudomonas fluorescens, Salmonella typhimurium,* and *Escherichia coli* (Pardee et al. 1966; Ota et al. 1971; Karbonowska et al. 1977; Ohtake et al. 1987; Sirko et al. 1990) and the slightly longer lag time in the sulfate permease triple mutant in *D. vulgaris* compared to the wild type alludes to these three permeases playing a role in sulfate and/or Cr(VI) transport. However, the effect does not seem to be merely a sulfate concentration threshold, because the EDL condition has more sulfate compared to the BAL condition (50 mM vs 30 mM) and yet the EDL condition has a longer lag time (at 20°C) compared to the BAL condition. It is important to note that the three resource ratios have similar growth rates without Cr(VI) at 20° and 30°C. In addition, when the resource ratios were normalized to sulfate level (5:10 mM versus 20:10 mM versus 50:10 for EDL, BAL, and EAL respectively), similar results were observed between EAL and BAL, and EDL had even a longer lag time. These results suggested that the co-metabolic

rate of lactate and sulfate utilization influences Cr(VI) influx and reduction, and thus, the subsequent overall cellular toxicity.

To further explore the hypothesis that limiting sulfate increases Cr(VI) toxicity in *D. vulgaris* due to competition between sulfate and chromate for transport across the cell membrane, growth experiments with increasing levels of sulfate and sulfate permease mutants were done. The results of the increasing sulfate experiment support our finding that cells grown under EAL conditions are more susceptible to Cr(VI) toxicity than those grown under BAL conditions. A previous transcriptomic study on *D. vulgaris* transitioning from exponential growth to stationary phase shows changes in expression of the annotated sulfate permease genes and other cell components for lactate oxidation as the cells transition from exponential to stationary phase (*i.e*., decreasing sulfate levels), indicating that perhaps different cell machinery is used to optimize the utilization of electron donors and acceptors (*i.e*., presumptive sulfate permeases have different affinities for sulfate) (Clark et al. 2006). Deletion of the three presumptive sulfate permease genes did not affect growth with lactate and sulfate, indicating that sulfate had additional ways to enter the cell. The triple mutant did have an increased lag time when cells were exposed to 50 μM Cr(VI), and this result suggested that the triple mutant had either a decreased affinity/capacity for sulfate influx and/or increased affinity/capacity for chromate influx. An alternative explanation could be an overall decreased metabolic flux due to limited transport, but the triple mutant had similar growth rates in the absence of

Cr(VI). Further work is needed to elucidate the additional mechanisms of sulfate transport in *Desulfovibrio* and the role of these transporters in Cr toxicity.

The decrease in biomass yield based on sulfate consumption when cells were exposed to 50 μM Cr(VI) could be explained by the expenditure of energy toward Cr(VI) detoxification and cellular repair from damaging Cr(VI) reduction intermediates instead of allocation towards growth. To determine whether the increased lag time under the EAL condition compared to the BAL condition was due to Cr(VI) causing a greater decrease in cell viability, we measured cell numbers throughout the lag phase in both EAL and BAL conditions with 50 μM Cr(VI). Results indicate that the increased lag time under EAL conditions was due to decreased cell viability, which indicates that Cr(VI) toxicity was more extensive in cells grown in the EAL condition compared to the BAL condition. The interplay between chromate and sulfate levels is most likely a result of a balance between Cr(VI) influx and the ability of cells to reduce Cr(VI) to the less toxic Cr(III), and this detoxification requires adequate reducing potential. The cellular response to Cr(VI) at different resource ratios suggests that *D. vulgaris* modulates metabolic flow in response to the ratio of e^-/C levels and e^- acceptors, and further work is needed to elucidate the mechanisms of metabolic control and the implications for desired activities. The increase in Cr(VI) toxicity for sulfate/lactate limited cells has large implications for applications such as bioremediation where carbon and electron sources are injected into the subsurface, most likely creating unbalanced pairings of energy/C sources (Figure 7).

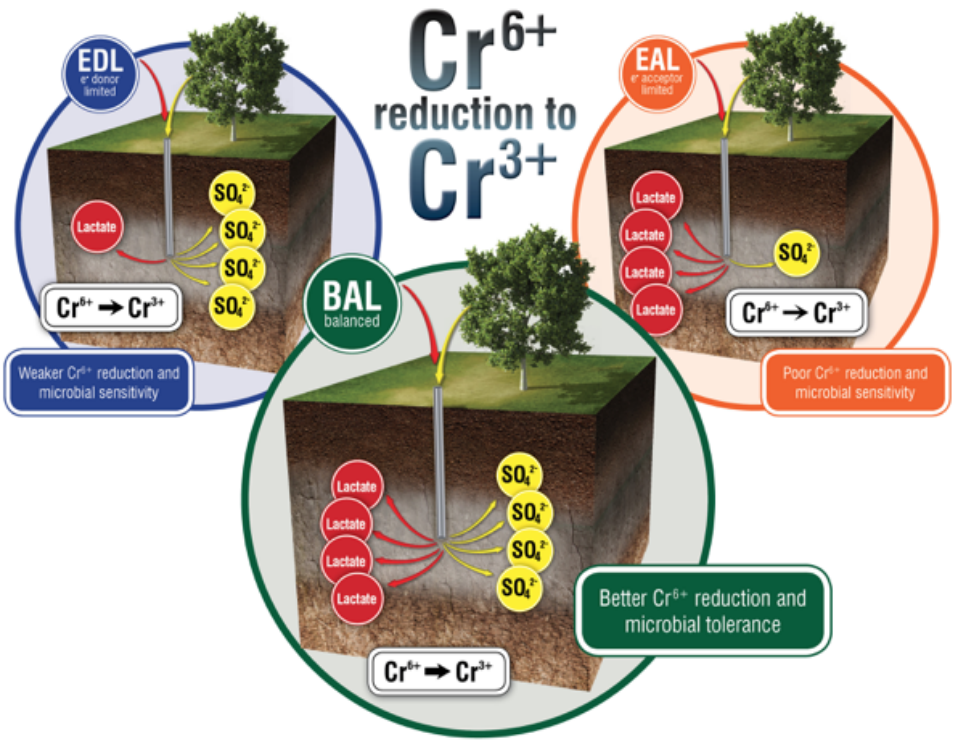


Figure 7. Three potential scenarios (EDL, BAL, EAL) in which nutrients are added to stimulate microbial activity and the ratio of resources are shifted. The different resource ratios can impact desired microbial activity.

In the subsurface, sulfate-reducing bacteria can account for a majority of biotic metal reduction via direct and indirect mechanisms, but little work has investigated the implications of biostimulation practices on microbial physiology and activity with respect to changing resource ratios and other environmentally-relevant conditions (*i.e.*, temperature). The impact of sulfate on Cr(VI) reduction has been previously reported in a yeast and a diatom, and increasing sulfate levels promoted improved efficiencies and rates of Cr(VI) reduction in the yeast and decreased Cr(VI) transport in the diatom (Riedel 1985; de María Guillén-Jiménez et al. 2008). Moreover, the Cr(VI)

concentrations that inhibited growth also inhibited sulfate uptake in the diatom (Riedel 1985). Given the role of SRBs in metal interactions in most anaerobic environments (both natural and man-made), further work is needed to ascertain the long-term implications of changing resource ratios on *in situ* metal-reduction and metal-toxicity.

REFERENCES CITED

Aguilar-Barajas E, Díaz-Pérez C, Ramírez-Díaz MI, Riveros-Rosas H, Cervantes C (2011) Bacterial transport of sulfate, molybdate, and related oxyanions. Biometals 24:687–707.

Aiyar J, Berkovits HJ, Floyd RA, Wetterhahn KE (1991) Reaction of chromium(VI) with glutathione or with hydrogen peroxide: identification of reactive intermediates and their role in chromium(VI)-induced DNA damage. Environ Health Perspect 92:53–62.

Appenroth K-J, Luther A, Jetschke G, Gabrys H (2008) Modification of chromate toxicity by sulphate in duckweeds (Lemnaceae). Aquat Toxicol 89:167–171.

ATSDR (2013) Toxicological Profile for Chromium. Agency for Toxic Substances and Disease Registry (US), Atlanta (GA)

Barnhart J (1997) Occurrences, uses, and properties of chromium. Regul Toxicol Pharmacol 26:S3–7.

Boonchayaanant B, Kitanidis PK, Criddle CS (2008) Growth and cometabolic reduction kinetics of a uranium- and sulfate-reducing Desulfovibrio/Clostridia mixed culture: Temperature effects. Biotechnol Bioeng 99:1107–1119.

Borglin S, Joyner D, Jacobsen J, Mukhopadhyay A, Hazen TC (2009) Overcoming the anaerobic hurdle in phenotypic microarrays: generation and visualization of growth curve data for Desulfovibrio vulgaris Hildenborough. J Microbiol Methods 76:159–168.

Brandis A, A. B, Thauer RK (1981) Growth of Desulfovibrio species on Hydrogen and Sulphate as Sole Energy Source. Microbiology 126:249–252.

Chardin B, Dolla A, Chaspoul F, Fardeau ML, Gallice P, Bruschi M (2002) Bioremediation of chromate: thermodynamic analysis of the effects of Cr(VI) on sulfate-reducing bacteria. Appl Microbiol Biotechnol 60:352–360.

Chardin B, Giudici-Orticoni M-T, De Luca G, Guigliarelli B, Bruschi M (2003a) Hydrogenases in sulfate-reducing bacteria function as chromium reductase. Appl Microbiol Biotechnol 63:315–321.

Chardin B, Giudici-Orticoni M-T, De Luca G, Guigliarelli B, Bruschi M (2003b) Hydrogenases in sulfate-reducing bacteria function as chromium reductase. Appl Microbiol Biotechnol 63:315–321.

Cieăślak-Golonka M, Raczko M, Staszak Z (1992) Synthesis, spectroscopic and magnetic studies of chromium(II) complexes isolated from in vitro reduction of the chromium(VI) ion with the main cellular reductants ascorbic acid, cysteine and glutathione*. Polyhedron 11:2549–2555.

Clark ME, He Q, He Z, Huang KH, Alm EJ, Wan X-F, Hazen TC, Arkin AP, Wall JD, Zhou J-Z, Fields MW (2006) Temporal transcriptomic analysis as Desulfovibrio vulgaris Hildenborough transitions into stationary phase during electron donor depletion. Appl Environ Microbiol 72:5578–5588.

Cypionka H (1989) Characterization of sulfate transport in Desulfovibrio desulfuricans. Arch Microbiol 152:237–243.

de María Guillén-Jiménez F, Morales-Barrera L, Morales-Jiménez J, Hernández-Rodríguez CH, Cristiani-Urbina E (2008) Modulation of tolerance to Cr (VI) and Cr (VI) reduction by sulfate ion in a Candida yeast strain isolated from tannery wastewater. J Ind Microbiol Biotechnol 35:1277–1287.

Dhal B, Thatoi HN, Das NN, Pandey BD (2013) Chemical and microbial remediation of hexavalent chromium from contaminated soil and mining/metallurgical solid waste: a review. J Hazard Mater 250-251:272–291.

Elias DA, Suflita JM, McInerney MJ, Krumholz LR (2004) Periplasmic Cytochrome c3 of Desulfovibrio vulgaris Is Directly Involved in H2-Mediated Metal but Not Sulfate Reduction. Appl Environ Microbiol 70:413–420.

Faybishenko B, Hazen TC, Long PE, Brodie EL, Conrad ME, Hubbard SS, Christensen JN, Joyner D, Borglin SE, Chakraborty R, Williams KH, Peterson JE, Chen J, Brown ST, Tokunaga TK, Wan J, Firestone M, Newcomer DR, Resch CT, Cantrell KJ, Willett A, Koenigsberg S (2008) In situ long-term reductive bioimmobilization of Cr(VI) in groundwater using hydrogen release compound. Environ Sci Technol 42:8478–8485.

Geets J, Vanbroekhoven K, Borremans B, Vangronsveld J, Diels L, van der Lelie D (2006) Column experiments to assess the effects of electron donors on the efficiency of in situ precipitation of Zn, Cd, Co and Ni in contaminated groundwater applying the biological sulfate removal technology. Environ Sci Pollution Res 13:362-378.

Goulhen F, Florence G, Alexandre G, Francois G, Mireille B (2005) Cr(VI) detoxification by *Desulfovibrio vulgaris* strain Hildenborough: microbe–metal interactions studies. Appl Microbiol Biotechnol 71:892–897.

Gustafsson JP, Persson I, Oromieh AG, van Schaik JWJ, Sjöstedt C, Kleja DB (2014) Chromium(III) complexation to natural organic matter: mechanisms and modeling. Environ Sci Technol 48:1753–1761.

Habibul N, Hu Y, Wang Y-K, Chen W, Yu H-Q, Sheng G-P (2016) Bioelectrochemical Chromium(VI) Removal in Plant-Microbial Fuel Cells. Environ Sci Technol 50:3882–3889.

Heidelberg JF, Seshadri R, Haveman SA, Hemme CL, Paulsen IT, Kolonay JF, Eisen JA, Ward N, Methe B, Brinkac LM, Daugherty SC, Deboy RT, Dodson RJ, Durkin AS, Madupu R, Nelson WC, Sullivan SA, Fouts D, Haft DH, Selengut J, Peterson JD, Davidsen TM, Zafar N, Zhou L, Radune D, Dimitrov G, Hance M, Tran K, Khouri H, Gill J, Utterback TR, Feldblyum TV, Wall JD, Voordouw G, Fraser CM (2004) The genome sequence of the anaerobic, sulfate-reducing bacterium Desulfovibrio vulgaris Hildenborough. Nat Biotechnol 22:554–559.

Jarvis B, Wilrich C, Wilrich P-T (2010) Reconsideration of the derivation of Most Probable Numbers, their standard deviations, confidence bounds and rarity values. J Appl Microbiol 109:1660–1667.

Karbonowska H, Wiater A, Hulanicka D (1977) Sulphate permease of Escherichia coli K12. Acta Biochim Pol 24:329–334.

Keller KL, Bender KS, Wall JD (2009) Development of a markerless genetic exchange system for Desulfovibrio vulgaris Hildenborough and its use in generating a strain with increased transformation efficiency. Appl Environ Microbiol 75:7682–7691.

Klonowska A, Clark ME, Thieman SB, Giles BJ, Wall JD, Fields MW (2008) Hexavalent chromium reduction in Desulfovibrio vulgaris Hildenborough causes transitory inhibition of sulfate reduction and cell growth. Appl Microbiol Biotechnol 78:1007–1016.

Liamleam W, Annachhatre AP (2007) Electron donors for biological sulfate reduction. Biotechnol Adv 25:452–463.

Li MZ, Elledge SJ (2007) Harnessing homologous recombination in vitro to generate recombinant DNA via SLIC. Nat Methods 4:251–256.

Li X, Krumholz LR (2009) Thioredoxin is involved in U(VI) and Cr(VI) reduction in Desulfovibrio desulfuricans G20. J Bacteriol 191:4924–4933.

Lovley DR, Phillips EJ (1994) Reduction of Chromate by Desulfovibrio vulgaris and Its c(3) Cytochrome. Appl Environ Microbiol 60:726–728.

Nriagu JO, Nieboer E (1988) Chromium in the natural and human environments. John Wiley & Sons

Ohtake H, Cervantes C, Silver S (1987) Decreased chromate uptake in Pseudomonas fluorescens carrying a chromate resistance plasmid. J Bacteriol 169:3853–3856.

Ota N, Galsworthy PR, Pardee AB (1971) Genetics of sulfate transport by Salmonella typhimurium. J Bacteriol 105:1053–1062.

Pardee AB, Prestidge LS, Whipple MB, Dreyfuss J (1966) A binding site for sulfate and its relation to sulfate transport into Salmonella typhimurium. J Biol Chem 241:3962–3969.

Parks JM, Johs A, Podar M, Bridou R, Hurt RA Jr, Smith SD, Tomanicek SJ, Qian Y, Brown SD, Brandt CC, Palumbo AV, Smith JC, Wall JD, Elias DA, Liang L (2013) The genetic basis for bacterial mercury methylation. Science 339:1332–1335.

Pepi M, Baldi F (1992) Modulation of chromium(VI) toxicity by organic and inorganic sulfur species in yeasts from industrial wastes. Biometals 5:179–185.

Riedel GF (1985) The relationship between chromium(VI) uptake, sulfate uptake, and chromium(VI) toxicity in the estuarine diatom Thalassiosira pseudonana. Aquat Toxicol 7:191–204.

Sirko A, Hryniewicz M, Hulanicka D, Böck A (1990) Sulfate and thiosulfate transport in Escherichia coli K-12: nucleotide sequence and expression of the cysTWAM gene cluster. J Bacteriol 172:3351–3357.

Stearns DM, Wetterhahn KE (1994) Reaction of Chromium(VI) with Ascorbate Produces Chromium(V), Chromium(IV), and Carbon-Based Radicals. Chem Res Toxicol 7:219–230.

Tyagi M, da Fonseca MMR, de Carvalho CCCR (2011) Bioaugmentation and biostimulation strategies to improve the effectiveness of bioremediation processes. Biodegradation 22:231–241.

Viamajala S, Peyton BM, Apel WA, Petersen JN (2002) Chromate/nitrite interactions in Shewanella oneidensis MR-1: evidence for multiple hexavalent chromium [Cr(VI)] reduction mechanisms dependent on physiological growth conditions. Biotechnol Bioeng 78:770–778.

Zayed AM, Terry N (2003) Chromium in the environment: factors affecting biological remediation. Plant Soil 249:139–156.

Zhang P, Van Nostrand JD, He Z, Chakraborty R, Deng Y, Curtis D, Fields MW, Hazen TC, Arkin AP, Zhou J (2015) A Slow-Release Substrate Stimulates Groundwater Microbial Communities for Long-Term in Situ Cr(VI) Reduction. Environ Sci Technol 49:12922–12931.

Zhitkovich A, Voitkun V, Costa M (1995) Glutathione and free amino acids form stable complexes with DNA following exposure of intact mammalian cells to chromate. Carcinogenesis 16:907–913.

SUPPLEMENTAL INFORMATION

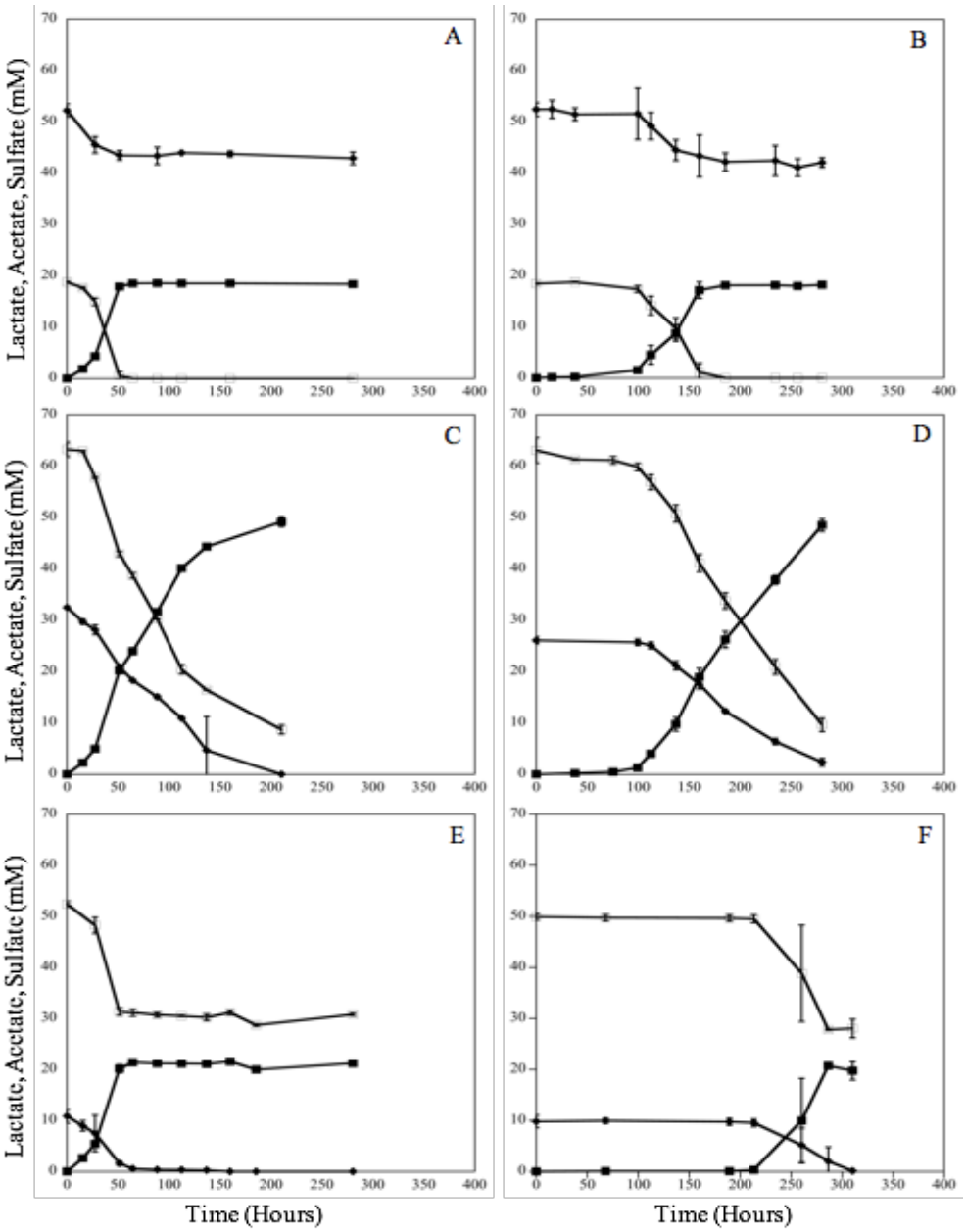


Figure S1. Lactate (●), acetate (■), and sulfate (◆) concentrations throughout growth at 20°C with 0 (a, c, e) and 50 (b, d, f) µM Cr(VI) under EDL (a,b), BAL (c,d), and EAL (e,f) conditions.

Strain	Features of Interest	Source
a-select	*deoR endA1 recA1 relA1 gyrA96 hsdR17* (r_k^- m_k^+) *supE44 thi-1 phoA* D*(lacZYA argF)U169* F80*lacZ* DM15 l^- F^-	Bioline
JW710	parental strain for deletion strains, D*upp*; $5FU^r$	(1)
JW9153	JW710 DDVU0053::(P_{npt}-*npt-upp*); Km^r $5FU^s$	This study
JW9155	JW710 DDVU0279::(P_{npt}-*npt-upp*); Km^r $5FU^s$	This study
JW9157	JW710 DDVU1999::(P_{npt}-*npt-upp*); Km^r $5FU^s$	This study
JW9167	JW9153 DDVU0053 D(P_{npt}-*npt-upp*); $5FU^r$	This study
JW9169	JW9155 DDVU0279 D(P_{npt}-*npt-upp*); $5FU^r$	This study
JW9171	JW9157 DDVU1999 D(P_{npt}-*npt-upp*); $5FU^r$	This study
JW9198	JW9167 DDVU0053 DDVU0279::(P_{npt}-*npt-upp*); Km^r $5FU^s$	This study
JW9199	JW9198 DDVU0053 DDVU0279 D(P_{npt}-*npt-upp*); $5FU^r$	This study
JW9200	JW9199 DDVU0053 DDVU0279 DDVU1999::(P_{npt}-*npt-upp*); Km^r $5FU^s$	This study
JW9201	JW9200 DDVU0053 DDVU0279 DDVU1999 D(P_{npt}-*npt-upp*); $5FU^r$	This study
Plasmids		
pCR8/GW/TOPO	parental plasmid, source for pUC Sp^r	Invitrogen
pSC27	source plasmid for P_{npt}-*npt*, Km^r	(1)
pMO746	source plasmid for P_{npt}-*npt-upp* selectable/counter-selectable cassette; Amp^r Km^r	(2)
pMO417	pCR8/GW/TOPO, marker-exchange plasmid for DVU0053; Sp^r Km^r	This study
pMO419	pCR8/GW/TOPO, marker-exchange plasmid for DVU0279; Sp^r Km^r	This study
pMO421	pCR8/GW/TOPO, marker-exchange plasmid for DVU1999; Sp^r Km^r	This study
pMO9152	pMO417, marker-exchange plasmid for DVU0053, P_{npt}-*npt-upp*; Sp^r Km^r	This study
pMO9154	pMO419, marker-exchange plasmid for DVU0279, P_{npt}-*npt-upp*; Sp^r Km^r	This study
pMO9156	pMO421, marker-exchange plasmid for DVU1999, P_{npt}-*npt-upp*; Sp^r Km^r	This study
pMO9166	pMO417, marker-less deletion plasmid for DVU0053; Sp^r	This study
pMO9168	pMO419, marker-less deletion plasmid for DVU0279; Sp^r	This study
pMO9170	pMO421, marker-less deletion plasmid for DVU1999; Sp^r	This study
pMO9154	pMO419, marker-exchange plasmid for DVU0279, P_{npt}-*npt-upp*; Sp^r Km^r	This study
pMO9156	pMO421, marker-exchange plasmid for DVU1999, P_{npt}-*npt-upp*; Sp^r Km^r	This study
pMO9166	pMO417, marker-less deletion plasmid for DVU0053; Sp^r	This study
pMO9168	pMO419, marker-less deletion plasmid for DVU0279; Sp^r	This study
pMO9170	pMO421, marker-less deletion plasmid for DVU1999; Sp^r	This study

Table S1. Strains used in this study.

Name	Sequence*	Purpose
DVU0053-1b	CGGGAAAGACCTCCGCCTTG	Cloning of upstream region of DVU0053
DVU0053-2	AAGACTGTAGCCGTACCTCGAATCTA CGTCCCGTGTTCCCTGTTTG	Cloning of upstream region of DVU0053, with overhang for annealing to kanamycin-resistance gene
DVU0053-3	AATCCGCTCACTAAGTTCATAGACCG CATATGGGTGCTGTCAGGTC	Cloning of downstream region of DVU0053, with overhang for annealing to

		kanamycin-resistance gene
DVU0053-4	AGCAGCCCATGTTGAGGTCG	Cloning of downstream region of DVU0053
bc0050f	TAGATTCGAGGTACGGCTACAGTCTT ATCTCTGAAGAAGCCGACAC CCCCAGAGTCCCGCTCAG	Amplification of kanamycin-resistance gene
bc0050r	CGGTCTATGAACTTAGTGAGCGGATT AGTAACAGTCGTGAACATCG GAGGTAGCTTGCAGTGGGCT	Amplification of kanamycin-resistance gene
DVU0279-1	GACTGCGGGAGCATCATGCG	Cloning of upstream region of DVU0279
DVU0279-2	AAGACTGTAGCCGTACCTCGAATCTA ATGCGCCTCCTTTGCGATTT	Cloning of upstream region of DVU0279, with overhang for annealing to kanamycin-resistance gene
DVU0279-3	AATCCGCTCACTAAGTTCATAGACCG CGTTGATGACAGACGTGACG	Cloning of downstream region of DVU0279, with overhang for annealing to kanamycin-resistance gene
DVU0279-4	ATGAGATTCGCGCCCTGTAC	Cloning of downstream region of DVU0279
bc0051-f	TAGATTCGAGGTACGGCTACAGTCTT ATCGAACTAACGTACATGCC CCCCAGAGTCCCGCTCAG	Amplification of kanamycin-resistance gene
bc0051-r	CGGTCTATGAACTTAGTGAGCGGATT ATCGCCTAACCTAGATACAG GAGGTAGCTTGCAGTGGGCT	Amplification of kanamycin-resistance gene
DVU1999-1	CCCCAAACCCCATCTCGATCGAG	Cloning of upstream region of DVU1999
DVU1999-2	AAGACTGTAGCCGTACCTCGAATCTA CTGGGGAGACGTTGCGTCTT	Cloning of upstream region of DVU1999, with overhang for annealing to kanamycin-resistance gene
DVU1999-3	AATCCGCTCACTAAGTTCATAGACCG ACCCGACAGTGAGCCGCCAG	Cloning of downstream region of DVU1999, with overhang for annealing to kanamycin-resistance gene
DVU1999-4	ATGATTTGGGCGGCTTCGGC	Cloning of downstream region of DVU1999
bc0052-f	TAGATTCGAGGTACGGCTACAGTCTT GTGTGACATGCTGCTAGAAC CCCCAGAGTCCCGCTCAG	Amplification of kanamycin-resistance gene
bc0052-r	CGGTCTATGAACTTAGTGAGCGGATT GCGTCGTAATAGTGGTTATC GAGGTAGCTTGCAGTGGGCT	Amplification of kanamycin-resistance gene
pMR->pMLD-Km	GAACACGGCGGCATCAGAG	Amplification of marker-replacement plasmid
pMR->pMLD-Cm	GCACCAAGTAAGACTGTAGCCGTACC TCGAATCTA	Amplification of marker-replacement plasmid
KanR-upp-pMR-F	AACAGACAATCGGCTGCTCTGATG	Amplification of kan^r-upp cassette
KanR-upp-pMR-R	TAGATTCGAGGTACGGCTACAGTCTT ACTTGGTGCCGAATATCTTGTCGCC	Amplification of kan^r-upp cassette; contains overhang for common sequence
DVU0053-	GGAACACGGGACGCATATGGGTGCTG	Amplification from marker-replacement

MLD-F	TCAGGTCTTCG	plasmid to construct the marker-less deletion plasmid for DVU0053
DVU0053-MLD-R	CAGCACCCATATG CGTCCCGTGTTCCCTGTTTGC	Amplification from marker-replacement plasmid to construct the marker-less deletion plasmid for DVU0053
DVU0279-MLD-F	AAAGGAGGCGCATCGTTGATGACAGA CGTGACGTTCC	Amplification from marker-replacement plasmid to construct the marker-less deletion plasmid for DVU0279
DVU0279-MLD-R	TCTGTCATCAACG ATGCGCCTCCTTTGCGATTT TCC	Amplification from marker-replacement plasmid to construct the marker-less deletion plasmid for DVU0279
DVU1999-MLD-F	AACGTCTCCCCAG ACCCGACAGTGAGCCGCCAG	Amplification from marker-replacement plasmid to construct the marker-less deletion plasmid for DVU1999
DVU1999-MLD-R	CTCACTGTCGGGT CTGGGGAGACGTTGCGTCTT	Amplification from marker-replacement plasmid to construct the marker-less deletion plasmid for DVU1999

* - underlined region represents overhang used for annealing to neighboring PCR product in SOE and SLIC reactions.

Table S2. Primers used in this study.

CHAPTER THREE

NUTRIENT LIMITATION CAUSES DECLINE IN METABOLITES IMPORTANT FOR CELL CYCLE PROGRESSION IN BACTERIAL BIOFILM

Contribution of Authors and Co-Authors

Author: Lauren Franco

Contributions: Experimental design, performed experiments, data analysis, wrote and revised manuscript

Co-Author: Julijana Ivanisevic

Contributions: Experimental design, performed experiments, data analysis, wrote and revised manuscript

Co-Author: Gary Siuzdak

Contributions: Experimental design, data analysis, revised manuscript

Co-Author: Matthew W. Fields

Contributions: Experimental design, performed experiments, data analysis, wrote and revised manuscript

Manuscript Information Page

Lauren C. Franco, Julijana Ivanisevic, Gary Siuzdak, Mathew W. Fields

Applied Microbiology and Microbiology

Status of Manuscript:
__x__ Prepared for submission to a peer-reviewed journal
____ Officially submitted to a peer-review journal
____ Accepted by a peer-reviewed journal
____ Published in a peer-reviewed journal

Abstract

The effect of nutrient limitation on *Desulfovibrio vulgaris* Hildenborough biofilm growth and metabolism is investigated in this chapter. *D. vulgaris* was grown in a CDC reactor under electron donor-limitation (EDL), electron acceptor-limitation (EAL) and electron donor to electron acceptor balanced (BAL) conditions. Biofilm growth was measured via protein and carbohydrate and were used to make biomass yield calculations based on lactate and sulfate consumption. Growth measurements normalized to protein and biomass yields did not differ between the three conditions. Although biofilm growth was not significantly affected by nutrient limitation, metabolomic analysis revealed significant dysregulation between *D. vulgaris* biofilm grown under the EAL condition compared to that grown under the BAL condition. Biofilm grown under the EAL condition had an overall down-regulation of metabolites compared to the BAL condition. Of those that could be confidently identified, metabolites involved in purine and pyrimidine synthesis, glutamine and glutamate synthesis, and peptidoglycan synthesis were down-regulated under the EAL condition, indicating an overall decrease in cell division and growth compared to the BAL condition. Interestingly, fatty acid metabolites were the majority of up-regulated metabolites that could be identified under the EAL condition compared to the BAL condition. Taken together, these results point to a metabolic switch from growth to biomass maintenance caused by electron acceptor-limitation. The results highlight the need to further explore the role of the fatty acids produced in *D. vulgaris* biofilm grown under the EAL condition and further emphasize the effects that nutrient limitation can have on microbial metabolism and physiology.

Introduction

The recognition of changing environmental conditions, such as nutrient availability, is essential to organismal growth and survival, and microorganisms are acutely adept at maximizing available resources for biomass and energy conservation. However, most microbial studies have been conducted on planktonic cells grown in suspension due to utility for study and sampling, and not the more predominant life-style of attached growth (*i.e*., biofilm). Bacteria have the ability to sense extracellular signals, via two-component regulatory systems for example, and can then feed those signals into transcriptional regulatory cascades, resulting in a change in gene expression and subsequent adjustment of metabolism to better perform under given external constraints. Another layer of extracellular sensing is the cell's ability to coordinate control of multiple inputs and adjust accordingly. For example, *Escherichia coli* carbon utilization can be coordinated with nitrogen availability, and carbohydrate transport can be coordinated with the regulation of carbohydrate-utilizing enzymes (*i.e*., glucose and the Lac operon). In the instance of coordinated N and C utilization, α-ketoglutarate inhibits enzyme I of the phosphotransferase system, and subsequently glucose uptake is adjusted in response to N availability (Doucette et al. 2011). Thereby, using the α-ketoglutarate/glutamate metabolic node of the TCA (tricarboxylic acid cycle) to help control influx of carbon (*i.e*., glucose) in light of available N in terms of α-ketoglutarate/glutamate/glutamine. In another example, carbon and sulfur metabolisms are linked by CysB, a transcriptional

regulator of the sulfur metabolism in *E. coli* and *Salmonella* that regulates an operon encoding genes required for uptake of sulfur sources and for the synthesis of cysteine. When *cysB* is mutated, the organism has 50% less activity of enzymes involved in carbon source uptake and utilization (Quan et al. 2002).

In *D. vulgaris,* dissimilatory sulfate reduction and carbon uptake and utilization are presumably coordinated as well, although the mechanism has not yet been elucidated. One potential player in this coordination is RexB, a repressor of sulfate adenylyl transferase (*sat*), the gene that encodes the enzyme responsible for activating sulfate in the first step of sulfate reduction. RexB is regulated by cellular levels of NAD/NADH+H^+ in that NADH+H^+, but not NAD^+, binds with RexB and prevents it from binding DNA. Elevated intracellular levels of NADH+H^+ therefore prevent RexB from repressing *sat* transcription, allowing the first step of sulfate reduction to commence (Christensen et al. 2015). While RexB certainly links sulfate reduction to the redox state of the cell through the NAD/NADH+H^+ ratio, it could also be a link to the central carbon metabolism, as NADH is a product of the TCA cycle.

Although it has been shown in *D. vulgaris* that the type of electron donor/carbon source and electron acceptor affects physiological responses to Cr(VI) and electron flow within the cell, little work has been done on how altering the electron donor/carbon source concentration affects its metabolism (Klonowska et al. 2008; Zhou et al. 2017). Moreover, limited work has been done with diverse microorganisms to better understand the overall metabolic state of biofilms. The work presented in this chapter investigates

how nutrient limitation, in the form of sulfate limitation, affects the metabolism and growth of *D. vulgaris* Hildenborough in the biofilm growth mode.

Materials and Methods

Bacterial Strains and Growth Conditions

D. vulgaris Hildenborough was grown in either batch or continuous mode. For batch growth, cells were inoculated into sterile N_2 gassed balch tubes containing LS4D, a lactate and sulfate medium (modified to 2.5 μM resazurin and 130 μM riboflavin in Thauer's vitamins) (Brandis and Thauer 1981; Borglin et al. 2009). The medium consisted of varying lactate and sulfate concentrations as follows: 60 mM sodium lactate and 30 mM sodium sulfate (balanced condition), 50 mM sodium lactate and 10 mM sodium sulfate (electron acceptor limited condition), and 18 mM sodium lactate and 50 mM sodium sulfate (electron donor limited condition). For continuous culture of *D. vulgaris* biofilm, cells were grown in a CDC reactor modified with continuous sparging of the headspace and medium with N_2. Exponential phase cells were inoculated into a CDC reactor containing electron acceptor limited, balanced, or electron donor limited LS4D medium. Cells were grown in batch mode for 48 hours and then continuous mode with a dilution rate of 0.04^{-hr}. Reactors were grown at room temperature (20-23°C), stirred at 60 rpm, and the headspace was continuously sparged with sterile N_2 gas to maintain anaerobic conditions. Coupons of glass slides were submerged in the reactor

body as a surface for biofilm growth.

Sample Collection

Biofilm samples were collected for biomass analysis at 168 hours (7 days). For biomass analyses glass slide coupons were removed from the reactor, gently submerged in PBS to remove any loosely attached biomass, and then biomass was scraped from both sides of the slide with a razor blade into 1 ml degassed water. Sulfide content was measured immediately after sampling, samples for protein and carbohydrate were measured after one freeze-thaw cycle to lyse cells.

Biomass Analyses

Protein was measured using the Qubit protein assay (Life Technologies, Carlsbad, CA). Carbohydrate in the form of hexose was measured using a colorimetric L-cysteine sulphuric acid assay with glucose as the standard (Chaplin and Kennedy 1986). Dissolved and precipitated sulfide was measured as described (Cord-Ruwisch 1985). All assays were performed in triplicate and error bars represent standard deviation. Results were compared using the unpaired student's t-test. Biomass yields were calculated by summing all of the biomass (biofilm and planktonic) in individual CDC reactors and dividing that by the amount of substrate consumed.

Metabolomic Analysis of Biofilm

Biofilm samples for metabolite analysis were harvested from reactors at 168 hrs,

quickly rinsed in ice cold 1:10 diluted phosphate buffered saline, flash frozen in liquid nitrogen, and stored at -80°C. Samples were extracted and analyzed at the Scripps Center for Metabolomics using an untargeted approach with a dual separation method (reversed-phase liquid chromatography and hydrophilic interaction chromatography) to maximize metabolite separation and recovery (Ivanisevic et al. 2013). Metabolite features were confirmed via tandem mass spectrometry (MS/MS) and identified by matching a standard in the METLIN database (Benton et al. 2015).

Results

Biofilm Growth under Nutrient-Limited and Balanced Conditions

D. vulgaris growth under continuous flow conditions as a biofilm was affected by altering electron donor and electron acceptor concentrations. More biomass, as quantified by protein, was produced under the balanced condition (47.6 ± 2.9 μg/cm^2) than under limiting conditions (22.1 ± 3.3 μg/cm^2 for EAL and 21.9 ± 1.4 μg/cm^2 for EDL) (Figure 1). This trend mimics the biomass production for *D. vulgaris* grown under batch planktonic conditions in which cells under the balanced condition reached a higher maximum O.D. compared to EAL and EDL (Chapter 2). Carbohydrate, as a measure for extracellular polymeric substances produced by the biofilm, also differed according to electron donor and acceptor limitation, but when normalized to protein, there was not a statistically significant difference between the three conditions (g carbohydrate/g protein

= 0.08±0.015 for EAL, 0.07±0.006 for BAL, and 0.06±0.005 for EDL; unpaired student's t-test p-value < 0.05 for all comparisons). Sulfide concentration within the biofilm biomass varied according to electron donor and electron acceptor concentration as well, but when sulfide was normalized to protein, there was no statistically significant difference between the three conditions (g sulfide/ g protein = 4.56±0.6 for EAL, 3.32±0.5 for BAL, 4.21±0.1 for EDL unpaired student's t-test p-value < 0.05 for all comparisons). Additionally, biomass yields for lactate and sulfate that included the biofilm and planktonic phase biomass, were not statistically different between the three conditions (Table 1) and the proportion of biomass in the biofilm phase compared to the planktonic phase was between 5 and 6% for all three conditions.

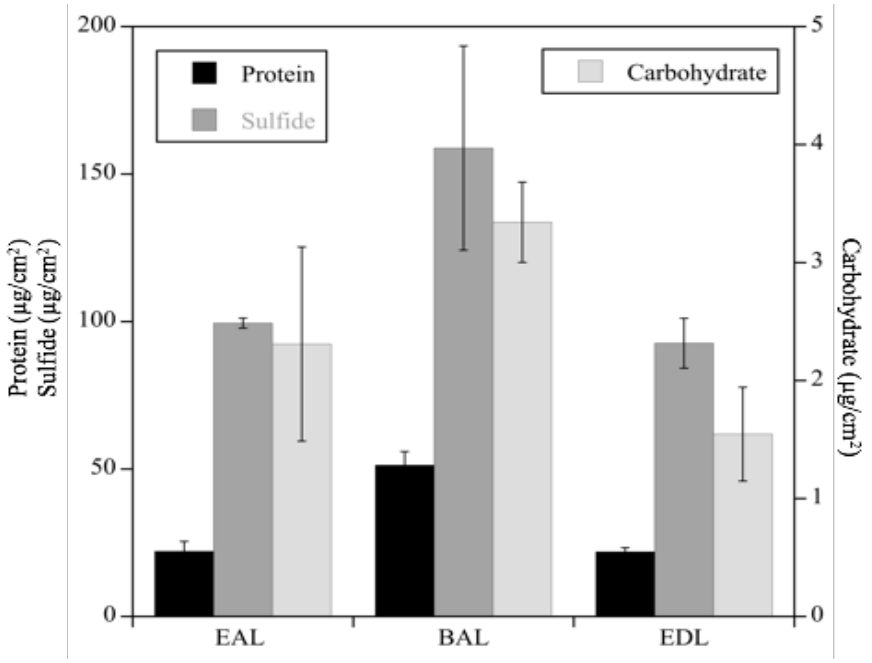


Figure 1. Protein, carbohydrate, and sulfide concentrations in *D. vulgaris* biofilm grown under EAL, BAL, and EDL conditions.

	Lactate: Sulfate Concentration (mM)	**Yield (g Protein/g Lactate)**	**Yield (g Protein/g Sulfate)**
Electron acceptor limited (EAL)	50:10	0.059 ± 0.006	0.113 ± 0.014
Balanced (BAL)	60:30	0.057 ± 0.004	0.112 ± 0.008
Electron donor limited (EDL)	18:50	0.066 ± 0.002	0.125 ± 0.003

Table 1. Lactate and Sulfate concentrations for the different nutrient ratios and biomass yields based on lactate and sulfate consumption.

Metabolomic Analysis of *D. vulgaris* Biofilm

To understand how nutrient limitation affects the metabolism of *D. vulgaris* biofilm, an untargeted metabolomic method was implemented. Overall, there were 552 dysregulated features with a p-value less than 0.01 and a fold-change greater than 1.5 when *D. vulgaris* biofilm grown under EAL was compared to that grown under BAL (Figure 2).

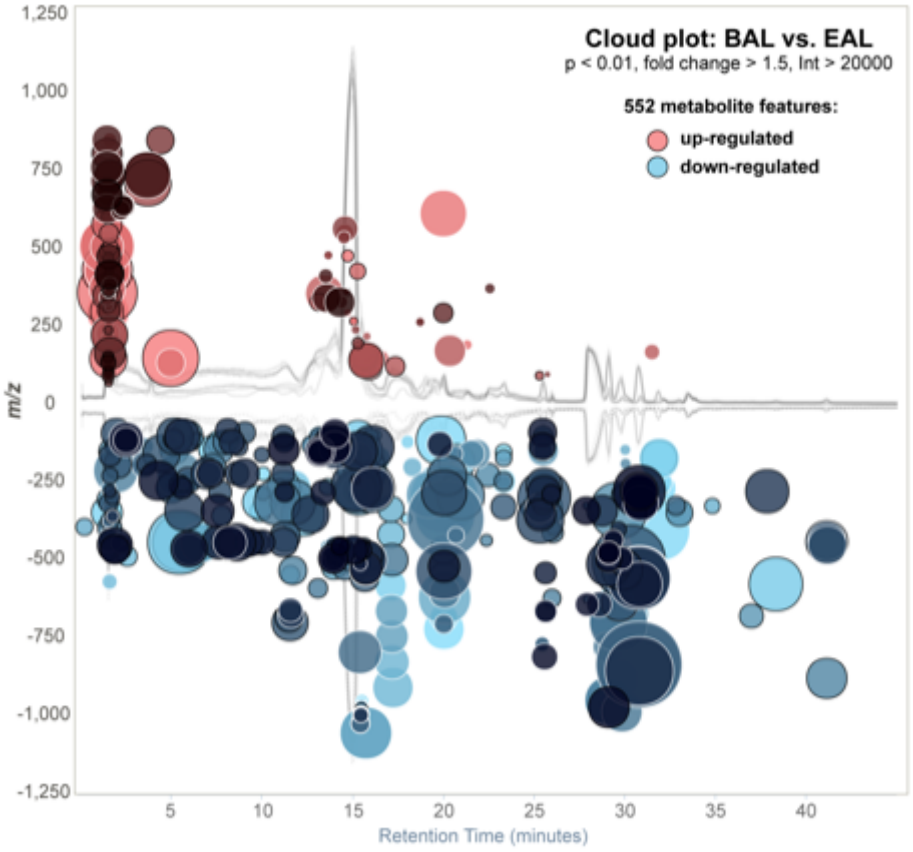


Figure 2. Cloud plot representation of dysregulated metabolites with a greater than 1.5 fold-change and p-value less than 0.01. Size of dot represents fold-change, with larger diameters representing greater fold change, and intensity of color represents p-value, with darker intensities representing smaller p-values.

Metabolites that were down-regulated under the EAL condition compared to the BAL condition fell into the categories of purine and pyrimidine metabolism, glutamine and glutamate metabolism, and peptidoglycan metabolism. Individual metabolites within these pathways are listed in Table 2 and pathways containing more than one down-regulated metabolite are depicted in Figure 3 (adapted from KEGG (Kanehisa 2000; Kanehisa et al. 2016; Kanehisa et al. 2017)).

Surprisingly, metabolites that were up-regulated under the EAL condition were almost entirely different types of fatty acids. These fatty acids are listed in Table 3. Taurine and possibly 3-deoxy-d-manno-octulosonate were also up-regulated under the EAL condition, but 3-deoxy-d-manno-octulosonate, a Lipid A precursor, could not be confirmed by MS/MS because there is no standard in the database. The up-expression of fatty acids in *D. vulgaris* biofilm is investigated further in Chapter 4.

Metabolite ID	Fold Change	p-value
Purine Metabolism		
Inosine	22.2	1.20E-03
Hypoxanthine	7.8	1.35E-05
Adenylylsulfate	6.5	1.10E-04
Guanosine	6.3	1.60E-02
Adenosine monophosphate (AMP)	5.5	3.70E-03
Guanine	4.3	9.00E-04
Adenine	2.7	6.00E-04
Pyrimidine Metabolism		
Uridine diphosphate (UDP)	13.3	4.00E-03
Glutamate	8.0	2.30E-02
Uracil	6.3	9.00E-05
Uridine monophosphate (UMP)	3.3	1.50E-03
UDP-glucose	3.2	2.00E-02
Cytidine monophosphate (CMP)	2.0	2.50E-02
Glutamine and Glutamate Metabolism		

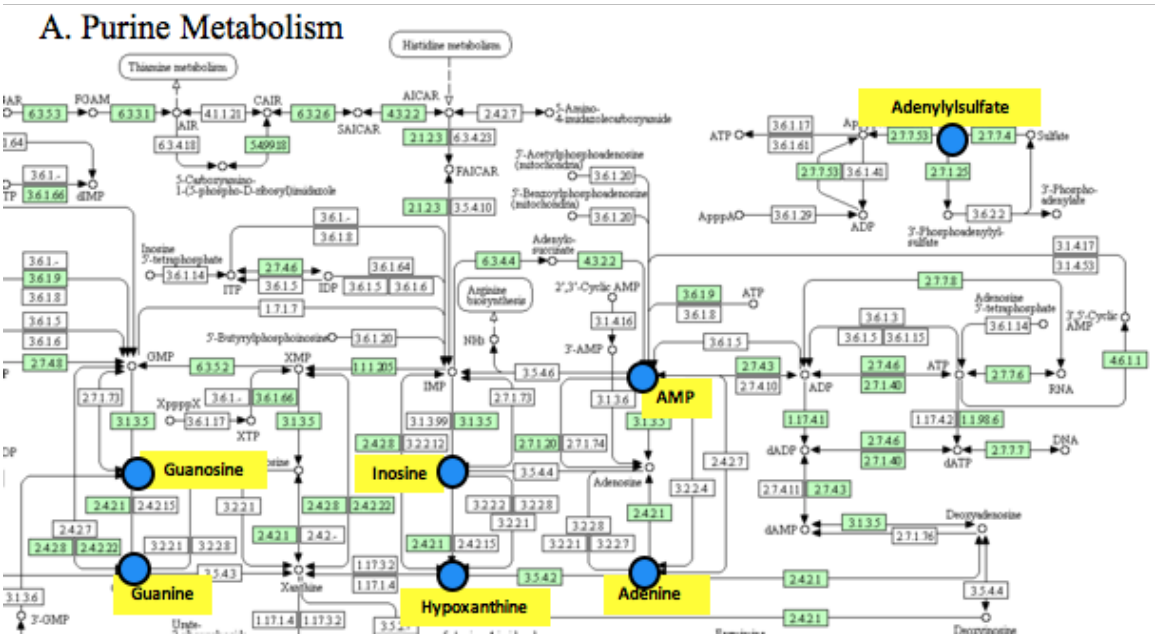
UDP-MurNAc-Ala-Glu	13.2	2.40E-03
D-Glutamine	8.0	2.30E-02
UDP-N-Acetyl-muramate	4.6	3.50E-03
L-Glutamate	3.7	2.20E-03
Peptidoglycan		
UDP-MurNAc-Ala-Glu	13.2	2.40E-03
Alanine	6.0	7.00E-06
UDP-N-Acetyl-muramate	4.6	3.50E-03
UMP	3.3	1.50E-03
Other		
Tryptophan	14.1	2.90E-03
2-C-Methyl-D-erythritol 2,4-cyclodiphosphate	10.7	8.50E-07
Lysophospholipid	9.4	3.00E-05
Methionine	7.8	2.70E-03
Methylthiouracil	6.6	4.00E-03
Lysophospholipid (17:1/0:0)	6.5	9.00E-04
Phosphoethanolamine (8:0/8:0)	6.0	2.00E-05
Aspartic acid	5.5	5.00E-06
Phosphatidylglycerol (15:1/0:0)	4.3	9.00E-04
NAD	4.0	1.00E-04
GDP-fucose	2.9	5.00E-03
Phenylalanine	2.5	5.80E-03
Phosphoethanolamine (8:0/8:0)	1.5	3.00E-02

Table 2. List of metabolites down-regulated under the EAL condition categorized by metabolic pathways they are linked to and associated fold change and p-value.

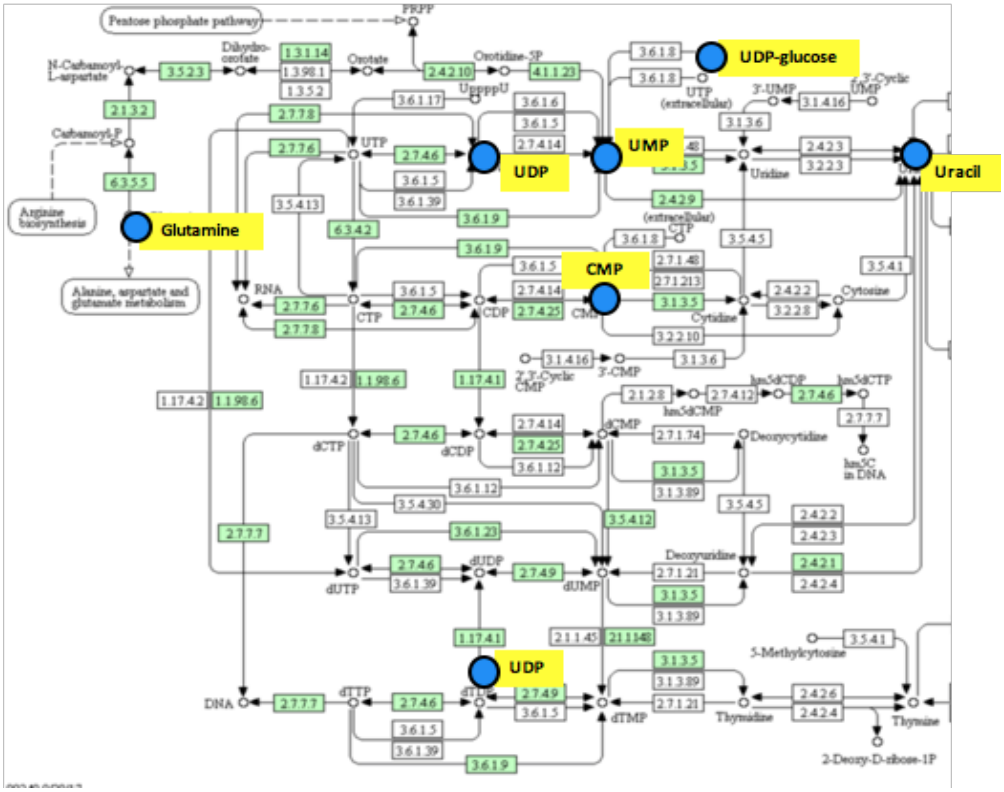
Metabolite ID	Fold Change	p-value
Fatty Acids		
Methyl-heptanoic acid	9.3	3.0E-03
Methyl-hexanoic acid	6.7	6.0E-03
Methyl-octanoic acid	5.2	5.0E-03
Decanoic acid	4.0	5.0E-03
Dihydroxy-octadecadienoic acid	3.8	6.0E-03
Hydroxy-octadecadienoic acid	3.5	5.0E-03
Methyl-decanoic acid	2.3	8.0E-03
Dodecanoic acid	2.0	2.0E-03
Methyl-hexadecanoic acid	1.7	8.0E-03
Hydroxy-undecenoic acid	1.6	8.0E-03
Hydroxy-hexadecanoic acid	1.4	4.0E-03
Methyl-tetradecanoic acid	1.3	8.0E-03
Other		
Taurine	2.9	3.00E-03
3-Deoxy-D-manno-octulosonate	1.9	7.20E-03

Table 3. List of metabolites up-regulated under the EAL condition, with associated fold change and p-value.

A. Purine Metabolism



B. Pyrimidine Metabolism



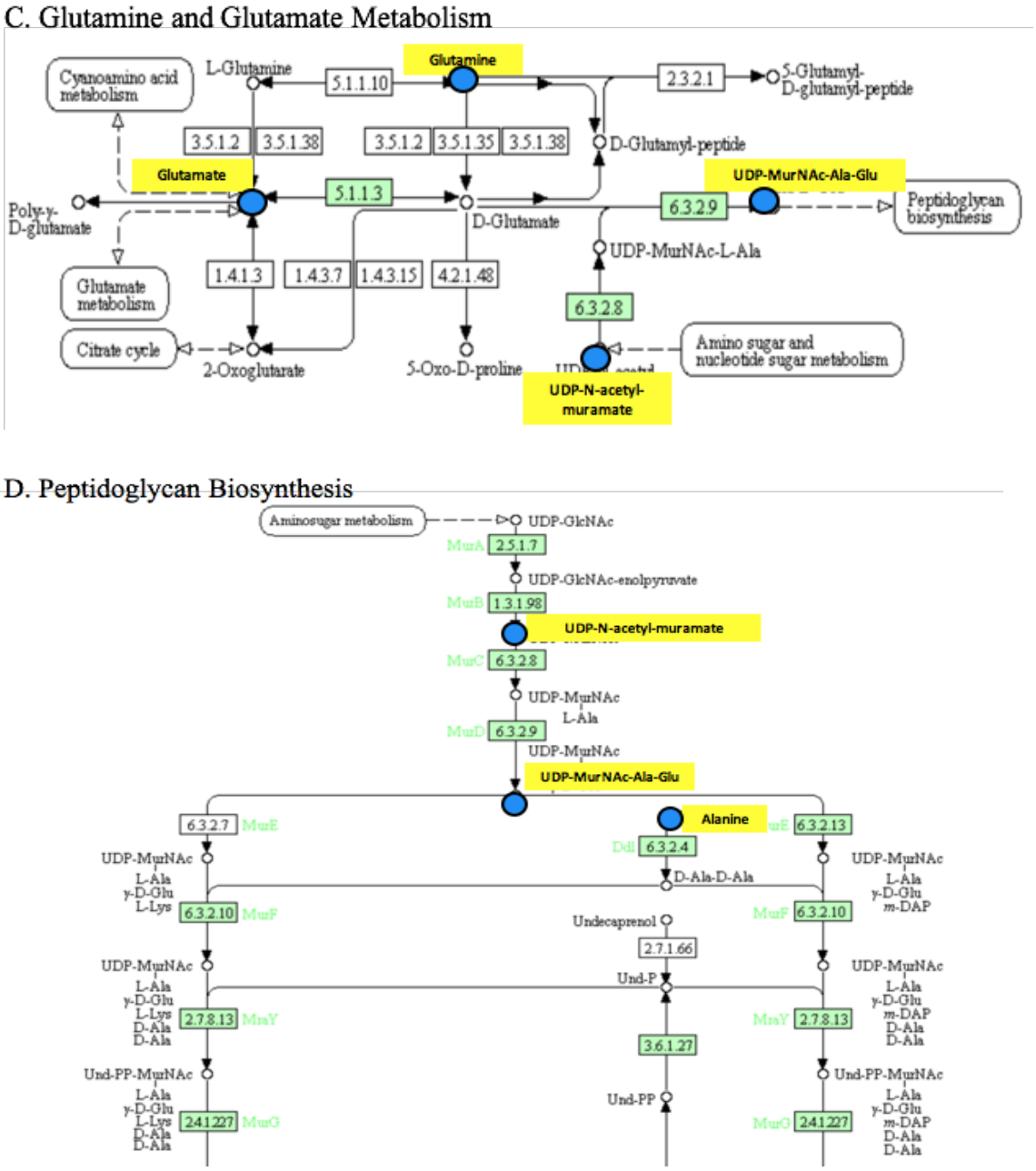


Figure 3. Metabolic pathways with multiple down-regulated metabolites, highlighted in yellow, under EAL conditions. Green boxes represent genes/proteins that are annotated in the *D. vulgaris* Hildenborough genome. Figures adapted from KEGG.

Discussion

Nutrient limitation, in the form of electron donor/carbon source or electron acceptor limitation, had notable effects on biofilm metabolism and growth. Growth, as measured by protein biomass, reached a higher density under the BAL condition, as was expected given that the BAL condition provides ~three times the amount electron flux compared to the EAL and EDL conditions (240, 80, and 72 electron equivalents, for BAL, EAL, and EDL, respectively). Although there was not three times the amount of biofilm biomass produced in accordance with the difference in lactate and sulfate concentration for the BAL condition, the biomass yields for the entire reactor (biofilm plus planktonic phase) for EAL, BAL, and EDL were similar to each other, indicating that the biomass produced, in either planktonic or biofilm phase, was consistent with how much lactate and sulfate was provided. Carbohydrate did not contribute a large portion of the total biofilm biomass under any of the three conditions, which is consistent with results from Clark *et al.*, in which the authors analyzed *D. vulgaris* Hildenborough biofilm grown at 30°C (Clark et al. 2007; Clark et al. 2012).

Despite similar biofilm biomass yields, there was a considerable amount of dysregulation in *D. vulgaris* biofilm grown under EAL compared to the BAL condition. Overall, the down-regulated metabolites for biofilm grown under EAL indicated that cellular growth was suppressed compared to biofilm under the BAL condition through the dysregulation of metabolites involved in purine and pyrimidine synthesis (for

nucleotide production), glutamine and glutamate synthesis (for amino acid production, purine and pyrimidine production, and NAD production), and peptidoglycan synthesis (for cell wall production). Under the condition of lower energy state (EAL), the data suggest that biofilm cells slow down "growth" related resource expenditure by decreasing the production of precursors for purine and pyrimidine biosynthesis and cell well biosynthesis. Because the comparison was between a nutrient limited biofilm and a nutrient balanced biofilm in reactors at the same dilution rate, the data suggest that the biofilm responded to energy limitation by decreasing metabolites important for new cell biosynthesis (*i.e.*, purines, pyrimidines, cell wall precursors).

This could be analogous to cell cycle check-points that stop or slow the cell cycle in eukaryotic cells under unfavorable conditions. Both glutamate and glutamine are crucial precursors to the de novo synthesis of both purines and pyrimidines as well as important amino acids for the coordination of N and C flux. Under the tested EAL condition, C and N are not limiting; however, electron acceptor is limiting and thus electron flux is lower. These results indicate that energy limitation causes a decline in precursors for purines, pyrimidines, and cell wall biosynthesis. This physiological biofilm state under energy limitation could be similar to a quiescent (Q0) or quiescent-like state in eukaryotic cells, and could possibly contribute to the increased tolerance of biofilms to stresses (*e.g.*, chemicals, metals, antibiotics). It has become increasingly evident that metabolic pathways are integrated and coupled to cell cycle progression and work in higher eukaryotes has shown that cell cycle progression and metabolism are

linked to body fat content in mice (Naaz 2004) as well as type II diabetes in humans (Saxena et al. 2007). However, little is known of the mechanisms involved and if bacteria and archaea display similar controls.

It is typically accepted that cells must sense the energetic status, and the energetic status is linked to the growth and cell cycle. Two commonly studied systems in eukaryotes are the AMP-activated protein kinase (AMPK) and mTOR (a serine/threonine kinase). It is not known if similar functions exist in bacteria and archaea, although interestingly, of the approximately 100 genes that were related to metabolic periodicity with the yeast cell cycle, two-thirds were involved in mitochrondrial function (Lee and Finkel 2013)

Few studies have used comprehensive metabolomics to characterize biofilm physiology and responses to nutrient deprivation. Interestingly, the metabolomic data suggested important roles for nucleotides and cell wall precursors. For purines, guanosine, guanine, inosine, hypoxanthine, and adenine were at lower levels compared to BAL conditions. Typically, inosine is a precursor that can lead to xanthine, guanine, and adenine. For pyrimidines, uridine monophosphate (UMP) was lower in EAL biofilms, and typically UMP is the precursor from which cytosine and thymine are produced. Glutamine and glutamate were also both lower in EAL biofilms, and these amino acids link DNA/RNA and cell wall turnover in several ways. Glutamine and glutamate are important for *de novo* nucleotide biosynthesis (amino donors), and the amino acids (D and L forms) can be placed into the peptide linkages between the glycan strands of the

cell wall. In addition, uridine-5'-triphosphate (UTP) serves as a donor for urdylated precursors during cell wall biosynthesis, and both UDP-N-acetyl-muramate and UDP-N-acetyl-muramate-A-E-A were at lower levels in the EAL biofilms. Moreover, a key intermediate to the biosynthesis of undecaprenyl-P, 2-C-methyl-D-erythritol 2,4-cyclodiphosphate, was depleted in EAL biofilms. Undecaprenyl-P is a crucial lipid carrier for cell wall biosynthesis, and previous work in *Escherichia coli* and *Bacillus subtilis* has shown loss of the synthase responsible for synthesizing this metabolite results in abnormal cell walls (Campbell and Brown 2002). In *E. coli*, a filamentous phenotype was observed, and in *B. subtilis* irregular morphology and thickened cell walls was observed. Purine and pyrimidine biosynthesis has also been linked to cell wall synthesis/rigidity in *Lactococcus lactis*, with mutations in the either *guaA* or *pyrB* genes causing changes in cell wall rigidity due to an accumulation of L-aspartate, which is an essential component of peptidoglycan crosslinking proteins, over conversion of L-Asp to pyrimidine precursors (Solopova et al. 2016). Purine biosynthesis has also been observed to be dysregulated during meiotic differentiation of yeast spores (Walther et al. 2014), and little is known of metabolic re-programming in bacterial biofilms or the repercussions for eukaryotic cell cycles and differentiation. In the context of the presented data with *D. vulgaris*, multiple metabolites crucial to DNA/RNA and cell wall turnover were dysregulated, and the data suggest a linkage between nucleotide and cell wall biosynthesis that could help coordinate the biofilm cell cycle and nutrient limitation.

Interestingly, the majority of the metabolites that were up-regulated under the EAL condition were fatty acids. Fatty acids are a major component of cellular membranes, but given that pathways critical to cellular growth were down-regulated, it does not make sense that metabolites associated with cellular membranes are up-regulated. This suggests that the fatty acids are not being produced as part of cellular membranes, but for another purpose. Fatty acid biosynthesis requires inputs of ATP and reducing equivalent in the form of NADPH, further supporting the idea that energy and reducing equivalents may be being used for fatty acid production rather than cellular growth. The up-regulation of fatty acids and their role in *D. vulgaris* biofilms grown under the EAL condition will be further explored in Chapter 4.

Of the other up-regulated metabolites under the EAL condition, only one could be positively identified in METLIN and that is taurine. Taurine is a sulfonic acid containing an amino group and its biosynthesis is widely distributed in eukaryotes. Taurine biosynthesis in bacteria is not as well understood, but a pathway has been elucidated in a *Synechococcus* species in and there may be similar pathways in other bacteria (Agnello et al. 2013). While certain *Desulfovibrio* strains can use sulfonates, including taurine, for electron acceptors, utilization of taurine as an electron acceptor by *D. vulgaris* Hildenborough has not been demonstrated (Laue et al. 1997; Lie et al. 1999). The production of taurine under sulfate-limiting conditions raises the question of whether taurine could be produced from cysteine as an electron acceptor when sulfate is limiting. This question is not addressed in this work, but could be a future direction for research.

While *D. vulgaris* biofilm growth under nutrient limited and balanced conditions was consistent with how much substrate was provided, and carbohydrate and sulfide concentrations were approximately the same when normalized to protein, the metabolomic analysis revealed significant dysregulation of metabolic features between the sulfate-limited and balanced conditions. The differences in metabolite regulation brings to light the ability of *D. vulgaris* to sense carbon/electron donor and sulfate/electron acceptor and adjust its metabolism accordingly. The mechanism by which this is coordinated is unknown, as is the utility of fatty acid production over growth, but the role of fatty acids produced under EAL conditions in *D. vulgaris* biofilms is explored further in Chapter 4.

REFERENCES CITED

Agnello G, Chang LL, Lamb CM, Georgiou G, Stone EM (2013) Discovery of a substrate selectivity motif in amino acid decarboxylases unveils a taurine biosynthesis pathway in prokaryotes. ACS Chem Biol 8:2264–2271.

Benton HP, Ivanisevic J, Mahieu NG, Kurczy ME, Johnson CH, Franco L, Rinehart D, Valentine E, Gowda H, Ubhi BK, Tautenhahn R, Gieschen A, Fields MW, Patti GJ, Siuzdak G (2015) Autonomous metabolomics for rapid metabolite identification in global profiling. Anal Chem 87:884–891.

Borglin S, Joyner D, Jacobsen J, Mukhopadhyay A, Hazen TC (2009) Overcoming the anaerobic hurdle in phenotypic microarrays: generation and visualization of growth curve data for Desulfovibrio vulgaris Hildenborough. J Microbiol Methods 76:159–168.

Brandis A, Thauer RK (1981) Growth of Desulfovibrio species on hydrogen and sulphate as sole energy source. Microbiology 126:249–252.

Campbell TL, Brown ED (2002) Characterization of the depletion of 2-C-methyl-D-erythritol-2,4-cyclodiphosphate synthase in Escherichia coli and Bacillus subtilis. J Bacteriol 184:5609–5618.

Chaplin MF, Kennedy JF (1986) Carbohydrate analysis: a practical approach. Oxford University Press, USA

Christensen GA, Zane GM, Kazakov AE, Li X, Rodionov DA, Novichkov PS, Dubchak I, Arkin AP, Wall JD (2015) Rex (encoded by DVU_0916) in Desulfovibrio vulgaris Hildenborough is a repressor of sulfate adenylyl transferase and is regulated by NADH. J Bacteriol 197:29–39.

Clark ME, Edelmann RE, Duley ML, Wall JD, Fields MW (2007) Biofilm formation in Desulfovibrio vulgaris Hildenborough is dependent upon protein filaments. Environ Microbiol 9:2844–2854.

Clark ME, He Z, Redding AM, Joachimiak MP, Keasling JD, Zhou JZ, Arkin AP, Mukhopadhyay A, Fields MW (2012) Transcriptomic and proteomic analyses of Desulfovibrio vulgaris biofilms: carbon and energy flow contribute to the distinct biofilm growth state. BMC Genomics 13:138.

Cord-Ruwisch R (1985) A quick method for the determination of dissolved and precipitated sulfides in cultures of sulfate-reducing bacteria. J Microbiol Methods 4:33–36.

Doucette CD, Schwab DJ, Wingreen NS, Rabinowitz JD (2011) α-Ketoglutarate coordinates carbon and nitrogen utilization via enzyme I inhibition. Nat Chem Biol 7:894–901.

Ivanisevic J, Zhu Z-J, Plate L, Tautenhahn R, Chen S, O'Brien PJ, Johnson CH, Marletta MA, Patti GJ, Siuzdak G (2013) Toward 'omic scale metabolite profiling: a dual separation--mass spectrometry approach for coverage of lipid and central carbon metabolism. Anal Chem 85:6876–6884.

Kanehisa M (2000) KEGG: Kyoto Encyclopedia of Genes and Genomes. Nucleic Acids Res 28:27–30.

Kanehisa M, Furumichi M, Tanabe M, Sato Y, Morishima K (2017) KEGG: new perspectives on genomes, pathways, diseases and drugs. Nucleic Acids Res 45:D353–D361.

Kanehisa M, Sato Y, Kawashima M, Furumichi M, Tanabe M (2016) KEGG as a reference resource for gene and protein annotation. Nucleic Acids Res 44:D457–62.

Klonowska A, Clark ME, Thieman SB, Giles BJ, Wall JD, Fields MW (2008) Hexavalent chromium reduction in Desulfovibrio vulgaris Hildenborough causes transitory inhibition of sulfate reduction and cell growth. Appl Microbiol Biotechnol 78:1007–1016.

Laue H, Denger K, Cook AM (1997) Taurine reduction in anaerobic respiration of Bilophila wadsworthia RZATAU. Appl Environ Microbiol 63:2016–2021.

Lee IH, Finkel T (2013) Metabolic regulation of the cell cycle. Curr Opin Cell Biol 25:724–729.

Lie TJ, Godchaux W, Leadbetter ER (1999) Sulfonates as terminal electron acceptors for growth of sulfite-reducing bacteria (Desulfitobacterium spp.) and sulfate-reducing bacteria: effects of inhibitors of sulfidogenesis. Appl Environ Microbiol 65:4611–4617.

Naaz A (2004) Loss of cyclin-dependent kinase inhibitors produces adipocyte hyperplasia and obesity. The FASEB Journal. doi: 10.1096/fj.04-2631fje

Quan JA, Schneider BL, Paulsen IT, Yamada M, Kredich NM, Saier MH Jr (2002) Regulation of carbon utilization by sulfur availability in Escherichia coli and Salmonella typhimurium. Microbiology 148:123–131.

Saxena R, Voight BF, Lyssenko V, Burtt NP, de Bakker PIW, Chen H, Roix JJ, Kathiresan S, Hirschhorn JN, Daly MJ, Hughes TE, Groop L, Altshuler D, Almgren P, Florez JC, Meyer J, Ardlie K, Boström KB, Isomaa B, Lettre G, Lindblad U, Lyon HN,

Melander O, Newton-Cheh C, Nilsson P, Orho-Melander M, Råstam L, Speliotes EK, Taskinen M-R, Tuomi T, Guiducci C, Berglund A, Carlson J, Gianniny L, Hackett R, Hall L, Holmkvist J, Laurila E, Sjögren M, Sterner M, Surti A, Svensson M, Svensson M, Tewhey R, Blumenstiel B, Parkin M, DeFelice M, Barry R, Brodeur W, Camarata J, Chia N, Fava M, Gibbons J, Handsaker B, Healy C, Nguyen K, Gates C, Sougnez C, Gage D, Nizzari M, Gabriel SB, Chirn G-W, Ma Q, Parikh H, Richardson D, Ricke D, Purcell S (2007) Genome-Wide Association Analysis Identifies Loci for Type 2 Diabetes and Triglyceride Levels. Science 316:1331–1336.

Solopova A, Formosa-Dague C, Courtin P, Furlan S, Veiga P, Péchoux C, Armalyte J, Sadauskas M, Kok J, Hols P, Dufrêne YF, Kuipers OP, Chapot-Chartier M-P, Kulakauskas S (2016) Regulation of Cell Wall Plasticity by Nucleotide Metabolism in Lactococcus lactis. J Biol Chem 291:11323–11336.

Walther T, Létisse F, Peyriga L, Alkim C, Liu Y, Lardenois A, Martin-Yken H, Portais J-C, Primig M, François JM (2014) Developmental stage-dependent metabolic regulation during meiotic differentiation in budding yeast. BMC Biol. doi: 10.1186/s12915-014-0060-x

Zhou C, Zhou Y, Rittmann BE (2017) Reductive precipitation of sulfate and soluble Fe(III) by Desulfovibrio vulgaris: Electron donor regulates intracellular electron flow and nano-FeS crystallization. Water Res 119:91–101.

CHAPTER FOUR

EXTRACELLULAR MEMBRANE STRUCTURES IN *DESULFOVIBRIO VULGARIS* HILDENBOROUGH BIOFILMS

Contribution of Authors and Co-Authors

Manuscript in Chapter 4

Author: Lauren C. Franco

Contributions: Developed experimental design, performed experiments, analyzed data, wrote and revised the manuscript.

Co-Author: Siva Wu

Contributions: Developed experimental design, performed experiments, analyzed data.

Co-Author: Michael Joo

Contributions: Developed experimental design, performed experiments, analyzed data.

Co-Author: Joel Mancuso, Jonathan Remis, Amita Gorur, Ambrose Leung, Danielle M. Jorgens, Joaquin Correa

Contributions: Developed experimental design, performed experiments, analyzed data.

Co-Author: Manfred Auer

Contributions: Developed experimental design, analyzed data, wrote and revised manuscript.

Co-Author: Matthew W. Fields

Contributions: Developed experimental design, analyzed data, wrote and revised the manuscript

Manuscript Information Page

Lauren C. Franco, Siva Wu, Michael Woo, Manfred Auer, Matthew W. Fields

Status of Manuscript:
__x_ Prepared for submission to a peer-reviewed journal
____ Officially submitted to a peer-review journal
____ Accepted by a peer-reviewed journal
____ Published in a peer-reviewed journal

Abstract

Biofilm samples of *Desulfovibrio vulgaris* Hildenborough grown under electron acceptor-limited (EAL), electron donor-limited (EDL), and electron donor to electron acceptor-balanced (BAL) conditions were analyzed via high resolution electron microscopy to investigate the composition and potential function of extracellular features in the biofilm matrix. Microscopy revealed the presence of membrane vesicles, extracellular filaments, and extracellular membranous structures. Membranous structures varied in shape, with some being sheet-like in structure, whereas others take on a more geometrical shape and form pockets in the biofilm that are devoid of cells. Transmission electron microscopy (TEM) images show that these structures connect to intact cells suggesting a biological origin and function. TEM imaging showed that membranous structures were associated with electron dense precipitates and energy dispersive x-ray spectroscopy (EDS) imaging analysis showed that these precipitates were composed of Fe, O and P. Wide-field montage TEM allowed observation of the biofilm grown under the three different conditions on a larger scale. Qualitatively, membranous structures produced in biofilm grown under the EAL condition were larger and more extensive than those produced under the EDL or BAL condition. Differential staining revealed that the structures were lipid-based. Fatty acid content of whole biofilm grown under BAL and EAL conditions was quantified and the results showed that biofilm grown under the EAL condition had ~3 times more fatty acid methyl ester (FAME) content. Since biofilm grown under the EAL condition had more extensive extracellular membranous structures, and these structures were associated with metal precipitates, biofilms grown under EAL and BAL were exposed to Cr(VI). Results suggested that biofilm grown under the EAL condition were more protected from Cr(VI) toxicity than those grown under the BAL condition, but the finding was not statistically significant. Together, the results presented here highlight lipids as an important and previously unrecognized part of the sulfate-reducing biofilm matrix and suggest that they might be involved in microbe-metal interactions. These results also continue to highlight the effects of nutrient limitation on microbial metabolism and physiology.

Introduction

The biofilm matrix is an all-inclusive term for the extracellular substances that allow cells to stick to surfaces and each other. These substances include, but are not limited to polysaccharides, extracellular DNA, membrane vesicles, cell debris from lysed cells, membrane vesicles, enzymes, small molecules, and lipids (Flemming and Wingender 2010). While some of these components have been identified and the function established for a particular species, there are still many matrix components that have not been identified or described. This chapter highlights extracellular membranes as an important constituent of sulfate reducing biofilm matrices.

Microorganisms are predicted to comprise the largest amount of biomass on earth (Whitman et al. 1998), are known to play vital roles in ecosystem function (Coleman and Whitman 2005; Duffy and Stachowicz 2006; Danovaro et al. 2008), and most likely represent immense, as yet undiscovered, biochemical capacities (Castelle et al. 2013). Additionally, microorganisms are known to play important roles in global biogeochemical processes such as carbon cycling and bioremediation (Anderson et al. 2003; Karl et al. 2012). It is well accepted that microorganisms can exist attached to surfaces and each other, often surrounded by extracellular polymeric substances (EPS) (Hall-Stoodley et al. 2004; Gross et al. 2007; Stewart and Franklin 2008). It is becoming increasingly clear that a mode of attached growth more closely resembles *in situ*

conditions for many microorganisms in different environments and might likely be a universal feature that presents an important physiology to explore in addition to the typically conducted studies on planktonic cells (Dunne 2002; Kolter 2005). Further, cells growing as a biofilm are known to have different physiologies and properties such as increased resistance to external stresses such as antimicrobials, heavy metal exposure, and desiccation (McKew et al. 2011; Clark et al. 2012; Stylo et al. 2015).

The presence of extracellular membranes in a biofilm matrix has not yet been reported, however structures of a similar appearance have been described in other metal-reducing organisms. *Shewanella oneidensis* MR-1 nanowires were originally thought to be proteinaceous filaments composed of pilin (Gorby et al. 2006), but have most recently been identified as extensions of the outer membrane and periplasm that contain the cytochromes MtrC and OmcA, similar to the previously described outer membrane vesicle chains and membrane tubes in *Myxococcus xanthus* planktonic cultures and biofilms (Remis et al. 2014; Pirbadian et al. 2014). *S. oneidensis* MR-1 biofilms have also been reported to produce extracellular polymeric substances (EPS) that play an active role in uranium reduction. The EPS-glycocalyx type structure was found to be lined with the MtrC and OmcA cytochromes that were in close association with UO_2 nanoparticles, indicating extracellular uranium (IV) reduction (Marshall et al. 2006).

Differences between planktonic and biofilm growth modes have been well documented in DvH; however, differences between biofilms grown under different conditions have not been as well studied (Clark et al. 2012). In the previous chapter the

metabolic effects of nutrient limitation on *D. vulgaris* biofilm were investigated. In the current chapter, the effect of nutrient limitation on biofilm structure and composition is explored. To do this, we employed a variety of advanced high-resolution imaging and chemical characterization techniques, including 2D transmission electron microscopy (TEM), 3D serial block face scanning electron microscopy (SBF/SEM) imaging, and elemental analysis via energy-dispersive x-ray spectroscopy. This work describes extracellular membranous structures that are produced by *D. vulgaris* biofilms grown under nutrient limited and balanced conditions. The prevalence of these structures in the biofilm suggests that they are an important, but understudied component of sulfate reducing biofilm matrices.

Materials and Methods

Bacterial Strains and Growth Conditions

D. vulgaris Hildenborough was grown in either batch or continuous mode. For batch growth, cells were inoculated into sterile N_2 gassed balch tubes containing LS4D, a lactate and sulfate medium (modified to 2.5 μM resazurin and 130 μM riboflavin in Thauer's vitamins) (Brandis and Thauer 1981; Borglin et al. 2009). The medium consisted of varying lactate and sulfate concentrations as follows: 60 mM sodium lactate and 30 mM sodium sulfate (balanced condition), 50 mM sodium lactate and 10 mM sodium sulfate (electron acceptor limited condition), and 18 mM sodium lactate and 50 mM sodium sulfate (electron donor limited condition). For continuous culture of *D.*

vulgaris biofilm, cells were grown in a modified CDC reactor equipped with additional gas lines to maintain anoxic conditions. Exponential phase cells were inoculated into a CDC reactor containing electron acceptor limited, balanced, or electron donor limited LS4D medium. Cells were grown in batch mode for 48 hours and then continuous mode with a dilution rate of 0.04^{-hr}. Reactors were grown at room temperature (20-23°C), stirred at 60 rpm, and the headspace was continuously sparged with sterile N_2 gas to maintain anaerobic conditions. Coupons of glass slides or aclar (7.8 mil thickness) (Electron Microscopy Sciences, Hatfield, PA) were submerged in the reactor body as a surface for biofilm growth.

Sample Collection

Biofilm samples were collected for biomass analysis and microscopic analysis. For biomass analyses glass slide coupons were removed from the reactor and biomass was scraped from both sides of the slide with a razor blade. Samples on aclar for microscopic analyses were collected at 168 hours. Immediately after sampling, aclar with attached biofilm was rinsed three times in phosphate buffered saline and then fixed in a 2.5% gluturaldehyde, 0.05M sodium cacodylate solution.

Biomass Analyses

Cell viability was determined via the most probable number method (Jarvis et al. 2010). Biofilm was scraped from glass slides, homogenized by vortexing and normalized by optical density to account for differing amounts of biomass between the different conditions. Normalized biofilm samples were then diluted to extinction and incubated at

30°C. After 3 weeks, growth was assessed and used to calculate the number of viable cells/ml for each biofilm condition. Lipid content from scraped biofilm (in triplicate) was chloroform extracted, transesterified, and measured by GC-MS according to the method described in Lohman *et al.* (Lohman et al. 2013).

Imaging Methods

Fluorescence Microscopy. Biofilms were fixed in 4% paraformaldehyde for 4 hours at room temperature, followed by incubation with the lipophilic fluorescent dye FM1-43 (www.thermofisher.com) and extensive washes with 20 mM HEPES buffer. Stained biofilm samples were either imaged on a Zeiss LSM 710 confocal microscope with Zen software or a Zeiss Axioskop Imaging platform with SPOT Basic software or embedded in O.C.T. freezing medium. Blocks of biofilm samples in O.C.T. were sectioned on the Leica Cryostat CM3050S (Leica Microsystems, Wetzlar, Germany) and ~10 μm-thick sections were imaged by epifluorescence microscopy.

High pressure freezing and freeze substitution. Biofilms, unfixed or fixed, were placed in 1 mm wide by 200 μm deep aluminum freezing hats, then surrounded with 10% glycerol-solution that acts as a cryo-protectant prior to freezing. The biofilms were then cryo-immobilized using a BAL-TEC HPM-010 high-pressure freezer (BAL-TEC, Inc., Carlsbad, CA). Alternatively, biofilms were subjected to routine bench-top processing. As discussed in the main text, different biofilm samples were subjected to different freeze-substitution/staining protocols, resulting in samples that were unstained (did not see any heavy metal staining during sample preparation), 0.1% uranyl acetate stained, or

stained by 1% osmium tetroxide plus 0.1% uranyl acetate. For all samples that were freeze-substituted we used either a Leica AFS2 (Leica Microsystems, Wetzlar, Germany) following a previously described protocol (McDonald et al. 2007) or adopted a method of super quick freeze substitution (McDonald and Webb 2011). Upon completion of freeze-substitution, the biofilm samples were rinsed five times in pure acetone and then progressively infiltrated with an epon-araldite resin (McDonald and Müller-Reichert 2002). Samples were flat embedded between two slides using two layers of parafilm as a spacer before being polymerized overnight in an oven at 60°C (McDonald and Müller-Reichert 2002; Müller-Reichert et al. 2003).

Transmission electron microscopy. 70-100 nm sections were collected on formvar-coated grids using a Reichert Ultracut E ultramicrotome (Leica Microsystems, Germany). For serial section TEM, 100 nm sections were collected in ribbons of ~5 sections upon each grid to preserve the order and orientation of the sectioned material. Sections were post-stained using 2% uranyl acetate in 70% methanol followed by Reynold's lead citrate. The sections were imaged in an FEI Tecnai 12 TEM (FEI, Hillsboro, OR) operated at 120 kV. Images were recorded using a Gatan CCD with Digital Micrograph software (Gatan Inc., Pleasanton, CA). ImageJ software (Abramoff et al. 2004) and Adobe Photoshop CS4 (Adobe Systems Inc., San Jose, CA) were used for further image processing and for the registration of the serial section images for 3D analysis.

Volume Electron Microscopy Imaging. For SBF-SEM, biofilms, embedded in

resin, were mounted onto an aluminum pin with a cyanoacrylate adhesive. The pin, which takes the place of a normal SEM stub, was loaded into a sample holder for the Gatan 3View (Gatan Inc., Pleasanton, Ca). Serial block face scanning electron microscopy was carried out as previously described (Denk and Horstmann 2004). SBF-SEM data was collected using a 3View system mounted on a Zeiss Sigma FE-SEM; serial images were acquired at 5 kV at 4k x 4k at 10 nm XY pixel size, and 50 nm Z slice dimensions.

Energy Dispersive X-ray Spectroscopy. High resolution scanning transmission electron microscopy (STEM) and energy-dispersive spectroscopy (EDS) were carried out on a Zeiss Sigma FE-SEM in backscatter or Scanning Transmission Electron Microscopy mode. Thin sections were mounted on continuous carbon-coated Formvar TEM grids. High-angle annual dark field (HAADF) scanning transmission electron microscopy (STEM) images and X-ray elemental line scans were acquired with a 1-nm probe at 120 or 200 kV. The specimens were tilted 10 degrees toward the X-ray detector to optimize the X-ray detection geometry. Collection times were 300 live seconds for each line scan.

The Effect of Cr(VI) on Whole and Scraped Biofilm

D. vulgaris biofilm grown under EAL or BAL conditions was harvested at 168 hours. For testing the effect of Cr(VI) on scraped and homogenized biofilm, biofilm CDC reactors were quickly moved into an anaerobic glove bag with gas, media input, and waste output lines clamped off. In the glove bag, biofilm slides were removed from the reactor, gently dipped in PBS three times, and then scraped into a microcentrifuge tube with 1 ml LS4D medium containing lactate and sulfate concentrations consistent with the

condition they were grown in. Scraped biomass was drawn up through a 16-gauge needle and transferred to a sterile, anaerobic balch tube containing 8 mls LS4D medium. Balch tubes containing the scraped biofilm grown under EAL or BAL conditions was homogenized via vortexing three times at 30 second intervals and then centrifuged at 5,750×*g* for 10 min at room temperature. To "wash" cells of sulfide that would abiotically reduce Cr(VI), the supernatant was removed anoxically and aseptically by needle attached to a vacuum flask under constant flow of N_2 gas to maintain neutral pressure. Pellets were then re-suspended in 9 ml fresh LS4D medium and washed once more, after which the pellets were re-suspended and concentrated in 1 ml fresh LS4D. Concentrated cell cultures were inoculated into 25 ml balch tubes with LS4D medium (10 ml) that contained Cr(VI) (potassium chromate) at 0 or 50 μM to an OD_{600} between 0.06 and 0.07. Growth was monitored by optical density (600 nm). All experiments were performed in triplicate.

To test how Cr(VI) affected viability of intact biofilm grown under EAL and BAL conditions, biofilm samples from the same CDC reactors as above in an anaerobic glove bag, were removed, gently dipped in anaerobic PBS and then transferred into tubes containing either EAL or BAL LS4D medium and 0 or 500 μM Cr(VI). The samples were incubated for 3 hours in the glove bag after which the slides were removed and biofilm was scraped into 1ml fresh LS4D medium. Scraped biofilm was then serially diluted in 96-well plates for MPN analysis as described above.

Cytochrome Staining and Heme Quantification

For cytochrome staining, periplasmic and spheroplast cellular fractions from scraped biofilm grown under BAL and EAL conditions were separated according to Baumgarten *et al.* and Badziong and Thauer (Badzjong and Thauer 1980; Baumgarten et al. 2001). Periplasmic fractions were incubated in 3 molar urea and 90 mM sodium dodecyl sulfate at room temperature for 1 hour before the sample was separated on a polyacrylamide gel (4-20%) via electrophoresis. Cytochromes were visualized via a peroxidase and 3,3',5,5'-tetramethylbenzadine stain (Thomas et al. 1976). Stained bands corresponding with the size of cytochrome c (~14 kDa) were qualitatively compared.

Heme content was measured from scraped and homogenized biofilm grown under EAL of BAL conditions as a quantitative way to detect any differences between the two conditions. Heme was measured using the QuantiChrom Heme Assay Kit (BioAssay Systems, Hayward, CA), a colorimetric assay for heme.

Results

2D TEM Imaging of *Desulfovibrio vulgaris* Biofilms

Using high pressure cryogenic preservation, followed by freeze-substitution and resin-embedding to preserve native biofilm structure, large portions of *D. vulgaris* biofilm grown under EAL, EDL, and BAL conditions were examined via wide-field TEM. Given the very large size typically encountered in a bacterial biofilm, we examined approximately 1 μm semi-thin sections of resin-embedded biofilms that were toluene blue-stained and subjected to montage optical microscopy imaging (Figure 1).

Selected regions with metal deposits were re-imaged by wide-field montage TEM using 70-100 nm ultrathin sections, and increasingly higher resolution images reveal typical metal deposits under EDL, BAL and EAL conditions. Metal deposits were observed under all three conditions, but they differed significantly in the amount of metals that were deposited onto these membrane structures and the overall dimensions of the metal deposits. It should be noted metal deposits were a highly regional phenomenon under all three conditions with most of the biofilm not showing any significant metal deposits. Imaging of DvH biofilms grown under EAL, EDL, and BAL conditions revealed the presence of heterogeneously distributed extracellular structures that were connected to some cells and were closely associated with metal precipitates.

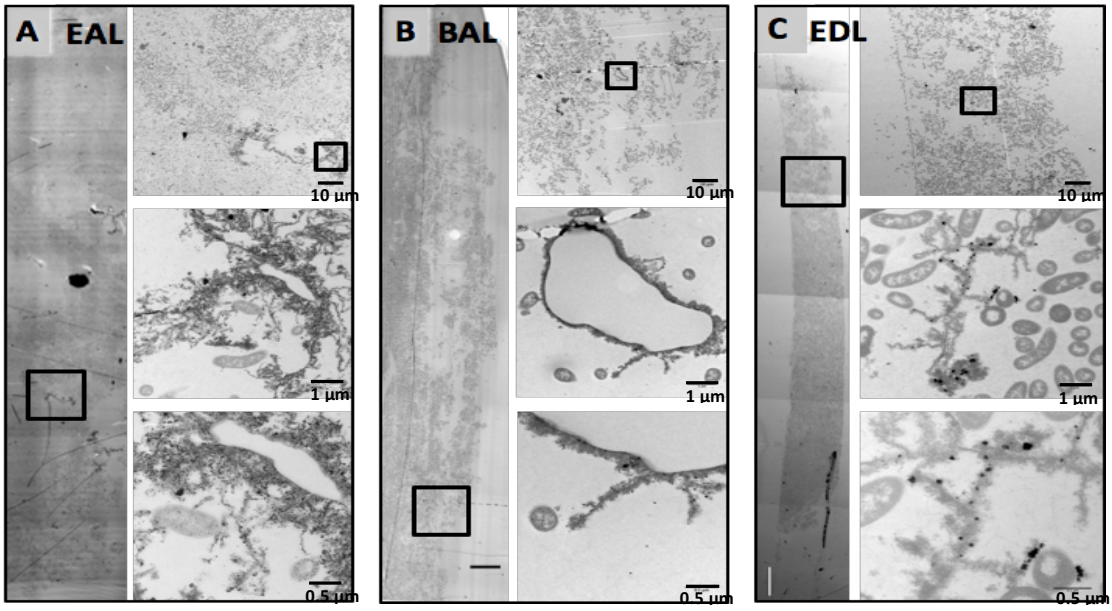


Figure 1. Large-scale microscopic analysis of sections of biofilms grown under EAL (A), BAL (B), and EDL (C) conditions highlighting differences in the extracellular membrane appearance. Each image shows progressively higher magnification within a panel.

It was initially, qualitatively, observed that biofilm grown under the EAL condition contained more, and larger, extracellular structures that those grown under the EDL or BAL conditions (Figure 1). Extracellular metal deposits, appearing as electron dense dark spots, were distributed in highly heterogeneous patterns throughout the biofilm (Figure 2). In areas of close proximity, metal deposition was varied, with metal deposits located in certain places between bacteria, whereas neighboring extracellular spaces were devoid of any metal deposits and appeared empty (Figure 2a). Metal deposits varied in proximity to cells, with some associated with cell surfaces (Figure 2a, b) and others being deposited on thin branched string-like structures (Figure 2c, d). On occasion, structures forming amorphous pockets devoid of cells were observed within the biofilm (Figure 2b). Close-up images of the connection between cells and the structures associated with metal deposits reveal that these structures appear to be connected to and continuous with the cellular outer membrane (Figure 2c, d). The fact that these objects of string-like appearance can be followed through large portions of approximately 70-100 nm ultrathin section of the biofilm suggests that these objects are not strings of metal deposits, but are sheet-like in structure, extending in three dimensions throughout the biofilm.

In favorably oriented biofilm sections we observed extracellular metal deposits with underlying structure directly connected at multiple sites to the bacterial outer membrane (Figures 2c, d). Note that the samples are not counterstained, thus the bacteria appear as light and rather featureless, although the outer and inner membrane can still be

detected (Figure 2c). The metal deposits appear dark and in many instances composed of nano-scale crystals decorating a continuous underlying biological structure. Interestingly, these extracellular features form rather complex large structures with many branches originating what appears in 2D to be ring-like core objects whose interior is devoid of any bacteria or other material (Figure 2b). Given the role that *Desulfovibrio* spp. play in catalyzing processes involving metal transformations (*i.e.*, biocorrosion, heavy metal reduction) and the observed physical connection between the bacterial outer membrane and extracellular structures decorated with metal deposits leads to the hypothesis that these structures are involved in microbe-metal interactions.

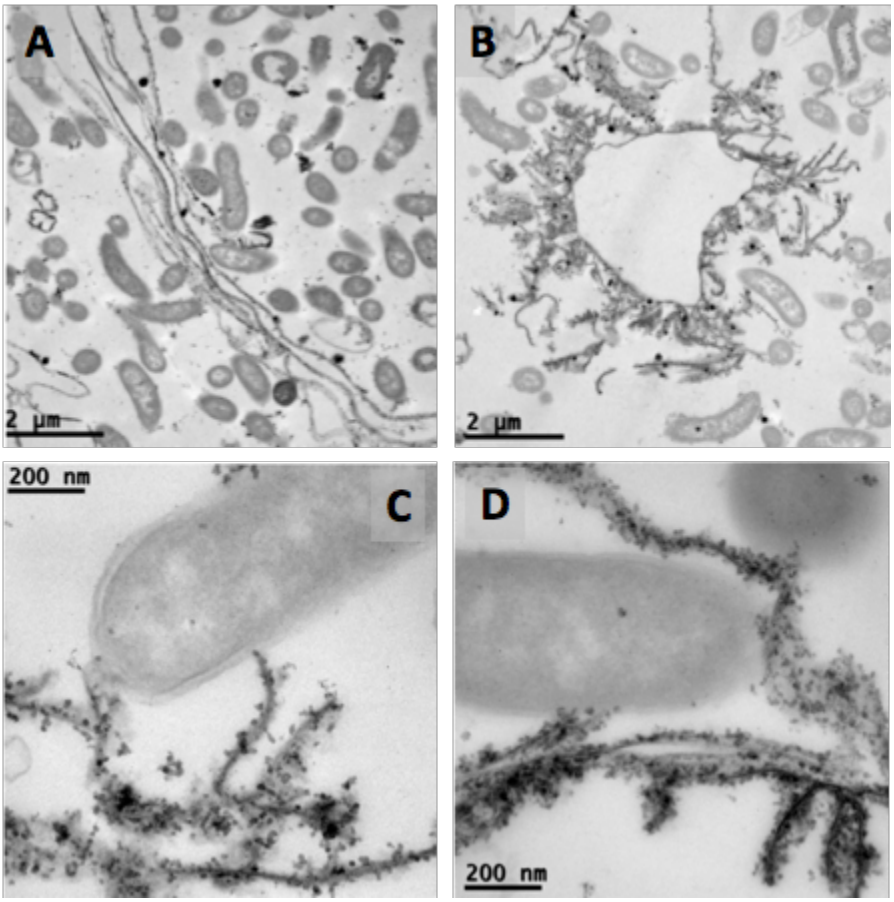


Figure 2. TEM images of *D. vulgaris* biofilm thin sections showing extracellular membrane structures. EMs vary in shape and size (A, B), connect with cells, and are associated with metal deposits (C, D).

Large Volume 3D SBF/SEM Imaging

Based on the 2D TEM imaging, it appeared that the extracellular structures extended three-dimensionally throughout the biofilm. To visualize the structures in 3D, we employed serial block face (SBF)-SEM. As observed in Figure 3a, which represents one of over 3,000 slices of the reconstructed 3D volume, metal deposits adopt lamellar,

spherical and/or barrel-like shapes (Figure 3a-c). The barrel-like shape of the metal deposit becomes clearer upon 3D rendering of approximately 3 µm of the respective volume (Figure 3d-f). For the sake of clarity only an approximately 1 µm thin central slab of the bacteria is rendered, illustrating their close proximity to the metal deposit (Figure 3f).

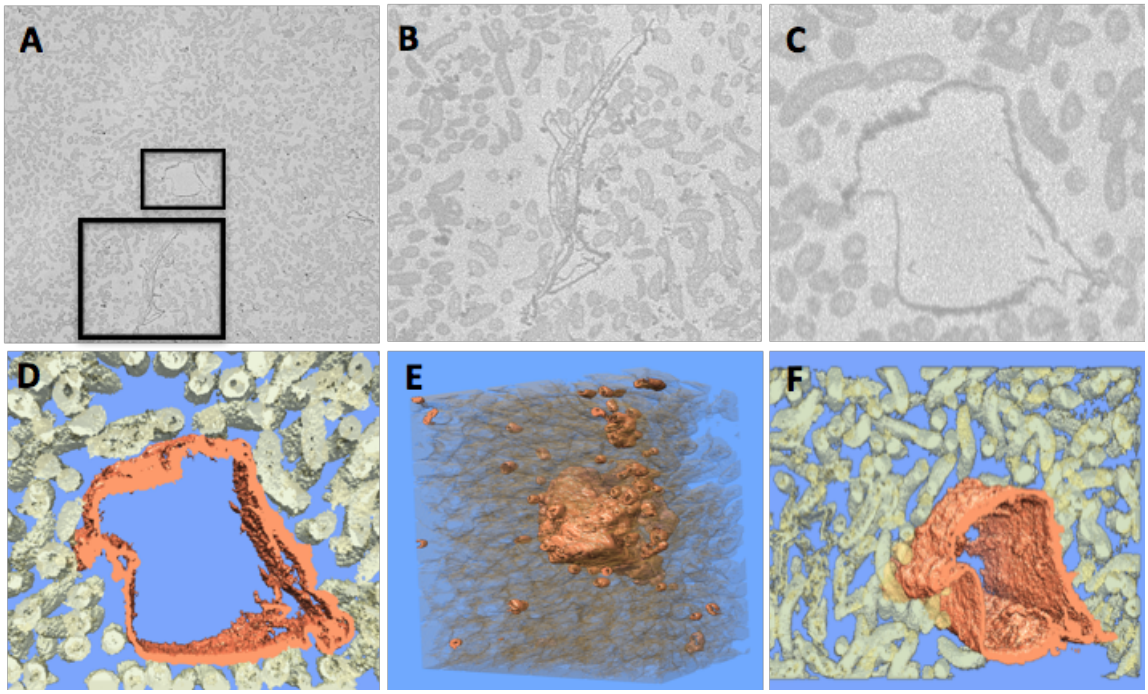


Figure 3. Thin sections of biofilm show extracellular membrane structures within the biofilm (B and C are magnifications of features in A). 3D renderings of extracellular membrane structures within the biofilm (D, E, F).

A 3D rendering of a 40µm x 40µm x 100µm sample of biofilm showed densely packed bacterial cells, extracellular structures, and metal deposits buried within the biofilm (Figure 4a). When the cells and extracellular structures are removed, leaving only the metal deposits, the heterogeneous distribution of the metal deposits throughout

the biofilm is apparent (Figure 4b). The extracellular structures shown in Figure 4b, extend through the entire 3D volume, thus extending for approximately 15 µm in the XY direction and at least 100 µm in the Z direction. Additionally, vesicular objects were observed nearby extracellular structures, with some vesicles apparently being in intimate contact or being in the process of and/or having fused with these objects. These presumptive vesicles are further investigated in Chapter 5.

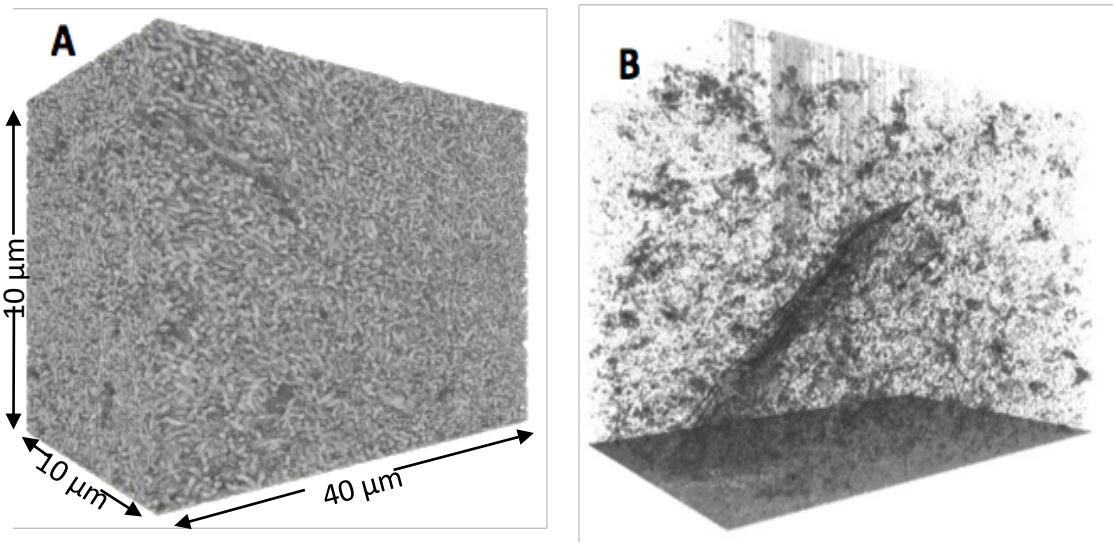


Figure 4. 3D reconstruction of 40 x 40 x 100 µm section of biofilm based on SBF imaging (A) and the same section with cells removed and only metal precipitates remaining (B).

Elemental Analysis of Extracellular Metal Deposits

Having determined that extracellular metal deposits are localized to thin lamellar sheets or stacks of sheets, which can connect to bacterial outer membranes and that can extend for at least 100 micrometers throughout a biofilm, the elemental composition of

the metal deposits were determined using line-profile dispersive X-ray spectroscopy scanning transmission electron microscopy (EDS STEM) imaging of non-osmicated, resin-embedded samples (Figure 5). The EDS STEM imaging line profiles (Figure 5c, e) showed very little background on the resin, but showed clear peaks that corresponded well with metal deposits (Figure 5d, f). Surprisingly, iron, oxygen and phosphorus, but no sulfur peak (Figures 5d, f) nor other commonly found elements such as nitrogen, carbon or chlorine was detected. This suggests, contrary to prior expectations, that metal deposits predominantly consist of iron oxides and possibly iron phosphates, but not iron sulfide, despite the presence of dissolved and precipitated sulfide detected within the biofilm during the experiment (Chapter 3) and abundance of H_2S gas throughout the experiment.

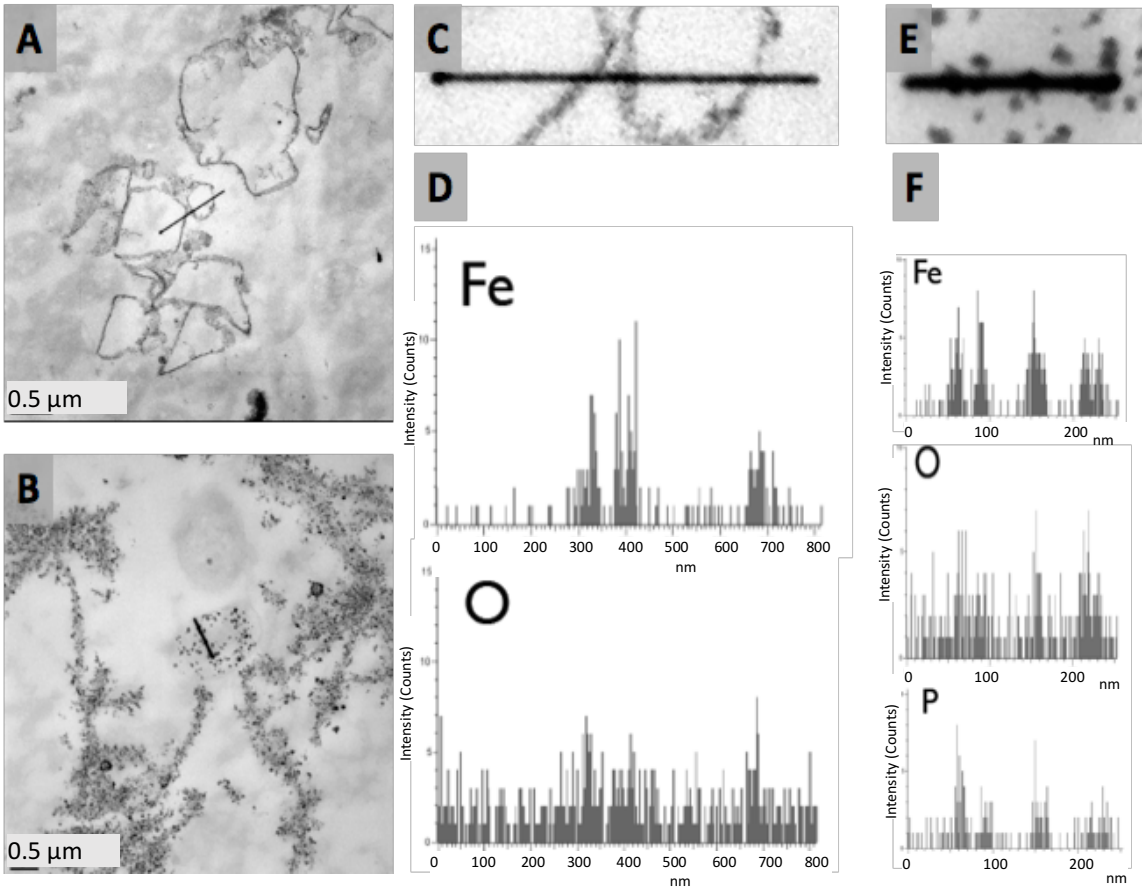


Figure 5. EDS elemental of metal precipitates associated with two different instances extracellular membranes within *D. vulgaris* biofilm (A, B). Path of analysis follows the lines shown in C, E and elemental composition is shown along the path in D, F.

Underlying Metal Deposition Sites are Biological Membranes

The images showing the connection between bacterial cellular membranes and the extracellular structures lead to the hypothesis that the structures may be composed of biological lipid membranes. In order to test this hypothesis, biofilm samples were differentially stained prior to resin-embedding. Unstained or uranyl acetate-only-stained samples reveal a ~10 nm gap between adjacent metal deposits (Figure 6a), whereas

osmicated samples did not display such a gap but instead a continuous filamentous structure onto which metal nanocrystals are deposited (Figure 6b). Additionally, ~5µm serial thick cryo-stat sections of unstained, frozen biofilm samples that were stained with the lipophilic dye, FM1-43, exhibited patterns of fluorescent structures (Figure 6d) that appeared to constitute a large portion of the biofilm matrix, consistent with the hypothesis that these structures are of biological lipid membrane origin. Ruthenium Red staining of biofilm samples (Figure 6e) showed very little to no carbohydrate associated with the extracellular structures under investigation compared to the control stained with osmium tetroxide and uranyl acetate only (Figure 6c).

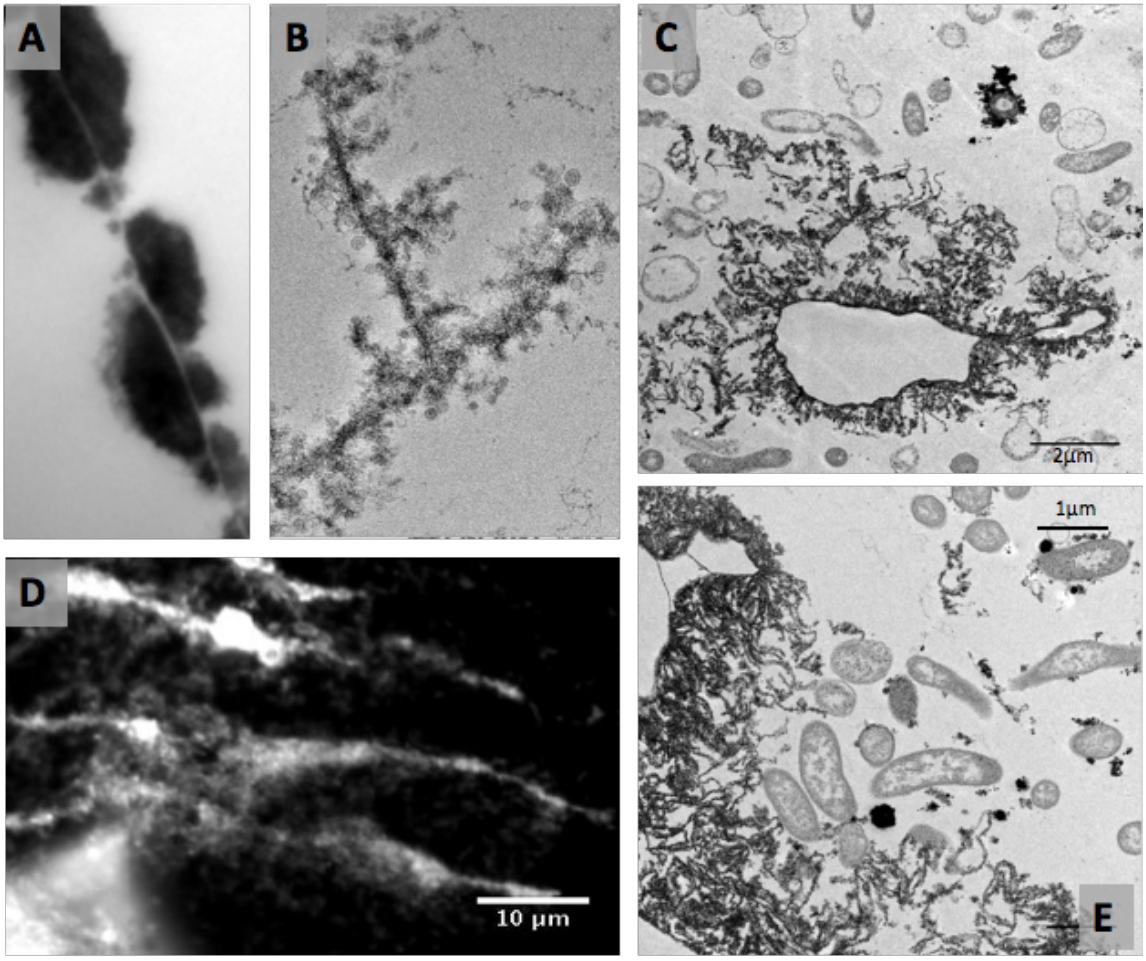


Figure 6. Differential staining of extracellular membranes. Uranyl acetate only stained structure (A), followed by osmium tetroxide and uranyl acetate stained structure (B). Ruthenium red stained thin section (E), compared to control (osmium tetroxide and uranyl acetate) (C). Staining with lipophilic fluorescent dye FM1-43 (D).

Because the differential staining evidence supports the hypothesis that the structures are lipid based, and because we qualitatively observed that there were more and larger structures produced under the EAL condition, total fatty acid methyl ester (FAME) content of biofilm grown under EAL and balanced conditions was quantified to

determine if there was a difference in fatty acid content. FAME content in DvH biofilms grown under the EAL condition was three times higher as compared to biofilm grown under balanced conditions when normalized to dry weight (18.9±0.36% vs. 6.38±0.59% dry weight) (Figure 7). The increase in fatty acid production under electron acceptor limitation is also biofilm specific, with planktonic cultures grown under balanced and electron acceptor limitation both yielding approximately 5-6% FAME per dry weight.

Due to the concern that the higher FAME content and presence of larger extracellular membranous structures for biofilm grown under the EAL condition could be due to a greater number of aggregated membrane material from dead cells under this condition compared to the BAL condition, cell viability between the three conditions was also tested. There was no statistically significant difference in viability between the EAL, BAL, and EDL conditions (Figure 8), indicating that the higher FAME content and larger, more extensive, membranous structures are not merely a consequence of decreased cell viability under the EAL condition.

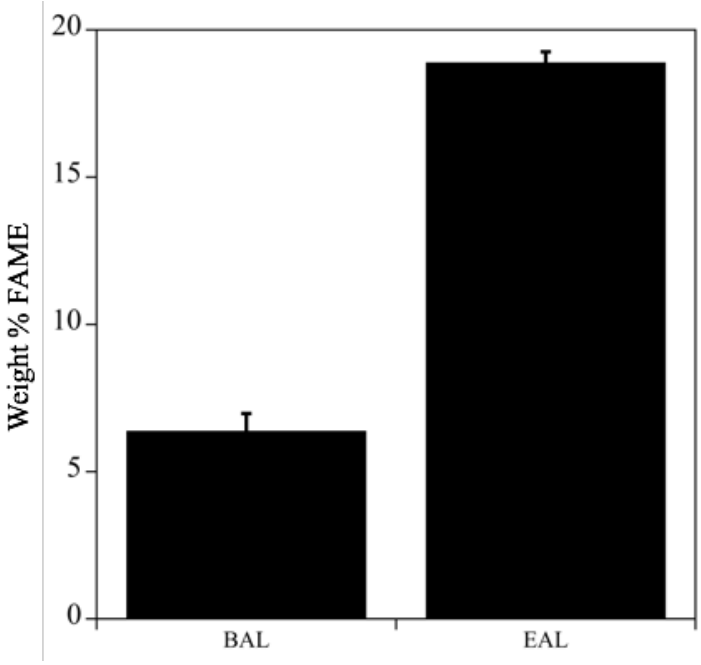


Figure 7. Weight percent of FAME content in dry weight of *D. vulgaris* biofilm grown under EAL and BAL conditions.

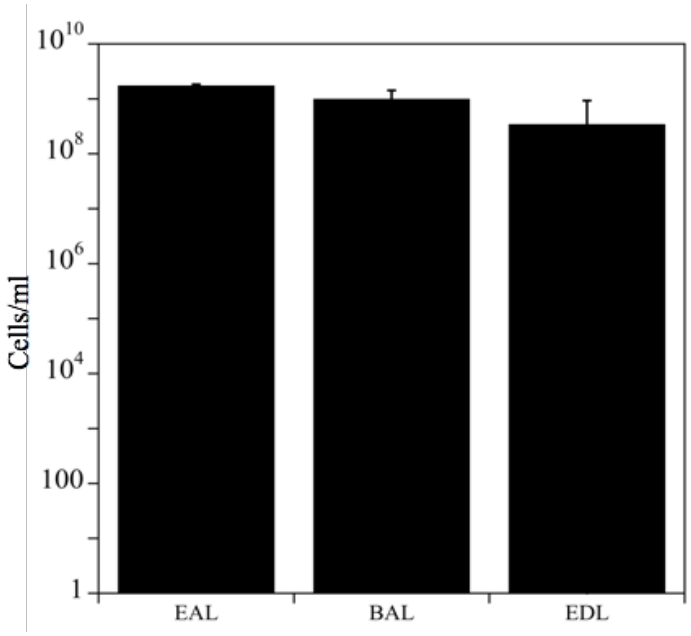


Figure 8. Viability (cells/ml) of scraped and homogenized biofilm grown under EAL, BAL, and EDL conditions normalized by optical density.

The Effect of Nutrient Limitation on Cr(VI) Toxicity in *D. vulgaris* Biofilm

Because *D. vulgaris* grown planktonically under EAL conditions was more susceptible to Cr(VI) toxicity compared to BAL conditions, as was shown in Chapter 2, the effect of Cr(VI) on *D. vulgaris* biofilm was investigated here. Measuring the biotic effect of heavy metal toxicity on sulfate-reducing biofilms is inherently difficult because the concentration of sulfide within the biofilm is so high that at field relevant levels of Cr(VI), most if not all of the Cr(VI) reduction will be abiotic. In a natural system, growth and therefore sulfide production may be slower, and other organisms may be utilizing the sulfide produced by the SRB, so understanding biological Cr(VI) reduction and toxicity is still warranted. The effect of Cr(VI) on *D. vulgaris* biofilm was investigated in two ways: the first with scraped, homogenized biofilm, and the second with intact biofilm. Scraping and homogenizing the biofilm was advantageous because more of the sulfide could be removed via washing of the cell pellet. Removing sulfide from the intact biofilm was not possible, and therefore the Cr(VI) concentration was 10-fold higher than that for the scraped and homogenized cells.

The lag time for scraped, homogenized *D. vulgaris* biofilm cells was ~75 hours for cells grown under both EAL or BAL conditions (Figure 9). This differed from the results presented in Chapter 2 in that there was no difference in lag time between the two conditions and the lag time was much shorter (approximately half) than the data presented in Chapter 2. The intact biofilm had a log reduction of 0.9±0.19 for cells

grown under the BAL condition and 0.5±0.37 for cells grown under the EAL condition, suggesting that cells growing under the BAL condition were slightly more susceptible to Cr(VI) toxicity than cells grown under the EAL condition (mixed effects ANOVA, p-value=0.06). It should also be noted that the biofilm grown under EAL and BAL conditions was exposed to the same concentration (500 μM) of Cr(VI) even though the biofilm grown under BAL contained approximately twice as many cells compared to biofilm grown under the EAL condition, so EAL biofilm had a higher concentration of Cr(VI) per cell, but a smaller log reduction compared to the BAL biofilm. Biofilm grown under the BAL condition also has a higher concentration of sulfide (Chapter 3), meaning that there was a higher potential for abiotic Cr(VI) reduction under the BAL condition. The results suggest that nutrient limitation/resource ratio affect Cr(VI) toxicity in the biofilm growth mode and this finding should be further investigated, especially given that this result was opposite of the results presented in Chapter 2 in which planktonic cells grown under the EAL condition were more susceptible to Cr(VI) compared to those grown under the BAL condition.

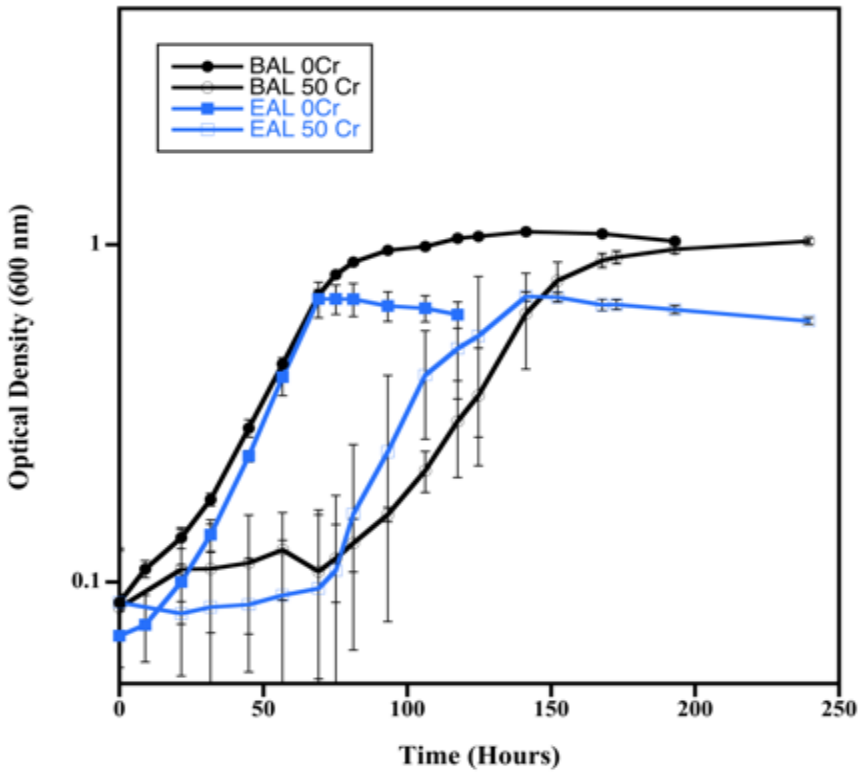


Figure 9. Planktonic growth of scraped and homogenized *D. vulgaris* biofilm grown under EAL (squares) and BAL (circles) conditions with 0 (filled) or 50 (empty) µM Cr(VI).

To determine if there was a difference in cytochrome quantity for biofilm grown under EAL compared to BAL that could help explain the difference in Cr(VI) toxicity between biofilm grown under EAL and BAL, cytochromes from purified periplasmic fractions was stained on a protein gel and visually compared and heme content was measured. There was a slight difference in band intensity of the two bands corresponding to cytochrome c at ~14 kDa (Figure 10), with the band associated with the BAL conditions being slightly darker. To determine if there was a quantifiable difference

between the two conditions, heme concentration was measured and compared in biofilm grown under EAL and BAL conditions. There was no difference in heme concentration between the two conditions (0.013 ± 0.004 µg heme/µg protein for BAL and 0.015 ± 0.005 µg heme/µg protein for EAL).

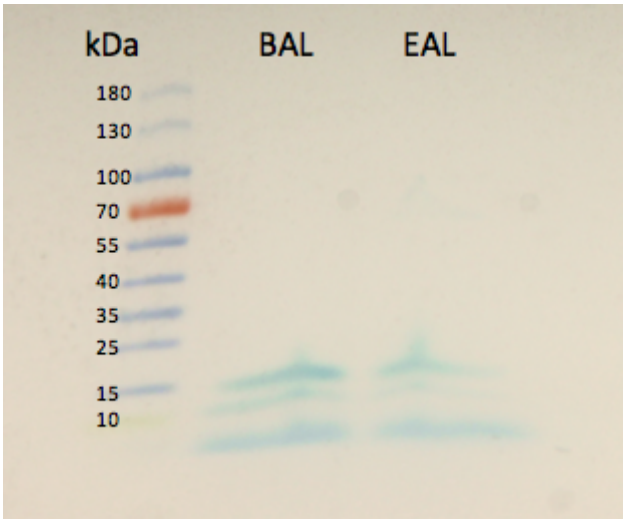


Figure 10. Protein gel showing ladder in kilodaltons (kDa) on right and stained cytochrome c at ~14-15 kDa from biofilm grown under BAL and EAL conditions.

Discussion

Hardiness of biofilm cells can be attributed to the distinct physiological state of cells existing and growing in the biofilm growth mode and also to the secreted matrix components that interact with surfaces and the external environment. The biofilm EPS is an all-inclusive term for the extracellular macromolecules that enable cells to adhere to surfaces and each other, and the understanding of the biofilm matrix has progressed to include, but are not limited to polysaccharides, extracellular DNA, membrane vesicles,

cell debris from lysed cells, enzymes, and structural proteins (reviewed in Flemming and Wingender, 2010). While some of these components have been identified and a function established for a particular species, there are still many matrix components that have not been identified or described, including membrane vesicles and related structures, particularly for environmental microorganisms. Membrane vesicles (MVs) in *Bacteria* and *Archaea* studied to date can play roles in nutrient acquisition, biofilm development, and pathogenesis dependent upon the organism (Schooling and Beveridge, 2006; Kulp and Kuehn, 2010; Manning and Kuehn, 2013). Moreover, the biofilm matrix is increasingly recognized to contain a variety of intra- and inter-matrix interactions that contribute and may control biofilm behavior (Schooling and Beveridge, 2006; Payne and Boles, 2016), and Manning and Kuehn (2013) likened the activity of MVs to that of intracellular membrane-bound processes. More recently, Hooper and Burstein posited that the minimization of extracellular space in prokaryotic (*i.e.*, *Bacteria* and *Archaea*) biofilms promoted cellular associations that impacted metabolism and may have contributed to the evolution of *Eukarya* (Hooper and Burstein 2014).

Identification of extracellular matrix components in biofilms is integral to our understanding of how biofilms form, persist, and evolve. The results of this study show that membranous structures contribute a previously unrecognized portion of the extracellular matrix of *D. vulgaris* biofilms. These structures connect to and are continuous with cellular membranes and the use of lipophilic dyes, metabolomic analyses, and fatty acid quantification support the hypothesis that these structures are

lipid-like in composition. The connection of these structures to the outer membrane of structurally intact, and hence presumably viable bacteria is highly significant as it suggests a metabolic connection to membrane structures and possibly neighboring bacteria. Metal precipitates co-localize with the membrane structures, and these observations suggest the structures may be involved in microbe-metal interactions. One possible function that these structures may fulfill is a mechanism to sequester metal precipitates away from the cell. A mechanism to remove or reduce metals away from the cell body would be beneficial given that planktonic *D. vulgaris* cells have been shown to accumulate reduced, precipitated Cr(III) in the periplasmic space along membranes, potentially encasing themselves (Goulhen et al. 2006). Given that the reduction of certain metals, such as Cr(VI), is not linked to growth for *D. vulgaris*, but is rather an energy-costing detoxification strategy (Chardin et al. 2002), the ability to reduce metals away from the cell body may be advantageous. Isolated *Shewanella* EPS has been shown to reduce U(VI), suggesting that this may be a strategy of metal-reducing bacteria (Cao et al. 2011).

Based on the idea that the extracellular structures could play a role in metal reduction, the effect on Cr(VI) toxicity on biofilm grown under EAL and BAL conditions was investigated. Given that there were more extensive extracellular membranes, three times more measured FAME content, and upregulated fatty acid metabolites observed in biofilms grown under the EAL condition, we hypothesized that biofilm grown under the EAL condition would be less susceptible to Cr(VI) toxicity compared to the BAL

condition. Scraped and homogenized biofilm cells grown under EAL and BAL conditions had similar lag-times (~75 hours) when exposed to 50 μM Cr(VI), which contradicted the results from Chapter 2 in which planktonic cells grown under the EAL condition were more susceptible to Cr(VI) toxicity. An overall shorter lag-time for biofilm cells is in agreement with the many reports of biofilm cells being more resistant to heavy metal stresses compared to planktonic cells. It is interesting to note that even when the structure of the biofilm is removed, the cells were still somewhat protected from Cr(VI) toxicity compared to planktonic cells. Previous results have shown that biofilm growth is a unique physiological state compared to planktonic (Clark et al., 2012), and the current results show that biofilms grown under different energy conditions (BAL vs. EAL) have different physiological responses to Cr(VI) even when intact biofilm structure is removed.

When intact *D. vulgaris* biofilm grown under EAL and BAL conditions were exposed to high concentrations of Cr(VI) to overcome abiotic Cr(VI) reduction, the cells grown under the BAL condition had a greater log-reduction of viable cells than those grown under the EAL condition. While the difference in log-reduction between the two conditions was not statistically significant at a p-value of 0.05, the finding is suggestive that in the biofilm growth mode, the EAL condition might confer increased resistance to Cr(VI) toxicity and warrants further investigation. It should be noted that BAL biofilms typically contain more sulfide than EAL biofilms and thus, EAL biofilms were likely more tolerant to Cr(VI) exposure.

Elemental analysis of extracellular membrane associated metal precipitates surprisingly did not show the presence of sulfur compounds, but rather iron oxides and iron phosphates. Interestingly, iron and phosphorus were also prevalent in the extracellular glycocalyx-like structures that *Shewanella oneidensis* MR-1 produces and the iron and phosphorus were closely associated with reduced UO_2 particles. The authors suggest that the iron was present due to heme containing proteins that were involved in the uranium reduction (Marshall et al. 2006). Additionally, intracellular membrane encapsulated iron-phosphorus granules have been reported in *Desulfovibrio magneticus* RS-1. These iron-phosphorus granules are distinct from the magnetite crystals but possible functions are unknown (Byrne et al. 2010). While quite different in lineage and growth conditions, these three findings together support a possible biological role of iron-phosphates in dissimilatory metal reducing bacteria that call for additional research.

Other components of *D. vulgaris* biofilm matrix have been analyzed in previous work as well as this one. In agreement with Clark et al. (Clark et al. 2007a; Clark et al. 2012), we observed that extracellular carbohydrate was not a significant part of the biofilm matrix under any of the tested nutrient ratios. Although carbohydrate is detected in whole biofilm samples (cells and extracellular materials), little carbohydrate is detected extracellularly by carbohydrate-sensitive staining. Extracellular proteins have been shown to be integral to biofilm formation and maintenance, and a proteomic analysis of *D. vulgaris* biofilm grown under different conditions from this study (60mM lactate, 50mM sulfate, 30°C) detected 188 extracellular proteins (Clark et al. 2007b;

Clark et al. 2012). Extracellular DNA has been shown to be important for biofilm formation and structure in other organisms, but DNase treatment of *D. vulgaris* biofilms did not affect structural integrity (data not shown). Membrane vesicles have also been observed in close association with cells and extracellular membranes in *D. vulgaris* biofilms and are the subject of Chapter 5.

In addition to the presence of extracellular membranes in the matrix, this study also highlighted how SRB biofilms respond to nutrient limitation. The lipid analysis revealed that the EAL biofilm produces approximately three times more fatty acids than the BAL biofilm. Also, metabolomic analysis from Chapter 3 showed an upregulation of fatty acid metabolites under the EAL condition. This indicates that sulfate limitation causes cells to shift to a lipid storing/excreting metabolism. Further, metabolic analysis shows that limiting sulfate causes dysregulation of 3303 metabolites (fold change $\geq$ 1.5, p-value $\leq$ 0.01), suggesting that many metabolic pathways are altered to cope with the limitation of sulfate. Previous studies have shown *Desulfovibrio* spp. response to electron acceptor limitation (Okabe et al. 1992; Villanueva et al. 2008), but none have investigated effects of electron acceptor limitation in a biofilm growth mode.

One of the key distinctions of this study is that it is by far the largest 3D volume of a bacterial biofilm ever studied at high resolution. This was possible by using a new 3D EM technology known as Serial Block Face Scanning Electron Microscopy, where 40 microns by 40 microns in XY have been recorded at ~10 nm stepsize, and ~100 microns

has been recorded at ~30 nm stepsize, using iterative SEM imaging of the block surface and subsequent removal of the block surface with a diamond knife. Likewise, correlative optical microscopy and 2D TEM was utilized to image toluene blue stained ~1 micron or unstained ~70 nm ultrathin sections, which allowed the study of biofilm on a larger scale. Identifying the frequency and locations of significant extracellular metal deposits by optical microscopy enabled qualitative observations to be made and then studied in much more detail by TEM analysis and other quantitative methods. The multiscale imaging analysis was key to this study, as metal deposits are highly heterogeneous; therefore, it was key to first gain an overview image of the entire biofilm, before examining certain areas at higher resolution. This result is also significant for bulk omic/chemical/analytical analysis, which is widely employed for many different environments and systems, but may be insufficient to detect highly significant local differences that only manifest themselves in a small fraction of sampled volume. The results presented here support the argument that bulk scale analysis may miss micro-environmental characteristics that could be significant for microbial biofilms.

REFERENCES CITED

Abramoff, Magalhães PJ, Ram SJ (2004) Image Processing with ImageJ. Biophotonics International 11:36–42.

Anderson RT, Vrionis HA, Ortiz-Bernad I, Resch CT, Long PE, Dayvault R, Karp K, Marutzky S, Metzler DR, Peacock A, White DC, Lowe M, Lovley DR (2003) Stimulating the in situ activity of Geobacter species to remove uranium from the groundwater of a uranium-contaminated aquifer. Appl Environ Microbiol 69:5884–5891.

Badzjong W, Thauer RK (1980) Vectorial electron transport in Degulfovibrio vulgaris (Marburg) growing on hydrogen plus sulfate as sole energy source. Arch Microbiol 125:167–174.

Baumgarten A, Redenius I, Kranczoch J, Cypionka H (2001) Periplasmic oxygen reduction by Desulfovibrio species. Arch Microbiol 176:306–309.

Borglin S, Joyner D, Jacobsen J, Mukhopadhyay A, Hazen TC (2009) Overcoming the anaerobic hurdle in phenotypic microarrays: generation and visualization of growth curve data for Desulfovibrio vulgaris Hildenborough. J Microbiol Methods 76:159–168.

Brandis A, Thauer RK (1981) Growth of Desulfovibrio species on hydrogen and sulphate as sole energy source. Microbiology 126:249–252.

Byrne ME, Ball DA, Guerquin-Kern J-L, Rouiller I, Wu T-D, Downing KH, Vali H, Komeili A (2010) Desulfovibrio magneticus RS-1 contains an iron- and phosphorus-rich organelle distinct from its bullet-shaped magnetosomes. Proc Natl Acad Sci U S A 107:12263–12268.

Cao B, Ahmed B, Kennedy DW, Wang Z, Shi L, Marshall MJ, Fredrickson JK, Isern NG, Majors PD, Beyenal H (2011) Contribution of Extracellular Polymeric Substances fromShewanellasp. HRCR-1 Biofilms to U(VI) Immobilization. Environ Sci Technol 45:5483–5490.

Castelle CJ, Hug LA, Wrighton KC, Thomas BC, Williams KH, Wu D, Tringe SG, Singer SW, Eisen JA, Banfield JF (2013) Extraordinary phylogenetic diversity and metabolic versatility in aquifer sediment. Nat Commun 4:2120.

Chardin B, Dolla A, Chaspoul F, Fardeau ML, Gallice P, Bruschi M (2002) Bioremediation of chromate: thermodynamic analysis of the effects of Cr(VI) on sulfate-reducing bacteria. Appl Microbiol Biotechnol 60:352–360.

Clark ME, Edelmann RE, Duley ML, Wall JD, Fields MW (2007a) Biofilm formation in

Desulfovibrio vulgaris Hildenborough is dependent upon protein filaments. Environ Microbiol 9:2844–2854.

Clark ME, Edelmann RE, Duley ML, Wall JD, Fields MW (2007b) Biofilm formation in Desulfovibrio vulgaris Hildenborough is dependent upon protein filaments. Environ Microbiol 9:2844–2854.

Clark ME, He Z, Redding AM, Joachimiak MP, Keasling JD, Zhou JZ, Arkin AP, Mukhopadhyay A, Fields MW (2012) Transcriptomic and proteomic analyses of Desulfovibrio vulgaris biofilms: carbon and energy flow contribute to the distinct biofilm growth state. BMC Genomics 13:138.

Coleman DC, Whitman WB (2005) Linking species richness, biodiversity and ecosystem function in soil systems. Pedobiologia 49:479–497.

Danovaro R, Gambi C, Dell'Anno A, Corinaldesi C, Fraschetti S, Vanreusel A, Vincx M, Gooday AJ (2008) Exponential decline of deep-sea ecosystem functioning linked to benthic biodiversity loss. Curr Biol 18:1–8.

Denk W, Horstmann H (2004) Serial block-face scanning electron microscopy to reconstruct three-dimensional tissue nanostructure. PLoS Biol 2:e329.

Duffy JE, Stachowicz JJ (2006) Why biodiversity is important to oceanography: potential roles of genetic, species, and trophic diversity in pelagic ecosystem processes. Mar Ecol Prog Ser 311:179–189.

Dunne WM Jr (2002) Bacterial adhesion: seen any good biofilms lately? Clin Microbiol Rev 15:155–166.

Flemming H-C, Wingender J (2010) The biofilm matrix. Nat Rev Microbiol 8:623–633.

Gorby YA, Yanina S, McLean JS, Rosso KM, Moyles D, Dohnalkova A, Beveridge TJ, Chang IS, Kim BH, Kim KS, Culley DE, Reed SB, Romine MF, Saffarini DA, Hill EA, Shi L, Elias DA, Kennedy DW, Pinchuk G, Watanabe K, Ishii S 'ichi, Logan B, Nealson KH, Fredrickson JK (2006) Electrically conductive bacterial nanowires produced by Shewanella oneidensis strain MR-1 and other microorganisms. Proc Natl Acad Sci U S A 103:11358–11363.

Goulhen F, Gloter A, Guyot F, Bruschi M (2006) Cr(VI) detoxification by Desulfovibrio vulgaris strain Hildenborough: microbe-metal interactions studies. Appl Microbiol Biotechnol 71:892–897.

Gross R, Hauer B, Otto K, Schmid A (2007) Microbial biofilms: new catalysts for

maximizing productivity of long-term biotransformations. Biotechnol Bioeng 98:1123–1134.

Hall-Stoodley L, Costerton JW, Stoodley P (2004) Bacterial biofilms: from the natural environment to infectious diseases. Nat Rev Microbiol 2:95–108.

Hooper SL, Burstein HJ (2014) Minimization of extracellular space as a driving force in prokaryote association and the origin of eukaryotes. Biol Direct 9:24.

Jarvis B, Wilrich C, Wilrich P-T (2010) Reconsideration of the derivation of Most Probable Numbers, their standard deviations, confidence bounds and rarity values. J Appl Microbiol 119:905.

Karl DM, Church MJ, Dore JE, Letelier RM, Mahaffey C (2012) Predictable and efficient carbon sequestration in the North Pacific Ocean supported by symbiotic nitrogen fixation. Proc Natl Acad Sci U S A 109:1842–1849.

Kolter R (2005) Surfacing views of biofilm biology. Trends Microbiol 13:1–2.

Lohman EJ, Gardner RD, Halverson L, Macur RE, Peyton BM, Gerlach R (2013) An efficient and scalable extraction and quantification method for algal derived biofuel. J Microbiol Methods 94:235–244.

Marshall MJ, Beliaev AS, Dohnalkova AC, Kennedy DW, Shi L, Wang Z, Boyanov MI, Lai B, Kemner KM, McLean JS, Reed SB, Culley DE, Bailey VL, Simonson CJ, Saffarini DA, Romine MF, Zachara JM, Fredrickson JK (2006) c-Type cytochrome-dependent formation of U(IV) nanoparticles by Shewanella oneidensis. PLoS Biol 4:e268.

McDonald KL, Morphew M, Verkade P, Müller-Reichert T (2007) Recent advances in high-pressure freezing: equipment- and specimen-loading methods. Methods Mol Biol 369:143–173.

McDONALD KL, Webb RI (2011) Freeze substitution in 3 hours or less. J Microsc 243:227–233.

McDonald K, Müller-Reichert T (2002) Cryomethods for thin section electron microscopy. Methods Enzymol 351:96–123.

McKew BA, Taylor JD, McGenity TJ, Underwood GJC (2011) Resistance and resilience of benthic biofilm communities from a temperate saltmarsh to desiccation and rewetting. ISME J 5:30–41.

Müller-Reichert T, Hohenberg H, O'Toole ET, McDonald K (2003) Cryoimmobilization and three-dimensional visualization of C. elegans ultrastructure. J Microsc 212:71–80.

Okabe S, Nielsen PH, Characklis WG (1992) Factors affecting microbial sulfate reduction by Desulfovibrio desulfuricans in continuous culture: Limiting nutrients and sulfide concentration. Biotechnol Bioeng 40:725–734.

Pirbadian S, Barchinger SE, Leung KM, Byun HS, Jangir Y, Bouhenni RA, Reed SB, Romine MF, Saffarini DA, Shi L, Gorby YA, Golbeck JH, El-Naggar MY (2014) Shewanella oneidensis MR-1 nanowires are outer membrane and periplasmic extensions of the extracellular electron transport components. Proc Natl Acad Sci U S A 111:12883–12888.

Remis JP, Wei D, Gorur A, Zemla M, Haraga J, Allen S, Witkowska HE, Costerton JW, Berleman JE, Auer M (2014) Bacterial social networks: structure and composition of Myxococcus xanthus outer membrane vesicle chains. Environ Microbiol 16:598–610.

Stewart PS, Franklin MJ (2008) Physiological heterogeneity in biofilms. Nat Rev Microbiol 6:199–210.

Stylo M, Neubert N, Roebbert Y, Weyer S, Bernier-Latmani R (2015) Mechanism of Uranium Reduction and Immobilization in Desulfovibrio vulgaris Biofilms. Environ Sci Technol 49:10553–10561.

Thomas PE, Ryan D, Levin W (1976) An improved staining procedure for the detection of the peroxidase activity of cytochrome P-450 on sodium dodecyl sulfate polyacrylamide gels. Anal Biochem 75:168–176.

Villanueva L, Haveman SA, Summers ZM, Lovley DR (2008) Quantification of Desulfovibrio vulgaris Dissimilatory Sulfite Reductase Gene Expression during Electron Donor- and Electron Acceptor-Limited Growth. Appl Environ Microbiol 74:5850–5853.

Whitman WB, Coleman DC, Wiebe WJ (1998) Prokaryotes: the unseen majority. Proc Natl Acad Sci U S A 95:6578–6583.

CHAPTER FIVE

OUTER MEMBRANE VESICLES AND ASSOCIATED PROTEINS PRODUCED BY *DESULFOVIBRIO VULGARIS* HILDENBOROUGH BIOFILMS

Contribution of Authors and Co-Authors

Author: Lauren Franco

Contributions: Developed experimental design, performed experiments, analyzed results, wrote and revised manuscript.

Co-Author: Chris Petzold

Contributions: Proteomic data acquisition, data analysis

Co-Author: Matthew W. Fields

Contributions: Developed experimental design, analyzed results, wrote and revised manuscript.

Manuscript Information Page

Lauren C. Franco, Chris Petzold, Mathew W. Fields

Applied Microbiology and Microbiology

Status of Manuscript:
__x__ Prepared for submission to a peer-reviewed journal
____ Officially submitted to a peer-review journal
____ Accepted by a peer-reviewed journal
____ Published in a peer-reviewed journal

Abstract

Outer membrane vesicles (OMVs) have been observed in *Desulfovibrio vulgaris* Hildenborough cultures, but their function is unknown. OMVs produced by other bacteria and archaea have a wide variety of functions and have been well studied in pathogenic bacteria, but are understudied in non-pathogenic organisms. Further, OMVs produced by biofilms have been shown to be distinct in protein content compared to their planktonic counterparts. In this study, OMVs were isolated from *D. vulgaris* biofilms grown under electron acceptor-limitation (EAL) and electron donor/electron acceptor balanced (BAL) conditions. Isolated OMVs were between 20-60 nm in diameter and OMV fractions also contained tube structures that appeared to be precursors to individual OMVs. Proteins in the isolated OMV fractions were identified by untargeted shotgun proteomics and revealed expected outer membrane and periplasmic components such as lipoproteins and porins. Proteins involved in oxidative stress and two hydrogenases were also detected in OMVs, suggesting a potential function for OMVs in *D. vulgaris*. Differences in abundance of the proteins detected between OMVs isolated from biofilm grown under EAL vs. BAL conditions were not detectable, but more biological replicates in the future may resolve this issue. Future studies might also incorporate metabolomic analysis to identify and unique metabolites that are contained within OMVs.

Introduction

Sulfate reducing bacteria are ubiquitous in the environment and play pivotal roles in natural and industrial processes such as biogeochemical cycling, biocorrosion, and bioremediation. Many of these processes involve the formation of biofilms by these microorganisms (Truper 1984; Neria-González et al. 2006; Liu et al. 2007; Marsili et al. 2007). *Desulfovibrio vulgaris* Hildenborough is a well-characterized model organism for sulfate reducing bacteria that has been studied in biofilm growth mode. It has been shown that *D. vulgaris* exhibits a distinct gene expression pattern when growing as a biofilm as opposed to the different phases of planktonic growth and some of these differences are due to the cellular production of biofilm matrix components (Clark et al. 2007; Clark et al. 2012).

The biofilm matrix can consist of many different components such as carbohydrates, proteins, lipids, pili and flagella, DNA, and outer membrane vesicles (OMVs) (Flemming and Wingender 2010). A variety of functions have been deduced from proteomic analyses of purified OMVs of many different organisms. These include, but are not limited to, DNA exchange, cell-cell communication, antibiotic resistance, heavy metal resistance, phage resistance, toxin release, and biofilm formation (Ciofu et al. 2000; Klieve et al. 2005; Mashburn and Whiteley 2005; Gorby et al. 2008; Yonezawa et al. 2009; Manning and Kuehn 2011; Guidi et al. 2013). Many of these studies have focused on pathogenic organisms and the role that OMVs play in pathogenesis and fewer

studies have examined the role that OMVs play in non-pathogenic bacteria. Further, there are very limited studies on how environmental changes or stress affects OMV production and composition, and the need for such work was emphasized in a recent review article (Orench-Rivera and Kuehn 2016).

While many studies have isolated and analyzed OMVs from planktonic cultures, relatively few studies have examined the function that OMVs have in biofilms. OMVs have been observed in naturally occurring biofilms in environments such as in a domestic sink drain, water treatment plants, and in a riverbed (Schooling and Beveridge 2006). Additionally, studies on cultured biofilms have shown that OMVs in biofilms are distinct compared to their planktonic counterparts. Schooling and Beveridge (2006) were the first to report on the differences between *Pseudomonas aeruginosa* OMVs from a biofilm versus planktonic cells: biofilms produced approximately 16 times more MVs according to dry weight, biofilm OMVs had smaller average diameters than planktonic OMVs, and SDS-PAGE analysis of biofilm and planktonic OMVs revealed different banding profiles, indicating potential differences in vesicle protein content. Further, protein composition in OMVs from *P. aeruginosa* biofilms differs from planktonic counterparts, pointing to differences in OMV function in biofilm versus planktonic produced OMVs (Park et al. 2015). *Helicobacter pylori* OMVs from biofilms have also been observed to be distinct from planktonic OMVs with biofilm produced OMVs containing double stranded DNA that is thought to contribute to biofilm structure and aggregation (Grande et al. 2015).

OMVs in *Desulfovibrio* species have been documented in the literature, but have yet to be purified and analyzed (Nanninga and Gottschal 1987). Given the role that sulfate reducing biofilms play in the natural environment and industrial processes, it is important to understand possible OMV functions in biofilms. Based upon observations of highly localized, extracellular membrane structures in *D. vulgaris* biofilms, we developed a method to determine if vesicles could be enriched from biofilm samples and potential protein content.

Materials and Methods

Bacterial Strains and Growth Conditions

Desulfovibrio vulgaris Hildenborough was obtained from Dr. Romy Chakraborty (Lawrence Berkeley National Lab). *D. vulgaris* was grown in LS4D medium, which contains lactate as the carbon source and electron donor and sulfate as the electron acceptor (Clark et al. 2006). Lactate and sulfate concentrations were altered to create balanced and electron acceptor limited conditions. The balanced condition was defined as 60 mM sodium lactate and 30 mM sodium sulfate and the electron acceptor limited condition was defined as 50 mM sodium lactate and 10 mM sodium sulfate. *D. vulgaris* was grown as a biofilm under continuous flow conditions in a modified CDC reactor. Exponential phase cells were inoculated into a reactor containing balanced or electron acceptor limited LS4D medium and were grown in batch mode for 48 hours. Reactors were grown at room temperature (20-23°C), with a dilution rate of 0.04^{-}

^{hr}, stirred at 60 rpm, and the headspace was continuously sparged with sterile N_2 gas to maintain anaerobic conditions. Coupons of glass slides were submerged in the reactor body as a surface for biofilm growth.

Isolation of outer membrane vesicles

Glass slides were removed from the reactor at 168 hours and biomass from each slide was aseptically scraped into a tube containing 1 ml 100mM HEPES buffer, pH 7.4. Scraped biomass was homogenized by vortexing for 5 minutes and then centrifuged at 12,000 x g for 20 minutes at 4°C. Supernatant was collected and kept on ice while the biomass pellet was resuspended in another 1 ml of HEPES buffer and the vortexing, centrifugation, and supernatant collection were repeated 2X. Supernatants were pooled, filtered through a 0.45 µm filter, then a 0.2 µm filter. Filtered supernatant was centrifuged at 125,000 x g for 1.5 hours to pellet OMVs and any other extracellular biofilm components. Pellets were resuspended in 45% optiprep (Sigma) in 100 mM HEPES buffer, pH 7.4. The samples were aliquoted into 5 ml ultracentrifuge tubes and optiprep in decreasing concentrations was layered on top (0.6 ml 45% with sample, 0.6 ml 40%, 0.8 ml 35%, 0.8 ml 30%, 0.8 ml 25%, 0.8 ml 20%, 0.4 ml 15%). Density gradients were centrifuged at 100,000 x g for 16 h at 4°C in a 30° fixed angle rotor (Thermo Scientific S110-AT rotor). Fractions were collected in 0.2 ml aliquots and screened for the presence of OMVs by transmission electron microscopy (TEM). Fractions containing isolated OMVs were concentrated via ultracentrifugation at

125,000 x g for 1.5 h, resuspended in 50 mM ammonium bicarbonate, flash frozen in liquid nitrogen, and stored at -80°C.

Transmission Electron Microscopy

Aliquots of the density gradient fractions (20 µl) was spotted on a 40nm silicon oxide membrane TEM grid (Ted Pella, Inc.), allowed to sit for 3 minutes, excess liquid wicked away, and then washed with sterile deionized water. After washing, samples were stained with 10 µl 2% w/v uranyl acetate for 1 min and then wicked dry. Samples were imaged on a Zeiss Leo 912AB transmission electron microscope.

Nucleic Acid Detection

The Qbit high sensitivity DNA assay kit (Life Technologies) was used according to the manufacturer's directions to measure DNA associated with OMVs. OMV samples were boiled at 95°C for 5 minutes prior to measuring to access any DNA held within the OMV.

Proteomic Analysis

An untargeted shotgun proteomics approach was taken for identifying peptides in isolated OMV samples. Proteins were extracted and precipitated from samples via a chloroform/methanol extraction protocol, digested with trypsin, and desalted according to established protocols (Parsons et al. 2013; González Fernández-Niño et al. 2015). Purified samples were analyzed on on an Agilent 6550 iFunnel Q-TOF mass

spectrometer (Agilent Technologies) coupled to an Agilent 1290 UHPLC system with the parameters described in (González Fernández-Niño et al. 2015) et al. (González Fernández-Niño et al. 2015). The 20 most intense ions within the 300-1,400 m/z mass range and above a threshold of 1,500 counts were selected for MS/MS analysis. MS/MS data was analyzed using Mascot (Matrix Biosciences) with the parameters listed in González Fernández-Niño et al. (2015) and matched with the annotated genome sequence of *D. vulgaris* Hildenborough (GenBank accession number AE017285 (chromosome) and AE017286 (plasmid)) (Heidelberg et al. 2004). Identified peptides were further analyzed with Scaffold (Proteome Software Inc.) and peptide identifications were accepted if they reached a >95% probability according to the Peptide Prophet algorithm (Keller et al. 2002). Protein identifications were accepted if the reached a >95% confidence according to the Protein Prophet algorithm and contained at least 1 identified peptide at >95% confidence (Nesvizhskii et al. 2003). To quantify protein abundance, total spectral counts were normalized to the amino acid length to account for total protein length, yielding a normalized spectral abundance factor (NSAF) (Zybailov et al. 2007).

Results and Discussion

Outer Membrane Vesicles and Tubes

Screening of density gradient fractions revealed that OMVs were found between 1.12 and 1.15 g/ml in the gradient. Surprisingly, density gradient fractions containing

OMVs also contained tubular structures that appeared to be OMV precursor structures, and observed OMV-tubes are presumed to be different stages of OMV development (Figure 1). In addition, numerous individual OMVs and tube structures with what look like OMVs forming at each end were observed (Figure 1). Further, OMVs in chain patterns can be observed, possibly individual OMVs in the process of forming from tube structures or tubes in the process of forming individual OMVs (Figure 1c). OMV-tube structures have been recently observed in other bacteria such as *Myxococcus xanthus*, *Francisella novicida*, and *Shewanella oneidensis* and more organisms may produce similar structures, but OMV isolation methods typically exclude the tube form from the enrichments *(Remis et al. 2013; McCaig et al. 2013; Pirbadian et al. 2014; Subramanian et al. 2016)*. Production of OMV-tubes instead of individual OMVs could be a "power in numbers" strategy that would guarantee a higher OMV concentration at a particular location rather than sending off individual OMVs with no control over localization or co-localization. OMVs varied in size between 20 to 60 nm in diameter and tubes were typically 20-30 nm in diameter. OMVs and OMV-tubes from *D. vulgaris* biofilms grown under EAL vs. BAL conditions did not differ in appearance.

Due to some reports of OMVs containing DNA and being involved in horizontal gene transfer, isolated *D. vulgaris* OMV fractions were tested for the presence of DNA (Pérez-Cruz et al. 2013; Fulsundar et al. 2014). DNA was measured before and after a boiling step (5 min) and detectable DNA was not measured in either instance, leading to

the conclusion that OMVs produced by *D. vulgaris* grown under the EAL and BAL condition were not vehicles for DNA transfer.

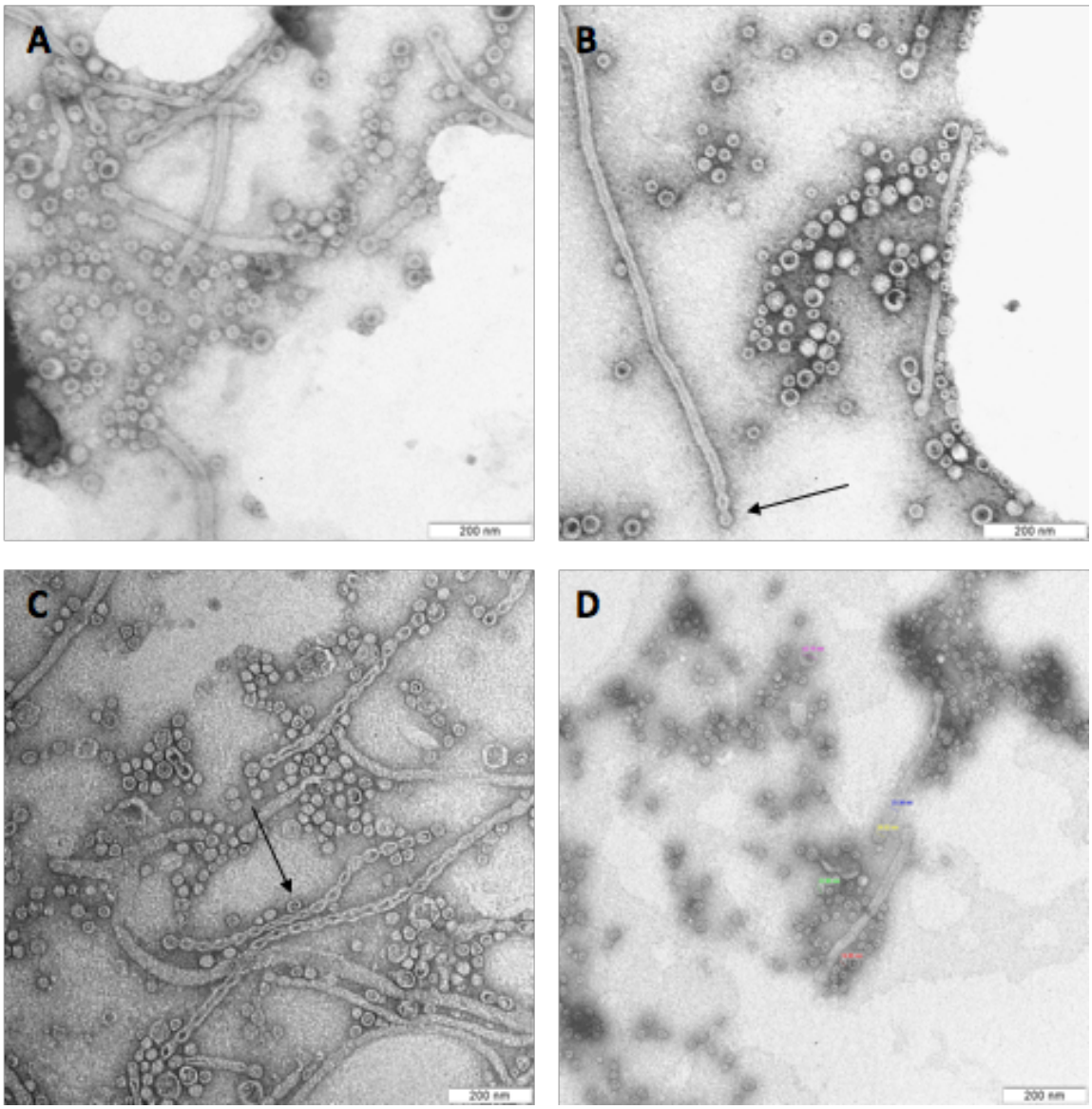


Figure 1. TEM images of isolated OMVs and OMV-tubes. Arrows in B and C point to OMV-tubes in different stages of vesicle differentiation.

Protein	Gene ID	NSAF	
		BAL	EAL
Outer Membrane			
Porin	DVU0799	0.114±0.082	0.109±0.023
Uncharacterized protein	DVU0797	0.045±0.045	0.039±0.015
Lipoprotein, putative	DVU1573	0.068±0.080	0.046±0.027
OmpA family protein	DVU1422	0.034±0.045	0.029±0.024
Lipoprotein, putative	DVU0761	0.069±0.088	0.036±0.028
Lipoprotein, putative	DVU3249	0.018±0.022	0.010±0.011
Transporter, putative	DVU0766	0.034±0.042	0.019±0.016
Lipoprotein, putative	DVU2428	0.049±0.031	0.022±0.004
Lipoprotein, putative	DVU3042	0.038±0.015	0.038±0.013
Peptidoglycan-associated lipoprotein, putative	DVU3104	0.028±0.035	0.006±0.006

Lipoprotein, putative	DVU3352	0.009±0.013	0.004±0.003
Uncharacterized protein	DVU0255	0.012±0.016	0.004±0.003
Periplasm			
Periplasmic [NiFeSe] hydrogenase, large subunit	DVU1918	0.067±0.067	0.078±0.033
Periplasmic [NiFe] hydrogenase, large subunit	DVU1922	0.021±0.036	0
Periplasmic [NiFeSe] hydrogenase, small subunit	DVU1917	0.024±0.030	0.021±0.010
TPR domain protein	DVU1930	0.014±0.017	0.009±0.008
Cytoplasm			
Sulfite reductase, dissimilatory-type subunit beta	DVU0403	0.030±0.008	0.035±0.005
Adenylyl-sulphate reductase, alpha subunit	DVU0847	0.017±0.002	0.011±0.005
Sulfite reductase, dissimilatory-type subunit alpha	DVU0402	0.016±0.003	0.012±0.005
Glyceraldehyde-3-phosphate dehydrogenase	DVU0565	0	0.033±0.018
Inorganic pyrophosphatase, manganese-dependent	DVU1636	0.021±0.039	0.007±0.007
Zinc resistance-associated protein homolog	DVU3384	0.039±0.047	0.010±0.012
50S ribosomal protein L21	DVU0927	0	0.016±0.021

50S ribosomal protein L23	DVU1305	0.029±0.045	0.021±0.021
Rubrerythrin	DVU3094	0.012±0.003	0.005±0.000
Rubredoxin-oxygen oxidoreductase	DVU3185	0.004±0.001	0.002±0.002
Inner Membrane			
Amino acid ABC transporter	DVU0966	0.025±0.027	0

Table 1. Proteins identified in purified OMV samples from *D. vulgaris* biofilm grown under BAL and EAL conditions. Protein abundance is estimated by normalized spectral abundance factor (NSAF).

Proteomic Analysis of OMVs

To understand the potential function of the OMVs in *D. vulgaris* biofilms grown under EAL and BAL conditions, protein content was analyzed by untargeted shotgun proteomics. The proteins detected for both the EAL and BAL conditions are presented in Table 1, organized based on cellular location. It is expected that OMVs contain proteins whose origin is the outer membrane or periplasmic space, but the detection of proteins belonging to the cytoplasm or inner membrane would indicate a specific sorting event or contamination of samples with cell lysis products during the OMV separation protocol. It is rare that proteomic studies of OMVs are free of cytoplasmic proteins, even when extremely stringent isolation protocols are used to avoid cell lysis (Schwechheimer and Kuehn 2015). In attempt to differentiate between cytoplasmic proteins detected due to contamination from lysed cells compared to intentional sorting, the Protein Abundance

Database (pax-db.org) was used to identify proteins of high abundance in *D. vulgaris*. Six out of ten cytoplasmic proteins detected in the OMV fractions were among the top 5% of proteins present in *D. vulgaris* based on a compilation of proteomic data, indicating that these are likely a contamination (Wang et al. 2012). Cytoplasmic associated proteins detected in OMV fractions that are typically less abundant in *D. vulgaris* cells are two ribosomal proteins (50S ribosomal proteins L21 and L23), rubrerythrin (provides protection from oxidative stress), and a zinc resistance-associated protein that has been shown to increase in abundance when *D. vulgaris* is exposed to oxygen (Mukhopadhyay et al. 2007). Interestingly, three out of the ten proteins of cytoplasmic origin that are associated with oxygen stress (rubrerthyrin, zinc resistance-associated protein, and rubredoxin-oxygen oxidoreductase), pointing toward a possible role for OMVs in oxidative stress protection.

The most abundant protein detected in OMVs was a porin that was recently characterized and found to form a homotrimeric structure, have a slight preference for anionic sugars over uncharged sugars, and is similar in permeability to the major porin of *Escherichia coli* (Zeng et al. 2017). This porin (encoded by DVU0799) is one of the most abundant outer membrane proteins, indicating its importance in controlling outer membrane permeability. Given that this porin is highly abundant in the outer membrane, it is not surprising that it is also highly abundant on OMVs. Another highly abundant, but uncharacterized, protein in the OMV fractions is encoded by DVU0797, which is separated from DVU0799 in the genome by a small (31 AA) hypothetical

protein. DVU0797 is similar in size to DVU0799 and has 60% sequence identity, making it another candidate for a porin (Walian et al. 2012).

Also present in *D. vulgaris* OMVs were eight different lipoproteins. Lipoproteins are typically associated with the cytoplasmic membrane, the inner leaflet of the outer membrane and the outer cell surface, as was recently demonstrated in Gram-negative cells (Wilson and Bernstein 2016). Lipoproteins have a wide range of functions, including nutrient acquisition, pathogenesis, sporulation, transport and folding of proteins, and membrane integrity (Mathiopoulos et al. 1991; Alloing et al. 1994; Berry and Paton 1996; Schmaler et al. 2010). Defects in lipoproteins have been shown to result in a decrease in membrane integrity and hyper-vesiculation, leading some researchers to propose that lipoproteins, or spacing of lipoproteins in the outer membrane, may be involved in OMV formation (Bernadac et al. 1998a; Cascales et al. 2002). *D. vulgaris* has 45 annotated lipoproteins in the genome, most of which are of unknown function. One of the eight that were identified in the isolated OMVs, DVU3104, has significant homology with Pal in *E. coli* (Walian et al. 2012), which is anchored in the outer membrane and binds with peptidoglycan, and when mutated causes hyper-vesiculation (Bernadac et al. 1998b). Several genes encoding lipoproteins in *D. vulgaris* were down-expressed after changing from syntrophic growth with a methanogen to a sulfidogenic metabolism, indicating that lipoproteins in *D. vulgaris* may also play an important role in interspecies interactions (Plugge et al. 2010).

Two periplasmic hydrogenases were identified in the OMV fractions as well. Both the [NiFeSe] hydrogenase and [NiFe] hydrogenase mature in the cytoplasm and are then transferred across the cytoplasmic membrane via the Tat system (Valente et al. 2005). The [NiFeSe] hydrogenase has been shown to also be a lipoprotein and it is hypothesized that the [NiFe] hydrogenase maybe is as well (Valente et al. 2007). Hydrogenases have an essential role in energy production in SRB as they oxidize H_2, donate the electrons to the electron transport chain and produce protons for generation of a proton motive force that is used for ATP production (Peck 1993). Additionally, isolated hydrogenases from different *Desulfovibrio* sp. are capable of Cr(VI) reduction (Chardin et al. 2003). Whether or not these hydrogenases function in an OMV or if they happen to be packaged in OMVs due to their location in the periplasm is not clear. However, vesicles that contained hydrogenase activity could be supplied with an electron source via H_2, and therefore, could feed electron transfer mechanisms away from the cell. Interspecies H_2 transfer is an important component of syntrophic relationships, with microbes forming aggregates and biofilms structured to maximize the availability of substrates (Ishii et al. 2005). In the example of *D. vulgaris* and *Methanococcus maripaludis*, hydrogen production by the SRB and consumption by the methanogen is critical to the syntrophy and extracellular hydrogenase activity could contribute to such relationships (Brileya et al. 2014). Further work is needed to ascertain long-distance, intra-species H_2 transfer in biofilms.

Another protein present in isolated OMVs contained a tetratricopeptide repeat domain (encoded by DVU1930) and has homology with CpoB, a cell division coordinator associated with regulating peptidoglycan synthesis and outer membrane invagination (Gray et al. 2015). A possible role for CpoB in isolated OMVs could be to regulate division of OMV-tube structures to individual OMVs, but it cannot be ruled out that its presence is a consequence of being an outer membrane associated protein. However, in a study that established an outer membrane protein dataset for *D. vulgaris*, this protein was not detected, further hinting at its involvement in OMV division (Walian et al. 2012).

Although OMVs were isolated from *D. vulgaris* biofilm grown under EAL and BAL conditions to look for differences in OMV protein content and quantity, more replicates are needed to make conclusions about protein abundance between the two conditions. This study does provide clues to the function of OMVs that could be further investigated: oxidative stress defense and hydrogenase activity. Metabolomic analyses of isolated OMVs could also help elucidate the functional role that OMVs play in *D. vulgaris* biofilm.

REFERENCES CITED

Alloing G, de Philip P, Claverys JP (1994) Three highly homologous membrane-bound lipoproteins participate in oligopeptide transport by the Ami system of the gram-positive Streptococcus pneumoniae. J Mol Biol 241:44–58.

Bernadac A, Gavioli M, Lazzaroni JC, Raina S, Lloubès R (1998) Escherichia coli tol-pal mutants form outer membrane vesicles. J Bacteriol 180:4872–4878.

Berry AM, Paton JC (1996) Sequence heterogeneity of PsaA, a 37-kilodalton putative adhesin essential for virulence of Streptococcus pneumoniae. Infect Immun 64:5255–5262.

Brileya KA, Camilleri LB, Zane GM, Wall JD, Fields MW (2014) Biofilm growth mode promotes maximum carrying capacity and community stability during product inhibition syntrophy. Front Microbiol 5:693.

Cascales E, Bernadac A, Gavioli M, Lazzaroni J-C, Lloubes R (2002) Pal Lipoprotein of Escherichia coli Plays a Major Role in Outer Membrane Integrity. J Bacteriol 184:754–759.

Chardin B, Giudici-Orticoni M-T, De Luca G, Guigliarelli B, Bruschi M (2003) Hydrogenases in sulfate-reducing bacteria function as chromium reductase. Appl Microbiol Biotechnol 63:315–321.

Ciofu O, Beveridge TJ, Kadurugamuwa J, Walther-Rasmussen J, Høiby N (2000) Chromosomal beta-lactamase is packaged into membrane vesicles and secreted from Pseudomonas aeruginosa. J Antimicrob Chemother 45:9–13.

Clark ME, Edelmann RE, Duley ML, Wall JD, Fields MW (2007) Biofilm formation in Desulfovibrio vulgaris Hildenborough is dependent upon protein filaments. Environ Microbiol 9:2844–2854.

Clark ME, He Q, He Z, Huang KH, Alm EJ, Wan X-F, Hazen TC, Arkin AP, Wall JD, Zhou J-Z, Fields MW (2006) Temporal transcriptomic analysis as Desulfovibrio vulgaris Hildenborough transitions into stationary phase during electron donor depletion. Appl Environ Microbiol 72:5578–5588.

Clark ME, He Z, Redding AM, Joachimiak MP, Keasling JD, Zhou JZ, Arkin AP, Mukhopadhyay A, Fields MW (2012) Transcriptomic and proteomic analyses of Desulfovibrio vulgaris biofilms: carbon and energy flow contribute to the distinct biofilm growth state. BMC Genomics 13:138.

Flemming H-C, Wingender J (2010) The biofilm matrix. Nat Rev Microbiol 8:623–633.

Fulsundar S, Harms K, Flaten GE, Johnsen PJ, Chopade BA, Nielsen KM (2014) Gene transfer potential of outer membrane vesicles of Acinetobacter baylyi and effects of stress on vesiculation. Appl Environ Microbiol 80:3469–3483.

González Fernández-Niño SM, Smith-Moritz AM, Chan LJG, Adams PD, Heazlewood JL, Petzold CJ (2015) Standard flow liquid chromatography for shotgun proteomics in bioenergy research. Front Bioeng Biotechnol 3:44.

Gorby Y, McLean J, Korenevsky A, Rosso K, El-Naggar MY, Beveridge TJ (2008) Redox-reactive membrane vesicles produced by Shewanella. Geobiology 6:232–241.

Grande R, Di Marcantonio MC, Robuffo I, Pompilio A, Celia C, Di Marzio L, Paolino D, Codagnone M, Muraro R, Stoodley P, Hall-Stoodley L, Mincione G (2015) Helicobacter pylori ATCC 43629/NCTC 11639 Outer Membrane Vesicles (OMVs) from Biofilm and Planktonic Phase Associated with Extracellular DNA (eDNA). Front Microbiol 6:1369.

Gray AN, Egan AJF, Van't Veer IL, Verheul J, Colavin A, Koumoutsi A, Biboy J, Altelaar AFM, Damen MJ, Huang KC, Simorre J-P, Breukink E, den Blaauwen T, Typas A, Gross CA, Vollmer W (2015) Coordination of peptidoglycan synthesis and outer membrane constriction during Escherichia coli cell division. Elife. doi: 10.7554/eLife.07118

Guidi R, Levi L, Rouf SF, Puiac S, Rhen M, Frisan T (2013) Salmonella enterica delivers its genotoxin through outer membrane vesicles secreted from infected cells. Cell Microbiol 15:2034–2050.

Heidelberg JF, Seshadri R, Haveman SA, Hemme CL, Paulsen IT, Kolonay JF, Eisen JA, Ward N, Methe B, Brinkac LM, Daugherty SC, Deboy RT, Dodson RJ, Durkin AS, Madupu R, Nelson WC, Sullivan SA, Fouts D, Haft DH, Selengut J, Peterson JD, Davidsen TM, Zafar N, Zhou L, Radune D, Dimitrov G, Hance M, Tran K, Khouri H, Gill J, Utterback TR, Feldblyum TV, Wall JD, Voordouw G, Fraser CM (2004) The genome sequence of the anaerobic, sulfate-reducing bacterium Desulfovibrio vulgaris Hildenborough. Nat Biotechnol 22:554–559.

Ishii S 'ichi, Kosaka T, Hori K, Hotta Y, Watanabe K (2005) Coaggregation facilitates interspecies hydrogen transfer between Pelotomaculum thermopropionicum and Methanothermobacter thermautotrophicus. Appl Environ Microbiol 71:7838–7845.

Keller A, Nesvizhskii AI, Kolker E, Aebersold R (2002) Empirical statistical model to estimate the accuracy of peptide identifications made by MS/MS and database search. Anal Chem 74:5383–5392.

Klieve AV, Yokoyama MT, Forster RJ, Ouwerkerk D, Bain PA, Mawhinney EL (2005) Naturally occurring DNA transfer system associated with membrane vesicles in cellulolytic Ruminococcus spp. of ruminal origin. Appl Environ Microbiol 71:4248–4253.

Liu H, Huang L, Huang Z, Zheng J (2007) Specification of sulfate reducing bacteria biofilms accumulation effects on corrosion initiation. Mater Corros 58:44–48.

Manning AJ, Kuehn MJ (2011) Contribution of bacterial outer membrane vesicles to innate bacterial defense. BMC Microbiol 11:258.

Marsili E, Beyenal H, Di Palma L, Merli C, Dohnalkova A, Amonette JE, Lewandowski Z (2007) Uranium immobilization by sulfate-reducing biofilms grown on hematite, dolomite, and calcite. Environ Sci Technol 41:8349–8354.

Mashburn LM, Whiteley M (2005) Membrane vesicles traffic signals and facilitate group activities in a prokaryote. Nature 437:422–425.

Mathiopoulos C, Mueller JP, Slack FJ, Murphy CG, Patankar S, Bukusoglu G, Sonenshein AL (1991) A Bacillus subtilis dipeptide transport system expressed early during sporulation. Mol Microbiol 5:1903–1913.

McCaig WD, Koller A, Thanassi DG (2013) Production of outer membrane vesicles and outer membrane tubes by Francisella novicida. J Bacteriol 195:1120–1132.

Mukhopadhyay A, Redding AM, Joachimiak MP, Arkin AP, Borglin SE, Dehal PS, Chakraborty R, Geller JT, Hazen TC, He Q, Joyner DC, Martin VJJ, Wall JD, Yang ZK, Zhou J, Keasling JD (2007) Cell-wide responses to low-oxygen exposure in Desulfovibrio vulgaris Hildenborough. J Bacteriol 189:5996–6010.

Nanninga HJ, Gottschal JC (1987) Properties of Desulfovibrio carbinolicus sp. nov. and Other Sulfate-Reducing Bacteria Isolated from an Anaerobic-Purification Plant. Appl Environ Microbiol 53:802–809.

Neria-González I, Wang ET, Ramírez F, Romero JM, Hernández-Rodríguez C (2006) Characterization of bacterial community associated to biofilms of corroded oil pipelines from the southeast of Mexico. Anaerobe 12:122–133.

Nesvizhskii AI, Keller A, Kolker E, Aebersold R (2003) A Statistical Model for Identifying Proteins by Tandem Mass Spectrometry. Anal Chem 75:4646–4658.

Orench-Rivera N, Kuehn MJ (2016) Environmentally controlled bacterial vesicle-mediated export. Cell Microbiol 18:1525–1536.

Park AJ, Murphy K, Surette MD, Bandoro C, Krieger JR, Taylor P, Khursigara CM (2015) Tracking the Dynamic Relationship between Cellular Systems and Extracellular Subproteomes in Pseudomonas aeruginosa Biofilms. J Proteome Res 14:4524–4537.

Parsons HT, González Fernández-Niño SM, Heazlewood JL (2013) Separation of the Plant Golgi Apparatus and Endoplasmic Reticulum by Free-Flow Electrophoresis. In: Methods in Molecular Biology. pp 527–539

Peck HD (1993) Bioenergetic Strategies of the Sulfate-Reducing Bacteria. In: Brock/Springer Series in Contemporary Bioscience. pp 41–76

Pérez-Cruz C, Carrión O, Delgado L, Martinez G, López-Iglesias C, Mercade E (2013) New type of outer membrane vesicle produced by the Gram-negative bacterium Shewanella vesiculosa M7T: implications for DNA content. Appl Environ Microbiol 79:1874–1881.

Pirbadian S, Barchinger SE, Leung KM, Byun HS, Jangir Y, Bouhenni RA, Reed SB, Romine MF, Saffarini DA, Shi L, Gorby YA, Golbeck JH, El-Naggar MY (2014) Shewanella oneidensis MR-1 nanowires are outer membrane and periplasmic extensions of the extracellular electron transport components. Proc Natl Acad Sci U S A 111:12883–12888.

Plugge CM, Scholten JCM, Culley DE, Nie L, Brockman FJ, Zhang W (2010) Global transcriptomics analysis of the Desulfovibrio vulgaris change from syntrophic growth with Methanosarcina barkeri to sulfidogenic metabolism. Microbiology 156:2746–2756.

Remis JP, Wei D, Gorur A, Zemla M, Haraga J, Allen S, Ewa Witkowska H, William Costerton J, Berleman JE, Auer M (2013) Bacterial social networks: structure and composition ofMyxococcus xanthusouter membrane vesicle chains. Environ Microbiol 16:598–610.

Schmaler M, Jann NJ, Götz F, Landmann R (2010) Staphylococcal lipoproteins and their role in bacterial survival in mice. Int J Med Microbiol 300:155–160.

Schooling SR, Beveridge TJ (2006) Membrane Vesicles: an Overlooked Component of the Matrices of Biofilms. J Bacteriol 188:5945–5957.

Schwechheimer C, Kuehn MJ (2015) Outer-membrane vesicles from Gram-negative bacteria: biogenesis and functions. Nat Rev Microbiol 13:605–619.

Subramanian P, Pirbadian S, El-Naggar MY, Jensen GJ (2016) Electron Cryo-Tomography of Nanowires in Shewanella Oneidensis MR-1. Biophys J 110:23a.

Truper HG (1984) Microorganisms and the Sulfur Cycle. In: Müller A, Krebs B (eds) Sulfur: Its Significance for Chemistry, for the Geo-, Bio-, and Cosmosphere and Technology. Elsevier, pp 351–365

Valente FMA, Oliveira ASF, Gnadt N, Pacheco I, Coelho AV, Xavier AV, Teixeira M, Soares CM, Pereira IAC (2005) Hydrogenases in Desulfovibrio vulgaris Hildenborough: structural and physiologic characterisation of the membrane-bound [NiFeSe] hydrogenase. J Biol Inorg Chem 10:667–682.

Valente FMA, Pereira PM, Venceslau SS, Regalla M, Coelho AV, Pereira IAC (2007) The [NiFeSe] hydrogenase fromDesulfovibrio vulgarisHildenborough is a bacterial lipoprotein lacking a typical lipoprotein signal peptide. FEBS Lett 581:3341–3344.

Walian PJ, Allen S, Shatsky M, Zeng L, Szakal ED, Liu H, Hall SC, Fisher SJ, Lam BR, Singer ME, Geller JT, Brenner SE, Chandonia J-M, Hazen TC, Ewa Witkowska H, Biggin MD, Jap BK (2012) High-throughput Isolation and Characterization of Untagged Membrane Protein Complexes: Outer Membrane Complexes ofDesulfovibrio vulgaris. J Proteome Res 121025102316001.

Wang M, Weiss M, Simonovic M, Haertinger G, Schrimpf SP, Hengartner MO, von Mering C (2012) PaxDb, a database of protein abundance averages across all three domains of life. Mol Cell Proteomics 11:492–500.

Wilson MM, Bernstein HD (2016) Surface-Exposed Lipoproteins: An Emerging Secretion Phenomenon in Gram-Negative Bacteria. Trends Microbiol 24:198–208.

Yonezawa H, Osaki T, Kurata S, Fukuda M, Kawakami H, Ochiai K, Hanawa T, Kamiya S (2009) Outer membrane vesicles of Helicobacter pylori TK1402 are involved in biofilm formation. BMC Microbiol 9:197.

Zeng L, Wooton E, Stahl DA, Walian PJ (2017) Identification and Characterization of the Major Porin of Desulfovibrio vulgaris Hildenborough. J Bacteriol. doi: 10.1128/JB.00286-17

Zybailov BL, Florens L, Washburn MP (2007) Quantitative shotgun proteomics using a protease with broad specificity and normalized spectral abundance factors. Mol Biosyst 3:354–360.

CHAPTER SIX

EPILOGUE

The motivation behind this work and the theme throughout this dissertation is understanding how nutrient limitation and resource ratio affect *D. vulgaris* growth, metabolism, and response to Cr(VI) toxicity in both planktonic and biofilm growth modes. While there have been many studies that have elucidated sensory systems in bacteria that control gene expression and therefore physiological responses to environmental changes, relatively few studies have investigated how nutrient limitation in terms of resource ratio affects microbial physiology, especially in response to heavy metal toxicity in both planktonic and biofilm growth modes. Investigating how nutrient limitation and resource ratio affected growth and metabolism of *D. vulgaris* Hildenborough in the biofilm growth mode led to the observation of complex extracellular structures and vesicles that warranted further investigation. The characterization of these structures and vesicles is the subject of Chapters 4 and 5.

The response of *D. vulgaris* to Cr(VI) toxicity is a secondary theme throughout this dissertation. Chapter 2 presents the response of *D. vulgaris* to Cr(VI) when grown planktonically in batch mode. Under all conditions tested (20 and 30°C, and EAL, BAL, and EDL resource ratios), *D. vulgaris* responded to Cr(VI) toxicity with an increased lag time compared to growth without Cr(VI). The length of the lag time increased with increased Cr(VI) concentration, but surprisingly lag time and Cr(VI) reduction rate was

also linked to resource ratio, with cells grown under the EAL condition being much more susceptible to Cr(VI) toxicity compared to cells grown under the BAL condition. In attempt to explain this, sulfate concentration was tested as a possible factor that could affect Cr(VI) toxicity. Increased sulfate concentration did provide some protection from Cr(VI) toxicity, but when sulfate levels were normalized, resource ratio still affected Cr(VI) toxicity, measured by lag time. These results indicate that there may be a dual effect of sulfate concentration and resource ratio that dictates Cr(VI) susceptibility in *D. vulgaris*. The effect of Cr(VI) on *D. vulgaris* biofilm grown under EAL and BAL conditions was also measured to determine if growth under the EAL condition in the biofilm growth mode had a similar effect on *D. vulgaris* Cr(VI) susceptibility as in planktonic growth. Surprisingly, in the biofilm growth mode, *D. vulgaris* grown under the EAL condition was equally susceptible or more resistant to Cr(VI) toxicity compared to the BAL condition. This finding, opposite of the results for planktonic growth with Cr(VI), is surprising, but is consistent with the plethora of literature documenting the physiological differences between biofilm and planktonic growth modes (Xu et al. 2000; Stewart 2002; Harrison et al. 2007). Although it is difficult to directly compare Cr(VI) susceptibility between biofilm and planktonic cells for SRB due to abiotic Cr(VI) reduction by sulfide, it seems that regardless of resource ratio, the biofilm growth mode confers increased Cr(VI) resistance for *D. vulgaris*, which is consistent with other organisms, such as *Pseudomonas* sp. (Teitzel and Parsek 2003; Chien et al. 2013).

Although there is not as much information available on the topic of increased resistance to heavy metals in biofilms compared to planktonic growth, the information that is available suggests similar mechanisms that contribute to biofilm resistance to antibiotics may be at play. These include the presence of slow growing cells within the biofilm due to heterogeneity in nutrient availability, dead cells/cell debris within the biofilm that may react with or sorb metal ions, and the production of extracellular matrix materials that might chelate or reduce metal ions (Rani et al. 2007; Harrison et al. 2007). The presence of slow growing cells and the role that extracellular matrix components play in biofilm resistance to heavy metals is particularly relevant to the work presented in Chapters 3 and 4.

Chapter 3 describes differences in the metabolism of *D. vulgaris* biofilms grown under EAL compared to BAL conditions. Biofilm grown under the EAL condition had many metabolites belonging to pathways essential for growth and cell division division down-regulated, indicating that *D. vulgaris* growing under the EAL condition may be growing more slowly, or in a biomass retention state. One theory for increased resistance of biofilms to external stressors (i.e. antibiotics, heavy metals), is that cells that are limited for an essential nutrient are forced to enter a very slow-growing or dormant state. Upon exposure to an external stress or antimicrobial agent, those cells within the biofilm that have nutrients available and therefore have a faster growth rate are more susceptible because they are prone to take up and metabolize the antimicrobial agent. The active cells also then serve to protect the less active cells by metabolizing the agent at their own

expense (Walters et al. 2003; Borriello et al. 2004). Further, linking purine/pyrimidine and glutamine/glutamate down-regulation to microbial resilience is a study in which removal of nucleobases and amino acids from medium supporting *E. coli* growth resulted in increased antibiotic resistance (Fung et al. 2010). The authors attribute increased resistance to induction of a stringent response, and/or additional unidentified mechanisms. Under the EAL condition, *D. vulgaris* is not limited for C or N, but sulfate limitation induces cellular regulation of C and N possibly through RexB or other unidentified mechanisms. The changes in metabolic state induced by electron acceptor limitation may therefore actually be protective in the biofilm growth mode whereas in the planktonic growth mode it is disadvantageous.

In Chapter 4 extracellular membranous structures are characterized and found to be closely associated with metal precipitants that were determined to be iron oxides and iron phosphates. The presence of larger and more extensive extracellular membrane structures produced under the EAL condition could also explain the opposing results for the effect of resource ratio on Cr(VI) toxicity for planktonic compared to biofilm cells if these structures have Cr(VI) reduction/sorption/chelating properties. Future studies should attempt to visualize such extracellular membrane structures within the biofilm after exposure to Cr(VI) and locate Cr(III) deposition within the biofilm.

While the exact function of the extracellular membranous structures still eludes us, there are multiple lines evidence supporting the hypothesis that they are involved in microbe-metal interactions. The first, mentioned above, is the association with iron

oxides/iron phosphates with the structures. There are metal deposits throughout the biofilm, with some seemingly far from cells and any extracellular structures and others adjacent to cells, but the association of metal precipitates with the extracellular membranous structures is quite notable. The identification of these precipitates as iron oxides and iron phosphates was surprising, as we would have otherwise assumed that they were iron sulfide precipitates since sulfide is abundant in the biofilm and readily reacts with ferrous iron (which is in the medium at a concentration of 0.063 mM as $FeCl_2$) to form mackinawite (FeS) or greigite (Fe_3S_4) (Haaningnielsen et al. 2005; Gramp et al. 2010). Because samples were processed and stored aerobically, it is possible that iron sulfides were oxidized to iron oxides in the time between sampling and analysis (Rickard and III Luther 2007). Still, it is surprising that no sulfur was detected and so we cannot rule out the possibility that these iron phosphates are not artifacts from sample preparation.

The second piece of evidence supporting the hypothesis that the extracellular membranous structures are involved in microbe-metal interactions is the presence of hydrogenases in OMVs. While it would be difficult to isolate the extracellular membranous structures away from the rest of the biofilm for further analysis, outer membrane vesicles were sometimes associated with and connecting to extracellular membranous structures and OMVs could be isolated and analyzed in an indirect attempt to learn more about the function of the extracellular membranous structures. Isolated OMVs contained [NiFe] and [NiFeSe] hydrogenases, which are critical to electron

transfer and hydrogen production and oxidation in cells. Extracellular hydrogenase activity in a biofilm has many implications for electron and hydrogen transfer over long distances. Additionally, hydrogenases isolated from SRB have been observed to reduce Cr(VI) (Michel et al. 2001; Chardin et al. 2003). Whether or not hydrogenases located within OMVs are capable of Cr(VI), or other metal, reduction if H_2 is present has not been tested, but these results suggest that OMVs could potentially contribute to metal reduction and resistance in both biofilm and planktonic growth modes. Further, the presence of hydrogenases in OMVs and the observation that OMVs are associated with extracellular membranous structures suggests that these two extracellular matrix components may be linked in structure and/or function.

Third, the overproduction of these structures under the EAL condition compared to BAL and EDL, suggests that their production may be in attempt to locate an alternative electron acceptor. Other dissimilatory metal-reducing organisms such as *Shewanella* sp. and *Geobacter* sp. produce extracellular nanowires in response to electron acceptor limitation (Gorby et al. 2006; Bond et al. 2012). While the topic of nanowires is one of intense debate and current hypotheses and models are continually changing, the production of extracellular structures in response to electron acceptor limitation in these other dissimilatory metal-reducing bacteria is well established. Extracellular electron transport has not been demonstrated and outer membrane cytochromes have not been detected in *Desulfovibrio* sp., making use of extracellular insoluble electron acceptors unlikely; however, there are parallels between the extracellular membrane structures and

nanowires produced by *S. oneidensis*. The most recent description of *S. oneidensis* nanowires shows that they are actually extensions of the outer membrane and periplasmic space that then differentiate into OMVs, which is seemingly very similar to the OMV-tube structures that we observed with the isolated OMVs (Pirbadian et al. 2014; Subramanian et al. 2016). Further, direct extracellular electron transfer via extracellular cytochromes is not the only mechanism for extracellular electron transfer. Transport of electrons via hydrogen (interspecies hydrogen transfer) is the foundation for many syntrophic microbial relationships, such as those between SRB, methanogens, or other fermentative microorganisms (Iannotti et al. 1973; Nakamura et al. 2010) and extracellular hydrogenases could facilitate the transfer of electrons from H_2 to an exogenous electron acceptor. While all of this taken together suggests that extracellular membranous structures play a role in microbe-metal interactions, other possible functions of these structures, such as waste extrusion and intercellular communication cannot be ruled out.

A unique aspect of the work presented in this dissertation is that all of the experiments were carried out at a room temperature (20-23°C), which is lower than the optimal growth temperature of 30°C for *D. vulgaris*. The experiments in the majority of published studies on dissimilatory metal-reducing bacteria are performed at 30°C, probably to be consistent with the body of literature available for comparison and to increase growth rate, and therefore reduce experiment length. With the rationale of perturbing resource ratio to better mimic "real world" scenarios, we thought it also

important to culture *D. vulgaris* at a temperature that was closer to subsurface temperatures (~5-17°C at Hanford Site, WA) (Truex et al. 2012). Decreased temperature resulted in a decreased growth rate for *D. vulgaris*, which is expected. Cells grown at 20°C were also more susceptible to Cr(VI) toxicity as measured by increased lag time and had slower Cr(VI) reduction rates compared to 30°C. A temperature increase of 10°C in a sulfate-reducing consortium resulted in a uranium reduction rate with three times the rate constant, indicating that temperature, growth rate, and enzyme reaction rates are linked (Boonchayaanant et al. 2008). The Cr(VI) reduction rate at 20°C was ~2 times slower than at 30°C, which most likely contributed to increased Cr(VI) toxicity at the lower temperature.

Additionally, temperature also affected production of extracellular filaments in *D. vulgaris* biofilms regardless of electron donor/electron acceptor ratio. Relatively few filaments were observed in biofilms grown at 30°C compared to those grown at 20°C and filament production in biofilms grown at 25°C was more than that of 30°C, but less than that of 20°C, suggesting that extracellular filament production is temperature dependent (Appendix A). To rule out that filament production was not based on growth rate, biofilms were also grown at 30°C, but at the dilution rate appropriate for a reactor grown at 20°C. This thermoregulation of filament production is not unique to *D. vulgaris*, as *Geobacter sulfurreducens* also produces pili at 25°C, but not 30°C and *E. coli* produces fimbrae at 37°C, but not 25°C (Goransson et al. 1989; Cologgi et al. 2011). Although we cannot determine what these filaments are in relation to the extracellular membranous

structures described in Chapter 4 due to possible sample distortion from ethanol dehydration and critical point drying, the presence of these extracellular structures at lower temperatures further emphasizes the importance of culturing organisms at temperatures that may be sub-optimal but field-relevant.

The work presented here investigated the effects of nutrient limitation and resource ratio on *D. vulgaris* growth, metabolism, and Cr(VI) susceptibility in the planktonic and biofilm growth modes. Measuring growth alone, whether planktonically or as a biofilm, revealed that *D. vulgaris* maximum biomass production is dictated by sulfate limitation in the EAL condition and lactate limitation in the EDL condition, which was expected. Cells grown under the EAL condition could have a growth advantage because they are able to produce H_2 for a short time after sulfate is depleted. This was measured in planktonic batch tube growth, but could not be detected in a CDC biofilm reactor (possibly due to H_2 consumption within the biofilm or the limit of detection on the gas chromatograph) and biomass yields were not significantly higher under the EAL condition, indicating that if H_2 production was occurring, it was not at a high enough level to contribute bo biomass production.

While measuring microbial growth in response to a stress and with different substrates or varying nutrient concentration can be an elegant way of discerning microbial physiology, complementing growth experiments with other analytical and "omics" approaches was instrumental to understanding how nutrient limitation and resource ratio affected *D. vulgaris* metabolism and biofilm matrix composition. The

combination of microscopy, differential staining, metabolomics, and fatty acid quantification in *D. vulgaris* biofilms was essential to the discovery and characterization of lipids as an important component of the biofilm matrix.

Based on the findings presented here, we conclude that nutrient limitation and resource ratio have notable effects on planktonic *D. vulgaris* Cr(VI) susceptibility and reduction, with electron acceptor limitation causing decreased Cr(VI) reduction rates and increased cell death in response to Cr(VI). In the biofilm growth mode, nutrient limitation altered the flow of carbon and energy in *D. vulgaris*, with electron acceptor limitation causing a switch to a biomass retention state with increased fatty acid production. Further, fatty acid content of biofilms was visualized and quantified and corresponded with extensive extracellular structures that connected to cells and were associated with extracellular metal deposits. The function of these structures is undetermined, but we hypothesize that they are involved in microbe-metal interactions and may confer protection against external stressors or antimicrobial agents. The identification of extracellular membranes as an important constituent of the biofilm matrix is significant because they have not been previously recognized, and because they may also be important to consider from an evolutionary perspective. Since containment of organelles within a membrane is a distinguishing factor between eukaryotic and prokaryotic organisms, the presence of extracellular membranes in biofilms where organisms from different domains of life are potentially coexisting and cooperating, has significant implications for the evolution of more complex life forms. The presence of

extracellular membranes in biofilms may not be unique to SRB, but the high-resolution imaging techniques that were used to identify them were unique to this study and it highlights the value of microscopy, as a tool to identify elements of biological systems that might be missed with other techniques. Overall, these results emphasize the effects that nutrient limitation or ratios of electron donor to electron acceptor in the environment can have on microbial physiology. Because SRB are important drivers of sulfur, carbon, and heavy metal cycling, and because they are implicated in destructive microbial corrosion and oil souring processes, understanding of how changes in nutrient concentrations affect their physiology is instrumental for their control and utilization.

REFERENCES CITED

Bond DR, Strycharz-Glaven SM, Tender LM, Torres CI (2012) On Electron Transport through Geobacter Biofilms. ChemSusChem 5:1099–1105.

Boonchayaanant B, Kitanidis PK, Criddle CS (2008) Growth and cometabolic reduction kinetics of a uranium- and sulfate-reducing Desulfovibrio/Clostridia mixed culture: Temperature effects. Biotechnol Bioeng 99:1107–1119.

Borriello G, Werner E, Roe F, Kim AM, Ehrlich GD, Stewart PS (2004) Oxygen limitation contributes to antibiotic tolerance of Pseudomonas aeruginosa in biofilms. Antimicrob Agents Chemother 48:2659–2664.

Chardin B, Giudici-Orticoni M-T, De Luca G, Guigliarelli B, Bruschi M (2003) Hydrogenases in sulfate-reducing bacteria function as chromium reductase. Appl Microbiol Biotechnol 63:315–321.

Chien C-C, Lin B-C, Wu C-H (2013) Biofilm formation and heavy metal resistance by an environmental Pseudomonas sp. Biochem Eng J 78:132–137.

Cologgi DL, Lampa-Pastirk S, Speers AM, Kelly SD, Reguera G (2011) Extracellular reduction of uranium via Geobacter conductive pili as a protective cellular mechanism. Proc Natl Acad Sci U S A 108:15248–15252.

Fung DKC, Chan EWC, Chin ML, Chan RCY (2010) Delineation of a bacterial starvation stress response network which can mediate antibiotic tolerance development. Antimicrob Agents Chemother 54:1082–1093.

Goransson M, Forsman K, Uhlin BE (1989) Regulatory genes in the thermoregulation of Escherichia coli pili gene transcription. Genes Dev 3:123–130.

Gorby YA, Yanina S, McLean JS, Rosso KM, Moyles D, Dohnalkova A, Beveridge TJ, Chang IS, Kim BH, Kim KS, Culley DE, Reed SB, Romine MF, Saffarini DA, Hill EA, Shi L, Elias DA, Kennedy DW, Pinchuk G, Watanabe K, Ishii S 'ichi, Logan B, Nealson KH, Fredrickson JK (2006) Electrically conductive bacterial nanowires produced by Shewanella oneidensis strain MR-1 and other microorganisms. Proc Natl Acad Sci U S A 103:11358–11363.

Gramp JP, Bigham JM, Jones FS, Tuovinen OH (2010) Formation of Fe-sulfides in cultures of sulfate-reducing bacteria. J Hazard Mater 175:1062–1067.

Haaningnielsen A, Lens P, Vollertsen J, Hvitvedjacobsen T (2005) Sulfide–iron

interactions in domestic wastewater from a gravity sewer. Water Res 39:2747–2755.

Harrison JJ, Ceri H, Turner RJ (2007) Multimetal resistance and tolerance in microbial biofilms. Nat Rev Microbiol 5:928–938.

Iannotti EL, Kafkewitz D, Wolin MJ, Bryant MP (1973) Glucose fermentation products in Ruminococcus albus grown in continuous culture with Vibrio succinogenes: changes caused by interspecies transfer of H 2. J Bacteriol 114:1231–1240.

Michel C, Brugna M, Aubert C, Bernadac A, Bruschi M (2001) Enzymatic reduction of chromate: comparative studies using sulfate-reducing bacteria. Key role of polyheme cytochromes c and hydrogenases. Appl Microbiol Biotechnol 55:95–100.

Nakamura N, Lin HC, McSweeney CS, Mackie RI, Gaskins HR (2010) Mechanisms of microbial hydrogen disposal in the human colon and implications for health and disease. Annu Rev Food Sci Technol 1:363–395.

Pirbadian S, Barchinger SE, Leung KM, Byun HS, Jangir Y, Bouhenni RA, Reed SB, Romine MF, Saffarini DA, Shi L, Gorby YA, Golbeck JH, El-Naggar MY (2014) Shewanella oneidensis MR-1 nanowires are outer membrane and periplasmic extensions of the extracellular electron transport components. Proc Natl Acad Sci U S A 111:12883–12888.

Rani SA, Pitts B, Beyenal H, Veluchamy RA, Lewandowski Z, Davison WM, Buckingham-Meyer K, Stewart PS (2007) Spatial patterns of DNA replication, protein synthesis, and oxygen concentration within bacterial biofilms reveal diverse physiological states. J Bacteriol 189:4223–4233.

Rickard D, III Luther GW (2007) Chemistry of Iron Sulfides. ChemInform. doi: 10.1002/chin.200719200

Stewart PS (2002) Mechanisms of antibiotic resistance in bacterial biofilms. Int J Med Microbiol 292:107–113.

Subramanian P, Pirbadian S, El-Naggar MY, Jensen GJ (2016) Electron Cryo-Tomography of Nanowires in Shewanella Oneidensis MR-1. Biophys J 110:23a.

Teitzel GM, Parsek MR (2003) Heavy metal resistance of biofilm and planktonic Pseudomonas aeruginosa. Appl Environ Microbiol 69:2313–2320.

Truex MJ, Oostrom M, Strickland CE, Johnson TC, Freedman VL, Johnson CD, Greenwood WJ, Ward AL, Clayton RE, Lindberg MJ, Peterson JE, Hubbard S, Chronister GB, Benecke MW (2012) Deep Vadose Zone Treatability Test for the

Hanford Central Plateau: Soil Desiccation Pilot Test Results.

Walters MC, Roe F, Bugnicourt A, Franklin MJ, Stewart PS (2003) Contributions of Antibiotic Penetration, Oxygen Limitation, and Low Metabolic Activity to Tolerance of Pseudomonas aeruginosa Biofilms to Ciprofloxacin and Tobramycin. Antimicrob Agents Chemother 47:317–323.

Xu KD, Stewart PS, McFeters GA (2000) Biofilm resistance to antimicrobial agents. Microbiology 146:547–549.

REFERENCES CITED

Abildgaard L (2006) Desulfovibrio alkalitolerans sp. nov., a novel alkalitolerant, sulphate-reducing bacterium isolated from district heating water. Int J Syst Evol Microbiol 56:1019–1024.

Abramoff, Magalhães PJ, Ram SJ (2004) Image Processing with ImageJ. Biophotonics International 11:36–42.

Agnello G, Chang LL, Lamb CM, Georgiou G, Stone EM (2013) Discovery of a substrate selectivity motif in amino acid decarboxylases unveils a taurine biosynthesis pathway in prokaryotes. ACS Chem Biol 8:2264–2271.

Aguilar-Barajas E, Díaz-Pérez C, Ramírez-Díaz MI, Riveros-Rosas H, Cervantes C (2011) Bacterial transport of sulfate, molybdate, and related oxyanions. Biometals 24:687–707.

Aiyar J, Berkovits HJ, Floyd RA, Wetterhahn KE (1991) Reaction of chromium(VI) with glutathione or with hydrogen peroxide: identification of reactive intermediates and their role in chromium(VI)-induced DNA damage. Environ Health Perspect 92:53–62.

Alazard D (2003) Desulfovibrio hydrothermalis sp. nov., a novel sulfate-reducing bacterium isolated from hydrothermal vents. Int J Syst Evol Microbiol 53:173–178.

Alazard D, Joseph M, Battaglia-Brunet F, Cayol J-L, Ollivier B (2010) Desulfosporosinus acidiphilus sp. nov.: a moderately acidophilic sulfate-reducing bacterium isolated from acid mining drainage sediments. Extremophiles 14:305–312.

Allen TD, Kraus PF, Lawson PA, Drake GR, Balkwill DL, Tanner RS (2008) Desulfovibrio carbinoliphilus sp. nov., a benzyl alcohol-oxidizing, sulfate-reducing bacterium isolated from a gas condensate-contaminated aquifer. Int J Syst Evol Microbiol 58:1313–1317.

Alloing G, de Philip P, Claverys JP (1994) Three highly homologous membrane-bound lipoproteins participate in oligopeptide transport by the Ami system of the gram-positive Streptococcus pneumoniae. J Mol Biol 241:44–58.

Alvarez AH, Moreno-Sánchez R, Cervantes C (1999) Chromate efflux by means of the ChrA chromate resistance protein from Pseudomonas aeruginosa. J Bacteriol 181:7398–7400.

Anderson RT, Vrionis HA, Ortiz-Bernad I, Resch CT, Long PE, Dayvault R, Karp K, Marutzky S, Metzler DR, Peacock A, White DC, Lowe M, Lovley DR (2003) Stimulating the in situ activity of Geobacter species to remove uranium from the groundwater of a uranium-contaminated aquifer. Appl Environ Microbiol 69:5884–5891.

Appenroth K-J, Luther A, Jetschke G, Gabrys H (2008) Modification of chromate toxicity by sulphate in duckweeds (Lemnaceae). Aquat Toxicol 89:167–171.

Badzjong W, Thauer RK (1980) Vectorial electron transport in Degulfovibrio vulgaris (Marburg) growing on hydrogen plus sulfate as sole energy source. Arch Microbiol 125:167–174.

Baena S, Fardeau ML, Labat M, Ollivier B, Garcia JL, Patel BK (1998) Desulfovibrio aminophilus sp. nov., a novel amino acid degrading and sulfate reducing bacterium from an anaerobic dairy wastewater lagoon. Syst Appl Microbiol 21:498–504.

Bansal R, Helmus RA, Stanley BA, Zhu J, Liermann LJ, Brantley SL, Tien M (2013) Survival during long-term starvation: global proteomics analysis of Geobacter sulfurreducens under prolonged electron-acceptor limitation. J Proteome Res 12:4316–4326.

Barchinger SE, Pirbadian S, Sambles C, Baker CS, Leung KM, Burroughs NJ, El-Naggar MY, Golbeck JH (2016) Regulation of Gene Expression in Shewanella oneidensis MR-1 during Electron Acceptor Limitation and Bacterial Nanowire Formation. Appl Environ Microbiol 82:5428–5443.

Bargar JR, Williams KH, Campbell KM, Long PE, Stubbs JE, Suvorova EI, Lezama-Pacheco JS, Alessi DS, Stylo M, Webb SM, Davis JA, Giammar DE, Blue LY, Bernier-Latmani R (2013a) Uranium redox transition pathways in acetate-amended sediments. Proceedings of the National Academy of Sciences 110:4506–4511.

Barnhart J (1997) Occurrences, uses, and properties of chromium. Regul Toxicol Pharmacol 26:S3–7.

Baumgarten A, Redenius I, Kranczoch J, Cypionka H (2001) Periplasmic oxygen reduction by Desulfovibrio species. Arch Microbiol 176:306–309.

Benton HP, Ivanisevic J, Mahieu NG, Kurczy ME, Johnson CH, Franco L, Rinehart D, Valentine E, Gowda H, Ubhi BK, Tautenhahn R, Gieschen A, Fields MW, Patti GJ, Siuzdak G (2015) Autonomous metabolomics for rapid metabolite identification in global profiling. Anal Chem 87:884–891.

Bernadac A, Gavioli M, Lazzaroni JC, Raina S, Lloubès R (1998a) Escherichia coli tol-pal mutants form outer membrane vesicles. J Bacteriol 180:4872–4878.

Berry AM, Paton JC (1996) Sequence heterogeneity of PsaA, a 37-kilodalton putative adhesin essential for virulence of Streptococcus pneumoniae. Infect Immun 64:5255–5262.

Beyenal H, Lewandowski Z (2004) Dynamics of lead immobilization in sulfate reducing biofilms. Water Res 38:2726–2736.

Beyenal H, Sani RK, Peyton BM, Dohnalkova AC, Amonette JE, Lewandowski Z (2004) Uranium immobilization by sulfate-reducing biofilms. Environ Sci Technol 38:2067–2074.

Blodau C, Mayer B, Peiffer S, Moore TR (2007) Support for an anaerobic sulfur cycle in two Canadian peatland soils. J Geophys Res. doi: 10.1029/2006jg000364

Böckelmann U, Janke A, Kuhn R, Neu TR, Wecke J, Lawrence JR, Szewzyk U (2006) Bacterial extracellular DNA forming a defined network-like structure. FEMS Microbiol Lett 262:31–38.

Bond DR, Strycharz-Glaven SM, Tender LM, Torres CI (2012) On Electron Transport through Geobacter Biofilms. ChemSusChem 5:1099–1105.

Boonchayaanant B, Kitanidis PK, Criddle CS (2008a) Growth and cometabolic reduction kinetics of a uranium- and sulfate-reducing Desulfovibrio/Clostridia mixed culture: Temperature effects. Biotechnol Bioeng 99:1107–1119.

Borglin S, Joyner D, Jacobsen J, Mukhopadhyay A, Hazen TC (2009a) Overcoming the anaerobic hurdle in phenotypic microarrays: generation and visualization of growth curve data for Desulfovibrio vulgaris Hildenborough. J Microbiol Methods 76:159–168.

Borriello G, Werner E, Roe F, Kim AM, Ehrlich GD, Stewart PS (2004) Oxygen limitation contributes to antibiotic tolerance of Pseudomonas aeruginosa in biofilms. Antimicrob Agents Chemother 48:2659–2664.

Bowles MW, Mogollón JM, Kasten S, Zabel M, Hinrichs K-U (2014) Global rates of marine sulfate reduction and implications for sub-sea-floor metabolic activities. Science 344:889–891.

Brandis A, Thauer RK (1981) Growth of Desulfovibrio species on hydrogen and sulphate as sole energy source. Microbiology 126:249–252.

Bridgewater LC, Manning FC, Woo ES, Patierno SR (1994) DNA polymerase arrest by adducted trivalent chromium. Mol Carcinog 9:122–133.

Brileya KA, Camilleri LB, Zane GM, Wall JD, Fields MW (2014) Biofilm growth mode promotes maximum carrying capacity and community stability during product inhibition syntrophy. Front Microbiol 5:693.

Brileya KA, Connolly JM, Downey C, Gerlach R, Fields MW (2013) Taxis toward hydrogen gas by Methanococcus maripaludis. Sci Rep 3:3140.

Byrne ME, Ball DA, Guerquin-Kern J-L, Rouiller I, Wu T-D, Downing KH, Vali H, Komeili A (2010) Desulfovibrio magneticus RS-1 contains an iron- and phosphorus-rich organelle distinct from its bullet-shaped magnetosomes. Proc Natl Acad Sci U S A 107:12263–12268.

Campbell TL, Brown ED (2002) Characterization of the depletion of 2-C-methyl-D-erythritol-2,4-cyclodiphosphate synthase in Escherichia coli and Bacillus subtilis. J Bacteriol 184:5609–5618.

Cao B, Ahmed B, Kennedy DW, Wang Z, Shi L, Marshall MJ, Fredrickson JK, Isern NG, Majors PD, Beyenal H (2011) Contribution of Extracellular Polymeric Substances fromShewanellasp. HRCR-1 Biofilms to U(VI) Immobilization. Environ Sci Technol 45:5483–5490.

Cascales E, Bernadac A, Gavioli M, Lazzaroni J-C, Lloubes R (2002) Pal Lipoprotein of Escherichia coli Plays a Major Role in Outer Membrane Integrity. J Bacteriol 184:754–759.

Castelle CJ, Hug LA, Wrighton KC, Thomas BC, Williams KH, Wu D, Tringe SG, Singer SW, Eisen JA, Banfield JF (2013) Extraordinary phylogenetic diversity and metabolic versatility in aquifer sediment. Nat Commun 4:2120.

Castro H (2000) Phylogeny of sulfate-reducing bacteria. FEMS Microbiol Ecol 31:1–9.

Chang W-S, van de Mortel M, Nielsen L, Nino de Guzman G, Li X, Halverson LJ (2007) Alginate production by Pseudomonas putida creates a hydrated microenvironment and contributes to biofilm architecture and stress tolerance under water-limiting conditions. J Bacteriol 189:8290–8299.

Chaplin MF, Kennedy JF (1986) Carbohydrate analysis: a practical approach. Oxford University Press, USA

Chardin B, Dolla A, Chaspoul F, Fardeau ML, Gallice P, Bruschi M (2002) Bioremediation of chromate: thermodynamic analysis of the effects of Cr(VI) on sulfate-reducing bacteria. Appl Microbiol Biotechnol 60:352–360.

Chardin B, Giudici-Orticoni M-T, De Luca G, Guigliarelli B, Bruschi M (2003a) Hydrogenases in sulfate-reducing bacteria function as chromium reductase. Appl Microbiol Biotechnol 63:315–321.

Chiang W-C, Nilsson M, Jensen PØ, Høiby N, Nielsen TE, Givskov M, Tolker-Nielsen T (2013) Extracellular DNA shields against aminoglycosides in Pseudomonas aeruginosa biofilms. Antimicrob Agents Chemother 57:2352–2361.

Chien C-C, Lin B-C, Wu C-H (2013) Biofilm formation and heavy metal resistance by an environmental Pseudomonas sp. Biochem Eng J 78:132–137.

Christensen BE, Characklis WG (1990) Physical and chemical properties of biofilms. In: Characklis WG, Marshall KC (eds) Biofilms. Wiley, New York, pp 93–103

Christensen GA, Zane GM, Kazakov AE, Li X, Rodionov DA, Novichkov PS, Dubchak I, Arkin AP, Wall JD (2015) Rex (encoded by DVU_0916) in Desulfovibrio vulgaris Hildenborough is a repressor of sulfate adenylyl transferase and is regulated by NADH. J Bacteriol 197:29–39.

Cieăślak-Golonka M, Raczko M, Staszak Z (1992) Synthesis, spectroscopic and magnetic studies of chromium(II) complexes isolated from in vitro reduction of the chromium(VI) ion with the main cellular reductants ascorbic acid, cysteine and glutathione*. Polyhedron 11:2549–2555.

Ciofu O, Beveridge TJ, Kadurugamuwa J, Walther-Rasmussen J, Høiby N (2000) Chromosomal beta-lactamase is packaged into membrane vesicles and secreted from Pseudomonas aeruginosa. J Antimicrob Chemother 45:9–13.

Clark ME, Edelmann RE, Duley ML, Wall JD, Fields MW (2007a) Biofilm formation in Desulfovibrio vulgaris Hildenborough is dependent upon protein filaments. Environ Microbiol 9:2844–2854.

Clark ME, He Q, He Z, Huang KH, Alm EJ, Wan X-F, Hazen TC, Arkin AP, Wall JD, Zhou J-Z, Fields MW (2006) Temporal transcriptomic analysis as Desulfovibrio vulgaris Hildenborough transitions into stationary phase during electron donor depletion. Appl Environ Microbiol 72:5578–5588.

Clark ME, He Z, Redding AM, Joachimiak MP, Keasling JD, Zhou JZ, Arkin AP, Mukhopadhyay A, Fields MW (2012) Transcriptomic and proteomic analyses of Desulfovibrio vulgaris biofilms: carbon and energy flow contribute to the distinct biofilm growth state. BMC Genomics 13:138.

Coleman DC, Whitman WB (2005) Linking species richness, biodiversity and ecosystem function in soil systems. Pedobiologia 49:479–497.

Cologgi DL, Lampa-Pastirk S, Speers AM, Kelly SD, Reguera G (2011) Extracellular reduction of uranium via Geobacter conductive pili as a protective cellular mechanism. Proc Natl Acad Sci U S A 108:15248–15252.

Cord-Ruwisch R (1985) A quick method for the determination of dissolved and precipitated sulfides in cultures of sulfate-reducing bacteria. J Microbiol Methods 4:33–36.

Cypionka H (1989) Characterization of sulfate transport in Desulfovibrio desulfuricans. Arch Microbiol 152:237–243.

Danovaro R, Gambi C, Dell'Anno A, Corinaldesi C, Fraschetti S, Vanreusel A, Vincx M, Gooday AJ (2008) Exponential decline of deep-sea ecosystem functioning linked to benthic biodiversity loss. Curr Biol 18:1–8.

Dar SA, Tan H, Peacock AD, Jaffe P, N'Guessan L, Williams KH, Strycharz-Glaven S (2013) Spatial Distribution ofGeobacteraceaeand Sulfate-Reducing Bacteria DuringIn SituBioremediation of Uranium-Contaminated Groundwater. Remediation Journal 23:31–49.

De León KB, Zane GM, Trotter VV, Krantz GP, Arkin AP, Butland GP, Walian PJ, Fields MW, Wall JD (2017) Unintended Laboratory-Driven Evolution Reveals Genetic Requirements for Biofilm Formation by Desulfovibrio vulgaris Hildenborough. MBio. doi: 10.1128/mBio.01696-17

de María Guillén-Jiménez F, Morales-Barrera L, Morales-Jiménez J, Hernández-Rodríguez CH, Cristiani-Urbina E (2008) Modulation of tolerance to Cr (VI) and Cr (VI) reduction by sulfate ion in a Candida yeast strain isolated from tannery wastewater. J Ind Microbiol Biotechnol 35:1277–1287.

Denk W, Horstmann H (2004) Serial block-face scanning electron microscopy to reconstruct three-dimensional tissue nanostructure. PLoS Biol 2:e329.

Dhal B, Thatoi HN, Das NN, Pandey BD (2013) Chemical and microbial remediation of hexavalent chromium from contaminated soil and mining/metallurgical solid waste: a review. J Hazard Mater 250-251:272–291.

Doucette CD, Schwab DJ, Wingreen NS, Rabinowitz JD (2011) α-Ketoglutarate coordinates carbon and nitrogen utilization via enzyme I inhibition. Nat Chem Biol 7:894–901.

Duffy JE, Stachowicz JJ (2006) Why biodiversity is important to oceanography: potential roles of genetic, species, and trophic diversity in pelagic ecosystem processes. Mar Ecol Prog Ser 311:179–189.

Dunne WM Jr (2002) Bacterial adhesion: seen any good biofilms lately? Clin Microbiol Rev 15:155–166.

Elasri MO, Miller RV (1999) Study of the response of a biofilm bacterial community to UV radiation. Appl Environ Microbiol 65:2025–2031.

Elias DA, Suflita JM, McInerney MJ, Krumholz LR (2004) Periplasmic Cytochrome c3 of Desulfovibrio vulgaris Is Directly Involved in H2-Mediated Metal but Not Sulfate Reduction. Appl Environ Microbiol 70:413–420.

Ellen AF, Albers S-V, Huibers W, Pitcher A, Hobel CFV, Schwarz H, Folea M, Schouten S, Boekema EJ, Poolman B, Driessen AJM (2009) Proteomic analysis of secreted membrane vesicles of archaeal Sulfolobus species reveals the presence of endosome sorting complex components. Extremophiles 13:67–79.

Enning D, Garrelfs J (2014) Corrosion of iron by sulfate-reducing bacteria: new views of an old problem. Appl Environ Microbiol 80:1226–1236.

Enning D, Venzlaff H, Garrelfs J, Dinh HT, Meyer V, Mayrhofer K, Hassel AW, Stratmann M, Widdel F (2012) Marine sulfate-reducing bacteria cause serious corrosion of iron under electroconductive biogenic mineral crust. Environ Microbiol 14:1772–1787.

Faybishenko B, Hazen TC, Long PE, Brodie EL, Conrad ME, Hubbard SS, Christensen JN, Joyner D, Borglin SE, Chakraborty R, Williams KH, Peterson JE, Chen J, Brown ST, Tokunaga TK, Wan J, Firestone M, Newcomer DR, Resch CT, Cantrell KJ, Willett A, Koenigsberg S (2008) In situ long-term reductive bioimmobilization of Cr(VI) in groundwater using hydrogen release compound. Environ Sci Technol 42:8478–8485.

Fishbain S, Dillon JG, Gough HL, Stahl DA (2003) Linkage of high rates of sulfate reduction in Yellowstone hot springs to unique sequence types in the dissimilatory sulfate respiration pathway. Appl Environ Microbiol 69:3663–3667.

Flemming H-C, Wingender J (2010) The biofilm matrix. Nat Rev Microbiol 8:623–633.

Foti M, Sorokin DY, Lomans B, Mussman M, Zacharova EE, Pimenov NV, Kuenen JG, Muyzer G (2007) Diversity, activity, and abundance of sulfate-reducing bacteria in saline and hypersaline soda lakes. Appl Environ Microbiol 73:2093–2100.

Frank KL, Rogers DR, Olins HC, Vidoudez C, Girguis PR (2013) Characterizing the distribution and rates of microbial sulfate reduction at Middle Valley hydrothermal vents. ISME J 7:1391–1401.

Friedman L, Kolter R (2004) Genes involved in matrix formation in Pseudomonas aeruginosa PA14 biofilms. Mol Microbiol 51:675–690.

Fulsundar S, Harms K, Flaten GE, Johnsen PJ, Chopade BA, Nielsen KM (2014) Gene transfer potential of outer membrane vesicles of Acinetobacter baylyi and effects of stress on vesiculation. Appl Environ Microbiol 80:3469–3483.

Fung DKC, Chan EWC, Chin ML, Chan RCY (2010) Delineation of a bacterial starvation stress response network which can mediate antibiotic tolerance development. Antimicrob Agents Chemother 54:1082–1093.

Gaal T, Bartlett MS, Ross W, Turnbough CL Jr, Gourse RL (1997) Transcription regulation by initiating NTP concentration: rRNA synthesis in bacteria. Science 278:2092–2097.

Gihring TM, Zhang G, Brandt CC, Brooks SC, Campbell JH, Carroll S, Criddle CS, Green SJ, Jardine P, Kostka JE, Lowe K, Mehlhorn TL, Overholt W, Watson DB, Yang Z, Wu W-M, Schadt CW (2011) A Limited Microbial Consortium Is Responsible for Extended Bioreduction of Uranium in a Contaminated Aquifer. Appl Environ Microbiol 77:5955–5965.

Giloteaux L, Goñi-Urriza M, Duran R (2010) Nested PCR and new primers for analysis of sulfate-reducing bacteria in low-cell-biomass environments. Appl Environ Microbiol 76:2856–2865.

González Fernández-Niño SM, Smith-Moritz AM, Chan LJG, Adams PD, Heazlewood JL, Petzold CJ (2015) Standard flow liquid chromatography for shotgun proteomics in bioenergy research. Front Bioeng Biotechnol 3:44.

Goransson M, Forsman K, Uhlin BE (1989) Regulatory genes in the thermoregulation of Escherichia coli pili gene transcription. Genes Dev 3:123–130.

Gorby YA, Yanina S, McLean JS, Rosso KM, Moyles D, Dohnalkova A, Beveridge TJ, Chang IS, Kim BH, Kim KS, Culley DE, Reed SB, Romine MF, Saffarini DA, Hill EA, Shi L, Elias DA, Kennedy DW, Pinchuk G, Watanabe K, Ishii S 'ichi, Logan B, Nealson KH, Fredrickson JK (2006) Electrically conductive bacterial nanowires produced by Shewanella oneidensis strain MR-1 and other microorganisms. Proc Natl Acad Sci U S A 103:11358–11363.

Gorby Y, McLean J, Korenevsky A, Rosso K, El-Naggar MY, Beveridge TJ (2008) Redox-reactive membrane vesicles produced by Shewanella. Geobiology 6:232–241.

Goulhen F, Florence G, Alexandre G, Francois G, Mireille B (2005a) Cr(VI) detoxification by Desulfovibrio vulgaris strain Hildenborough: microbe–metal interactions studies. Appl Microbiol Biotechnol 71:892–897.

Goulhen F, Gloter A, Guyot F, Bruschi M (2006) Cr(VI) detoxification by Desulfovibrio vulgaris strain Hildenborough: microbe-metal interactions studies. Appl Microbiol Biotechnol 71:892–897.

Gramp JP, Bigham JM, Jones FS, Tuovinen OH (2010) Formation of Fe-sulfides in cultures of sulfate-reducing bacteria. J Hazard Mater 175:1062–1067.

Grande R, Di Marcantonio MC, Robuffo I, Pompilio A, Celia C, Di Marzio L, Paolino D, Codagnone M, Muraro R, Stoodley P, Hall-Stoodley L, Mincione G (2015) Helicobacter pylori ATCC 43629/NCTC 11639 Outer Membrane Vesicles (OMVs) from Biofilm and Planktonic Phase Associated with Extracellular DNA (eDNA). Front Microbiol 6:1369.

Gray AN, Egan AJF, Van't Veer IL, Verheul J, Colavin A, Koumoutsi A, Biboy J, Altelaar AFM, Damen MJ, Huang KC, Simorre J-P, Breukink E, den Blaauwen T, Typas A, Gross CA, Vollmer W (2015) Coordination of peptidoglycan synthesis and outer membrane constriction during Escherichia coli cell division. Elife. doi: 10.7554/eLife.07118

Gross R, Hauer B, Otto K, Schmid A (2007) Microbial biofilms: new catalysts for maximizing productivity of long-term biotransformations. Biotechnol Bioeng 98:1123–1134.

Guidi R, Levi L, Rouf SF, Puiac S, Rhen M, Frisan T (2013) Salmonella enterica delivers its genotoxin through outer membrane vesicles secreted from infected cells. Cell Microbiol 15:2034–2050.

Gustafsson JP, Persson I, Oromieh AG, van Schaik JWJ, Sjöstedt C, Kleja DB (2014) Chromium(III) complexation to natural organic matter: mechanisms and modeling. Environ Sci Technol 48:1753–1761.

Haaningnielsen A, Lens P, Vollertsen J, Hvitvedjacobsen T (2005) Sulfide–iron interactions in domestic wastewater from a gravity sewer. Water Res 39:2747–2755.

Habibul N, Hu Y, Wang Y-K, Chen W, Yu H-Q, Sheng G-P (2016) Bioelectrochemical Chromium(VI) Removal in Plant-Microbial Fuel Cells. Environ Sci Technol 50:3882–3889.

Hall-Stoodley L, Costerton JW, Stoodley P (2004) Bacterial biofilms: from the natural environment to infectious diseases. Nat Rev Microbiol 2:95–108.

Harrison JJ, Ceri H, Turner RJ (2007) Multimetal resistance and tolerance in microbial biofilms. Nat Rev Microbiol 5:928–938.

Harrison JJ, Turner RJ, Ceri H (2005) Persister cells, the biofilm matrix and tolerance to metal cations in biofilm and planktonic Pseudomonas aeruginosa. Environ Microbiol 7:981–994.

Heidelberg JF, Seshadri R, Haveman SA, Hemme CL, Paulsen IT, Kolonay JF, Eisen JA, Ward N, Methe B, Brinkac LM, Daugherty SC, Deboy RT, Dodson RJ, Durkin AS, Madupu R, Nelson WC, Sullivan SA, Fouts D, Haft DH, Selengut J, Peterson JD, Davidsen TM, Zafar N, Zhou L, Radune D, Dimitrov G, Hance M, Tran K, Khouri H, Gill J, Utterback TR, Feldblyum TV, Wall JD, Voordouw G, Fraser CM (2004b) The genome sequence of the anaerobic, sulfate-reducing bacterium Desulfovibrio vulgaris Hildenborough. Nat Biotechnol 22:554–559.

Hentzer M, Teitzel GM, Balzer GJ, Heydorn A, Molin S, Givskov M, Parsek MR (2001) Alginate overproduction affects Pseudomonas aeruginosa biofilm structure and function. J Bacteriol 183:5395–5401.

Hockin SL, Gadd GM (2003) Linked redox precipitation of sulfur and selenium under anaerobic conditions by sulfate-reducing bacterial biofilms. Appl Environ Microbiol 69:7063–7072.

Hooper SL, Burstein HJ (2014) Minimization of extracellular space as a driving force in prokaryote association and the origin of eukaryotes. Biol Direct 9:24.

Hubert C, Voordouw G (2007) Oil field souring control by nitrate-reducing Sulfurospirillum spp. that outcompete sulfate-reducing bacteria for organic electron donors. Appl Environ Microbiol 73:2644–2652.

Hwang C, Wu W, Gentry TJ, Carley J, Corbin GA, Carroll SL, Watson DB, Jardine PM, Zhou J, Criddle CS, Fields MW (2009a) Bacterial community succession during in situ uranium bioremediation: spatial similarities along controlled flow paths. ISME J 3:47–64.

Iannotti EL, Kafkewitz D, Wolin MJ, Bryant MP (1973) Glucose fermentation products in Ruminococcus albus grown in continuous culture with Vibrio succinogenes: changes caused by interspecies transfer of H 2. J Bacteriol 114:1231–1240.

Inaba T, Hori T, Aizawa H, Ogata A, Habe H (2017) Architecture, component, and microbiome of biofilm involved in the fouling of membrane bioreactors. NPJ Biofilms Microbiomes 3:5.

Ishii S 'ichi, Kosaka T, Hori K, Hotta Y, Watanabe K (2005) Coaggregation facilitates interspecies hydrogen transfer between Pelotomaculum thermopropionicum and Methanothermobacter thermautotrophicus. Appl Environ Microbiol 71:7838–7845.

Itoh M, Nakamura M, Suzuki T, Kawai K, Horitsu H, Takamizawa K (1995) Mechanism of chromium(VI) toxicity in Escherichia coli: is hydrogen peroxide essential in Cr(VI) toxicity? J Biochem 117:780–786.

Ivanisevic J, Zhu Z-J, Plate L, Tautenhahn R, Chen S, O'Brien PJ, Johnson CH, Marletta MA, Patti GJ, Siuzdak G (2013) Toward 'omic scale metabolite profiling: a dual separation--mass spectrometry approach for coverage of lipid and central carbon metabolism. Anal Chem 85:6876–6884.

Ivanov IE, Boyd CD, Newell PD, Schwartz ME, Turnbull L, Johnson MS, Whitchurch CB, O'Toole GA, Camesano TA (2012) Atomic force and super-resolution microscopy support a role for LapA as a cell-surface biofilm adhesin of Pseudomonas fluorescens. Res Microbiol 163:685–691.

Jackson BE, McInerney MJ (2000) Thiosulfate Disproportionation by Desulfotomaculum thermobenzoicum. Appl Environ Microbiol 66:3650–3653.

Jarvis B, Wilrich C, Wilrich P-T (2010a) Reconsideration of the derivation of Most Probable Numbers, their standard deviations, confidence bounds and rarity values. J Appl Microbiol 109:1660–1667.

Jurcisek JA, Bakaletz LO (2007) Biofilms formed by nontypeable Haemophilus influenzae in vivo contain both double-stranded DNA and type IV pilin protein. J Bacteriol 189:3868–3875.

Kadiiska MB, Xiang Q-H, Mason RP (1994) In vivo Free Radical Generation by Chromium (VI): An Electron Spin Resonance Spin-Trapping Investigation. Chem Res Toxicol 7:800–805.

Kanehisa M (2000) KEGG: Kyoto Encyclopedia of Genes and Genomes. Nucleic Acids Res 28:27–30.

Kanehisa M, Furumichi M, Tanabe M, Sato Y, Morishima K (2017) KEGG: new perspectives on genomes, pathways, diseases and drugs. Nucleic Acids Res 45:D353–D361.

Kanehisa M, Sato Y, Kawashima M, Furumichi M, Tanabe M (2016) KEGG as a reference resource for gene and protein annotation. Nucleic Acids Res 44:D457–62.

Kaplan D, Christiaen D, Arad SM (1987) Chelating Properties of Extracellular Polysaccharides from Chlorella spp. Appl Environ Microbiol 53:2953–2956.

Karbonowska H, Wiater A, Hulanicka D (1977b) Sulphate permease of Escherichia coli K12. Acta Biochim Pol 24:329–334.

Karl DM, Church MJ, Dore JE, Letelier RM, Mahaffey C (2012) Predictable and efficient carbon sequestration in the North Pacific Ocean supported by symbiotic nitrogen fixation. Proc Natl Acad Sci U S A 109:1842–1849.

Karnachuk OV, Mardanov AV, Avakyan MR, Kadnikov VV, Vlasova M, Beletsky AV, Gerasimchuk AL, Ravin NV (2015) Draft genome sequence of the first acid-tolerant sulfate-reducing deltaproteobacterium Desulfovibrio sp. TomC having potential for minewater treatment. FEMS Microbiol Lett. doi: 10.1093/femsle/fnv007

Kawanishi S, Inoue S, Sano S (1986) Mechanism of DNA cleavage induced by sodium chromate(VI) in the presence of hydrogen peroxide. J Biol Chem 261:5952–5958.

Keller A, Nesvizhskii AI, Kolker E, Aebersold R (2002) Empirical statistical model to estimate the accuracy of peptide identifications made by MS/MS and database search. Anal Chem 74:5383–5392.

Keller JK, Bridgham SD (2007) Pathways of anaerobic carbon cycling across an ombrotrophic-minerotrophic peatland gradient. Limnol Oceanogr 52:96–107.

Keller KL, Bender KS, Wall JD (2009) Development of a markerless genetic exchange system for Desulfovibrio vulgaris Hildenborough and its use in generating a strain with increased transformation efficiency. Appl Environ Microbiol 75:7682–7691.

Keller KL, Wall JD (2011a) Genetics and Molecular Biology of the Electron Flow for Sulfate Respiration in Desulfovibrio. Front Microbiol. doi: 10.3389/fmicb.2011.00135

Kim S-Y, Kim J-H, Kim C-J, Oh D-K (1996) Metal adsorption of the polysaccharide produced from Methylobacterium organophilum. Biotechnol Lett 18:1161–1164.

Kimura KR, Nakata M, Sumitomo T, Kreikemeyer B, Podbielski A, Terao Y, Kawabata S (2012) Involvement of T6 pili in biofilm formation by serotype M6 Streptococcus pyogenes. J Bacteriol 194:804–812.

Klausen M, Heydorn A, Ragas P, Lambertsen L, Aaes-Jørgensen A, Molin S, Tolker-Nielsen T (2003) Biofilm formation by Pseudomonas aeruginosa wild type, flagella and type IV pili mutants. Mol Microbiol 48:1511–1524.

Klieve AV, Yokoyama MT, Forster RJ, Ouwerkerk D, Bain PA, Mawhinney EL (2005) Naturally occurring DNA transfer system associated with membrane vesicles in cellulolytic Ruminococcus spp. of ruminal origin. Appl Environ Microbiol 71:4248–4253.

Klonowska A, Clark ME, Thieman SB, Giles BJ, Wall JD, Fields MW (2008) Hexavalent chromium reduction in Desulfovibrio vulgaris Hildenborough causes transitory inhibition of sulfate reduction and cell growth. Appl Microbiol Biotechnol 78:1007–1016.

Knoblauch C, Jørgensen BB, Harder J (1999) Community size and metabolic rates of psychrophilic sulfate-reducing bacteria in Arctic marine sediments. Appl Environ Microbiol 65:4230–4233.

Koch GH, United States. Federal Highway Administration (2002) Corrosion Cost and Preventive Strategies in the United States.

Kolter R (2005) Surfacing views of biofilm biology. Trends Microbiol 13:1–2.

Kuehn MJ (2005) Bacterial outer membrane vesicles and the host-pathogen interaction. Genes Dev 19:2645–2655.

Kulp A, Kuehn MJ (2010) Biological functions and biogenesis of secreted bacterial outer membrane vesicles. Annu Rev Microbiol 64:163–184.

Kwak YH, Lee DS, Kim HB (2003a) Vibrio harveyi nitroreductase is also a chromate reductase. Appl Environ Microbiol 69:4390–4395.

Labrenz M, Banfield JF (2004) Sulfate-Reducing Bacteria-Dominated Biofilms That Precipitate ZnS in a Subsurface Circumneutral-pH Mine Drainage System. Microb Ecol. doi: 10.1007/s00248-003-1025-8

Laue H, Denger K, Cook AM (1997) Taurine reduction in anaerobic respiration of Bilophila wadsworthia RZATAU. Appl Environ Microbiol 63:2016–2021.

Lee E-Y, Choi D-Y, Kim D-K, Kim J-W, Park JO, Kim S, Kim S-H, Desiderio DM, Kim Y-K, Kim K-P, Gho YS (2009) Gram-positive bacteria produce membrane vesicles: proteomics-based characterization of Staphylococcus aureus-derived membrane vesicles. Proteomics 9:5425–5436.

Lee IH, Finkel T (2013) Metabolic regulation of the cell cycle. Curr Opin Cell Biol 25:724–729.

Liamleam W, Annachhatre AP (2007) Electron donors for biological sulfate reduction. Biotechnol Adv 25:452–463.

Liao S, Klein MI, Heim KP, Fan Y, Bitoun JP, Ahn S-J, Burne RA, Koo H, Brady LJ, Wen ZT (2014) Streptococcus mutans extracellular DNA is upregulated during growth in biofilms, actively released via membrane vesicles, and influenced by components of the protein secretion machinery. J Bacteriol 196:2355–2366.

Lie TJ, Godchaux W, Leadbetter ER (1999) Sulfonates as terminal electron acceptors for growth of sulfite-reducing bacteria (Desulfitobacterium spp.) and sulfate-reducing bacteria: effects of inhibitors of sulfidogenesis. Appl Environ Microbiol 65:4611–4617.

Li MZ, Elledge SJ (2007) Harnessing homologous recombination in vitro to generate recombinant DNA via SLIC. Nat Methods 4:251–256.

Liu H, Huang L, Huang Z, Zheng J (2007) Specification of sulfate reducing bacteria biofilms accumulation effects on corrosion initiation. Mater Corros 58:44–48.

Liu X, Ferenci T (1998) Regulation of porin-mediated outer membrane permeability by nutrient limitation in Escherichia coli. J Bacteriol 180:3917–3922.

Li X, Krumholz LR (2009a) Thioredoxin is involved in U(VI) and Cr(VI) reduction in Desulfovibrio desulfuricans G20. J Bacteriol 191:4924–4933.

Lloyd JR, Nolting H‐F, Solé VA, Bosecker K, Macaskie LE (1998) Technetium reduction and precipitation by sulfate‐reducing bacteria. Geomicrobiol J 15:45–58.

Lohman EJ, Gardner RD, Halverson L, Macur RE, Peyton BM, Gerlach R (2013) An efficient and scalable extraction and quantification method for algal derived biofuel. J Microbiol Methods 94:235–244.

Lovley DR, Phillips EJ (1994) Reduction of Chromate by Desulfovibrio vulgaris and Its c(3) Cytochrome. Appl Environ Microbiol 60:726–728.

Lovley DR, Widman PK, Woodward JC, Phillips EJ (1993) Reduction of uranium by cytochrome c3 of Desulfovibrio vulgaris. Appl Environ Microbiol 59:3572–3576.

Ludwig W, Strunk O, Westram R, Richter L, Meier H, Yadhukumar, Buchner A, Lai T, Steppi S, Jobb G, Förster W, Brettske I, Gerber S, Ginhart AW, Gross O, Grumann S, Hermann S, Jost R, König A, Liss T, Lüssmann R, May M, Nonhoff B, Reichel B,

Strehlow R, Stamatakis A, Stuckmann N, Vilbig A, Lenke M, Ludwig T, Bode A, Schleifer K-H (2004) ARB: a software environment for sequence data. Nucleic Acids Res 32:1363–1371.

Magot M, Basso O, Tardy-Jacquenod C, Caumette P (2004) Desulfovibrio bastinii sp. nov. and Desulfovibrio gracilis sp. nov., moderately halophilic, sulfate-reducing bacteria isolated from deep subsurface oilfield water. Int J Syst Evol Microbiol 54:1693–1697.

Ma L, Jackson KD, Landry RM, Parsek MR, Wozniak DJ (2006) Analysis of Pseudomonas aeruginosa conditional psl variants reveals roles for the psl polysaccharide in adhesion and maintaining biofilm structure postattachment. J Bacteriol 188:8213–8221.

Manning AJ, Kuehn MJ (2011) Contribution of bacterial outer membrane vesicles to innate bacterial defense. BMC Microbiol 11:258.

Marozava S, Röling WFM, Seifert J, Küffner R, von Bergen M, Meckenstock RU (2014) Physiology of Geobacter metallireducens under excess and limitation of electron donors. Part II. Mimicking environmental conditions during cultivation in retentostats. Syst Appl Microbiol 37:287–295.

Marshall MJ, Beliaev AS, Dohnalkova AC, Kennedy DW, Shi L, Wang Z, Boyanov MI, Lai B, Kemner KM, McLean JS, Reed SB, Culley DE, Bailey VL, Simonson CJ, Saffarini DA, Romine MF, Zachara JM, Fredrickson JK (2006) c-Type cytochrome-dependent formation of U(IV) nanoparticles by Shewanella oneidensis. PLoS Biol 4:e268.

Marsili E, Beyenal H, Di Palma L, Merli C, Dohnalkova A, Amonette JE, Lewandowski Z (2007) Uranium immobilization by sulfate-reducing biofilms grown on hematite, dolomite, and calcite. Environ Sci Technol 41:8349–8354.

Mashburn LM, Whiteley M (2005) Membrane vesicles traffic signals and facilitate group activities in a prokaryote. Nature 437:422–425.

Mathiopoulos C, Mueller JP, Slack FJ, Murphy CG, Patankar S, Bukusoglu G, Sonenshein AL (1991) A Bacillus subtilis dipeptide transport system expressed early during sporulation. Mol Microbiol 5:1903–1913.

Matsuyama T, Nakagawa Y (1996) Surface-active exolipids: analysis of absolute chemical structures and biological functions. J Microbiol Methods 25:165–175.

McCaig WD, Koller A, Thanassi DG (2013) Production of outer membrane vesicles and outer membrane tubes by Francisella novicida. J Bacteriol 195:1120–1132.

McDonald KL, Morphew M, Verkade P, Müller-Reichert T (2007) Recent advances in high-pressure freezing: equipment- and specimen-loading methods. Methods Mol Biol 369:143–173.

McDONALD KL, Webb RI (2011) Freeze substitution in 3 hours or less. J Microsc 243:227–233.

McDonald K, Müller-Reichert T (2002) Cryomethods for thin section electron microscopy. Methods Enzymol 351:96–123.

McGrath SP (1995) Chromium and Nickel. In: Heavy Metals in Soils. pp 152–178

McInerney MJ, Sieber JR, Gunsalus RP (2009) Syntrophy in anaerobic global carbon cycles. Curr Opin Biotechnol 20:623–632.

McKew BA, Taylor JD, McGenity TJ, Underwood GJC (2011) Resistance and resilience of benthic biofilm communities from a temperate saltmarsh to desiccation and rewetting. ISME J 5:30–41.

McLean RJ, Beauchemin D, Clapham L, Beveridge TJ (1990) Metal-Binding Characteristics of the Gamma-Glutamyl Capsular Polymer of Bacillus licheniformis ATCC 9945. Appl Environ Microbiol 56:3671–3677.

Mello BL, Alessi AM, McQueen-Mason S, Bruce NC, Polikarpov I (2016) Nutrient availability shapes the microbial community structure in sugarcane bagasse compost-derived consortia. Sci Rep. doi: 10.1038/srep38781

Michel C, Brugna M, Aubert C, Bernadac A, Bruschi M (2001) Enzymatic reduction of chromate: comparative studies using sulfate-reducing bacteria. Key role of polyheme cytochromes c and hydrogenases. Appl Microbiol Biotechnol 55:95–100.

Mogensen GL, Kjeldsen KU, Ingvorsen K (2005) Desulfovibrio aerotolerans sp. nov., an oxygen tolerant sulphate-reducing bacterium isolated from activated sludge. Anaerobe 11:339–349.

Molin S, Tolker-Nielsen T (2003) Gene transfer occurs with enhanced efficiency in biofilms and induces enhanced stabilisation of the biofilm structure. Curr Opin Biotechnol 14:255–261.

Moore CM, Mills MM, Arrigo KR, Berman-Frank I, Bopp L, Boyd PW, Galbraith ED, Geider RJ, Guieu C, Jaccard SL, Jickells TD, La Roche J, Lenton TM, Mahowald NM, Marañón E, Marinov I, Moore JK, Nakatsuka T, Oschlies A, Saito MA, Thingstad TF,

Tsuda A, Ulloa O (2013) Processes and patterns of oceanic nutrient limitation. Nat Geosci 6:701–710.

Mukhopadhyay A, Redding AM, Joachimiak MP, Arkin AP, Borglin SE, Dehal PS, Chakraborty R, Geller JT, Hazen TC, He Q, Joyner DC, Martin VJJ, Wall JD, Yang ZK, Zhou J, Keasling JD (2007) Cell-wide responses to low-oxygen exposure in Desulfovibrio vulgaris Hildenborough. J Bacteriol 189:5996–6010.

Müller AL, Kjeldsen KU, Rattei T, Pester M, Loy A (2015) Phylogenetic and environmental diversity of DsrAB-type dissimilatory (bi)sulfite reductases. ISME J 9:1152–1165.

Müller-Reichert T, Hohenberg H, O'Toole ET, McDonald K (2003) Cryoimmobilization and three-dimensional visualization of C. elegans ultrastructure. J Microsc 212:71–80.

Muyzer G, Stams AJM (2008) The ecology and biotechnology of sulphate-reducing bacteria. Nat Rev Microbiol 6:441–454.

Naaz A (2004) Loss of cyclin-dependent kinase inhibitors produces adipocyte hyperplasia and obesity. The FASEB Journal. doi: 10.1096/fj.04-2631fje

Nakamura N, Lin HC, McSweeney CS, Mackie RI, Gaskins HR (2010) Mechanisms of microbial hydrogen disposal in the human colon and implications for health and disease. Annu Rev Food Sci Technol 1:363–395.

Nanninga HJ, Gottschal JC (1987) Properties of Desulfovibrio carbinolicus sp. nov. and Other Sulfate-Reducing Bacteria Isolated from an Anaerobic-Purification Plant. Appl Environ Microbiol 53:802–809.

Neria-González I, Wang ET, Ramírez F, Romero JM, Hernández-Rodríguez C (2006) Characterization of bacterial community associated to biofilms of corroded oil pipelines from the southeast of Mexico. Anaerobe 12:122–133.

Nesvizhskii AI, Keller A, Kolker E, Aebersold R (2003) A Statistical Model for Identifying Proteins by Tandem Mass Spectrometry. Anal Chem 75:4646–4658.

Nielsen PH, Jahn A, Palmgren R (1997) Conceptual model for production and composition of exopolymers in biofilms. Water Sci Technol. doi: 10.1016/s0273-1223(97)00318-1

Nishio A, Uyeki EM (1985) Inhibition of DNA synthesis by chromium compounds. J Toxicol Environ Health 15:237–244.

Nriagu JO, Nieboer E (1988) Chromium in the natural and human environments. John Wiley & Sons

Odom J (1981) Hydrogen cycling as a general mechanism for energy coupling in the sulfate-reducing bacteria, Desulfovibrio sp. FEMS Microbiol Lett 12:47–50.

Ohtake H, Cervantes C, Silver S (1987a) Decreased chromate uptake in Pseudomonas fluorescens carrying a chromate resistance plasmid. J Bacteriol 169:3853–3856.

Okabe S, Nielsen PH, Characklis WG (1992) Factors affecting microbial sulfate reduction byDesulfovibrio desulfuricansin continuous culture: Limiting nutrients and sulfide concentration. Biotechnol Bioeng 40:725–734.

Ollivier B, Cord-Ruwisch R, Hatchikian EC, Garcia JL (1988) Characterization of Desulfovibrio fructosovorans sp. nov. Arch Microbiol 149:447–450.

Orench-Rivera N, Kuehn MJ (2016) Environmentally controlled bacterial vesicle-mediated export. Cell Microbiol 18:1525–1536.

Ota N, Galsworthy PR, Pardee AB (1971a) Genetics of sulfate transport by Salmonella typhimurium. J Bacteriol 105:1053–1062.

Ouattara AS, Cuzin N, Traore AS, -L. Garcia J (1992) Anerobic degradation of 1,2-propanediol by a new Desulfovibrio strain and D. alcoholovorans. Arch Microbiol 158:218–225.

Pardee AB, Prestidge LS, Whipple MB, Dreyfuss J (1966a) A binding site for sulfate and its relation to sulfate transport into Salmonella typhimurium. J Biol Chem 241:3962–3969.

Park AJ, Murphy K, Surette MD, Bandoro C, Krieger JR, Taylor P, Khursigara CM (2015) Tracking the Dynamic Relationship between Cellular Systems and Extracellular Subproteomes in Pseudomonas aeruginosa Biofilms. J Proteome Res 14:4524–4537.

Parks JM, Johs A, Podar M, Bridou R, Hurt RA Jr, Smith SD, Tomanicek SJ, Qian Y, Brown SD, Brandt CC, Palumbo AV, Smith JC, Wall JD, Elias DA, Liang L (2013) The genetic basis for bacterial mercury methylation. Science 339:1332–1335.

Parsons HT, González Fernández-Niño SM, Heazlewood JL (2013) Separation of the Plant Golgi Apparatus and Endoplasmic Reticulum by Free-Flow Electrophoresis. In: Methods in Molecular Biology. pp 527–539

Payne RB, Gentry DM, Rapp-Giles BJ, Casalot L, Wall JD (2002) Uranium Reduction by Desulfovibrio desulfuricans Strain G20 and a Cytochrome c3 Mutant. Appl Environ Microbiol 68:3129–3132.

Peck HD (1993) Bioenergetic Strategies of the Sulfate-Reducing Bacteria. In: Brock/Springer Series in Contemporary Bioscience. pp 41–76

Pepi M, Baldi F (1992) Modulation of chromium(VI) toxicity by organic and inorganic sulfur species in yeasts from industrial wastes. Biometals 5:179–185.

Pérez-Cruz C, Carrión O, Delgado L, Martinez G, López-Iglesias C, Mercade E (2013) New type of outer membrane vesicle produced by the Gram-negative bacterium Shewanella vesiculosa M7T: implications for DNA content. Appl Environ Microbiol 79:1874–1881.

Pimentel BE, Moreno-SÃ¡nchez R, Cervantes C (2002) Efflux of chromate byPseudomonas aeruginosacells expressing the ChrA protein. FEMS Microbiol Lett 212:249–254.

Pirbadian S, Barchinger SE, Leung KM, Byun HS, Jangir Y, Bouhenni RA, Reed SB, Romine MF, Saffarini DA, Shi L, Gorby YA, Golbeck JH, El-Naggar MY (2014) Shewanella oneidensis MR-1 nanowires are outer membrane and periplasmic extensions of the extracellular electron transport components. Proc Natl Acad Sci U S A 111:12883–12888.

Plugge CM, Scholten JCM, Culley DE, Nie L, Brockman FJ, Zhang W (2010) Global transcriptomics analysis of the Desulfovibrio vulgaris change from syntrophic growth with Methanosarcina barkeri to sulfidogenic metabolism. Microbiology 156:2746–2756.

Pratt LA, Kolter R (1998) Genetic analysis of Escherichia coli biofilm formation: roles of flagella, motility, chemotaxis and type I pili. Mol Microbiol 30:285–293.

Priester JH, Olson SG, Webb SM, Neu MP, Hersman LE, Holden PA (2006) Enhanced exopolymer production and chromium stabilization in Pseudomonas putida unsaturated biofilms. Appl Environ Microbiol 72:1988–1996.

Pruesse E, Peplies J, Glöckner FO (2012) SINA: accurate high-throughput multiple sequence alignment of ribosomal RNA genes. Bioinformatics 28:1823–1829.

Qatibi AI, Garcia J-L (1990) 1, 2 - and 1, 3 - Propanediol Degradation by Desulfovibrio Alcoholovorans SP. Nov., in Pure Culture or Through H2 Interspecies Transfer. In: Microbiology and Biochemistry of Strict Anaerobes Involved in Interspecies Hydrogen Transfer. pp 451–453

Quan JA, Schneider BL, Paulsen IT, Yamada M, Kredich NM, Saier MH Jr (2002) Regulation of carbon utilization by sulfur availability in Escherichia coli and Salmonella typhimurium. Microbiology 148:123–131.

Ramos AR, Grein F, Oliveira GP, Venceslau SS, Keller KL, Wall JD, Pereira IAC (2015) The FlxABCD-HdrABC proteins correspond to a novel NADH dehydrogenase/heterodisulfide reductase widespread in anaerobic bacteria and involved in ethanol metabolism inDesulfovibrio vulgaris Hildenborough. Environ Microbiol 17:2288–2305.

Ramsay BD, Hwang C, Woo HL, Carroll SL, Lucas S, Han J, Lapidus AL, Cheng J-F, Goodwin LA, Pitluck S, Peters L, Chertkov O, Held B, Detter JC, Han CS, Tapia R, Land ML, Hauser LJ, Kyrpides NC, Ivanova NN, Mikhailova N, Pagani I, Woyke T, Arkin AP, Dehal P, Chivian D, Criddle CS, Wu W, Chakraborty R, Hazen TC, Fields MW (2015) High-Quality Draft Genome Sequence of Desulfovibrio carbinoliphilus FW-101-2B, an Organic Acid-Oxidizing Sulfate-Reducing Bacterium Isolated from Uranium(VI)-Contaminated Groundwater. Genome Announc. doi: 10.1128/genomeA.00092-15

Rani SA, Pitts B, Beyenal H, Veluchamy RA, Lewandowski Z, Davison WM, Buckingham-Meyer K, Stewart PS (2007) Spatial patterns of DNA replication, protein synthesis, and oxygen concentration within bacterial biofilms reveal diverse physiological states. J Bacteriol 189:4223–4233.

Remis JP, Wei D, Gorur A, Zemla M, Haraga J, Allen S, Witkowska HE, Costerton JW, Berleman JE, Auer M (2014) Bacterial social networks: structure and composition of Myxococcus xanthus outer membrane vesicle chains. Environ Microbiol 16:598–610.

Rey FE, Gonzalez MD, Cheng J, Wu M, Ahern PP, Gordon JI (2013) Metabolic niche of a prominent sulfate-reducing human gut bacterium. Proc Natl Acad Sci U S A 110:13582–13587.

Rickard D, III Luther GW (2007) Chemistry of Iron Sulfides. ChemInform. doi: 10.1002/chin.200719200

Riedel GF (1985) The relationship between chromium(VI) uptake, sulfate uptake, and chromium(VI) toxicity in the estuarine diatom Thalassiosira pseudonana. Aquat Toxicol 7:191–204.

Robins KJ, Hooks DO, Rehm BHA, Ackerley DF (2013a) Escherichia coli NemA Is an Efficient Chromate Reductase That Can Be Biologically Immobilized to Provide a Cell Free System for Remediation of Hexavalent Chromium. PLoS One 8:e59200.

Sakaguchi T, Arakaki A, Matsunaga T (2002) Desulfovibrio magneticus sp. nov., a novel sulfate-reducing bacterium that produces intracellular single-domain-sized magnetite particles. Int J Syst Evol Microbiol 52:215–221.

Sasi Jyothsna TS, Sasikala C, Ramana CV (2008) Desulfovibrio psychrotolerans sp. nov., a psychrotolerant and moderately alkaliphilic sulfate-reducing deltaproteobacterium from the Himalayas. Int J Syst Evol Microbiol 58:821–825.

Saxena R, Voight BF, Lyssenko V, Burtt NP, de Bakker PIW, Chen H, Roix JJ, Kathiresan S, Hirschhorn JN, Daly MJ, Hughes TE, Groop L, Altshuler D, Almgren P, Florez JC, Meyer J, Ardlie K, Boström KB, Isomaa B, Lettre G, Lindblad U, Lyon HN, Melander O, Newton-Cheh C, Nilsson P, Orho-Melander M, Råstam L, Speliotes EK, Taskinen M-R, Tuomi T, Guiducci C, Berglund A, Carlson J, Gianniny L, Hackett R, Hall L, Holmkvist J, Laurila E, Sjögren M, Sterner M, Surti A, Svensson M, Svensson M, Tewhey R, Blumenstiel B, Parkin M, DeFelice M, Barry R, Brodeur W, Camarata J, Chia N, Fava M, Gibbons J, Handsaker B, Healy C, Nguyen K, Gates C, Sougnez C, Gage D, Nizzari M, Gabriel SB, Chirn G-W, Ma Q, Parikh H, Richardson D, Ricke D, Purcell S (2007) Genome-Wide Association Analysis Identifies Loci for Type 2 Diabetes and Triglyceride Levels. Science 316:1331–1336.

Schmaler M, Jann NJ, Götz F, Landmann R (2010) Staphylococcal lipoproteins and their role in bacterial survival in mice. Int J Med Microbiol 300:155–160.

Schooling SR, Beveridge TJ (2006) Membrane Vesicles: an Overlooked Component of the Matrices of Biofilms. J Bacteriol 188:5945–5957.

Schwechheimer C, Kuehn MJ (2015) Outer-membrane vesicles from Gram-negative bacteria: biogenesis and functions. Nat Rev Microbiol 13:605–619.

Sena-Vélez M, Redondo C, Graham JH, Cubero J (2016) Presence of Extracellular DNA during Biofilm Formation by Xanthomonas citri subsp. citri Strains with Different Host Range. PLoS One 11:e0156695.

Shi XG, Dalal NS (1990a) On the hydroxyl radical formation in the reaction between hydrogen peroxide and biologically generated chromium(V) species. Arch Biochem Biophys 277:342–350.

Shi XL, Dalal NS (1990b) NADPH-dependent flavoenzymes catalyze one electron reduction of metal ions and molecular oxygen and generate hydroxyl radicals. FEBS Lett 276:189–191.

Sirko A, Hryniewicz M, Hulanicka D, Böck A (1990a) Sulfate and thiosulfate transport in Escherichia coli K-12: nucleotide sequence and expression of the cysTWAM gene cluster. J Bacteriol 172:3351–3357.

Solopova A, Formosa-Dague C, Courtin P, Furlan S, Veiga P, Péchoux C, Armalyte J, Sadauskas M, Kok J, Hols P, Dufrêne YF, Kuipers OP, Chapot-Chartier M-P, Kulakauskas S (2016) Regulation of Cell Wall Plasticity by Nucleotide Metabolism in Lactococcus lactis. J Biol Chem 291:11323–11336.

Spain AM, Krumholz LR (2011) Nitrate-Reducing Bacteria at the Nitrate and Radionuclide Contaminated Oak Ridge Integrated Field Research Challenge Site: A Review. Geomicrobiol J 28:418–429.

Stams AJM, Plugge CM (2009) Electron transfer in syntrophic communities of anaerobic bacteria and archaea. Nat Rev Microbiol 7:568–577.

Stearns DM, Wetterhahn KE (1994) Reaction of Chromium(VI) with Ascorbate Produces Chromium(V), Chromium(IV), and Carbon-Based Radicals. Chem Res Toxicol 7:219–230.

Steinberger RE, Holden PA (2005) Extracellular DNA in single- and multiple-species unsaturated biofilms. Appl Environ Microbiol 71:5404–5410.

Stewart PS (2002) Mechanisms of antibiotic resistance in bacterial biofilms. Int J Med Microbiol 292:107–113.

Stewart PS, Franklin MJ (2008) Physiological heterogeneity in biofilms. Nat Rev Microbiol 6:199–210.

Stylo M, Neubert N, Roebbert Y, Weyer S, Bernier-Latmani R (2015) Mechanism of Uranium Reduction and Immobilization in Desulfovibrio vulgaris Biofilms. Environ Sci Technol 49:10553–10561.

Subramanian P, Pirbadian S, El-Naggar MY, Jensen GJ (2016a) Electron Cryo-Tomography of Nanowires in Shewanella Oneidensis MR-1. Biophys J 110:23a.

Sun B, Cole JR, Sanford RA, Tiedje JM (2000) Isolation and Characterization of Desulfovibrio dechloracetivorans sp. nov., a Marine Dechlorinating Bacterium Growing by Coupling the Oxidation of Acetate to the Reductive Dechlorination of 2-Chlorophenol. Appl Environ Microbiol 66:2408–2413.

Teitzel GM, Parsek MR (2003) Heavy metal resistance of biofilm and planktonic Pseudomonas aeruginosa. Appl Environ Microbiol 69:2313–2320.

Thomas PE, Ryan D, Levin W (1976) An improved staining procedure for the detection of the peroxidase activity of cytochrome P-450 on sodium dodecyl sulfate polyacrylamide gels. Anal Biochem 75:168–176.

Truex MJ, Oostrom M, Strickland CE, Johnson TC, Freedman VL, Johnson CD, Greenwood WJ, Ward AL, Clayton RE, Lindberg MJ, Peterson JE, Hubbard S, Chronister GB, Benecke MW (2012) Deep Vadose Zone Treatability Test for the Hanford Central Plateau: Soil Desiccation Pilot Test Results.

Truper HG (1984) Microorganisms and the Sulfur Cycle. In: Müller A, Krebs B (eds) Sulfur: Its Significance for Chemistry, for the Geo-, Bio-, and Cosmosphere and Technology. Elsevier, pp 351–365

Tyagi M, da Fonseca MMR, de Carvalho CCCR (2011a) Bioaugmentation and biostimulation strategies to improve the effectiveness of bioremediation processes. Biodegradation 22:231–241.

Valente FMA, Oliveira ASF, Gnadt N, Pacheco I, Coelho AV, Xavier AV, Teixeira M, Soares CM, Pereira IAC (2005) Hydrogenases in Desulfovibrio vulgaris Hildenborough: structural and physiologic characterisation of the membrane-bound [NiFeSe] hydrogenase. J Biol Inorg Chem 10:667–682.

Valente FMA, Pereira PM, Venceslau SS, Regalla M, Coelho AV, Pereira IAC (2007) The [NiFeSe] hydrogenase fromDesulfovibrio vulgarisHildenborough is a bacterial lipoprotein lacking a typical lipoprotein signal peptide. FEBS Lett 581:3341–3344.

Vandieken V, Knoblauch C, Jørgensen BB (2006) Desulfovibrio frigidus sp. nov. and Desulfovibrio ferrireducens sp. nov., psychrotolerant bacteria isolated from Arctic fjord sediments (Svalbard) with the ability to reduce Fe(III). Int J Syst Evol Microbiol 56:681–685.

Vats N, Lee SF (2000) Active detachment of Streptococcus mutans cells adhered to epon-hydroxylapatite surfaces coated with salivary proteins in vitro. Arch Oral Biol 45:305–314.

Viamajala S, Peyton BM, Apel WA, Petersen JN (2002) Chromate/nitrite interactions in Shewanella oneidensis MR-1: evidence for multiple hexavalent chromium [Cr(VI)] reduction mechanisms dependent on physiological growth conditions. Biotechnol Bioeng 78:770–778.

Villanueva L, Haveman SA, Summers ZM, Lovley DR (2008) Quantification of Desulfovibrio vulgaris Dissimilatory Sulfite Reductase Gene Expression during Electron Donor- and Electron Acceptor-Limited Growth. Appl Environ Microbiol 74:5850–5853.

Wagner M, Roger AJ, Flax JL, Brusseau GA, Stahl DA (1998) Phylogeny of dissimilatory sulfite reductases supports an early origin of sulfate respiration. J Bacteriol 180:2975–2982.

Walian PJ, Allen S, Shatsky M, Zeng L, Szakal ED, Liu H, Hall SC, Fisher SJ, Lam BR, Singer ME, Geller JT, Brenner SE, Chandonia J-M, Hazen TC, Ewa Witkowska H, Biggin MD, Jap BK (2012) High-throughput Isolation and Characterization of Untagged Membrane Protein Complexes: Outer Membrane Complexes ofDesulfovibrio vulgaris. J Proteome Res 121025102316001.

Walters MC, Roe F, Bugnicourt A, Franklin MJ, Stewart PS (2003) Contributions of Antibiotic Penetration, Oxygen Limitation, and Low Metabolic Activity to Tolerance of Pseudomonas aeruginosa Biofilms to Ciprofloxacin and Tobramycin. Antimicrob Agents Chemother 47:317–323.

Walther T, Létisse F, Peyriga L, Alkim C, Liu Y, Lardenois A, Martin-Yken H, Portais J-C, Primig M, François\ JM (2014) Developmental stage-dependent metabolic regulation during meiotic differentiation in budding yeast. BMC Biol. doi: 10.1186/s12915-014-0060-x

Wang M, Weiss M, Simonovic M, Haertinger G, Schrimpf SP, Hengartner MO, von Mering C (2012) PaxDb, a database of protein abundance averages across all three domains of life. Mol Cell Proteomics 11:492–500.

Whitchurch CB (2002) Extracellular DNA Required for Bacterial Biofilm Formation. Science 295:1487–1487.

Whitman WB, Coleman DC, Wiebe WJ (1998) Prokaryotes: the unseen majority. Proc Natl Acad Sci U S A 95:6578–6583.

Widdel F (1988) Microbiology and ecology of sulfate- and sulfur-reducing bacteria. In: Zehnder AJB (ed) Biology of anaerobic microorganisms. Wiley & Sons, New York, pp 469–575

Williams KH, Long PE, Davis JA, Wilkins MJ, Lucie N'Guessan A, Steefel CI, Yang L, Newcomer D, Spane FA, Kerkhof LJ, McGuinness L, Dayvault R, Lovley DR (2011) Acetate Availability and its Influence on Sustainable Bioremediation of Uranium-Contaminated Groundwater. Geomicrobiol J 28:519–539.

Wilson MM, Bernstein HD (2016) Surface-Exposed Lipoproteins: An Emerging Secretion Phenomenon in Gram-Negative Bacteria. Trends Microbiol 24:198–208.

Wu W-M, Carley J, Fienen M, Mehlhorn T, Lowe K, Nyman J, Luo J, Gentile ME, Rajan R, Wagner D, Hickey RF, Gu B, Watson D, Cirpka OA, Kitanidis PK, Jardine PM, Criddle CS (2006) Pilot-Scale in Situ Bioremediation of Uranium in a Highly Contaminated Aquifer. 1. Conditioning of a Treatment Zone. Environ Sci Technol 40:3978–3985.

Xu KD, Stewart PS, McFeters GA (2000) Biofilm resistance to antimicrobial agents. Microbiology 146:547–549.

Yaron S, Kolling GL, Simon L, Matthews KR (2000) Vesicle-mediated transfer of virulence genes from Escherichia coli O157:H7 to other enteric bacteria. Appl Environ Microbiol 66:4414–4420.

Yonezawa H, Osaki T, Kurata S, Fukuda M, Kawakami H, Ochiai K, Hanawa T, Kamiya S (2009) Outer membrane vesicles of Helicobacter pylori TK1402 are involved in biofilm formation. BMC Microbiol 9:197.

Zayed AM, Terry N (2003) Chromium in the environment: factors affecting biological remediation. Plant Soil 249:139–156.

Zeng L, Wooton E, Stahl DA, Walian PJ (2017a) Identification and Characterization of the Major Porin of Desulfovibrio vulgaris Hildenborough. J Bacteriol. doi: 10.1128/JB.00286-17

Zeng L, Wooton E, Stahl DA, Walian PJ (2017b) Identification and Characterization of the Major Porin of Desulfovibrio vulgaris Hildenborough. J Bacteriol. doi: 10.1128/JB.00286-17

Zhang P, Van Nostrand JD, He Z, Chakraborty R, Deng Y, Curtis D, Fields MW, Hazen TC, Arkin AP, Zhou J (2015) A Slow-Release Substrate Stimulates Groundwater Microbial Communities for Long-Term in Situ Cr(VI) Reduction. Environ Sci Technol 49:12922–12931.

Zhang X, Bishop PL (2003) Biodegradability of biofilm extracellular polymeric substances. Chemosphere 50:63–69.

Zhitkovich A, Voitkun V, Costa M (1995) Glutathione and free amino acids form stable complexes with DNA following exposure of intact mammalian cells to chromate. Carcinogenesis 16:907–913.

Zhou C, Zhou Y, Rittmann BE (2017) Reductive precipitation of sulfate and soluble Fe(III) by Desulfovibrio vulgaris: Electron donor regulates intracellular electron flow and nano-FeS crystallization. Water Res 119:91–101.

Zybailov BL, Florens L, Washburn MP (2007) Quantitative shotgun proteomics using a protease with broad specificity and normalized spectral abundance factors. Mol Biosyst 3:354–360.

(2013) Toxicological Profile for Chromium. Agency for Toxic Substances and Disease Registry (US), Atlanta (GA)

APPENDICES

APPENDIX A

PRODUCTION OF EXTRACELLULAR FILAMENTS IN *DESULFOVIBRIO VULGARIS* BIOFILMS IS TEMPERATURE-DEPENDENT

Introduction

Initial experiments to characterize *Desulfovibrio vulgaris* Hildenborough biofilm were carried out at 30°C (optimal growth temperature) and room temperature (20-23°C) to determine if culturing biofilm at room temperature was feasible. Biofilms grown at 30, 25, and 20°C were examined for extracellular matrix structure via SEM.

Materials and Methods

Biofilm Growth Conditions

Biofilm samples were grown in a CDC reactor (Biosurface Tech.) under electron acceptor limitation at 30°C, 25°C or 20°C in LS4D media described in Chapter 3. Dilution rates (D) were dependent on growth rate at said temperature with the exception of the sample shown in Figure 1b. Biofilm grown on glass slides were sampled at 72 hours for samples grown at 30°C and 168 hours for samples grown at 25 and 20°C.

Scanning Electron Microscopy and Sample Preparation

Biofilm coated slides were gently washed with phosphate buffered saline to remove loosely attached cells and then fixed overnight in a 2% paraformaldehyde, 2.5% gluturaldehyde, 0.05M sodium cacodylate solution. Samples were then dehydrated with increasing amounts of ethanol (25%, 50%, 75%, 95%, 100%x3 v/v EtOH, 20 min each treatment) and then critical point dried in a Tousimis Samdri-795 drier to preserve bacterial cell structure. Samples were mounted on aluminum stubs, coated with iridium,

and viewed on a Zeiss SUPRA 55VP field emission scanning electron microscope at 1.0 kV.

Results

Extracellular filament production in *D. vulgaris* biofilms grown at 30, 25, and 20°C varied according to temperature with biofilms grown at 30°C producing very few extracellular filaments (Figure 1a). Biofilm grown at room temperature (~20°C) produced many extracellular filaments that connected cells and cells to the surface (Figure 1d). Biofilm grown at a middle temperature of 25°C produced an intermediate number of extracellular filaments (Figure 1c). To determine if filament production was actually dependent on temperature or if it could be linked to growth rate/dilution rate, biofilm grown in a third reactor at 30°C, but with the same dilution rate of those grown at 20°C ($D=0.04^{-hr}$) was examined. These samples showed minimal filament production (Figure 1b), similar to those grown at 30°C with a higher dilution rate, indicating that filament production is temperature-dependent, not growth rate-dependent.

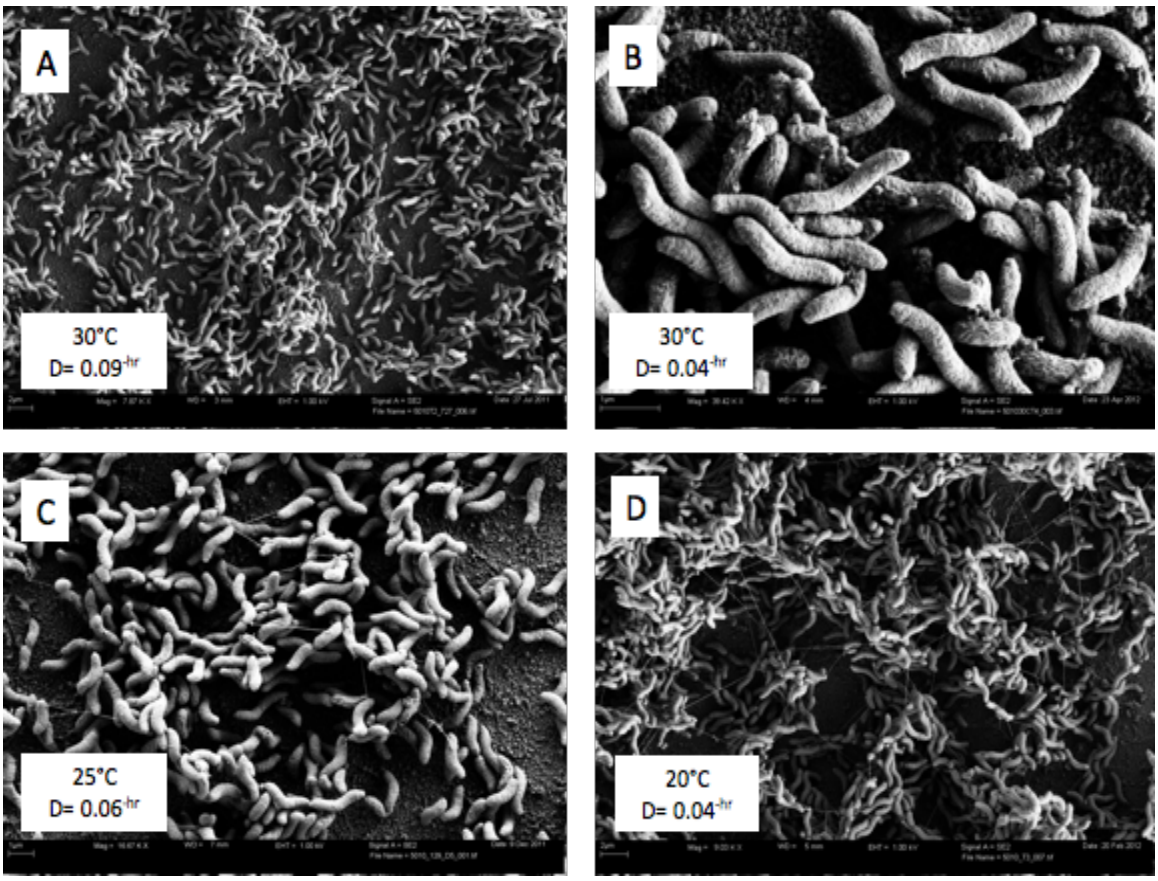


Figure 1. FE-SEM images of *D. vulgaris* biofilm grown at different temperatures and dilution rates.

APPENDIX B

DESULFOVIBRIO CARBINOLIPHILUS OAKRIDGENSIS, SPP. NOV., AN ORGANIC ACID-OXIDIZING, SULFATE REDUCING BACTERIUM ISOLATED FROM URANIUM(VI)-CONTAMINATED GROUNDWATER

Contribution of Authors and Co-Authors

Manuscript in Appendix B

Author: Bradley D. Ramsey

Contributions: Developed experimental design, performed experiments, analyzed data, wrote manuscript.

Co-Author: Lauren C. Franco

Contributions: Developed experimental design, performed experiments, analyzed data, wrote and revised manuscript.

Co-Author: Matthew W. Fields

Contributions: Developed experimental design, analyzed data, wrote and revised manuscript.

Manuscript Information Page

Bradley D. Ramsay, Lauren C. Franco, Matthew W. Fields

International Journal of Systematic and Evolutionary Microbiology

Status of Manuscript:
__x__ Prepared for submission to a peer-reviewed journal
____ Officially submitted to a peer-review journal
____ Accepted by a peer-reviewed journal
____ Published in a peer-reviewed journal

The Microbiology Society

Abstract

A novel sulfate-reducing bacterium was isolated from a uranium and nitrate contaminated well (FW-101) at the Oak Ridge Field Research Center. Phylogenetic analysis revealed that it is closely related to *Desulfovibrio carbinoliphilus* D41^T, although physiological studies indicate distinguish the two strains. The isolate could utilize pyruvate, lactate, formate, malate, maleate, methanol, ethanol, 1,2-propanediol, 1,3-propanediol, and fumarate and substrates and sulfate, sulfite, and thiosulfate as electron acceptors. Nitrate could be used as an N-source if ammonium was absent, but could not be used as an electron acceptor. The isolate grew in the presence of 100μM U(VI) or Cr(VI), but could not use U(VI) or C(VI) as a sole electron acceptor linked to growth. Based on the similarities in phylogeny, but distinctions in growth characteristics between this isolate and *D. carbinoliphilus* D41^T, the novel strain *Desulfovibrio carbinoliphilus* Oakridgensis is proposed.

Introduction

The Field Research Center (FRC) at Oak Ridge National Lab (ORNL) offers a unique research opportunity to study bioremediation *in situ*. Part of the Y-12 security complex, the FRC is located in the Bear Creek drainage near Oak Ridge, Tennessee. Beginning in the 1950s, and ending in 1983, an estimated 300 million liters of mixed acid, organics, and heavy metal wastes were deposited in four unlined waste disposal ponds. Capped with an asphalt parking lot in 1988, wastes from this area have seeped into the underlying bedrock and groundwater table. Some of the many mobile subsurface contaminants at this site include nitrate, uranium, thorium, technetium, and several volatile organics (Wu et al. 2006). ICP-MS of samples collected in late 2001 from well FW-101 has yielded uranium concentrations between 20 and 250ppm, and chromium concentrations between 35 and 85ppm. For comparison, US EPA drinking water standards in April 2017 for uranium and total chromium are 30ppb and 100ppb, respectively (www.epa.gov). Because of these highly contaminated zones within the FRC, it is hypothesized that novel denitrifying and metal-reducing microorganisms may live in these areas and therefore attempts to culture them could lead to discoveries of new metabolisms or lineages.

Dissimilatory metal-reducing bacteria are of particular interest at sites such as the ORNL FRC due to their ability to transform contaminants such as U(VI) and Cr(VI) from soluble to insoluble forms. One group capable of such metal reduction is the sulfate-

reducing bacteria (SRB) which contains the genus *Desulfovibrio*. Belonging to the δ-proteobacteria class, the *Desulfovibrio* genus consists of flagellated, Gram-negative curved-rods, that live in a variety of anoxic environments. Representatives from *Desulfovibrio* have been found in environments from cold (Vandieken et al. 2006; Sasi Jyothsna et al. 2008) to hot (Alazard 2003); from acidic (Karnachuk et al. 2015) to basic (Abildgaard 2006); and from freshwater to hypersaline (Magot et al. 2004). While sulfate is the preferred electron acceptor, electron donors for *Desulfovibrio* include alcohols (Ouattara et al. 1992; Allen et al. 2008), sugars (Ollivier et al. 1988), amino acids (Baena et al. 1998), and a number of different organic acids (Sun et al. 2000).

Previous studies have demonstrated reduction of nitrate and uranium levels in the subsurface upon bio-stimulation with ethanol (Hwang et al. 2009). During bio-stimulation, an increase was observed in DNA sequences corresponding to SRB. Here we present physiological and phylogenetic characterization of one novel SRB isolated from the ORNL FRC that belongs to the genus *Desulfovibrio*.

Materials and Methods

Groundwater from well FW-101 at the FRC site was collected during the uranium-reduction phase of a previously described biostimulation experiment (Hwang et al. 2009) and used as inoculum for a culture enriching for sulfate-reducing bacteria. The enrichment was grown at room temperature anaerobically in **ES4**D media with the

following composition: 40mM ethanol (**E**), 50mM sodium sulfate (**S4**), 8mM magnesium chloride, 20mM ammonium chloride, 2.2mM orthophosphate, 600μM calcium chloride, 1% (w/v) PIPES, 0.1% (v/v) 1000X Thauer's vitamins (Brandis and Thauer 1981), and 1.25% (v/v) 80X trace minerals solution. pH of the media was not adjusted, and was approximately 6.7. The trace mineral solution consisted of 50mM nitrilotriacetic acid, 5mM iron(II) chloride, 2.5mM manganese(II) chloride, 1.3mM cobalt(II) chloride, 1.5mM zinc chloride, 380M nickel(II) sulfate, 320M boric acid, 210M sodium molybdate, 30M sodium selenite, 20M sodium tungstate and 10M copper(II) chloride, pH adjusted to 6.5. All growth conditions were performed anaerobically under an atmosphere of 100% nitrogen.

The grown enrichment culture was transferred for increased growth rates of SRBs into liquid **L**S4D media: ES4D where ethanol was replaced with 40mM lactate (**L**), and 2.2mM orthophosphate replaced with 2.2mM potassium phosphate. Cultures grown in LS4D cultures were plated on solid LS4D agar: LS4D with 1.5% (w/v) agar added. Plates were incubated at 25ºC in a glove-bag with an atmosphere of nitrogen with ~2.5% hydrogen. Several colony morphologies arose; each was re-streaked and subsequently transferred into liquid LS4D media and grown at room temperature.

For sequencing of the small-subunit (SSU) ribosomal RNA gene of the isolate FW-101-2B, standard PCR methods were used to amplify the gene with previously described primers (Ye et al. 2004): FD1 (5'-AGAGTTTGATCCTGGCTCAG-3') and 1540R (5'-AAGGAGGTGATCCAGCC-3'). The resulting ~1500bp band was submitted

for capillary Sanger sequencing using each of the following primers, previously described (Ye et al. 2004): FD1, 350R (5'-CTGCTGCSYCCCGTAG-3'), 519F (5'-CAGCAGCCGCGGTAA-3'), 529R (5'-CGCGGCTGCTGGCAC-3'), 788F (5'-ATTAGATACCCTGGTA-3'), 925R (5'-CCGTCAATTCMTTTRAGTTT-3'), 1099F (5'-GCAACGAGCGCAACCC-3'), and 1540R. Resulting sequences were spliced to form one contiguous sequence representing the entire gene which was entered into NCBI's nucleotide BLAST engine (http://www.ncbi.nlm.nih.gov/blast/Blast.cgi).

Whole genome sequencing of isolate FW-101-2B was performed by the Joint Genome Institute. The sequence for the organism's *dsr*AB gene was obtained from the genome sequence. The *dsr*AB gene from *D. carbinoliphilus* D41T was amplified using standard PCR methods, and the sequence was determined by capillary Sanger sequencing, using previously described primers in both cases (Wagner et al. 1998; Giloteaux et al. 2010).

16s small subunit ribosomal RNA sequences were aligned with the SILVA Incremental Aligner (Pruesse et al. 2012) and a phylogenetic tree was constructed using the RAxML maximum likelihood algorithm with an inverse gamma distribution (Ludwig et al. 2004). *dsr*AB phylogenetic trees were constructed using the same method but with a *dsr*AB sequence database (Müller et al. 2015).

Batch cultures of isolate FW-101-2B were used to determine growth characteristics in differing conditions. To test for utilized phosphate sources, cells grown in LS4D were transferred into tubes containing either potassium phosphate,

triethylphosphate, sodium metaphosphate, or sodium trimetaphosphate in place of 2.2mM orthophosphate, each added so that the total phosphorus input was 2.2mM. Each condition was performed once.

Metabolism of different electron donors was tested in duplicates in LS4D media with 40mM of each of the following added: methanol; ethanol; 1-propanol; 2-propanol; 1,2-propanediol; 1,3-propanediol; glycerol (1,2,3-propanetriol); 1-butanol; 2-butanol; 1,4-butanediol; 2,3-butanediol; isoamyl alcohol (3-methyl-1-butanol); benzyl alcohol; 2-phenylethanol; sodium formate; sodium acetate; propionic acid; sodium butyrate; sodium lactate; sodium pyruvate; sodium malate; sodium maleate; sodium fumarate; D-fructose; and triethylphosphate. The poly-lactate mixtures Metals Remediation Compound and Hydrogen Releasing Compound (Regenesis, San Clemente, CA) were also tested at an overall lactate concentration of 40mM. Those cultures which grew with both lactate and the additional carbon source were transferred in duplicates into fresh tubes with only 40mM of the substrate in question. Positives were scored by an increase in turbidity (OD600) and successful growth after a transfer into fresh media. As pyruvate was the preferred carbon source and potassium phosphate was utilized as a phosphorus source, the remaining growth tests were carried out using pyruvate (**P**) and potassium phosphate (**P**S4D).

To determine optimum growth temperature, isolate FW-101-2B was grown in PS4D at 4, 10, 16, 25, 30, 37, 42, and 60ºC in duplicates while monitoring the increase in optical density at 600nm. To determine optimum pH for growth initiation, PS4D was

prepared without PIPES but with 30mM potassium phosphate in its stead, then was adjusted with sodium hydroxide or hydrochloric acid to pH 4.5, 5, 6, 6.5, 7, and 8.5. Media above pH 6.5 required the magnesium concentration to be lowered from 8mM to 4mM due to precipitation with dibasic phosphate ions. Growth was performed in triplicates at each pH.

PS4D and LS4D media lacking ammonium chloride was prepared to test the isolate for nitrate reduction and assimilation. A culture of FW-101-2B grown in normal PS4D or LS4D was pelleted and rinsed in nitrogen-free PS4D/LS4D, re-pelleted and inoculated into fresh nitrogen-free media to an OD_{600} of ~0.1. Nitrate was added to media containing sulfate at 0, 1, or 10 mM concentrations and with or without ammonium added. Nitrate was measured with ion chromatography over the growth period. Ammonium was measured with a Hach Ammonium Ion Selective Probe according to manufacturer protocols (Hach, CO).

Four electron acceptors were tested with the isolate: sulfate, sulfite, thiosulfate, and fumarate. PS4D media was prepared without sulfate (P--D), and electron acceptors were added individually for each experiment. Cells grown in normal PS4D were pelleted and rinsed in P--D, re-pelleted and inoculated into fresh media to an OD600 of ~0.1. Growth was tested on sulfite, thiosulfate, and fumarate at 50mM concentration with pyruvate as the carbon source and electron donor.

Uranium(VI) and chromium(VI) tolerance tests were carried out in PS4D with the sulfate concentration reduced to 25mM. The isolate was grown in duplicates in varying

concentrations of uranyl chloride, UO_2Cl_2: 1M, 10M, and 100M. Chromium(VI) toxicity was assessed in duplicates by growth in varying concentrations of potassium chromate, K_2CrO_4, with 25mM sulfate: 20mM, 50mM, and 100mM.

Results and Discussion

One colony chosen for study, isolate FW-101-2B formed a very dark brown glossy colony on solid LS4D agar approximately 3mm in diameter and 4mm tall. Viewed from underneath, the colony was light tan colored. A BLAST search of the SSU rRNA gene sequence revealed the isolate's closest known relative is *Desulfovibrio carbinoliphilus* D41^T at 99.0% identity. Although the SSU rRNA sequence showed remarkable similarities, whole genome sequencing of the isolate has revealed a G+C DNA content of 66.5%, compared to 63% in *D. carbinoliphilus* (Allen et al. 2008; Ramsay et al. 2015). Based upon SSU rRNA sequences, isolate FW-101-2B belongs to a clade of *Desulfovibrio* species including *D. fructosovorans*, *D. marrakechenisis*, *D. alcoholvorans*, *D. carbinoliphilus*, *D. aerotolerans*, *D. burkinensis*, *D. carbinolicus*, and *D. magneticus*. The tree of these species placed in the context of other Desulfovibrio spp. is shown below (Figure 1). Based upon *dsr*AB sequences, isolate FW-101-2B belongs to a clade of the same organisms. The *dsr*AB gene of the isolate matches the sequence from *Desulfovibrio carbinoliphilus* D41^T at 91.64% identity. The tree of *dsr*AB Desulfovibrio sequences is shown in Figure 2.

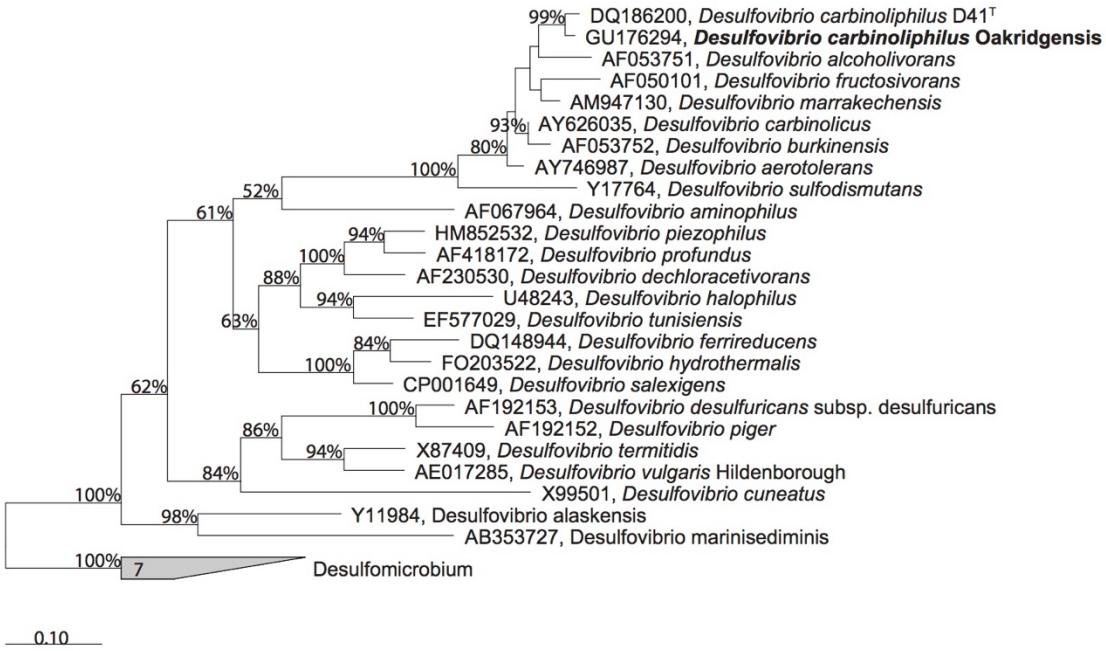


Figure 1. Maximum likelihood phylogenetic tree of 16s small subunit RNA sequences from representatives of the *Desulfovibrio* genus. Branch length indicates number of nucleotide substitutions per site.

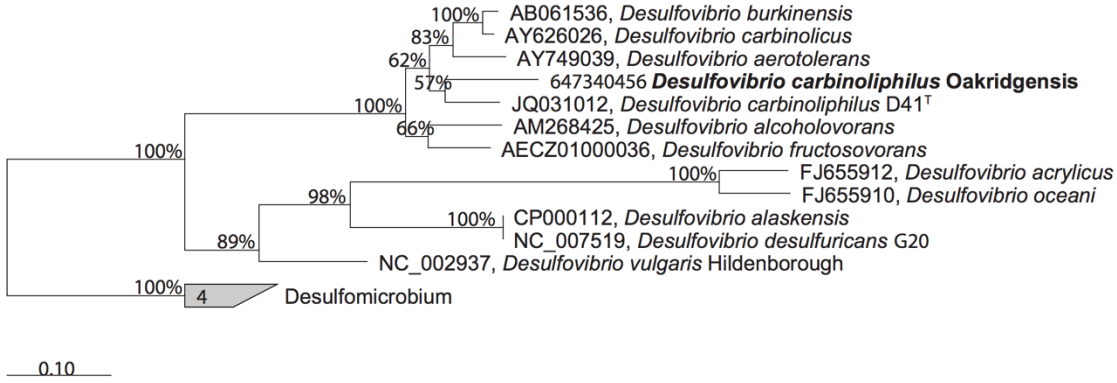


Figure 2. Maximum likelihood tree of the dissimilatory sulfite reductase alpha and beta subunit (*dsr*AB) genes from species belonging to the *Desulfovibrio* genus. Branch lengths represent nucleotide substitutions per site.

Isolate FW-101-2B was found to thrive in many different growth conditions. No difference in growth was observed between each of the phosphate sources tested. Substrates that supported growth were methanol; ethanol; 1,2-propanediol; 1,3-propanediol; formate; fumarate; maleate; malate; lactate; and pyruvate. Presence of 40mM benzyl alcohol, propionic acid, hydrogen releasing compound, and metals remediation compound were inhibitory for growth. A trend towards relative non-toxicity of secondary alcohols and diols compared to primary alcohols is noticeable.

The maximum growth rate was determined to lie between 30 and 37ºC with no measured growth occurring at 42ºC or warmer. Growth at 10ºC and colder was extremely slow. Growth rates of cultures at pH values greater than 7 were skewed due to vast production of iron sulfide. No difference in growth rate was detected by changing

the magnesium concentration at pH 6.5. Interestingly, final pH values were measured after growth and showed a sharp trend of neutralization towards pH 6.5, ranging from 5.75 to7.1. Only pH 6.5 remained unchanged. Only miniscule growth was detected below pH 6. Although optical growth determination is not reliable in the basic pH conditions due to mass production of sulfides, it is believed that the organism's preferred pH is at or very near 6.5.

Cultures provided with nitrate as their only electron acceptor did not grow and there was no decrease in nitrate concentration over time, indicating that this organism cannot use nitrate as an electron acceptor. Cultures provided with sulfate and nitrate, but no ammonium could grow and they consumed ~1.5mmol nitrate, indicating that the isolate is capable of assimilatory nitrate reduction. While no growth occurred when nitrate was the only nitrogen source, but the isolate grew with sulfate in the presence of nitrate, the organism appears to be nitrate tolerant, but will not reduce nitrate to meet nitrogen demands. Nitrate tolerance is expected considering the high nitrate levels present at the organism's source of isolation.

FW-101-2B cultures grew with sulfite and thiosulfate as electron acceptors. Growth on sulfite was similar to that on sulfate, but with thiosulfate growth occurred at a diminished rate (0.019^{-hr} compared to 0.029^{-hr}) and reached a lower maximum optical density (0.99 compared to 1.26). Two likely fates of thiosulfate are reduction and disproportionation of thiosulfate (Jackson and McInerney 2000). Both lead to double the HS^- production generated during sulfate reduction, but thiosulfate reduction also

generates sulfite. The isolate could not use fumarate as an electron acceptor. P--D media with no electron acceptor supported very slow growth representative of pyruvate fermentation.

Growth was not affected by addition of uranium(VI) at tested concentrations up to 100μM. Although the isolate experienced significant lag phases in 100μM chromate, otherwise normal growth occurred in each concentration. No growth occurred in the presence of U(VI) or Cr(VI) without sulfate. Considering the high level of uranium and chromium toxicity in this organism's source environment, these findings are not unexpected.

	1	2	3	4	5	6	7
Substrate							
Formate	+	+	+	+	w	-	+
Lactate	+	+	+	+	+	+	+
Pyruvate	+	+	+	+	+	+	+
Maleate	+	+	ND	ND	w	-	ND
Malate	+	+	+	+	-	+	+
Methanol	+	+	+	ND	ND	ND	+
Ethanol	+	+	+	+	+	+	+
Fumarate	+	+	+	+	+	ND	+
1-propanol	-	+	+	ND	w	-	+
2-propanol	-	+	-	ND	ND	-	ND
1-butanol	-	+	+	ND	ND	ND	+
2-butanol	-	+	-	ND	ND	ND	ND
1,2-propanediol	+	+	+	ND	ND	-	ND
1,3-propanediol	+	+	+	ND	ND	ND	ND
1,4-butanediol	ND	+	+	ND	ND	ND	ND
Isoamyl alcohol	-	+	ND	ND	ND	-	-
Ethelyne glycol	ND	+	+	ND	ND	ND	ND
Benzoyl alcohol	-	+	ND	ND	ND	ND	ND
Phenylethanol	-	-	ND	ND	ND	ND	ND
H_2+CO_2	ND	+	+	+	ND	ND	ND
Acetate+H_2+CO_2	ND	ND	+	-	+	-	-
Acetate	-	-	ND	-	-	-	-
Fructose	-	-	-	+	ND	-	ND
Glycerol	ND	-	+	+	+	+	-
Tert-amyl alcohol	-	-	ND	ND	ND	ND	ND
2,3-butanediol	-	-	-	ND	ND	ND	ND
Electron Acceptors							
Sulfate	+	+	+	+	+	+	+
Thiosulfate	+	+	+	+	+	+	+
Elemental sulfur	ND	-	+	+	+	-	i
Sulfite	+	+	+	+	+	-	+
Nitrate	-	-	-	-	-	-	-
Fumarate	-	-	-	+	ND	+	-

Table 1. Summary of substrate and electron acceptor utilization of FW-101 isolate and closely related strains. 1, *D. carbinoliphilus* sp. nov. Oakridgensis; 2, *D. carbinoliphilus* D41^T (Allen et al. 2008); 3, *D. alcoholovorans* (Qatibi and Garcia 1990); 4, *D. fructosovorans* (Ollivier et al. 1988); 5, *D. aerotolerans* (Mogensen et al. 2005); 6, *D. magneticus (Sakaguchi et al. 2002)*; 7, *D. carbinolicus (Nanninga and Gottschal 1987)*. ND - not determined, i - incomplete, w - weak.

Description of *Desulfovibrio carbinoliphilus* Oakridgensis spp. nov.

Desulfovibrio carbinoliphilus Oakridgensis (oak · ridg · en´ · sis M.L. fem. adj. Oakridgensis coming from Oak Ridge, the city in the state of Tennessee whence the organism was isolated).

Isolate FW-101-2B will utilize inorganic phosphate, metaphosphate, orthometaphosphate, and triethylphosphate has phosphorus sources. Carbon sources and electron donors utilized are methanol, ethanol, 1,2-propanediol, 1,3-propanediol, formate, fumarate, malate, maleate, pyruvate, and lactate. *D. carbinoliphilus* Oakridgensis will reduce sulfate, sulfite, and thiosulfate and will ferment pyruvate in the lack of electron acceptor. The organism has a maximum growth temperature of 30-37ºC and an optimum pH of 6.5. *D. carbinoliphilus* Oakridgensis cannot use nitrate as a dissimilatory electron acceptor, but it can assimilate nitrate when ammonium is not available. Finally, *D. carbinoliphilus* Oakridgensis is tolerant to soluble uranium and chromate at tested levels up to 100μM.

Although physiological evidence would support classification of a new species, isolate FW-101-2B is phylogenetically very similar to *D. carbinoliphilus* D41^T based upon small-subunit rRNA and dsrAB sequences, thus we propose its classification as new strain *Desulfovibrio carbinoliphilus* strain Oakridgensis. The GenBank accession number for the small-subunit ribosomal RNA gene of *D. carbinoliphilus* Oakridgensis is GU176294.

References

Abildgaard L (2006) Desulfovibrio alkalitolerans sp. nov., a novel alkalitolerant, sulphate-reducing bacterium isolated from district heating water. Int J Syst Evol Microbiol 56:1019–1024.

Alazard D (2003) Desulfovibrio hydrothermalis sp. nov., a novel sulfate-reducing bacterium isolated from hydrothermal vents. Int J Syst Evol Microbiol 53:173–178.

Allen TD, Kraus PF, Lawson PA, Drake GR, Balkwill DL, Tanner RS (2008) Desulfovibrio carbinoliphilus sp. nov., a benzyl alcohol-oxidizing, sulfate-reducing bacterium isolated from a gas condensate-contaminated aquifer. Int J Syst Evol Microbiol 58:1313–1317.

Baena S, Fardeau ML, Labat M, Ollivier B, Garcia JL, Patel BK (1998) Desulfovibrio aminophilus sp. nov., a novel amino acid degrading and sulfate reducing bacterium from an anaerobic dairy wastewater lagoon. Syst Appl Microbiol 21:498–504.

Brandis A, Thauer RK (1981) Growth of Desulfovibrio species on hydrogen and sulphate as sole energy source. Microbiology 126:249–252.

Giloteaux L, Goñi-Urriza M, Duran R (2010) Nested PCR and new primers for analysis of sulfate-reducing bacteria in low-cell-biomass environments. Appl Environ Microbiol 76:2856–2865.

Hwang C, Wu W, Gentry TJ, Carley J, Corbin GA, Carroll SL, Watson DB, Jardine PM, Zhou J, Criddle CS, Fields MW (2009) Bacterial community succession during in situ uranium bioremediation: spatial similarities along controlled flow paths. ISME J 3:47–64.

Jackson BE, McInerney MJ (2000) Thiosulfate Disproportionation by Desulfotomaculum thermobenzoicum. Appl Environ Microbiol 66:3650–3653.

Karnachuk OV, Mardanov AV, Avakyan MR, Kadnikov VV, Vlasova M, Beletsky AV, Gerasimchuk AL, Ravin NV (2015) Draft genome sequence of the first acid-tolerant sulfate-reducing deltaproteobacterium Desulfovibrio sp. TomC having potential for minewater treatment. FEMS Microbiol Lett. doi: 10.1093/femsle/fnv007

Ludwig W, Strunk O, Westram R, Richter L, Meier H, Yadhukumar, Buchner A, Lai T, Steppi S, Jobb G, Förster W, Brettske I, Gerber S, Ginhart AW, Gross O, Grumann S, Hermann S, Jost R, König A, Liss T, Lüssmann R, May M, Nonhoff B, Reichel B, Strehlow R, Stamatakis A, Stuckmann N, Vilbig A, Lenke M, Ludwig T, Bode A,

Schleifer K-H (2004) ARB: a software environment for sequence data. Nucleic Acids Res 32:1363–1371.

Magot M, Basso O, Tardy-Jacquenod C, Caumette P (2004) Desulfovibrio bastinii sp. nov. and Desulfovibrio gracilis sp. nov., moderately halophilic, sulfate-reducing bacteria isolated from deep subsurface oilfield water. Int J Syst Evol Microbiol 54:1693–1697.

Mogensen GL, Kjeldsen KU, Ingvorsen K (2005) Desulfovibrio aerotolerans sp. nov., an oxygen tolerant sulphate-reducing bacterium isolated from activated sludge. Anaerobe 11:339–349.

Müller AL, Kjeldsen KU, Rattei T, Pester M, Loy A (2015) Phylogenetic and environmental diversity of DsrAB-type dissimilatory (bi)sulfite reductases. ISME J 9:1152–1165.

Nanninga HJ, Gottschal JC (1987) Properties of Desulfovibrio carbinolicus sp. nov. and Other Sulfate-Reducing Bacteria Isolated from an Anaerobic-Purification Plant. Appl Environ Microbiol 53:802–809.

Ollivier B, Cord-Ruwisch R, Hatchikian EC, Garcia JL (1988) Characterization of Desulfovibrio fructosovorans sp. nov. Arch Microbiol 149:447–450.

Ouattara AS, Cuzin N, Traore AS, -L. Garcia J (1992) Anerobic degradation of 1,2-propanediol by a new Desulfovibrio strain and D. alcoholovorans. Arch Microbiol 158:218–225.

Pruesse E, Peplies J, Glöckner FO (2012) SINA: accurate high-throughput multiple sequence alignment of ribosomal RNA genes. Bioinformatics 28:1823–1829.

Qatibi AI, Garcia J-L (1990) 1, 2 - and 1, 3 - Propanediol Degradation by Desulfovibrio Alcoholovorans SP. Nov., in Pure Culture or Through H2 Interspecies Transfer. In: Microbiology and Biochemistry of Strict Anaerobes Involved in Interspecies Hydrogen Transfer. pp 451–453

Ramsay BD, Hwang C, Woo HL, Carroll SL, Lucas S, Han J, Lapidus AL, Cheng J-F, Goodwin LA, Pitluck S, Peters L, Chertkov O, Held B, Detter JC, Han CS, Tapia R, Land ML, Hauser LJ, Kyrpides NC, Ivanova NN, Mikhailova N, Pagani I, Woyke T, Arkin AP, Dehal P, Chivian D, Criddle CS, Wu W, Chakraborty R, Hazen TC, Fields MW (2015) High-Quality Draft Genome Sequence of Desulfovibrio carbinoliphilus FW-101-2B, an Organic Acid-Oxidizing Sulfate-Reducing Bacterium Isolated from Uranium(VI)-Contaminated Groundwater. Genome Announc. doi: 10.1128/genomeA.00092-15

Sakaguchi T, Arakaki A, Matsunaga T (2002) Desulfovibrio magneticus sp. nov., a novel sulfate-reducing bacterium that produces intracellular single-domain-sized magnetite particles. Int J Syst Evol Microbiol 52:215–221.

Sasi Jyothsna TS, Sasikala C, Ramana CV (2008) Desulfovibrio psychrotolerans sp. nov., a psychrotolerant and moderately alkaliphilic sulfate-reducing deltaproteobacterium from the Himalayas. Int J Syst Evol Microbiol 58:821–825.

Sun B, Cole JR, Sanford RA, Tiedje JM (2000) Isolation and Characterization of Desulfovibrio dechloracetivorans sp. nov., a Marine Dechlorinating Bacterium Growing by Coupling the Oxidation of Acetate to the Reductive Dechlorination of 2-Chlorophenol. Appl Environ Microbiol 66:2408–2413.

Vandieken V, Knoblauch C, Jørgensen BB (2006) Desulfovibrio frigidus sp. nov. and Desulfovibrio ferrireducens sp. nov., psychrotolerant bacteria isolated from Arctic fjord sediments (Svalbard) with the ability to reduce Fe(III). Int J Syst Evol Microbiol 56:681–685.

Wagner M, Roger AJ, Flax JL, Brusseau GA, Stahl DA (1998) Phylogeny of dissimilatory sulfite reductases supports an early origin of sulfate respiration. J Bacteriol 180:2975–2982.

Wu W-M, Carley J, Fienen M, Mehlhorn T, Lowe K, Nyman J, Luo J, Gentile ME, Rajan R, Wagner D, Hickey RF, Gu B, Watson D, Cirpka OA, Kitanidis PK, Jardine PM, Criddle CS (2006) Pilot-Scale in Situ Bioremediation of Uranium in a Highly Contaminated Aquifer. 1. Conditioning of a Treatment Zone. Environ Sci Technol 40:3978–3985.

Supplemental Figures

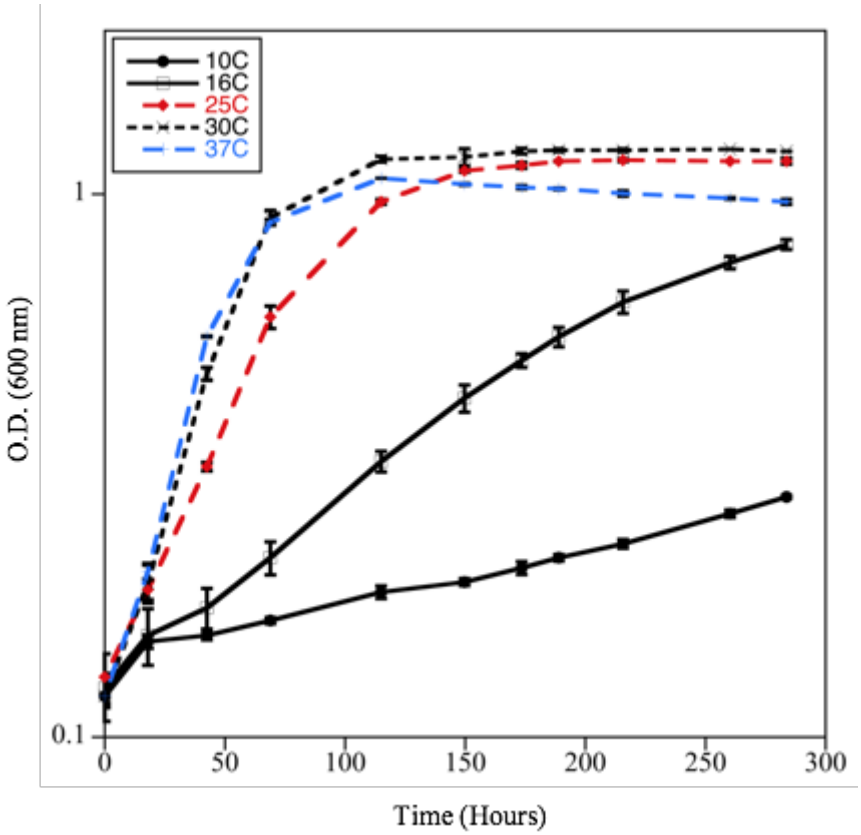


Figure S1. Growth of *D. carbinoliphilus* Oakridgensis at 10, 16, 25, 30, and 37°C.

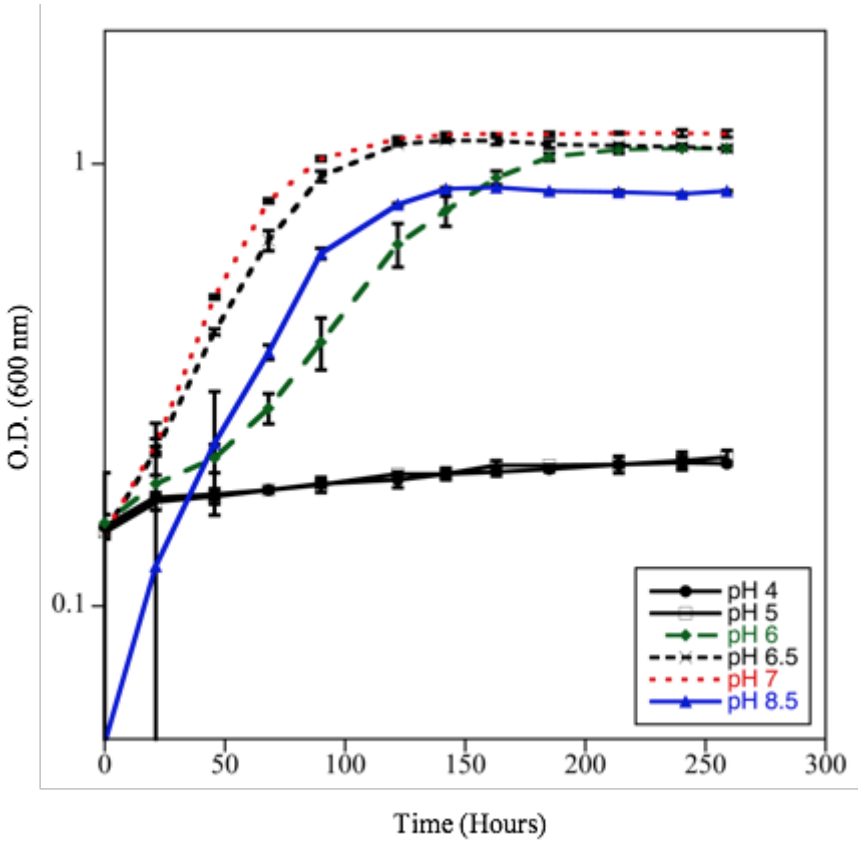


Figure S2. Growth of *D. carbinoliphilus* Oakridgensis at pH 4, 5, 6, 6.5, 7, and 8.5.

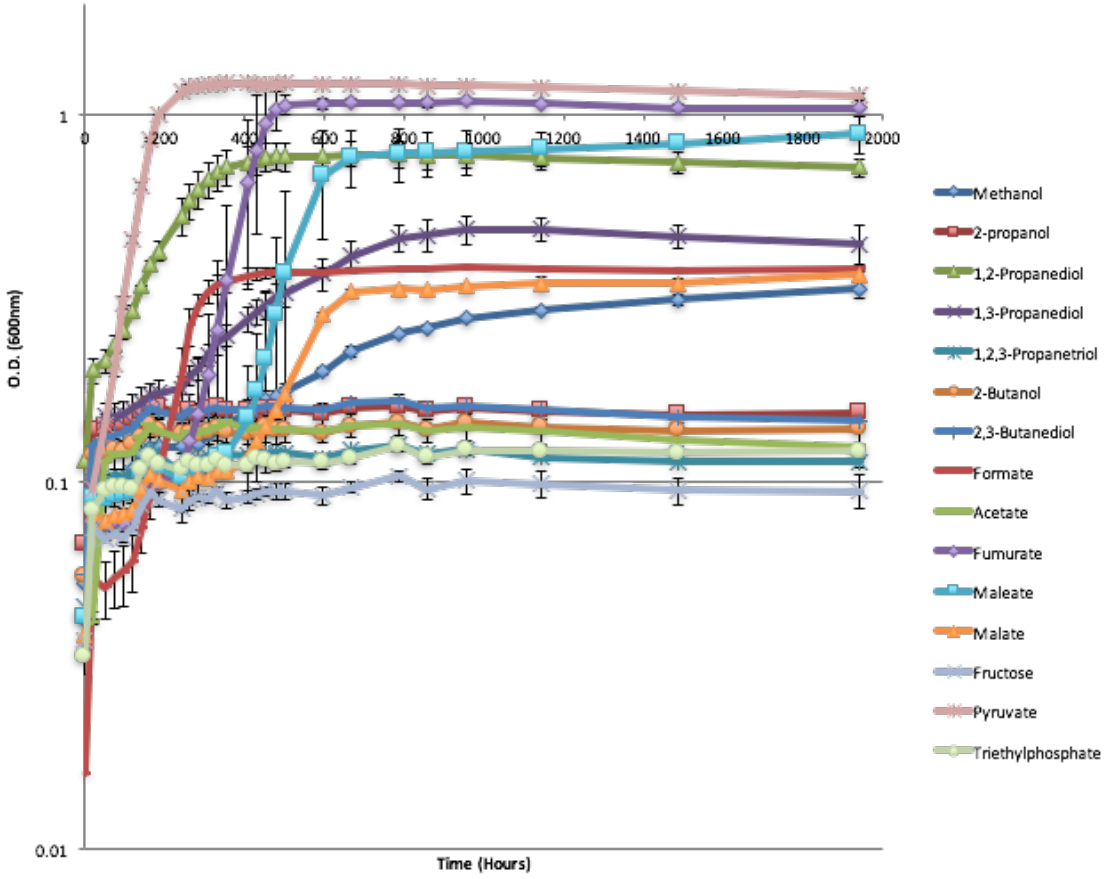


Figure S3. Growth of *D. carbinoliphilus* Oakridgensis with different substrates and sulfate as the electron acceptor.

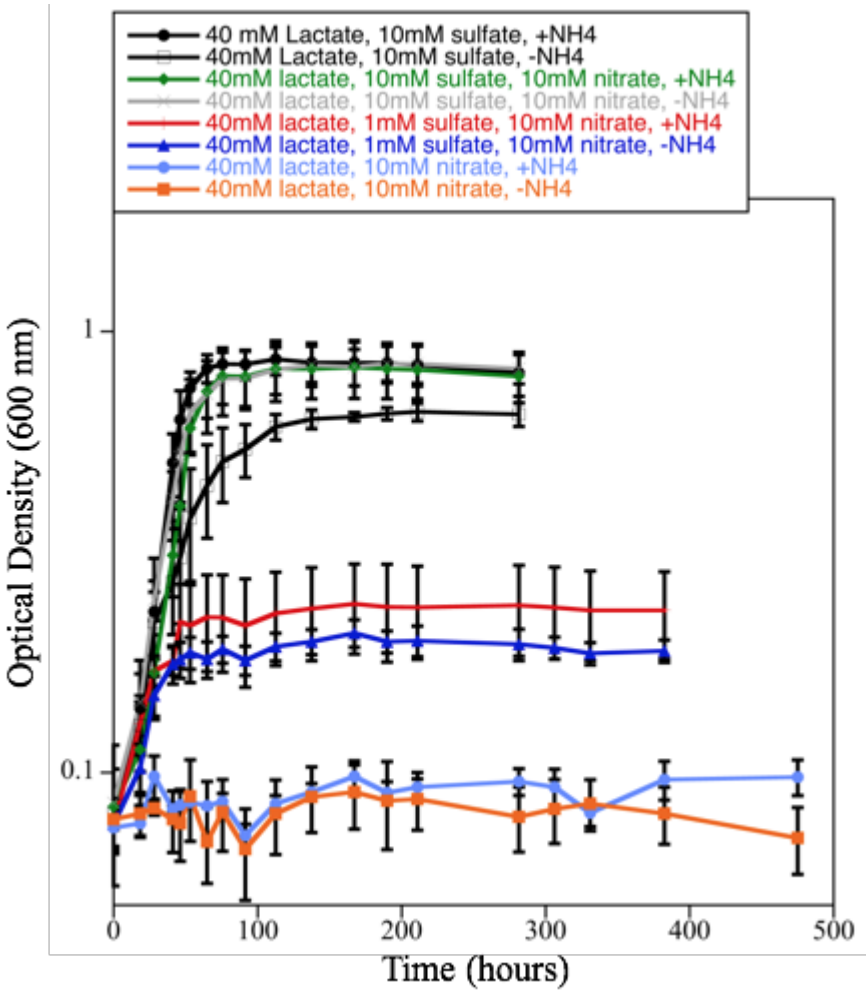


Figure S4. Growth of *D. carbinoliphilus* Oakridgensis with nitrate and/or ammonium as the nitrogen source.

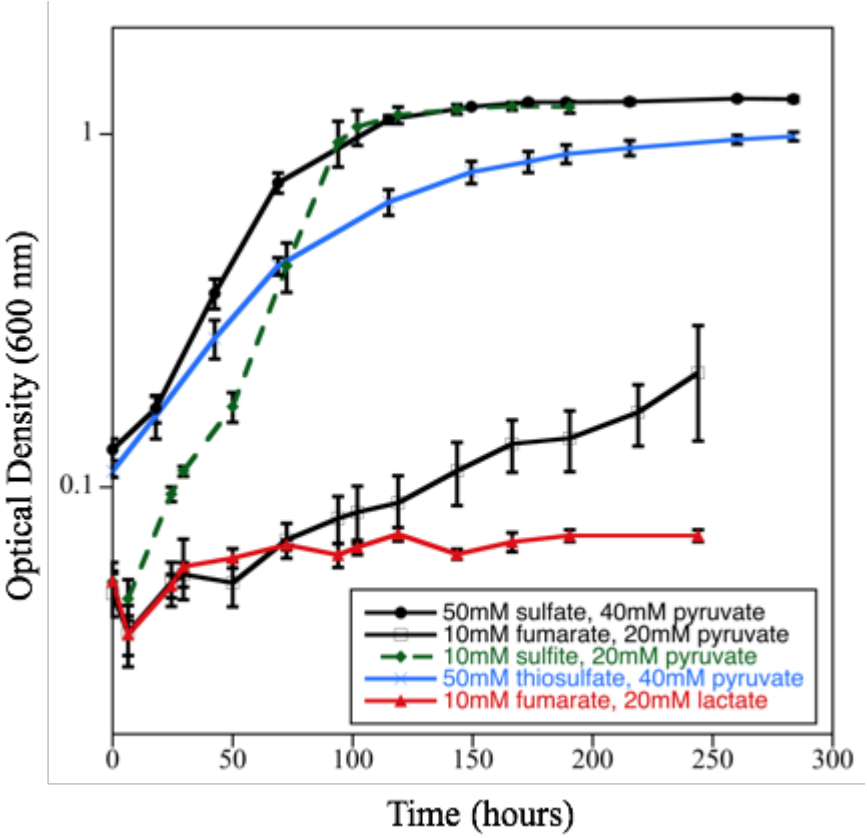


Figure S5. Growth of *D. carbinoliphilus* Oakridgensis with different electron acceptors.

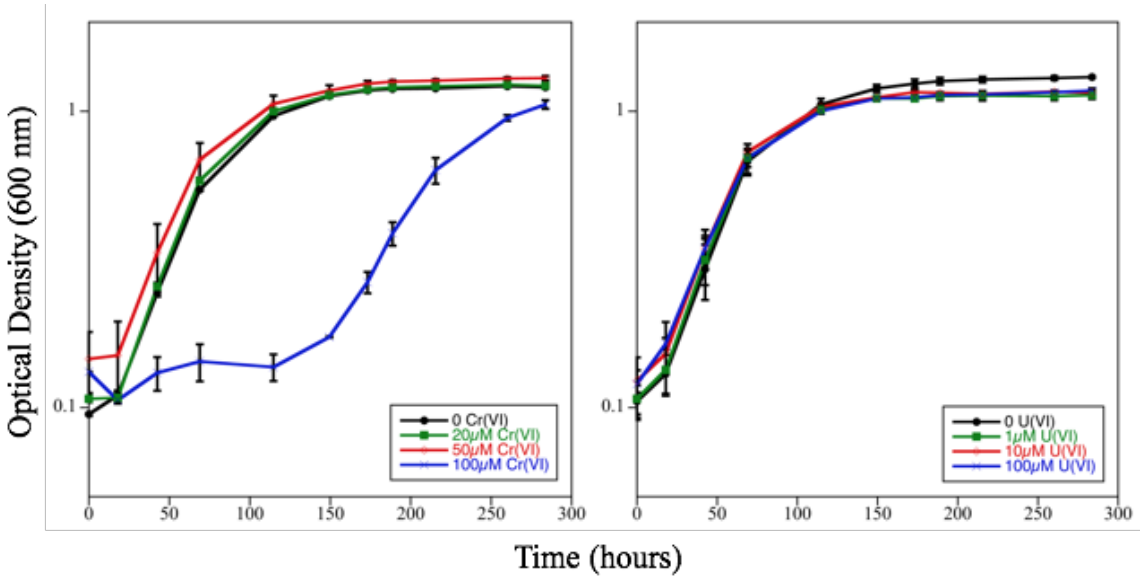


Figure S6. Growth of *D. carbinoliphilus* Oakridgensis with Cr(VI) or U(VI).

APPENDIX C

AUTONOMOUS METABOLOMICS FOR RAPID METABOLITE IDENTIFICATION IN GLOBAL PROFILING

Contribution of Authors and Co-Authors

Manuscript in Appendix C

Author: Paul H. Benton

Contributions: Experimental design, performed experiments, data acquisition and analysis, prepared and revised manuscript.

Co-Authors: Julijana Ivanisevic, Nathaniel G. Mahieu, Michael E. Kurczy, Caroline H. Johnson, Lauren Franco, Duane Rinehart, Elizabeth Valentine, Harsha Gowda, Baljit K. Ubhi, Ralf Tautenhahn, Andrew Gieschen, Matthew W. Fields, Gary J. Patti

Contributions: Performed experiments, revised manuscript.

Co-Author: Gary Siuzdak

Contributions: Experimental design, data analysis, prepared and revised manuscript.

Manuscript Information Page

H. Paul Benton, Julijana Ivanisevic, Nathaniel G. Mahieu, Michael E. Kurczy, Caroline H. Johnson, Lauren Franco, Duane Rinehart, Elizabeth Valentine, Harsha Gowda, Baljit K. Ubhi, Ralf Tautenhahn, Andrew Gieschen, Matthew W. Fields, Gary J. Patti, and Gary Siuzdak

Analytical Chemistry

Status of Manuscript:
____ Prepared for submission to a peer-reviewed journal
____ Officially submitted to a peer-review journal
____ Accepted by a peer-reviewed journal
__x_ Published in a peer-reviewed journal

ACS Publications
2015, *87* (2), pp 884–891

This is an open access article published under an ACS AuthorChoice License, which permits copying and redistribution of the article or any adaptations for non-commercial purposes.

analytical chemistry

Article

pubs.acs.org/ac

Autonomous Metabolomics for Rapid Metabolite Identification in Global Profiling

H. Paul Benton,[†] Julijana Ivanisevic,[†] Nathaniel G. Mahieu,[‡] Michael E. Kurczy,[†] Caroline H. Johnson,[†] Lauren Franco,[§] Duane Rinehart,[†] Elizabeth Valentine,[#] Harsha Gowda,[†,¶] Baljit K. Ubhi,[∫] Ralf Tautenhahn,[†,∥] Andrew Gieschen,[⊥] Matthew W. Fields,[§] Gary J. Patti,*[,‡] and Gary Siuzdak*

[†]Scripps Center for Metabolomics and Mass Spectrometry, The Scripps Research Institute, 10550 North Torrey Pines Road, La Jolla, California 92037, United States

[‡]Departments of Chemistry, Genetics and Medicine, Washington University, One Brookings Drive, St. Louis, Missouri 63130, United States

[§]Department of Microbiology and Immunology and Center for Biofilm Engineering, Montana State University, 109 Lewis Hall, Bozeman, Montana 59717, United States

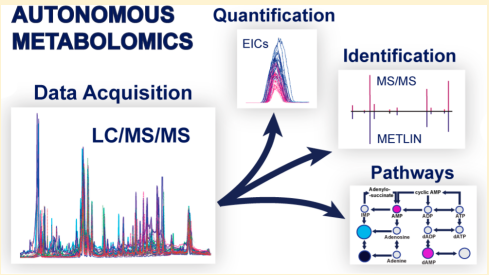
[∫]AB SCIEX, 1201 Radio Road, Redwood City, California 94065, United States

[⊥]Agilent Technologies, 11011 North Torrey Pines Road, La Jolla, California 92037, United States

[#]The Skaggs Institute for Chemical Biology, The Scripps Research Institute, 10550 North Torrey Pines Road, La Jolla, California 92037, United States

Supporting Information

ABSTRACT: An autonomous metabolomic workflow combining mass spectrometry analysis with tandem mass spectrometry data acquisition was designed to allow for simultaneous data processing and metabolite characterization. Although previously tandem mass spectrometry data have been generated on the fly, the experiments described herein combine this technology with the bioinformatic resources of XCMS and METLIN. As a result of this unique integration, we can analyze large profiling datasets and simultaneously obtain structural identifications. Validation of the workflow on bacterial samples allowed the profiling on the order of a thousand metabolite features with simultaneous tandem mass spectra data acquisition. The tandem mass spectrometry data acquisition enabled automatic search and matching against the METLIN tandem mass spectrometry database, shortening the current workflow from days to hours. Overall, the autonomous approach to untargeted metabolomics provides an efficient means of metabolomic profiling, and will ultimately allow the more rapid integration of comparative analyses, metabolite identification, and data analysis at a systems biology level.



Untargeted metabolomic experiments performed on complex biological matrices with high-resolution, high-throughput, and sensitive mass spectrometry (MS) technology have enabled the detection of thousands of metabolite features from a single experiment.[1−4] However, the identification of these features presents a major bottleneck in the metabolomics workflow. It is not only a time-consuming process, taking weeks to carry out, but often results in a low yield of correctly identified metabolites. This is partly due to the manual interpretation required by the investigator and also the number of metabolites currently characterized in metabolite databases.[5] This process can be potentially shortened by integrating metabolite profiling and identification into a single autonomous workflow.

Current metabolomic studies typically adopt a multistep workflow (Figure 1). Comparative profiling is first carried out in MS mode; the data is then processed using bioinformatics software such as XCMS[6,7] to reveal features of interest that show statistically significant differences. The features are then subjected to tandem mass spectrometry (MS/MS) acquisition and identified through MS/MS matching to standards in metabolite databases such as METLIN.[8,9] This conventional approach typically involves the generation of a list of dysregulated metabolite features from an initial set of experiments followed by statistical analysis and manual selection of precursor ions, which are then fragmented to obtain mass spectra used for metabolite characterization.[10]

Received: July 11, 2014
Accepted: December 12, 2014
Published: December 12, 2014

 © 2014 American Chemical Society

DOI: 10.1021/ac5025649
Anal. Chem. 2015, 87, 884−891

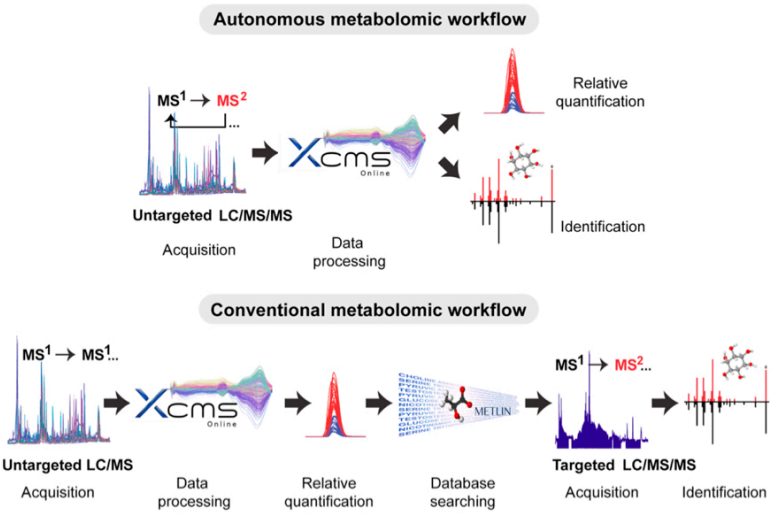


Figure 1. An autonomous vs conventional mass spectrometry-based metabolomic workflow. The autonomous workflow is based on parallel untargeted MS^1 and MS^2 data acquisition, where cycle time is optimized as a compromise for high peak definition (MS^1 for comparative quantitative analysis) and high quality MS^2 (for MS/MS matching to facilitate metabolite identification). The conventional workflow, the untargeted MS^1 data acquisition for comparative quantitative analysis and targeted MS^2 data acquisition of dysregulated features of interest (for metabolite identification) are performed in two subsequent steps. The autonomous workflow can be accomplished through the direct link between XCMS software and METLIN metabolite database.

Similar to the early days of proteomics, this time-consuming metabolomic workflow relies heavily on investigator input and manual data analysis.

To facilitate a more efficient and autonomous approach toward 'omic scale profiling, we have been developing XCMS Online, a software package for untargeted metabolomics to enable the integration of metabolite profiling and identification into one step (Figure 1). XCMS Online has integrated algorithms for peak detection, retention time correction, chromatogram alignment, and relative quantification based on peak area. In addition, a number of univariate and multivariate statistical tools have been incorporated into the workflow to aid in elucidating the features that have the highest statistical significance and drive sample clustering.[11] However, one of the most important aspects of XCMS Online is its integrated metabolite database, METLIN, a spectral library with MS/MS data available for more than ten thousand endogenous and exogenous metabolites, enabling automatic putative identification of metabolites.

The basis of the autonomous metabolomic workflow is high resolution sequential MS and MS/MS data acquisition (Figure 1). High-quality MS and MS/MS data are a prerequisite to extract accurate quantitative information and simultaneously characterize metabolite features by MS/MS data matching.[12] This one-step autonomous approach requires coordinated acquisition of MS and MS/MS data to ensure efficient and accurate comparative analysis and identification. Mass spectrometers that have high scan speeds and can alternate between MS and MS/MS modes in the same run are essential for this type of simultaneous data acquisition. Indeed, most modern quadrupole-time-of-flight (Q-TOF) instruments have high sensitivity and rapid scan speeds ensuring the acquisition of a sufficient amount of data points across a chromatographic peak while simultaneously acquiring fragmentation data which is necessary for metabolite characterization.

Key to the autonomous approach has been the development, over the last ten years, of databases to facilitate identification of metabolites in metabolomic experiments. The METLIN tandem mass spectrometry database,[13,14] Human Metabolome Database (HMDB),[15] MassBank,[16] and LipidMaps[17] databases have been generated largely from the analysis of pure standard compounds to provide for accurate identification of metabolites from biological samples. Most of these repositories allow researchers to compare MS/MS data from their research samples to MS/MS data recorded from standards one at a time for metabolite identification.

Here, we have designed an autonomous untargeted metabolomic workflow that acquires MS and MS/MS data sequentially. Quantitative information is extracted from MS data using XCMS Online and metabolite features are simultaneously characterized by matching MS/MS data to the METLIN database. The effectiveness of this workflow is demonstrated using standard mixture and a bacterial extract samples.

EXPERIMENTAL SECTION

Chemicals. Ammonium acetate (NH_4Ac) and ammonium hydroxide (NH_4OH) were purchased from Sigma-Aldrich (St. Louis, MO, USA). LC-MS grade methanol (MeOH) was purchased from Honeywell (Muskegon, MI, USA). LC-MS

DOI: 10.1021/ac5025649
Anal. Chem. 2015, 87, 884−891

grade acetonitrile was purchased from Fisher Scientific (Morris Plains, NJ, USA) and water was purchased from J.T. Baker (Phillipsburg, NJ, USA).

Bacterial Strain and Biofilm Growth Conditions. *Desulfovibrio vulgaris* Hildenborough (DvH) was obtained from Dr. Romy Chakraborty (Lawrence Berkeley National Lab). DvH was grown in LS4D medium, which contains lactate as the carbon source and electron donor and sulfate as the electron acceptor[18] (modified to 2.5 μM resazurin and 130 μM riboflavin in modified Thauer's vitamins stock).[19] Lactate and sulfate concentrations were altered to create balanced and electron acceptor limited conditions. The balanced condition was defined as 60 mM sodium lactate and 30 mM sodium sulfate and the electron acceptor limited condition was defined as 50 mM sodium lactate and 10 mM sodium sulfate. DvH was grown as a biofilm under continuous flow conditions in a modified CDC reactor. Exponential phase cells were inoculated into a reactor containing balanced or electron acceptor limited LS4D medium and were grown in batch mode for 48 h. Reactors were grown at room temperature (20−23 °C), with a dilution rate of 0.04^{-hr}, stirred at 60 rpm, and the headspace was continually sparged with sterile N_2 gas to maintain anaerobic conditions. Coupons of aclar (7.8 mil thickness) (Electron Microscopy Sciences, Hatfield, PA) supported by glass slides were submerged in the reactor body as a surface for biofilm growth. Aclar coupons were removed from the reactor at 144 h, rinsed three times in ice-cold phosphate buffered saline, wicked dry, and flash frozen in liquid nitrogen. Samples were stored at −70 °C until further analysis.

Growth of Credentialed *Escherichia coli* Standards. *Escherichia coli* cultures were grown in a rotary shaker at 37 °C. A preculture of K12 MG1655 strain was grown in LB broth for 16 h. M9 minimal salts were prepared and 100 mL aliquoted into 2 sterile 1 L Erlenmeyer flasks. To each aliquot 2 mL of 200 mg/mL glucose was added via fresh filtered syringe. One aliquot received $U^{13}C$-labeled glucose and the second received natural abundance glucose. Each aliquot was then inoculated with the equivalent of 1 mL of OD600 = 0.6 preculture as determined by dilution. Cultures were grown to OD600 = 1.0 at which point they were harvested. Cell quench solution of 10 mM ammonium acetate in 3:2 methanol/water was aliquoted into 50 conical tubes, 30 mL per tube. Tubes were chilled to −60 °C using a dry ice and 60% ethylene glycol in ethanol bath. Upon reaching OD600 = 1.0 flasks were removed from the shaker and rapidly aliquoted into the prechilled tubes. Pairs of tubes were prepared, with one being mixed at 8:11 and the other 11:8 ^{12}C culture to ^{13}C culture, respectively. Cells were pelleted by centrifugation at 0 °C and 3200 RCF for 15 min.

Metabolite Extraction. Bacteria biofilm and cell pellets (DVH and *E. coli*) were extracted using a MeOH/ACN/H_2O (2:2:1, v/v) solvent mixture. A volume of 1 mL of cold solvent was added to each pellet, vortexed for 30 s and incubated in liquid nitrogen for 1 min. Samples were allowed to thaw and sonicated for 10 min. This cycle of cell lysis in liquid nitrogen combined with sonication was repeated three times. To precipitate proteins, the samples were incubated for 1 h at −20 °C, followed by 15 min centrifugation at 13,000 rpm and 4 °C. The resulting supernatant was removed and evaporated to dryness in a vacuum concentrator. The dry extracts were then reconstituted in 100 μL of ACN:H_2O (1:1, v/v), sonicated for 10 min and centrifuged for 15 min at 13000 rpm and 4 °C to remove insoluble debris. The supernatants were transferred to HPLC vials and stored at −80 °C prior to LC/MS analysis.

LC/MS/MS Analysis. Analyses were performed using an HPLC system (1200 series, Agilent Technologies) coupled to a quadrupole time-of-flight (AB Sciex TripleTOF 5600, and Agilent Q-TOF 6530). Samples were analyzed using a Phenomenex (Torrance, CA, USA) Luna Aminopropyl column for HILIC-MS analysis.[20] The mobile phase A = 20 mM NH_4Ac and 20 mM NH_4OH in 95% water and B = 95% acetonitrile was used. A linear gradient elution from 100% B (0−5 min) to 100% A (45−50 min) was used. The 10 min postrun was applied to ensure column re-equilibration and maintain the reproducibility. The total gradient time was 60 min. The flow rate was 50 μL/min and the sample injection volume was 5 μL. DVH biofilm samples and standard mixture were analyzed using AB Sciex TripleTOF 5600 instrument whereas credentialed *E. coli* standards were analyzed using Agilent Q-TOF 6530.

ESI source conditions on TripleTOF were set as following: Ion Source Gas 1 (GS1) as 35, Ion Source Gas 2 (GS2) as 35, Curtain gas (CUR) as 30, source temperature 550 °C, IonSpray Voltage Floating (ISVF) −4500 V in negative mode. In MS only acquisition, the instrument was set to acquire over the m/z range 50−1000 Da with TOF MS scan, and the accumulation time for TOF MS scan was set at 0.25 s/spectra. In auto MS/MS acquisition, the instrument was set to acquire over the m/z range 50−1000 Da for TOF MS scan and the m/z range 25−1000 for product ion scan. The accumulation time for TOF MS scan was set at 0.25 s/spectra and product ion scan at 0.05 s/spectra (cycle time = 1 sec). The product ion scan is acquired using information dependent acquisition (IDA) with high sensitivity mode selected. IDA triggers MS/MS during the full scan experiment based on a set of criteria that the user inputs. The unit resolution is selected for precursor ion selection, and the collision energy (CE) was fixed at −30 V with ±15 spread. Declustering potential (DP) was set as −100 V. IDA settings were set as following: charge state 1 to 1, intensity 500 cps, exclude isotopes within 4 Da, mass tolerance 10 ppm and maximum number of candidate ions 15. The "exclude former target ions" was set as 9 s after 2 occurrences. In IDA Advanced tab, "dynamic background subtract" was also chosen.

ESI source settings on Agilent 6530 instrument were as follows: gas temp, 250 °C; gas flow, 6 L/min; nebulizer pressure, 25 psi; sheath flow, 9 L/min; sheath temperature, 350 °C; fragmentor, 120 V; capillary, 2000 V; nozzle, 1500 V. All MS and MS/MS acquisition settings were as listed above for TripleTOF.

Data Processing of DVH Biofilm Samples. The raw MS data (wiff.scan files) were converted to mzXML files using ProteoWizard MSConvert and processed using XCMS for feature detection, retention time correction and alignment. The parameters in XCMS were set as follows: centWave settings for feature detection (Δ m/z = 15 ppm, minimum peak width = 10 s and maximum peak width = 120 s) and mzwid = 0.015, minfrac = 0.5, and bw = 5 for chromatogram alignment. After careful evaluation retention time alignment was shown not to be required. Isotopic peaks and adducts were detected using CAMERA.[21] Paramater ID was 12480 and the data sets are shared as public data sets ID: 1039270 (Auto MS/MS job) and 1039276 (MS Only job). Each mzXML file was processed separately to ensure features were not missed. For each file a global noise intensity level was calculated using the XCMS noise function on each scan. The median from the distribution was used as a filter to remove peak below this value in each spectrum. The precursor was then matched to METLIN at 20

DOI: 10.1021/ac5025649
Anal. Chem. 2015, 87, 884−891

ppm accuracy. The database currently contains MS/MS data for more than 12 000 metabolites and 61 000 MS/MS spectra. Matches with MS/MS data were scored using a cosine similarity metric (0−1) to the closest collision energy in the database. Spectral mirror plots were created for conformation of positive matches.

Data Processing of Credentialed *E. coli* Standards. A pair of *E. coli* samples (8:11 and 11:8) were analyzed as above in both MS1 only mode and auto MS/MS mode. These samples were credentialed using the github pattilab/credential R package (http://pattilab.wustl.edu/software/credential/). Parameters used were mixed_ratio_factor = 4, mixed_ratio_ratio_factor = 1.8, mpc_factor = 1.1. The list of credentialed features was then formatted as a preferred MS/MS list and the samples were analyzed again in Preferred Auto MS/MS mode.

■ RESULTS AND DISCUSSION

Autonomous Workflow Optimization: Auto MS/MS method. The overall design of the autonomous workflow approach is to simultaneously acquire MS and MS/MS data during each LC/MS run (Figure 1). The quality of both MS and MS/MS data were of equal importance and a balance between the amounts of time spent on the acquisition of each needed to be made. While MS/MS data were necessary to generate fragmentation patterns for metabolite identification, too long accumulation times to maximize signal-to-noise and collect high quality MS/MS data can compromise MS data quality. MS data acquisition is crucial for metabolite feature detection, profile alignment, comparative and statistical analyses; however excessive time acquiring MS data could limit the number of MS/MS spectra and weaken MS/MS spectral quality. Fortunately, modern Q-TOF mass spectrometers have fast scan rates and high sensitivities making it possible to collect both MS and MS/MS data simultaneously, throughout the same run, without compromising overall data quality.

In this study, biological samples were extracted and analyzed on a Q-TOF mass spectrometer coupled to a capillary LC. The MS/MS spectra were generated using automated Information Dependent Acquisition (IDA), whereby the instrument software continuously evaluates the profile of the precursor ions (MS data) in the full survey scan and triggers MS/MS acquisition based on a set of criteria that the user inputs into the method. Instrument settings including acquisition rate, number of precursor candidate ions, collision energy, and dynamic exclusion time were optimized for IDA. In the optimized Auto MS/MS method, MS/MS acquisition was triggered on selected precursor ions that met the defined criteria of intensity and charge state. A cycle time of 1 s was used for data acquisition where each MS scan was followed by 15 MS/MS events. MS data were acquired at 4 Hz (250 ms accumulation time for each spectrum) while MS/MS data were acquired at 20 Hz (50 ms accumulation time for each spectrum, and 750 ms in total for 15 MS/MS events). This ensured an approximate duty cycle of 25% on MS acquisition while simultaneously acquiring up to 15 MS/MS spectra in the remaining time period. Chromatographic base peak widths for ions in HILIC HPLC mode were 30 s on average. A cycle time of 1 s ensured at least 15−30 MS data points acquired for each extracted ion chromatogram (EIC) peak. Multiple MS data points along the chromatographic peak are crucial for reliable peak detection, peak area integration, comparative and statistical analyses. The accumulation time for both MS and MS/MS acquisitions by UHPLC separation can be reduced 3 to 5 times as features tend to be 3 to 5 times narrower when compared to capillary LC separation. However, shortening the accumulation time compromises the sensitivity and data quality.

Some of the crucial parameters for precursor ion selection in IDA mode included a precursor ion intensity threshold of 500 counts, monoisotopic precursor selection and charge state screening to exclude any feature that was not singly charged (see Methods). Dynamic exclusion in IDA mode has been enabled to further reduce the redundancy of precursor ion selection and expand the MS/MS acquisition coverage. Every precursor ion that qualified using the preset criteria, was selected for fragmentation two consecutive times, and was dynamically excluded for the next nine seconds. Repeated acquisition on the same precursor ion and short exclusion times were chosen to maintain sufficient redundancy for MS/MS data acquisition providing higher quality data.

Validation of Autonomous Workflow: Auto MS/MS versus MS Only. To test the efficacy of our autonomous workflow a complex biological matrix from bacterial biofilm culture was investigated. *Desulfovibrio vulgaris* Hildenborough (DvH) biofilm samples were grown in balanced (BAL, $n = 4$) and in electron acceptor limited conditions (EAL, $n = 4$) to obtain insight into the altered metabolic activity and understand how it could be associated with a particular phenotype. The metabolic response of DVH biofilms grown in EAL conditions versus balanced conditions were characterized and compared using the optimized MS sampling rate and duty cycle as described above. Analysis was carried out in both MS Only mode (i.e., only MS^1 acquisition) and Auto MS/MS mode (i.e., MS^1 and MS^2 acquisition). Out of total aligned features, thirty six percent of the features that were observed using MS only method were also observed using the auto MS/MS method (Figure 2A). Forty nine percent of additional unique features detected by MS only method were likely due to frequent MS^1 data acquisition, and therefore higher MS^1 signal intensity and peak definition. Furthermore, 29% of the dysregulated features (p-value ≤ 0.05, intensity ≥ 1000) detected with the MS only method were also observed using the Auto MS/MS acquisition (Figure 2A). The other 28% were related to chemical noise and false positives or negatives, likely because of lower peak definition quality. Fold-change is an important parameter to characterize the degree of metabolite change in perturbed biological system. An example of one down-regulated metabolite feature characterized by m/z 132.030 and retention time of 24.6 min acquired with both methods was used to demonstrate the consistency of the Auto MS/MS method compared to the MS only method (Figure 2B). Both acquisition methods showed similar fold change and statistical significance (Welch t test). MS/MS data acquired using the Auto MS/MS method allowed for identification of the selected metabolite feature as aspartic acid. Together, these data demonstrated that Auto MS/MS acquisition with a 25% duty cycle for MS data collection can reduce data quality for metabolite feature detection, although the majority of dysregulated features from comparative analysis were correctly assigned and identified. In general, the results from the autonomous or conventional untargeted workflow should be validated using targeted quantification of identified dysregulated metabolites of interest.[22]

Autonomous Metabolomic Analysis of Bacterial Biofilm. Further data analysis of DVH biofilm grown in EAL conditions and using Auto MS/MS acquisition in negative

DOI: 10.1021/ac5025649
Anal. Chem. 2015, 87, 884−891

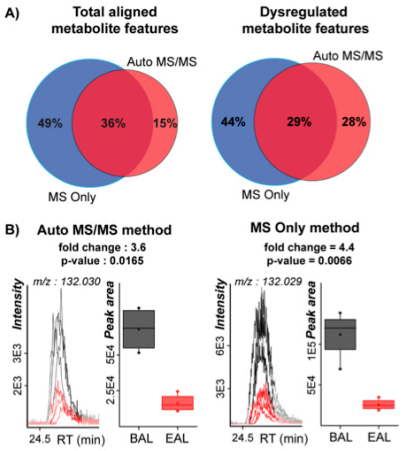


Figure 2. Characterization of the metabolic response of *Desulfovibrio vulgaris* (DVH) biofilm grown in the electron acceptor limited (EAL) conditions, using both auto MS/MS and MS-only acquisition method. (A) The overlap between metabolite features acquired with auto MS/MS method vs MS only method. Dysregulated metabolite features were defined using following parameters: p-value $\leq$ 0.05, intensity $\geq$ 1000. (B) Metabolite feature characterized by m/z 132.030 and retention time 24.6 min (MS/MS match, aspartic acid), its extracted ion chromatograms (EICs), p-values and fold-changes when acquired with auto MS/MS and MS only method. Red lines, biofilm grown in EAL conditions (n = 4); black lines, biofilm grown in balanced conditions (n = 4).

ionization mode revealed 34% of significantly dysregulated metabolite features (339 features with p-value $\leq$ 0.05, and intensity $\geq$ 1000) out of total aligned metabolite features (Figure 3A). Sixty seven of these had MS/MS matches (20%) to the METLIN metabolite database and 46 were identified using matching score $\geq$0.5 (Figure 3B). Of these, 36 had KEGG IDs which were used for biochemical pathway mapping using KEGG small molecules database. The results of pathway mapping suggested several perturbed pathways at the cell level, relevant to DVH as a response to biofilm growth in EAL conditions. The affected purine metabolism was chosen as an example to demonstrate the effectiveness of the autonomous workflow for identifying biologically relevant metabolites (Figure 3C). Specifically, 6 metabolites were mapped onto the purine metabolism pathway (Figure 3C) and all of which were down-regulated as much as 6.5 fold (e.g., hypoxanthine). Statistical information (e.g., fold-change and p-value) and identification (MS/MS spectral match, METLIN, and KEGG ID) can be extracted from data set (acquired in Auto MS/MS mode) for each metabolite in the pathway to facilitate interpretation (Figure 3B). As shown here, the development of the autonomous metabolomic workflow offered simultaneous metabolite profiling and metabolite identification, further supporting the use of metabolomics as a systems biology tool.

A false discovery rate (FDR) used in proteomics is not feasible here for the MS/MS spectral matching as no appropriate decoy metabolite databases can be constructed,[23] therefore the results need to be further manually assessed by the user. The relatively low match percentage (up to 20%) is likely due to incompleteness of the METLIN database and metabolite databases in general. However, METLIN is rapidly expanding and the number of successful matches is likely to improve over time. In the past 3 years METLIN has added more than 6,000 metabolites with MS/MS data. As of September 2014 METLIN housed more than 12 000 compounds with MS/MS data. This demonstrates the importance of having a comprehensive metabolite database and its impact on the metabolite identification process. As more and more fragmentation data from metabolites and their derivatives are deposited into METLIN, we expect that our ability to identify metabolites from biological samples will greatly improve. The scoring algorithm can also affect the results. Here, we have used the cosine similarity score for its ease of implementation and interpretation. However, there are many other scoring algorithms in use today, such as X-rank[24] weighted cosine,[16] and others.

Addressing the Coverage of Autonomous MS/MS Spectra Acquisition. Additional experiments were performed to demonstrate the effectiveness of the autonomous workflow for metabolite identification through METLIN tandem mass spectral matches. In addition to the limitation presented by the incomplete database two major factors limit the number of matched features; MS/MS spectral coverage and the match percentage. To determine the coverage of the autonomous metabolomic approach, we measured a standard metabolite mixture (40 metabolites, Supporting Information Table 1) by optimized Auto MS/MS method, and the results revealed that MS/MS spectra were acquired for 85% of the metabolites present in the standard mixture. All of these metabolites could be identified through MS/MS matching against METLIN metabolite database. The future improvements in instrument scan speed as new instruments are developed will likely increase this already high MS/MS spectral coverage. However, increasing the scan speed comes at the detriment of acquiring good quality MS/MS spectra, therefore, in our case; a 20 Hz acquisition rate was employed as a compromise to achieve higher numbers of metabolite identifications (Figure 4).

To maximize scan time, and therefore maximize MS/MS spectral quality, we opted to narrow down the number of candidate features via "credentialing" or defining the real, biologically relevant nonartifactual features. In an autonomous metabolomic experiment, the objective is to acquire MS/MS data for all monoisotopic ions of biological origin. Out of the thousands of ions that are typically detected in an untargeted metabolomic experiment only a small percentage of these will be relevant, biological ions. Selecting the appropriate ions for MS/MS analysis, thus, is a challenge. As demonstrated herein, modern instruments are capable of intelligently excluding isotopes, charge states, and low abundance ions from MS/MS analysis. Still, using auto MS/MS, many ions will be analyzed which are irrelevant to the experiment. This is due to many monoisotopic, high abundance ions which are the result of contamination and chemical noise rather than the biological sample. These peaks waste scans, taking time away from true, relevant metabolites and effectively decreasing MS/MS coverage. To investigate and address the challenge of coverage in auto MS/MS experiments we utilized a credentialing approach. In this approach we performed auto MS/MS on an extract of *E. coli* specifically prepared for the credentialing informatic workflow. This workflow allows the distinction of biological

DOI: 10.1021/ac5025649
Anal. Chem. 2015, 87, 884−891

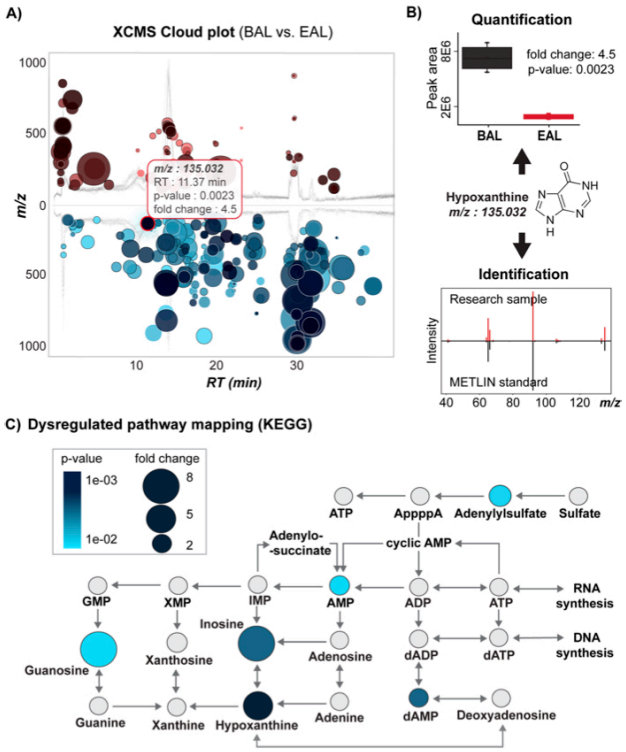


Figure 3. Autonomous metabolomic approach for simultaneous comparative analysis and identification of metabolites. (A) XCMS Cloud plot representation of the dysregulated metabolite features from *Desulfovibrio vulgaris* biofilm grown in electron acceptor limited conditions: red bubbles represent up-regulated features and blue bubbles represent down-regulated features. (B) Relative quantification and MS/MS matching identification of hypoxanthine as intermediary metabolite in purine metabolism. (C) Pathway mapping of dysregulated metabolite features using KEGG. Identified metabolites and their role in the purine metabolism pathway: blue circles represent down-regulated metabolites and the size of the circle represents the fold change.

features and artifactual features (such as contamination and chemical noise).[25]

Using this information, we assess the coverage of Auto MS/MS and whether this coverage can be improved with guided precursor ion selection (preferred auto MS/MS). As shown in Figure 5, after deisotoping and credentialing, the 12 420 total original features decreased to 836 credentialed features. The removed artifactual features correspond to various noise sources, contamination, and isotopes. The remaining 836 credentialed features represent the biologically relevant signals of which MS/MS data is desired.

The initial experiment resulted in 2606 features being chosen during auto MS/MS mode, from the 12 420 total features, of these, 2288 (88%) were artifactual. After credentialing, only 836 features were detected compared to 12 420, and out of these 836, only 38% (318 features) were picked up by the original auto MS/MS experiment without credentialing. This low coverage of credentialed features, and the high number of noncredentialed features assayed, illustrates the challenge of prioritizing relevant ions for analysis.

To improve the coverage of relevant ions we applied a preferred ion list to guide MS/MS precursor selection. The 836 credentialed features were imported as a preferred ion list and the auto MS/MS experiment repeated. After addition of the preferred ion list 660 credentialed features were analyzed by MS/MS corresponding to a 207% increase. This represents 342 new credentialed features which were analyzed by MS/MS and a large increase in coverage of our method. The use of a credentialed, preferred auto MS/MS list is a valuable addition to the autonomous metabolomic workflow for any sample type. Biological ions from a standard *E. coli* extract are easily annotated using the feature credentialing workflow.[25] These credentialed features are then used to generate a preferred ion list and included in the autonomous method. While this preferred list was generated using *E. coli*, it is applicable to any biological sample. Preferred ions are only analyzed if they are present at the proper retention time, so extraneous ions in the

DOI: 10.1021/ac5025649
Anal. Chem. 2015, 87, 884–891

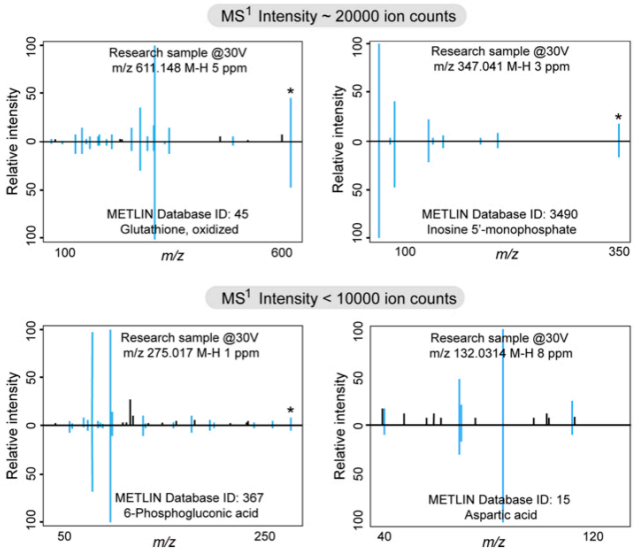


Figure 4. MS/MS spectral matching of the MS/MS data, acquired "on-the-fly", against METLIN metabolite database. MS/MS data were acquired at 50 ms scanning rate per spectra.

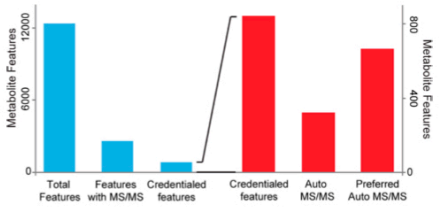


Figure 5. Preferred auto MS/MS increased MS/MS coverage of credentialed features relative to a naive experiment. Credentialed or biologically relevant features comprise only a portion of a metabolomic data set. The utilization of credentialed features to generate a preferred ion list increased auto MS/MS coverage to 78% of credentialed features.

list will not detract from the analysis. Further, the shared metabolite content of various biological samples ensures that many metabolites (central carbon metabolism, amino acids, etc.) are preferentially analyzed over artifactual peaks.

CONCLUSIONS

An autonomous workflow that allows for simultaneous MS and MS/MS data acquisition will enable relative quantification and structural characterization for the thousands of features observed using untargeted metabolomics. High quality data acquisition can be accomplished by taking advantage of the high sensitivity, high mass accuracy and resolution, and fast scanning speeds of modern mass spectrometers. Key to this workflow is utilizing the well-established XCMS bioinformatic platform and the largest metabolite database METLIN that facilitates feature assignment and identification. Our results revealed that Integrated MS and MS/MS data acquisition in the autonomous approach significantly improved the throughput performance, reducing the amount of sample and time required for the metabolomic experiments. An autonomous metabolomic approach will thus ultimately allow the more rapid integration of comparative analyses, metabolite identification, and data analysis at a systems biology level.

ASSOCIATED CONTENT

Supporting Information

Additional material as described in the text. This material is available free of charge via the Internet at http://pubs.acs.org.

AUTHOR INFORMATION

Corresponding Authors

*E-mail: gjpattij@wustl.edu.
*E-mail: siuzdak@scripps.edu.

Present Addresses

[¶]H.G.: Institute of Bioinformatics, International Tech Park, Bangalore 560066, India and
[‖]R.T.: Thermo Fisher Scientific, 355 River Oaks Parkway, San Jose, CA 95134.

Author Contributions

H.P.B. and J.I. contributed equally.

Notes

The authors declare no competing financial interest.

ACKNOWLEDGMENTS

This work was supported by US National Institutes of Health grants R01 CA170737 (G.S.), P30 MH062261 (G.S.), RC1

DOI: 10.1021/ac5025649
Anal. Chem. 2015, 87, 884−891

HL101034 (G.S.), P01 DA026146 (G.S.) and R01 ES022181 (G.J.P.), L30 AG0 038036 (G.J.P.), and Department of Defense grant W81XWH-13-1-0402. This material by ENIGMA-Ecosystems and Networks Integrated with Genes and Molecular Assemblies (http://enigma.lbl.gov), a Scientific Focus Area Program at Lawrence Berkeley National Laboratory is also based upon work supported by the U.S. Department of Energy, Office of Science, Office of Biological & Environmental Research under contract number DE-AC02-05CH11231 (G.S.).

■ REFERENCES

(1) Patti, G. J.; Yanes, O.; Siuzdak, G. *Nat. Rev. Mol. Cell Biol.* **2012**, *13*, 263−269.
(2) Fiehn, O.; Kopka, J.; Dormann, P.; Altmann, T.; Trethewey, R. N.; Willmitzer, L. *Nat. Biotechnol.* **2000**, *18*, 1157−1161.
(3) Dettmer, K.; Aronov, P. A.; Hammock, B. D. *Mass Spectrom. Rev.* **2007**, *26*, 51−78.
(4) van der Greef, J.; van Wietmarschen, H.; van Ommen, B.; Verheij, E. *Mass Spectrom. Rev.* **2013**, *32*, 399−415.
(5) Johnson, C. H.; Gonzalez, F. J. *J. Cell. Physiol.* **2012**, *227*, 2975−2981.
(6) Smith, C. A.; Want, E. J.; O'Maille, G.; Abagyan, R.; Siuzdak, G. *Anal. Chem.* **2006**, *78*, 779−787.
(7) Tautenhahn, R.; Patti, G. J.; Rinehart, D.; Siuzdak, G. *Anal. Chem.* **2012**, *84*, 5035−5039.
(8) Smith, C. A.; O'Maille, G.; Want, E. J.; Qin, C.; Trauger, S. A.; Brandon, T. R.; Custodio, D. E.; Abagyan, R.; Siuzdak, G. *Ther. Drug Monit.* **2005**, *27*, 747−751.
(9) Tautenhahn, R.; Cho, K.; Uritboonthai, W.; Zhu, Z.; Patti, G. J.; Siuzdak, G. *Nat. Biotechnol.* **2012**, *30*, 826−828.
(10) Zhu, Z.-J.; Schultz, A. W.; Wang, J. H.; Johnson, C. H.; Yannone, S. M.; Patti, G. J.; Siuzdak, G. *Nat. Protoc.* **2013**, *8*, 451−460.
(11) Gowda, H.; Ivanisevic, J.; Johnson, C. H.; Kurczy, M. E.; Benton, H. P.; Rinehart, D.; Nguyen, T.; Ray, J.; Kuehl, J.; Arevalo, B.; Westenskow, P. D.; Wang, J.; Arkin, A. P.; Deutschbauer, A. M.; Patti, G. J.; Siuzdak, G. *Anal. Chem.* **2014**, *86*, 6931−6939.
(12) Benton, H. P.; Wong, D. M.; Trauger, S. A.; Siuzdak, G. *Anal. Chem.* **2008**, *80*, 6382−6389.
(13) Smith, C. A.; Maille, G. O.; Want, E. J.; Qin, C.; Trauger, S. A.; Brandon, T. R.; Custodio, D. E.; Abagyan, R.; Siuzdak, G. *Ther. Drug Monit.* **2005**, *27*, 747−751.
(14) Tautenhahn, R.; Cho, K.; Uritboonthai, W.; Zhu, Z. J.; Patti, G. J.; Siuzdak, G. *Nat. Biotechnol.* **2012**, *30*, 826−828.
(15) Wishart, D. S.; Jewison, T.; Guo, A. C.; Wilson, M.; Knox, C.; Liu, Y.; Djoumbou, Y.; Mandal, R.; Aziat, F.; Dong, E.; Bouatra, S.; Sinelnikov, I.; Arndt, D.; Xia, J.; Liu, P.; Yallou, F.; Bjorndahl, T.; Perez-Pineiro, R.; Eisner, R.; Allen, F.; Neveu, V.; Greiner, R.; Scalbert, A. *Nucleic Acids Res.* **2013**, *41*, D801−D807.
(16) Horai, H.; Arita, M.; Kanaya, S.; Nihei, Y.; Ikeda, T.; Suwa, K.; Ojima, Y.; Tanaka, K.; Tanaka, S.; Aoshima, K.; Oda, Y.; Kakazu, Y.; Kusano, M.; Tohge, T.; Matsuda, F.; Sawada, Y.; Hirai, M. Y.; Nakanishi, H.; Ikeda, K.; Akimoto, N.; Maoka, T.; Takahashi, H.; Ara, T.; Sakurai, N.; Suzuki, H.; Shibata, D.; Neumann, S.; Iida, T.; Tanaka, K.; Funatsu, K.; Matsuura, F.; Soga, T.; Taguchi, R.; Saito, K.; Nishioka, T. *J. Mass Spectrom.* **2010**, *45*, 703−714.
(17) Fahy, E.; Subramaniam, S.; Murphy, R. C.; Nishijima, M.; Raetz, C. R. H.; Shimizu, T.; Spener, F.; van Meer, G.; Wakelam, M. J. O.; Dennis, E. A. *J. Lipid Res.* **2009**, *50*, S9−S14.
(18) Borglin, S.; Joyner, D.; Jacobsen, J.; Mukhopadhyay, A.; Hazen, T. C. *J. Microbiol. Meth.* **2009**, *76*, 159−168.
(19) Brandis, A.; Thauer, R. K. *J. Gen Microbiol* **1981**, *126*, 249−252.
(20) Ivanisevic, J.; Zhu, Z. J.; Plate, L.; Tautenhahn, R.; Chen, S.; O'Brien, P. J.; Johnson, C. H.; Marletta, M. A.; Patti, G. J.; Siuzdak, G. *Anal. Chem.* **2013**, *85*, 6876−6884.
(21) Kuhl, C.; Tautenhahn, R.; Böttcher, C.; Larson, T. R.; Neumann, S. *Anal. Chem.* **2011**, *84*, 283−289.
(22) Johnson, C. H.; Ivanisevic, J.; Benton, H. P.; Siuzdak, G. *Anal. Chem.* **2014**, DOI: 10.1021/ac5040693.
(23) Käll, L.; Storey, J. D.; MacCoss, M. J.; Noble, W. S. *J. Proteome Res.* **2007**, *7*, 29−34.
(24) Mylonas, R.; Mauron, Y.; Masselot, A.; Binz, P. A.; Budin, N.; Fathi, M.; Viette, V.; Hochstrasser, D. F.; Lisacek, F. *Anal. Chem.* **2009**, *81*, 7604−7610.
(25) Mahieu, N. G.; Huang, X.; Chen, Y. J.; Patti, G. J. *Anal. Chem.* **2014**, *86*, 9583−9589.

DOI: 10.1021/ac5025649
Anal. Chem. 2015, 87, 884−891

APPENDIX D

COMPREHENSIVE BIOIMAGING WITH FLUORINATED NANOPARTICLES USING BREATHABLE LIQUIDS

Contribution of Authors and Co-Authors

Manuscript in Appendix D

Author: Michael Kurczy

Contributions: Experimental design, performed experiments, data acquisition and analysis, prepared and revised manuscript.

Co-Authors: Zheng-Jiang Zhu, Julijana Ivanisevic, Adam M. Schuyler, Kush Lalwani, Antonio F. Santidrian, John M. David, Anand Giddabasappa, Amanda J. Roberts, Hernando J. Olivos, Peter J. O'Brien, Lauren Franco, Matthew W. Fields, Liliana P. Paris, Martin Friedlander, Caroline H. Johnson, Adrian A. Epstein, Howard E. Gendelman, Malcolm R. Wood, Brunhilde H. Felding, Gary J. Patti, Mary E. Spilker

Contributions: Performed experiments, revised manuscript.

Co-Author: Gary Siuzdak

Contributions: Experimental design, data analysis, prepared and revised manuscript.

Manuscript Information Page

Michael Kurczy, Zheng-Jiang Zhu, Julijana Ivanisevic, Adam M. Schuyler, Kush Lalwani, Antonio F. Santidrian, John M. David, Anand Giddabasappa, Amanda J. Roberts, Hernando J. Olivos, Peter J. O'Brien, Lauren Franco, Matthew W. Fields, Liliana P. Paris, Martin Friedlander, Caroline H. Johnson, Adrian A. Epstein, Howard E. Gendelman, Malcolm R. Wood, Brunhilde H. Felding, Gary J. Patti, Mary E. Spilker, and Gary Siuzdak

Nature Communications

Status of Manuscript:
____ Prepared for submission to a peer-reviewed journal
____ Officially submitted to a peer-review journal
____ Accepted by a peer-reviewed journal
__x_ Published in a peer-reviewed journal

Nature Publishing Group
6: 5998 (2015)

nature COMMUNICATIONS

ARTICLE

Received 26 May 2014 | Accepted 28 Nov 2014 | Published 20 Jan 2015

DOI: 10.1038/ncomms6998

Comprehensive bioimaging with fluorinated nanoparticles using breathable liquids

Michael E. Kurczy[1], Zheng-Jiang Zhu[1], Julijana Ivanisevic[1], Adam M. Schuyler[1], Kush Lalwani[2], Antonio F. Santidrian[3], John M. David[2], Anand Giddabasappa[2], Amanda J. Roberts[4], Hernando J. Olivos[5], Peter J. O'Brien[2], Lauren Franco[6], Matthew W. Fields[6], Liliana P. Paris[7], Martin Friedlander[7], Caroline H. Johnson[1], Adrian A. Epstein[8], Howard E. Gendelman[8], Malcolm R. Wood[9], Brunhilde H. Felding[3], Gary J. Patti[10,11], Mary E. Spilker[2] & Gary Siuzdak[1,12]

Fluorocarbons are lipophobic and non-polar molecules that exhibit remarkable biocompatibility, with applications in liquid ventilation and synthetic blood. The unique properties of these compounds have also enabled mass spectrometry imaging of tissues where the fluorocarbons act as a Teflon-like coating for nanostructured surfaces to assist in desorption/ionization. Here we report fluorinated gold nanoparticles (f-AuNPs) designed to facilitate nanostructure imaging mass spectrometry. Irradiation of f-AuNPs results in the release of the fluorocarbon ligands providing a driving force for analyte desorption. The f-AuNPs allow for the mass spectrometry analysis of both lipophilic and polar (central carbon) metabolites. An important property of AuNPs is that they also act as contrast agents for X-ray microtomography and electron microscopy, a feature we have exploited by infusing f-AuNPs into tissue via fluorocarbon liquids to facilitate multimodal (molecular and anatomical) imaging.

[1] Scripps Center for Metabolomics and Mass Spectrometry, The Scripps Research Institute, 10550 North Torrey Pines Road, La Jolla, California 92037, USA. [2] Pfizer Worldwide Research and Development, 10724 Science Center Dr, San Diego, CA 92121, USA. [3] Departments of Chemical Physiology and Molecular and Experimental Medicine, The Scripps Research Institute, 10550 North Torrey Pines Road, La Jolla, California 92037, USA. [4] Department of Molecular and Cellular Neuroscience, The Scripps Research Institute, 10550 North Torrey Pines Road, La Jolla, California 92037, USA. [5] Waters Corporation, 100 Cummings Center, Beverly, Massachusetts 01915, USA. [6] Department of Microbiology and Immunology and Center for Biofilm Engineering, Montana State University, 109 Lewis Hall, Montana State University, Bozeman, Montana 59717, USA. [7] Department of Cell and Molecular Biology, The Scripps Research Institute, 10550 North Torrey Pines Road, La Jolla, California 92037, USA. [8] The Department of Pharmacology and Experimental Neuroscience, University of Nebraska Medical Center, Omaha, Nebraska 68198-5880, USA. [9] The Core Microscopy Facility, The Scripps Research Institute, 10550 North Torrey Pines Road, La Jolla, CA 92037, USA. [10] Department of Chemistry, Washington University in St. Louis, One Brookings Drive, St. Louis, Missouri 63130, USA. [11] Departments Genetics and Medicine, Washington University School of Medicine, 660 South Euclid Ave., St Louis, Missouri 63110, USA. [12] Departments of Chemistry, Molecular and Computational Biology, The Scripps Research Institute, 10550 North Torrey Pines Road, La Jolla, California 92037, USA. Correspondence and requests for materials should be addressed to G.S. (email: siuzdak@scripps.edu).

© 2015 Macmillan Publishers Limited. All rights reserved.

Fluorocarbons have remarkable chemical and physical characteristics that allow unique surface properties, high stability, low reactivity and an ability to solubilize gases. The biocompatibility of fluorocarbons has been demonstrated[1–5] and has inspired researchers to utilize these compounds for a wide range of biomedical and research applications. For example, these properties have enabled fluorocarbons to be applied in areas as diverse as surface coatings[6], drug delivery[4], liquid ventilation[1], synthetic blood[2] and several imaging modalities[4,5,7,8] including mass spectrometry imaging[9].

Mass spectrometry imaging facilitates the spatially resolved mass analysis of metabolites *in situ*[10–12] where investigators have a choice of multiple technologies each with their inherent advantages and disadvantages[9,13–18]. These techniques include matrix-assisted laser desorption/ionization mass spectrometry (MALDI-MS)[15], secondary ion mass spectrometry[13], desorption electrospray ionization[14], MALDESI[18], and others[9,16,17,19]. While there have been some successful developments in low energy[20] and low background[21] matrices for MALDI-MS, the most widely used of these technologies, these matrices do not facilitate multiple modes imaging.

Gold nanoparticles (AuNPs) are well known as contrast agents for X-ray imaging technologies[22–24] and electron microscopy[25]. For example, the attenuation property of X-rays by AuNPs has led to their use as contrast agents in computed tomography (CT) imaging[26,27]. AuNP have also been exploited for mass spectrometry molecular imaging, thus presenting a single platform capable of supporting comprehensive bioimaging. However, AuNPs' ability to facilitate molecular imaging via mass spectrometry is limited due to the required high laser energies, resulting in significant fragmentation and generally poor sensitivity[28]. While AuNPs are attractive biomedical imaging agents, they have not been explored as agents to correlate structure with molecular information given their limitations with mass spectrometry. Indeed, when performing mass spectrometry-based metabolomic imaging, correlating metabolite localization patterns with tissue anatomy is key to data interpretation but has represented a serious challenge. Traditionally, correlations have been based on immunohistochemistry. Given that immunohistochemistry chemically alters tissue sections immunohistochemistry and mass spectrometry imaging cannot be performed on the same tissue samples.

Here we introduce f-AuNPs as an agent for nanostructure imaging mass spectrometry (NIMS). The use of fluorocarbons as a covalent modification of AuNPs for this application is a natural choice given the history[17] of fluorocarbons facilitating NIMS, specifically nanostructured silicon has benefited from fluorine modifications[9]. Fluorinated silicon nanostructures used for laser desorption/ionization have been shown to generate low background interference, have minimal ultraviolet absorbance, generate little fragmentation and, given their unique super-hydrophobicity, readily allow for the desorption of metabolites from their surface with high sensitivity. In addition, fluorous initiators containing amino groups can be used to promote $[M-H]^-$ production[29,30], which, similar to basic MALDI matrices[31,32], have been successfully applied to mass spectrometry imaging of central carbon metabolites. In addition to mass spectrometry imaging, f-AuNPs, unlike MALDI matricies, are also capable of acting as contrast agents for X-ray analysis and electron microscopy[22–24,25]. We demonstrate f-AuNP multimodal imaging to generate X-ray (μCT) and electron microscopy structural images, as well as facilitating mass spectrometry imaging, providing both anatomical and molecular information.

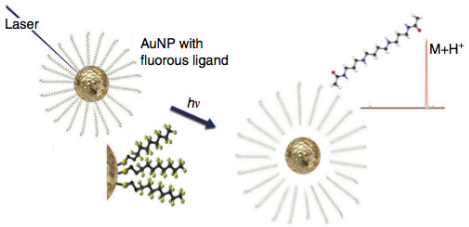


Figure 1 | Decoupling laser-induced nanoparticle heating from desorption/ionization. Schematic illustration of the possible desorption mechanism: on irradiation, gold core efficiently absorbs the laser energy and transfers the energy to thermally release fluorinated ligands. The desorbed fluorinated ligands provide the kinetic energy (and driving force) for analyte desorption and serve to protect the analyte from thermal degradation. Protonated diacetylspermine is shown as an example of f-AuNP desorption/ionization.

Results

Fluorinated AuNPs for mass spectrometry imaging. Given the advantages that fluorocarbon modifications impart on silicon nanostructure mass spectrometry imaging, our goal in these studies was to adapt fluorocarbon ligands to the more versatile AuNPs. In laser desorption/ionization experiments, silicon nanostructures and AuNPs absorb energy extremely well in the ultraviolet region[33–35] and in the case of AuNPs, the core can reach ~2,000 K in a few nanoseconds[36]. While AuNPs alone have limited ability to facilitate molecular imaging via mass spectrometry due to the required high laser energies resulting in significant fragmentation and generally poor sensitivity[28]. AuNPs with fluorocarbon ligands (f-AuNPs) are designed to initiate the desorption/ionization mass spectrometry event while attenuating energy transfer to the analyte. This is accomplished through the fluorinated ligand, which serves to insulate the analyte from the thermal energy of the AuNP (~2,000 K) while the laser-induced release of the ligand allows it to act as a conduit for analyte desorption. We posit that the thermal desorption of the ligand provides enough kinetic energy to drive analyte desorption into the gas phase with minimal energy input, as illustrated in Fig. 1.

In a representative experiment, we have demonstrated the utility of these f-AuNPs to carry out MS analysis of pure standards (Supplementary Fig. 1) and human plasma (Supplementary Fig. 2) using two instruments designed for MALDI, an AB SCIEX TOF/TOF 5800 and a Waters Synapt G2. AuNPs also offer a straight-forward platform for functionalization using gold-thiol chemistry. Here we used two separate commercially available thiols, 1H,1H,2H,2H-perfluorodecanethiol (fC10) and 1H,1H,2H,2H-perfluorooctanethiol (fC8). However, there is also the opportunity to design new ligands for the AuNPs that could enhance ionization, for example, amine fluorocarbon ligands could facilitate desorption/ionization of negatively charged metabolites since the ligand's amine would act as a proton acceptor.

Soft ionization with fluorinated AuNPs. To illustrate the laser-induced thermal energy generated at f-AuNPs, 4-nm f-AuNPs were measured with transmission electron microscopy (TEM) before and after laser irradiation (Fig. 2). The size distribution in the top panel of Fig. 2 shows an increase in size (to ~6 nm) indicating that the particles melt and anneal following exposure to the laser pulses. The accompanying TEM images in Fig. 2b offer further evidence that laser radiation has melted and fused the f-AuNPs. The thermal energy responsible for melting the

© 2015 Macmillan Publishers Limited. All rights reserved.

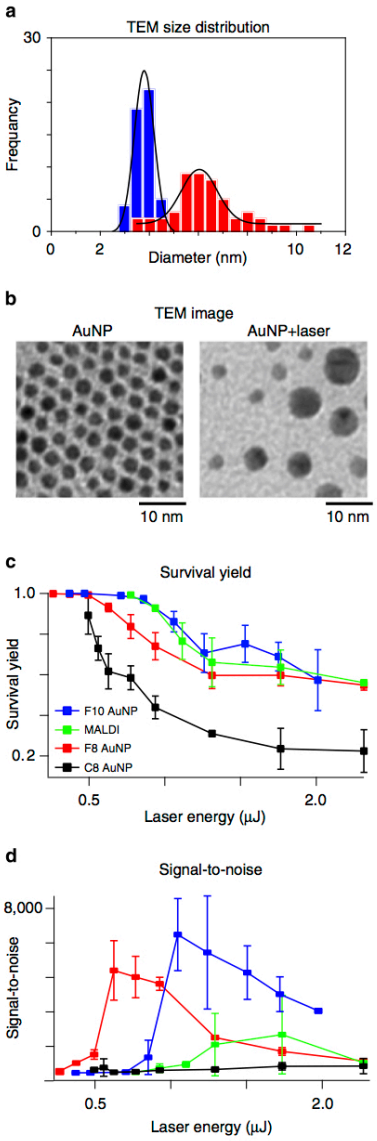


Figure 2 | Soft ionization with f-AuNPs. (**a**) The diameter of AuNPs increases from 3.5 ± 0.5 nm to 6.0 ± 1.4 nm after laser irradiation. (**b**) TEM images of AuNPs before and after laser irradiation. Scale bar, 10 nm. (**c**) Survival yield versus laser energy plot of methoxybenzyl pyridinium for F8-AuNP, F10-AuNP, C8-AuNP and MALDI (error bars are s.d.). (**d**) Signal-to-noise versus laser energy plot for $[M]^+$ ($m/z = 200$) for F8-AuNP, F10-AuNP, C8-AuNP and MALDI (error bars are s.d.).

particles can be used to desorb the fluorocarbon ligand, thus indirectly desorbing analyte molecules into the gas phase for mass spectrometry analysis. Thermal desorption, however, typically requires high energy, which leads to significant fragmentation, including the formation of ions that are primarily cation adducts[33] and the formation of gold cluster ions[37]. Therefore, our next set of experiments explored the performance of the f-AuNPs and whether thermal release of the fluorocarbon ligand was beneficial to the mass spectrometry analyses. To do this, the f-AuNPs were compared with MALDI and AuNPs functionalized with the non-fluorous ligand octanethiol (C8-AuNPs) by tracking the survival yield of the thermally labile molecule methoxybenzyl pyridinium with respect to laser energy (Fig. 2). Survival yield was calculated as the ratio of $[M]^+$ ($m/z = 200$) to the major fragment at $m/z = 121$. Desorption of methoxybenzyl pyridinium was initiated at energies above 0.78 μJ; when using MALDI with α-cyano-4-hydroxycinnamic acid, (C8-AuNP) initiated desorption at energies above 0.50 μJ, while the f-AuNP initiated desorption at energies above 0.25 μJ for the 8-carbon fluorous ligand (F8-AuNP) and 0.34 μJ for the 10-carbon fluorous ligand (F10-AuNP). The low-energy behaviour of f-AuNPs allows NIMS experiments to be carried out at energies that are below the threshold for gold cluster formation (Supplementary Fig. 3), a significant advantage since these ion clusters can complicate the mass spectrum in the low mass region. In addition, the low energies used tend to create minimal background signal compared with typical MALDI matrices (Supplementary Figs 4–15).

The survival yield plot in Fig. 2 shows that the f-AuNPs performed exceptionally well in terms of fragmentation as compared with the C8-AuNPs. We observed that fragmentation begins immediately at the threshold energy required for desorption and levels out at ~20% survival for C8-AuNP, whereas the F8-AuNP maintained 100% survival over 0.25–0.50 μJ and reached a steady state of 60% at 1.25 μJ. These results suggest that the fluorous-thiol functionality effectively insulates the sample from the potentially damaging thermal energy from the irradiated AuNPs. This is further evidenced by the observation that the longer fluorinated alkane thiol functionalized F10-AuNPs maintain 100% survival over a longer range (0.34–0.80 μJ) as presumably the longer chain better insulates the analyte from the heat generated at the particle surface. It is also interesting to note that fragmentation begins at energies far below the threshold for desorption of bare nanoparticles, showing the inherent harshness of nanoparticle-based thermal desorption. The comparison to be made with MALDI-MS is more nuanced; at very low energies, desorption does not occur in MALDI-MS, while it does occur using f-AuNP with essentially no damage to the molecular ion. As the energy approaches the threshold for MALDI, the survival yield for f-AuNPs begins to decrease and continues to decrease at a slower rate than MALDI until both desorption methods reach a steady state of 60% at 1.25 μJ.

Generally, we observed that the f-AuNPs outperform MALDI at low energy and perform comparably at higher energies. The signal-to-noise ratios plotted in Fig. 2 show that the particles perform better than both MALDI and the C8-AuNP in terms of the generation of $[M]^+$ signal. This result is again most likely due to the low energy requirements for this type of desorption/ionization. In addition, the longer chain appears to perform slightly better than the shorter chain. The length of the chain appears to shift and extend the optimal energy range for this experiment; however, in both cases, it should be noted that the maximum signal-to-noise occurs at energies above 100% survival. Furthermore, it could be the case that the trend would continue with the use of a perfluorododecanethiol (F12); however, this ligand was not readily available.

© 2015 Macmillan Publishers Limited. All rights reserved.

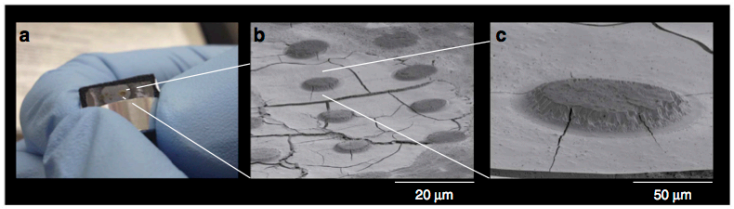


Figure 3 | Characterization of desorption/ionization using fluorinated nanoparticles. (**a**) Silicon substrate with a thaw-mounted section of mouse lung spotted with a f-AuNP solution. (**b**) SEM characterization of the mouse lung section spotted with f-AuNPs after laser irradiation. (**c**) The plateau-shaped spots (50–60 µm in diameters) formed on the tissue surface after laser irradiation.

In addition to the low-energy requirements of the f-AuNP observed in the survival yield experiments, scanning electron microscopy (SEM) data indicate that the desorption process is particularly soft. Unlike the typical ablation 'craters' observed in MALDI-MS analysis of the tissue (Supplementary Fig. 16), we observed plateau-like structures in the f-AuNP experiments. Figure 3 shows a slice of lung tissue that was spotted with the f-AuNP solution and irradiated with a Nd:YAG laser. In the treated area, the laser pulses create raised protrusions. Outside of this f-AuNP-coated region, no protrusions were formed. Interestingly, the laser pulses that occurred at the interface create partial plateau structures. We suspect that the protrusion of the surface following laser radiation is a side product brought about by the heating of the f-AuNPs. We speculate that the heat of the f-AuNPs vaporizes the more volatile components in the tissue, creating the plateau-like effect, however this phenomenon requires further investigation.

NIMS and SEM imaging of biofilms. The overarching goals of this technology are to increase both the accessibility and the functionality of nanostructure-based imaging. Using f-AuNPs as a platform accomplishes these goals by adding multiple methods of imaging capabilities. To this point, another advantage of f-AuNPs is their solubility in biologically inert fluorocarbon solvents that can be applied to the top of a tissue sample. This contrasts to classic silicon NIMS experiments, which require that the sample be thinly sliced and placed on top of a nanostructured surface. We tested the versatility of the f-AuNPs on a biofilm sample that would not be immediately accessible to silicon nanostructure-based techniques due to the thickness of the sample[38]. To analyse these samples, the aclar substrates that the biofilms were grown on were attached directly to the target plate where, following desiccation, the f-AuNPs were deposited drop wise.

The NIMS data shown in Fig. 4 illustrate that f-AuNP can be used to initiate desorption/ionization from these irregular biofilm surfaces. This image compares two biofilm cultures of *Desulfovibrio vulgaris* (DVH)—one that was grown in balanced conditions and one that was grown in stressed conditions. Stressed conditions refer to an electron acceptor-limited (EAL) environment, which affects the biofilm growth of sulfate reducing bacteria, like DVH. The mass spectra extracted from the balanced and stressed bacteria (Fig. 4) show several differences, the most dramatic one at m/z 551, which has been mapped to the right of the mass spectra in Fig. 4. This ion was putatively identified (Supplementary Fig. 17 and Supplementary Table 1) diglyceride (16:0/16:0) (ref. 39) and might be indicative of perturbed metabolism in the stressed bacteria; however, this is still a very preliminary finding. In addition, f-AuNPs were successfully applied to the bacteria sample, following fixation and dehydration, to act as a contrast agent for the comparatively high-resolution SEM images shown in Fig. 4. Surprisingly, we found that the density of the EAL bacteria was in fact increased relative to the balanced bacteria. This result was confirmed using a standard SEM procedure and is currently under further investigation.

NIMS and X-ray µCT imaging of mouse lung tissue. The success of the mass spectrometric detection of metabolites using f-AuNPs (Fig. 4) has allowed for the further integration of the f-AuNPs NIMS analysis with µCT. Together these two modes of imaging allow for the correlation of three-dimensional anatomical (structural) and molecular information (Supplementary Fig. 18). For example, this has been demonstrated in the analysis of metastatic mouse lungs. Specifically, 500 µl of the biologically inert f-AuNP solution was intratracheally introduced into mouse lungs and immediately distributed into the lung tissue. The liquid ventilated lung was then embedded into OCT (optimal cutting temperature) material and preserved in −80 °C until analysis. The mouse lung was then imaged with µCT to construct high-resolution three-dimensional image (Fig. 5 Supplementary Video 1). F-AuNPs were well distributed into the lung tissue and characterized the airway and porosity of the lung. The blood vessels appear as dark areas and the regions of the lungs carrying metastases revealed dark spots consistent with the exclusion of nanoparticle from the metastatic lesions (Supplementary Fig. 19).

To obtain molecular information from liquid ventilated metastatic lung tissue, OCT-embedded lungs were sectioned (20 µm) and analysed. Since the f-AuNPs solution had been passed through the trachea into the lung, no additional f-AuNPs were applied to the tissue. A mass spectrometry image of the f-AuNP-ventilated left lobe of the lung is shown in Fig. 5. In general, mass spectrometry analysis is a multiplexed analysis where multiple molecular ions can be simultaneously detected in one experiment. Here we chose to map a phosphatidylcholine (Supplementary Fig. 20) at m/z 756 to demonstrate molecular information and its distribution in this tissue (Fig. 5). To confirm that the areas lacking nanoparticle signal did contain cancerous tissue, metastases in an intact liquid ventilated mouse lung were identified by haematoxylin and eosin staining and compared with an adjacent NIMS image (Supplementary Fig. 19). To better access these structures, it might be possible to approach the metastases from the blood stream by perfusing the animal with a synthetic blood form of the f-AuNP or to coat the tissue following sectioning (Supplementary Fig. 21).

To enable NIMS and X-ray µCT imaging of blood vessels *in situ*, we took advantage of fluorocarbons utility as a blood substitute[2,40]. The f-AuNPs were dissolved in the fluorocarbon

© 2015 Macmillan Publishers Limited. All rights reserved.

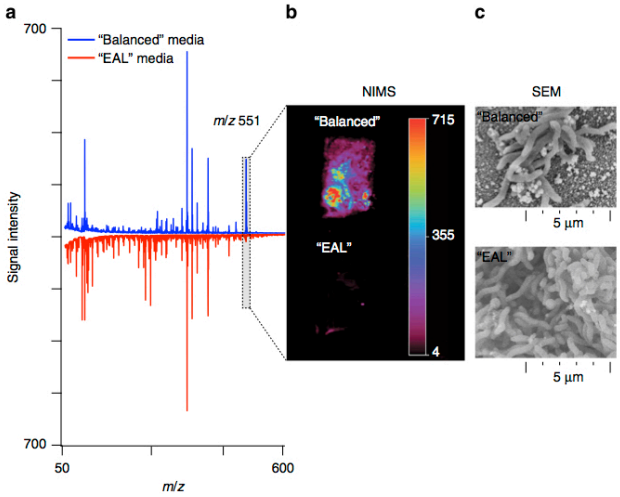


Figure 4 | NIMS and SEM imaging using fluorinated AuNPs. (**a**) Mass spectra generated from two regions of interest in the f-AuNP MSI—one corresponds to the biofilm grown in balanced media (blue) and one corresponding to the biofilm grown in EAL media (red). The inset (**b**) shows the ion image for *m/z* 551. (**c**) SEM images of balanced and stressed biofilms treated with f-AuNP.

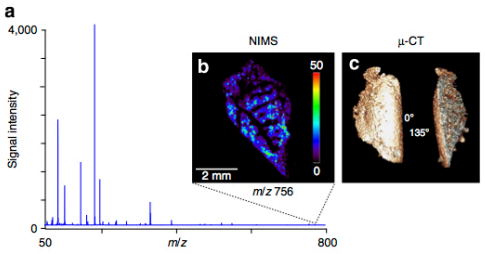


Figure 5 | NIMS and µCT imaging using fluorinated AuNPs. (**a**) Mass spectra generated from a single-lobe metastatic mouse lung ventilated with f-AuNPs. The inset (**b**) shows the ion image for *m/z* 756. (**c**) µCT images of the same lobe of the f-AuNP-ventilated metastatic mouse lung at 0° and 135° where gold indicates the surfaces of the f-AuNP-ventilated lung and silver represents the volume.

perfluordecalin, which was emulsified to approximate the only the Food and Drug Administration-approved fluorocarbon-based blood substitute[40]. The f-AuNP emulsion was perfused into the circulatory system to demonstrate the ability to obtain structural and chemical information from the circulatory system associated with the lung (Supplementary Fig. 22) as well the liver (Supplementary Fig. 23) of the mouse. In addition, we also applied these imaging approaches to investigate the structural and chemical effects of hyperoxia on the lung tissue of juvenile mice (Supplementary Figs 24 and 25).

NIMS for analysis of central carbon metabolites. The majority of central carbon metabolites are anionic and thus are better suited for analysis in negative ion mode imaging mass spectrometry. One successful approach used for the *in situ* ionization and imaging of central carbon metabolites employs amine-functionalized initiators[30] and MALDI matrices[31]. Presumably, these adjuvants work well because the basic amine group acts as a proton acceptor to promote $M-H^-$ production. Thus, to enable the application of this imaging platform to the analysis of central carbon metabolites in negative ionization mode, we have to enrich the fluorocarbon solvent with the basic initiator 1H,1H,2H,2H,3H,3H-perfluoroundecylamine (PFUA).

As it was not clear that the f-AuNPs would transfer the requisite energy to the initiator molecule needed to induce desorption/ionization, we tested the enriched f-AuNPs using a standard mixture of nine metabolites in negative mode. A mass spectrum generated from this experiment is shown in Fig. 6; in addition to the peaks for each individual metabolite, we also observe peaks for Au^- and $PO_4H_2^-$. We attribute the emergence of these ions to the higher energy used in this experiment. The spectra in Supplementary Fig. 3 show that under the standard operation energy of 1.4 µJ no Au ions are formed; the addition of PFUA, however, increased the energy requirement to ~2 µJ. Just as the energy threshold increases with chain length (Fig. 2), the incorporation of the PFUA shifted this threshold even further by ostensibly adding a second barrier between the AuNP and the analyte. However, even at this increased energy, the enriched f-AuNPs performed well in negative ion mode.

The enriched f-AuNPs were then used to demonstrate central carbon metabolite imaging in tissue using negative ionization mode. The enriched particles were applied to the top of a sagittal slice from one half of a bifurcated mouse brain after desiccation. In Fig. 6, we have mapped the ions corresponding to lactate, glutamate and docosahexenoic acid. The presence of each mapped metabolite was then confirmed by LC-MS/MS analysis of the second half of the brain. Here we have demonstrated that this platform like Si-based NIMS[30] has the ability to use specialized initiators to expand the number of metabolites that are amicable to mass spectrometry imaging.

© 2015 Macmillan Publishers Limited. All rights reserved.

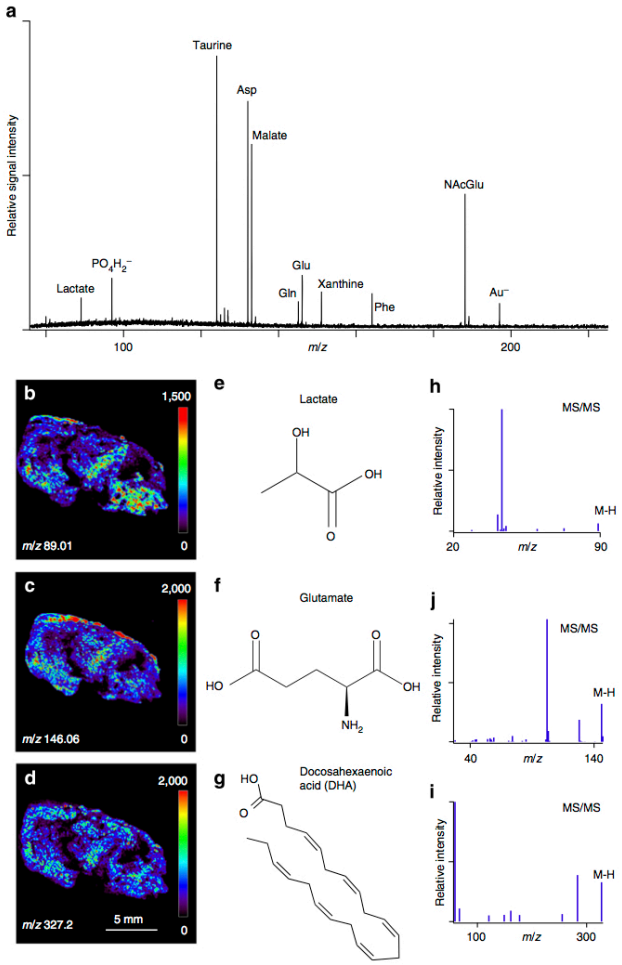


Figure 6 | NIMS for the analysis of central carbon metabolites. (**a**) A mass spectrum for nine metabolites in a standard mixture. (**b**–**d**) NIMS images of a sagittal slice of a mouse brain collected in negative ion mode. Each image is paired with (**e**–**g**) the structure of the identified metabolite and (**h**–**j**) tandem MS data that were collected using LC-MS/MS.

Discussion

Fluorinated AuNPs (f-AuNPs) were designed to facilitate NIMS as well as act as contrast agents for EM and μCT. An important feature of the f-AuNPs is that they promote a gentle laser desorption/ionization mechanism facilitating intact molecular ion formation with little background interference or molecular ion fragmentation. The utility of AuNPs for structural μCT measurements is well established but the primary advance of employing fluorinated ligands to these structures has allowed for structural data (μCT) to be combined for the first time with molecular mass spectrometry information (f-AuNPs NIMS). This multimodal imaging approach is particularly useful for performing mass spectrometry-based metabolite imaging, where correlating metabolite concentrations with anatomical structure is key to data interpretation. The fluorocarbon liquid component of the method affords versatility in the delivery of the agent, which can be carried out via direct coating, liquid ventilation or perfusion allowing analysis of morphologically diverse biological samples.

Methods

Chemicals. Octanethiol-functionalized AuNPs (2–4 nm DLS, 2% w/v in toluene) and fluorinated ligands 1H,1H,2H,2H-perfluorodecanethiol (fC10) and 1H,1H,2H,2H-perfluorooctanethiol (fC8), methoxybenzyl pyridinium chloride and perfluorodecalin were purchased from Sigma-Aldrich (St Louis, MO, USA) and 10% Gibco Pluronic F-68 was from Life Technologies (Grand Island, NY)

© 2015 Macmillan Publishers Limited. All rights reserved.

1H,1H,2H,2H,3H,3H-perfluoroundecylamine was from Santa Cruz Biotechnology (Dallas, TX).

Nanoparticle synthesis. Octanethiol-functionalized AuNPs were in toluene with a concentration of 20 mg ml^{-1}. One ml of octanethiol-functionalized AuNPs (20 mg) was added to ~20 ml of ethanol to precipitate the AuNPs with centrifugation at 4,000 r.p.m. for 15 min. The precipitated AuNP were then washed with acetone, briefly sonicated and centrifuged again. The cleaning procedure was repeated three times before being dissolved in 1 ml of hexane. The AuNP solution (1 µl) was then analysed using LDI-MS to test for the presence of tetraoctyl ammonium bromide by monitoring the tetraoctyl ammonium ion at *m/z* 466, which is commonly used as a phase transfer additive in nanoparticle synthesis. More acetone washes were conducted until tetraoctyl ammonium ion was not detected. An additional 1 ml of hexane and 400 µl of 1H,1H,2H,2H-perfluorooctanethiol (fC8) or 1H,1H,2H,2H-perfluorodecanethiol (fC10) was added and the vial was purged with nitrogen gas to remove air. The solution was stirred for one to three days until AuNPs precipitated. The solvent was evaporated with nitrogen gas flow and nanoparticles were washed three times with hexane, three times with acetone and two times with 1:1:1 methanol/acetone/water, respectively, to remove excess ligand and impurities. Following washing, the AuNP was dried in the oven (~80 °C) for several minutes and stored as a solid. Before use, the AuNP was dissolved in tetradecafluorohexane (PFH) at 3 mg ml^{-1} for mass spectrometry and electron microscopy analyses and 10 mg ml^{-1} in perfluorodecalin for mouse lung perfusion experiments.

Enriched f-AuNPs were made by dissolving 3 mg ml^{-1} f-AuNPs into 5% 1H,1H,2H,2H,3H,3H-perfluoroundecylamine perfluorodecalin solution.

The blood substitute f-AuNP solution was made by combining 50% 20 mg ml^{-1} f-AuNP/prefluorodecilin and 50% Pluronic F-68 (0.5%) in Milli-Q water. The immiscible solutions were sonicated for 5 min at 50% duty cycle with a probe sonicator.

Electron microscopy characterization. For TEM imaging, fluorinated AuNPs were deposited on 400 mesh copper grids and characterized by a Philips CM100 electron microscope (FEI, Hillsborough, OR) at 80 kV. Images were collected using a Megaview III CCD camera (Olympus Soft Imaging Solutions, Münster, Germany). Fluorinated AuNPs deposited on copper grids were also irradiated with (355 nm, laser energy 6.6 µJ, 2,000 shots), and then measured with TEM. For SEM analysis, 10 µl of 3 mg ml^{-1} fluorinated AuNPs in PFH were first deposited onto mouse brain or lung tissue which was then irradiated by a laser with a predefined 250-µm step size. Subsequently, the samples were imaged with a Hitachi S4800 SEM at 5 kV. SEM was done on biofilms from the same batch. Aclar slides with adhered biofilm were aldehyde fixed (2.5% w/v glutaraldehyde, 2.0% w/v paraformaldehyde, 0.05 M sodium cacodylate buffer pH 7.0) overnight. Samples were rinsed with double-distilled H_2O and ethanol dehydrated. Critical point drying was then carried on the samples using CO_2 and spotted with f-AuNP solution (1 mg ml^{-1}). Samples were also viewed on a Hitachi S4800 SEM.

Bacterial strains and growth conditions. DVH RCH1 was obtained from Dr Romy Chakraborty (Lawrence Berkeley National Lab) and was isolated from Cr-contaminated groundwater at the U.S. Department of Energy Hanford reservation. DVH RCH1 was grown in LS4D medium, which contains lactate as the carbon source and electron donor and sulfate as the electron acceptor[41]. Lactate and sulfate concentrations were altered to create balanced and EAL conditions. The balanced condition was defined as 60 mM sodium lactate and 30 mM sodium sulfate and the EAL condition was defined as 50 mM sodium lactate and 10 mM sodium sulfate. DVH RCH1 was grown as a biofilm under continuous flow conditions in a modified Center for Disease Control reactor. Exponential phase cells were inoculated into a reactor containing balanced or EAL lactate–sulfate media (LS4D) and were grown in batch mode for 48 h. Biofilms were grown at room temperature (20–23 °C), with a dilution rate of 0.04 per hour, stirred at 60 r.p.m. and the headspace was continually purged with sterile N_2 gas to maintain anaerobic conditions. Coupons of aclar (7.8 m.i.l. thickness; Electron Microscopy Sciences, Hatfield, PA) supported by glass slides were submerged in the reactor body as a surface for biofilm growth. Aclar coupons were removed from the reactor after 144, rinsed three times in ice-cold PBS, wicked dry and flash frozen in liquid nitrogen. Samples were stored at −80 °C until analysis.

Animals and µCT imaging. All animal work complied with the National Institutes of Health and institutional guidelines (TSRI is AAALAC, International accredited). Female 11-week-old CB17-*Prkdc*^{SCID} mice were euthanized by overdose of isoflurane before exsanguination by cutting the abdominal aorta. A small incision was performed in the trachea to insert a 20 gauge blunt needle, which was secured by a piece of suture. Approximately 500 µl of 10 mg ml^{-1} f-AuNP in PFH solution was then injected into the lungs up to full lung inflation. Intact lungs were immediately harvested, placed in OCT compound embedding medium, frozen in liquid nitrogen and stored at −80 °C before analysis.

For the hyperoxia experiment, the experimental group consisted of C57BL/6J P7 pups (7 days old) exposed to 75% oxygen for 5 days and returned to room air at P12 (12-day-old pups). The control group consisted of age-matched pups raised in normoxia (21% O2) for the same period. Pups were killed at P12. As was the case with adult mice, the pups were euthanized by overdose of isoflurane before exsanguination by cutting the abdominal aorta. Ventilation of the f-AuNPs in this case was carried out directly via the mouth to the trachea. Approximately 250 µl of 10 mg ml^{-1} f-AuNP in perfluorodecalin solution was then injected into the lungs up to full lung inflation. Again, the intact lungs were immediately harvested, placed in OCT compound embedding medium, frozen in liquid nitrogen and stored at −80 °C before analysis.

For the blood substitute experiment, a male mouse (C57BL/6J, 24 days of age) was anaesthetized with isoflurane and the heart was exposed. A 23-gauge needle attached by tubing to a syringe was inserted into the left ventricle, the right atria was pierced and 40 ml saline was perfused through the animal at a rate of 3.1 ml min^{-1} to clear all of the blood. A three-way valve was switched so that 3 ml of the f-AuNP blood substitute was then pumped through the mouse at the same rate. The lung and liver were harvested and imbedded in OCT until µCT analysis.

The intact mouse lungs and liver were imaged by µCT (vivaCT 75; Scanco Medical AG; Basserdorf, Switzerland) in standard resolution using the following parameters: 55 kVP, 145 µA, 300-ms integration time and 41-µm voxel size. The scanning protocol was programmed to acquire images via a rotating gantry, resulting in a total of 500 step-projections per scan. The projections were reconstructed with a matrix of 1,024 × 1,024 using Scanco's µCT Tomography V5.4C software. The two-dimensional binary digital imaging communication files obtained from Scanco's software were later analysed using 64-bit OsiriX v.3.9.2 (Pixmeo; Geneva, Switzerland) software.

Mass spectrometry analysis and imaging. For the analysis of standard compounds, 0.5 µl of f-AuNP solution (3 mg ml^{-1}) was first deposited onto a *p*-type silicon chip and allowed to air dry. Then, 0.1–0.5 µl of standard compound solution was deposited on top of dried f-AuNP layer and dried under vacuum. An AB SCIEX TOF/TOF 5800 MS system was used for data collection. The instrument was operated at reflectron mode with a repetition frequency of 400 Hz and an accelerating voltage of 15 kV. Each sample spectrum was averaged from 400 laser shots.

Plasma was analysed using a MALDI SYNAPT G2S (Waters, Milford, MA) equipped with a Nd:YAG laser (355 nm) with a repetition frequency of 1,000 Hz and variable laser energy (8–10 µJ). Nitrogen was used in the ion mobility cell and the mobility experiments were collected with a variable wave velocity of 320 to 900 m s^{-1} for the 50 to 1,200 *m/z* region.

Mouse lung and liver tissue treated with AuNPs was sliced with a Leica CM1900 cryostat to a thickness of 20 µm, and then thaw-mounted directly onto *p*-type silicon chip. The tissues were directly imaged by an AB SCIEX TOF/TOF 5800 MS system without additional sample preparation. Tissue slices were imaged with a 100 µm step size and each recorded mass spectrum resulted from the average of 400 laser shots. Representative sections of the cancer metastasized lungs were collected on Superfrost Plus slides and stained with hematoxylin and eosin using routine histological techniques.

LC-MS/MS. Lung tissue and biofilm samples were analysed using reversed phase liquid chromatography/MS analysis in ESI-positive mode. The extracts were analysed on 6550 iFunnel QTOF mass spectrometer (Agilent Technologies) interfaced with 1200 series HPLC system (Agilent Technologies). For reversed phase liquid chromatography separation, 0.1% formic acid in water was used as mobile phase A and 0.1% formic acid in acetonitrile was used as mobile phase B. The metabolite extract was loaded onto a C18 column using 5% mobile phase B at a flow rate of 100 µl min^{-1} and resolved using a linear gradient of 5% B–95% B over 60 min.

References

1. Clark, L. C. & Gollan, F. Survival of mammals breathing organic liquids equilibrated with oxygen at atmospheric pressure. *Science* **152,** 1755–1756 (1966).
2. Sloviter, H. A. & Kamimoto, T. Erythrocyte substitute for perfusion of brain. *Nature* **216,** 458–460 (1967).
3. Ubel, F. A., Sorenson, S. D. & Roach, D. E. Health-status of plant workers exposed to fluorochemicals - a preliminary-report. *Am. Ind. Hyg. Assoc. J.* **41,** 584–589 (1980).
4. Krafft, M. P. Fluorocarbons and fluorinated amphiphiles in drug delivery and biomedical research. *Adv. Drug Deliv. Rev.* **47,** 209–228 (2001).
5. Mattrey, R. F. Perfluorooctylbromide - A new contrast agent for CT, sonography, and MR imaging. *Am. J. Roentgenol.* **152,** 247–252 (1989).
6. McBee, E. Fluorine chemistry. *Ind. Eng. Chem.* **39,** 236–237 (1947).
7. Mattrey, R. F. *et al.* Perfluorochemicals as US contrast agents for tumor imaging and hepatosplenography - preliminary clinical-results. *Radiology* **163,** 339–343 (1987).
8. Bruneton, J. N., Falewee, M. N., Balumaestro, C., Normand, F. & Mattrey, R. F. Perfluoroctylbromide and hepatosplenic computed-tomography - preliminary clinical-study. *Invest. Radiol.* **23,** 306–307 (1988).
9. Northen, T. R. *et al.* Clathrate nanostructures for mass spectrometry. *Nature* **449,** 1033–U1033 (2007).

© 2015 Macmillan Publishers Limited. All rights reserved.

10. Khatib-Shahidi, S., Andersson, M., Herman, J. L., Gillespie, T. A. & Caprioli, R. M. Direct molecular analysis of whole-body animal tissue sections by imaging MALDI mass spectrometry. *Anal. Chem.* **78,** 6448–6456 (2006).
11. Amaya, K. R., Sweedler, J. V. & Clayton, D. F. Small molecule analysis and imaging of fatty acids in the zebra finch song system using time-of-flight-secondary ion mass spectrometry. *J. Neurochem.* **118,** 499–511 (2011).
12. Lanekoff, I., Geydebrekht, O., Pinchuk, G. E., Konopka, A. E. & Laskin, J. Spatially resolved analysis of glycolipids and metabolites in living Synechococcus sp PCC 7002 using nanospray desorption electrospray ionization. *Analyst* **138,** 1971–1978 (2013).
13. Herzog, R. F. K. & Viehbock, F. P. Ion sourse for mass spectrography. *Phys. Rev.* **76,** 855–856 (1949).
14. Takats, Z., Wiseman, J. M., Gologan, B. & Cooks, R. G. Mass spectrometry sampling under ambient conditions with desorption electrospray ionization. *Science* **306,** 471–473 (2004).
15. Hillenkamp, F., Karas, M., Beavis, R. C. & Chait, B. T. Matrix-assisted laser desorption ionization mass-spectrometry of biopolymers. *Anal. Chem.* **63,** A1193–A1202 (1991).
16. Roach, P. J., Laskin, J. & Laskin, A. Nanospray desorption electrospray ionization: an ambient method for liquid-extraction surface sampling in mass spectrometry. *Analyst* **135,** 2233–2236 (2010).
17. Wei, J., Buriak, J. M. & Siuzdak, G. Desorption-ionization mass spectrometry on porous silicon. *Nature* **399,** 243–246 (1999).
18. Sampson, J. S., Hawkridge, A. M. & Muddiman, D. C. Generation and detection of multiply-charged peptides and proteins by matrix-assisted laser desorption electrospray ionization (MALDESI) Fourier transform ion cyclotron resonance mass spectrometry. *J. Am. Soc. Mass Spectrom.* **17,** 1712–1716 (2006).
19. Shrivas, K., Hayasaka, T., Sugiura, Y. & Setou, M. Method for simultaneous imaging of endogenous low molecular weight metabolites in mouse brain using TiO2 nanoparticles in nanoparticle-assisted laser desorption/ionization-imaging mass spectrometry. *Anal. Chem.* **83,** 7283–7289 (2011).
20. Wang, X. D. *et al.* Hydroxyflavones as a new family of matrices for MALDI tissue imaging. *Anal. Chem.* **85,** 7566–7573 (2013).
21. Shroff, R., Rulisek, L., Doubsky, J. & Svatos, A. Acid-base-driven matrix-assisted mass spectrometry for targeted metabolomics. *Proc. Natl Acad. Sci. USA* **106,** 10092–10096 (2009).
22. De, M., Ghosh, P. S. & Rotello, V. M. Applications of nanoparticles in biology. *Adv. Mater.* **20,** 4225–4241 (2008).
23. Boisselier, E. & Astruc, D. Gold nanoparticles in nanomedicine: preparations, imaging, diagnostics, therapies and toxicity. *Chem. Soc. Rev.* **38,** 1759–1782 (2009).
24. Mieszawska, A. J., Mulder, W. J. M., Fayad, Z. A. & Cormode, D. P. Multifunctional gold nanoparticles for diagnosis and therapy of disease. *Mol. Pharm.* **10,** 831–847 (2013).
25. Hermann, R., Walther, P. & Müller, M. Immunogold labeling in scanning electron microscopy. *Histochem. Cell Biol.* **106,** 31–39 (1996).
26. Lusic, H. & Grinstaff, M. W. X-ray-computed tomography contrast agents. *Chem. Rev.* **113,** 1641–1666 (2012).
27. Popovtzer, R. *et al.* Targeted gold nanoparticles enable molecular CT imaging of cancer. *Nano Lett.* **8,** 4593–4596 (2008).
28. Zhu, Z. J., Ghosh, P. S., Miranda, O. R., Vachet, R. W. & Rotello, V. M. Multiplexed screening of cellular uptake of gold nanoparticles using laser desorption/ionization mass spectrometry. *J. Am. Chem. Soc.* **130,** 14139–14143 (2008).
29. Amantonico, A., Flamigni, L., Glaus, R. & Zenobi, R. Negative mode nanostructure-initiator mass spectrometry for detection of phosphorylated metabolites. *Metabolomics* **5,** 346–353 (2009).
30. Ivanisevic, J. *et al.* Brain region mapping using global metabolomics. *Chem. Biol.* **21,** 1575–1584.
31. Edwards, J. L. & Kennedy, R. T. Metabolomic analysis of eukaryotic tissue and prokaryotes using negative mode MALDI time-of-flight mass spectrometry. *Anal. Chem.* **77,** 2201–2209 (2005).
32. Miura, D. *et al.* Ultrahighly sensitive in situ metabolomic imaging for visualizing spatiotemporal metabolic behaviors. *Anal. Chem.* **82,** 9789–9796 (2010).
33. Zhu, Z. J., Rotello, V. M. & Vachet, R. W. Engineered nanoparticle surfaces for improved mass spectrometric analyses. *Analyst* **134,** 2183–2188 (2009).
34. Chiang, C.-K., Chen, W.-T. & Chang, H.-T. Nanoparticle-based mass spectrometry for the analysis of biomolecules. *Chem. Soc. Rev.* **40,** 1269–1281 (2011).
35. McLean, J. A., Stumpo, K. A. & Russell, D. H. Size-selected (2–10 nm) gold nanoparticles for matrix assisted laser desorption ionization of peptides. *J. Am. Chem. Soc.* **127,** 5304–5305 (2005).
36. Pustovalov, V. K. Theoretical study of heating of spherical nanoparticle in media by short laser pulses. *Chem. Phys.* **308,** 103–108 (2005).
37. Hsieh, Y. T., Chen, W. T. & Chang, H. T. Detection of nucleoside monophosphates through surface-assisted laser desorption/ionization mass spectrometry using CTAB-adsorbed gold nanoparticles. *J. Chin. Chem. Soc.* **58,** 761–768 (2011).
38. Louie, K. B. *et al.* 'Replica-extraction-transfer' nanostructure-initiator mass spectrometry imaging of acoustically printed bacteria. *Anal. Chem.* **85,** 10856–10862 (2013).
39. Passarelli, M. K. & Winograd, N. Lipid imaging with time-of-flight secondary ion mass spectrometry (ToF-SIMS). *Biochim. Biophys. Acta* **1811,** 976–990 (2011).
40. Maugh, T. H. Blood substitute passes its first test. *Science* **206,** 205 (1979).
41. Clark, M. E. *et al.* Temporal transcriptomic analysis as *Desulfovibrio vulgaris* hildenborough transitions into stationary phase during electron donor depletion. *Appl. Environ. Microbiol.* **72,** 5578–5588 (2006).

Acknowledgements

This work was supported by the California Institute of Regenerative Medicine grant number TR1-01219 (G.S. and M.F.), the Department of Defense (DoD) number W81XWH-13-1-0402 and ENIGMA- Ecosystems and Networks Integrated with Genes and Molecular Assemblies (http://enigma.lbl.gov), a Scientific Focus Area Program at Lawrence Berkeley National Laboratory is based upon work supported by the U.S. Department of Energy, Office of Science, Office of Biological & Environmental Research under contract number DE-AC02-05CH11231 (G.S. and M.W.F.). It was also supported by the US National Institutes of Health numbers R01 CA170737 (B.H.F.), R24 EY017540 (G.S. and M.F.), P30 MH062261 (G.S.), RC1 HL101034 (G.S.) and P01 DA026146 (G.S.).

Author contributions

Z.J.Z, M.E.K, J.I., M.E.S, P.J.O.B. and G.S. designed the experiments; Z.J.Z, A.M.S, M.E.K. and J.I. performed the MS experiments. M.R.W. performed the electron microscopy. H.J.O. performed the IM-MS experiments. K.L, J.M.D and A.G. collected the μCT data. A.F.S, A.J.R, L.P.P, C.H.J, M.F., J.M.D and B.H.F. performed the animal experiments. A.A.E. and H.E.G. prepared the brain tissue samples for analyses. L.F., J.I. and M.W.F. performed the bacterial experiments. M.E.K, J.I., Z.J.Z, A.M.S, G.J.P. and G.S. analysed data and wrote the paper.

Additional information

Supplementary Information accompanies this paper at http://www.nature.com/naturecommunications

Competing financial interests: The authors declare no competing financial interests.

Reprints and permission information is available online at http://npg.nature.com/reprintsandpermissions/

How to cite this article: Kurczy, M. E. *et al.* Comprehensive bioimaging with fluorinated nanoparticles using breathable liquids. *Nat. Commun.* 6:5998 doi: 10.1038/ncomms6998 (2015).

© 2015 Macmillan Publishers Limited. All rights reserved.